

Sheffield Hallam University

Desulphurisation of iron-carbon melts.

HORNE, Stephen A.

Available from the Sheffield Hallam University Research Archive (SHURA) at:

<http://shura.shu.ac.uk/19827/>

A Sheffield Hallam University thesis

This thesis is protected by copyright which belongs to the author.

The content must not be changed in any way or sold commercially in any format or medium without the formal permission of the author.

When referring to this work, full bibliographic details including the author, title, awarding institution and date of the thesis must be given.

Please visit <http://shura.shu.ac.uk/19827/> and <http://shura.shu.ac.uk/information.html> for further details about copyright and re-use permissions.

SHEFFIELD CITY
POLYTECHNIC LIBRARY
POND STREET
SHEFFIELD S1 1WB

6819

794745101 X

TELEPEN



Sheffield City Polytechnic Library

REFERENCE ONLY

ProQuest Number: 10697133

All rights reserved

INFORMATION TO ALL USERS

The quality of this reproduction is dependent upon the quality of the copy submitted.

In the unlikely event that the author did not send a complete manuscript and there are missing pages, these will be noted. Also, if material had to be removed, a note will indicate the deletion.



ProQuest 10697133

Published by ProQuest LLC (2017). Copyright of the Dissertation is held by the Author.

All rights reserved.

This work is protected against unauthorized copying under Title 17, United States Code
Microform Edition © ProQuest LLC.

ProQuest LLC.
789 East Eisenhower Parkway
P.O. Box 1346
Ann Arbor, MI 48106 – 1346

DESULPHURISATION OF IRON-CARBON MELTS

by

STEPHEN ALAN HORNE

A THESIS SUBMITTED TO THE COUNCIL FOR NATIONAL
ACADEMIC AWARDS IN PARTIAL FULFILMENT FOR THE DEGREE OF
DOCTOR OF PHILOSOPHY

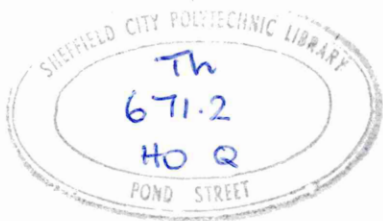
COLLABORATING ESTABLISHMENT:-

British Steel Corporation,
Scunthorpe Works,
P.O. Box No. 1,
SCUNTHORPE,
South Humberside, DN16 1BP.

SPONSORING ESTABLISHMENT:-

Department of Metallurgy,
Sheffield City Polytechnic,
Pond Street,
SHEFFIELD, S1 1WB.

December, 1984.



7947451-01

PREFACE

The work reported in this thesis was carried out while the candidate was registered for a higher degree.

During this period, the author attended post graduate lectures organised by the Department of Metallurgy, Sheffield City Polytechnic, on the following topics:-

- (i) The Physical Chemistry of Desulphurisation
- (ii) Refractories Technology
- (iii) Arc Furnace Steelmaking

A visual aid programmed learning course on Gas Liquid Chromatography organised by the Department of Chemistry was completed.

The work described in this thesis is, to the best of my knowledge, original except where reference is made to others, and no part of it has been submitted for an award at any other College or University.

ACKNOWLEDGEMENTS

The author would like to express his gratitude to Dr. R. Smith and Dr. R. Acheson for their guidance and advice during the supervision of this work.

Thanks are also given to my industrial supervisor, Dr. D.J. Price of B.S.C. Scunthorpe Works. The use of the GLC facilities in the Department of Chemistry, Sheffield City Polytechnic, under the guidance of Dr. D. Leathard, is gratefully acknowledged.

The author would also like to express his gratitude to the technical staff of the Metallurgy Department, particularly D.O. Latimer, J. Bradshaw, R. Grant and G.E. Gregory. Especial thanks go to my research colleagues, notably J. Cawley, G.Ekebuisi, A. Vassiliou and P. Williams for their enthusiasm and many stimulating discussions. The author is indebted to Mrs. N. Cooke for her considerable patience and skill in the typing of this thesis.

Special thanks to my family, particularly Debbie, for their patience and support throughout the period of this work.

The provision of a Research Assistantship by the LEA is gratefully acknowledged.

Desulphurisation of Iron-Carbon Melts

by

Stephen Alan Horne

Abstract

Desulphurisation of iron-carbon melts by CaO-FeO-SiO₂ slags (Fayalite to 38 mass % CaO-Fayalite) at 1300 °C has been investigated under conditions similar to those encountered in LD steelmaking practice. Techniques were developed to introduce a single metal droplet into a liquid slag contained in an iron crucible. Reaction was terminated by quenching the droplet and slag, the former being analysed to determine sulphur concentration. Equivalent techniques were employed to monitor decarburisation.

Results showed an initial efficient desulphurisation followed by a period of slow sulphur removal rate for droplets, initially containing 0.120 mass % S and higher, reacted with the 38 mass % CaO slag. Droplets of lower initial sulphur content experienced sulphur reversion for the first two to five minutes of droplet-slag interaction. Similar trends were established for experiments employing slags containing up to 28 mass % CaO but the reversion phenomenon was mainly restricted to droplets initially containing 0.030 mass % S. Decarburisation data indicated two dominant mechanisms, slag phase control followed by dispersed phase control.

The initial desulphurisation period was attributed to conditions imposed at the droplet-slag interface by slag phase controlled decarburisation in conjunction with the presence of FeO. A finite carbon and low oxygen concentration at the droplet surface, coupled with the availability of oxygen anions, created conditions conducive to sulphur removal. The FeO prevented formation of an acid CaO-SiO₂ interfacial slag of low oxygen anion concentration. Reversion of lower sulphur concentration droplets was related to gradual depletion of interfacial FeO which moved the slag towards an acid composition and lowered oxygen anion concentration. Replenishment of FeO at the reaction interface due to a transition to mixed or dispersed phase controlled decarburisation enabled desulphurisation to commence.

An attempt to determine silicate anion constitutions of synthetic and industrial slags was made using trimethylsilylation - GLC techniques. Similarity of results for slags of appreciable FeO concentration irrespective of SiO₂ content suggested that massive anionic redistribution had occurred during trimethylsilylation.

SYMBOLS

A	Area
a	Activity
C	Molar concentration
C_S	Sulphide capacity
C_D	Drag coefficient
D	Diffusivity
d	Diameter
e	Interaction parameter
f	Henrian activity coefficient
f	Fraction of solute extracted
f	Detector response factor
g	Acceleration due to gravity
K	Equilibrium constant
K	Toop and Samis 'Equilibrium constant' for silicate polymerisation
K_{11}	Masson 'Equilibrium constant' for silicate polymerisation
K'	Flood mixed equilibrium quotient
k	Mass transfer coefficient
m	Mass
N	Temkin anionic fraction
N'	Flood electrically equivalent ionic fraction
N_n	Ionic fraction of $Si_n O_{3n+1}^{2(n+1)-}$; Masson Models
n_i	Number of i species in slag
n	Molar rate of transport
O^-	Singly bonded oxygen
O^0	Double bonded oxygen
O^{2-}	Free oxygen anion

P Partial pressure

t Time

u Velocity

x Mole fraction

δ Fraction of droplet surface in contact with slag phase

ρ Density

σ Surface tension

μ Viscosity

SUBSCRIPTS

C	Carbon
Ca	Calcium
Ca ²⁺	Calcium cation
con	Pertaining to the continuous phase
d	Pertaining to droplets
Fe	Iron
Fe ²⁺	Iron cation
FeO	Ferrous oxide
i	At an interface
M ²⁺	Metal cation
Mg	Magnesium
Mn	Manganese
MO	Metal oxide
Na	Sodium
Na ⁺	Sodium cation
O	Oxygen
O ²⁻	Free oxygen anion
S	Sulphur
S ²⁻	Sulphur anion
Sl	Pertaining to the slag phase

SUPERSCRIPTS

b Within the bulk of the phase
i At an interface

DIMENSIONLESS GROUPS

Gr Grashof Number
Re Reynolds Number
Sc Schmidt Number
Sh Sherwood Number
We Weber Number

[] Pertaining to metal phase
() Pertaining to slag phase
{ } Pertaining to gaseous phase

CONTENTS

List of symbols, subscripts and superscripts

	Page
<u>CHAPTER ONE</u> <u>INTRODUCTION</u>	1
<u>CHAPTER TWO</u> <u>LITERATURE REVIEW</u>	5
2.1 LD Steelmaking	5
2.1.1 Introduction	5
2.1.2 Decarburisation in the LD process	8
2.1.3 Foams, emulsions and slag formation	10
2.1.4 Desulphurisation in the LD process	13
2.2 Desulphurisation as a Metal to Slag Reaction	18
2.2.1 Introduction	18
2.2.2 Experimental interpretation of sulphur transfer	18
2.2.3 Ionic slag theories	22
2.2.3(a) The Temkin Model	22
2.2.3(b) The Flood Model	24
2.3 Thermodynamics and Constitution of Silicate Melts	28
2.3.1 The classical theory of silicate melts	28
2.3.2 Thermodynamic models of silicate melts	31
2.3.2(a) The Toop and Samis Model	31
2.3.2(b) The Models of Masson	34
2.3.3 Constitution of silicate melts	39
2.3.3(a) Practical attempts to determine silicate melt structures	39
2.3.3(b) The trimethylsilylation of silicates	41
2.4 Single Droplet Studies of Slag-Metal Reaction Systems	48

2.4.1	Hydrodynamic behaviour of falling droplets	48
2.4.2	Mass transfer models	49
2.4.3	Surface phenomena	51
2.4.4	The refining of single droplets	52
<u>CHAPTER THREE</u> EXPERIMENTAL PROCEDURE		59
3.1	Preliminary Single Droplet Work	59
3.1.1	Introduction	59
3.1.2	Low temperature droplet model	60
	3.1.2(a) Components	60
	3.1.2(b) Droplet production	60
	3.1.2(c) Information from the low temperature model	61
3.1.3	Iron-Carbon-Sulphur droplet trial	61
	3.1.3(a) Stopper and seat components	61
	3.1.3(b) Stopper and seat arrangement	62
	3.1.3(c) Furnace used for the droplet trial	63
	3.1.3(d) Production of droplets	64
	3.1.3(e) Photography of droplets	64
	3.1.3(f) Implications of the preliminary work	65
3.2	Experimental Apparatus and Procedures for Droplet Experiments	67
3.2.1	Metal melt preparation	67
	3.2.1(a) Melting procedure	67
	3.2.1(b) Pin sample preparation for experiments	67
	3.2.1(c) High sulphur melts	68
3.2.2	Synthetic slag preparation	69

3.2.3	Crucible preparation	70
	3.2.3(a) Selection of crucible	70
	3.2.3(b) Preparation and coating of crucibles	71
3.2.4	Furnace used for droplet experiments	72
3.2.5	The stopper and seat technique	73
	3.2.5(a) Stopper and seat components	73
	3.2.5(b) Stopper and seat assembly	74
	3.2.5(c) Droplet production procedure	76
	3.2.5(d) Quenching and droplet collection	77
	3.2.5(e) Examination of crucibles	77
3.2.6	The suspended droplet technique	79
	3.2.6(a) Suspended droplet experiment equipment	79
	3.2.6(b) Suspended droplet experimental procedure	79
	3.2.6(c) Droplet analysis	81
	3.2.6(d) Droplet and platinum examination	82
3.3	Trimethylsilylation - GLC; Apparatus and Procedures	83
3.3.1	Materials	83
	3.3.1(a) Silicate materials	83
	3.3.1(b) Reagents	83
3.3.2	Trimethylchlorosilane purification	84
3.3.3	Trimethylsilyl derivative preparation	85
	3.3.3(a) The Lentz technique	85
	3.3.3(b) The Masson technique	86
	3.3.3(c) Internal standard	86
3.3.4	Gas liquid chromatography	87

3.3.4(a)	Principles of chromatography	87
3.3.4(b)	The gas liquid chromatograph	88
3.3.4(c)	Operating conditions	90
<u>CHAPTER FOUR</u>	RESULTS	92
4.1	Droplet Experiments	92
4.1.1	The determination of the initial composition of the metal droplets	92
4.1.2	The stopper and seat technique	95
4.1.2(a)	Desulphurisation results	95
4.1.2(b)	Decarburisation results	99
4.1.2(c)	Condition of reacted droplets	99
4.1.2(d)	Slag-crucible examination	103
4.1.2(e)	Reacted slag analyses	105
4.1.3	The suspended droplet technique	106
4.1.3(a)	Desulphurisation results	106
4.1.3(b)	Decarburisation results	114
4.1.3(c)	Condition of reacted droplets	116
4.1.3(d)	Droplet metal-Pt wire examination	119
4.1.3(e)	Reacted slag analyses	119
4.2	Trimethylsilylation - GLC Experiments	121
4.2.1	Treatment of results	121
4.2.2	The Lentz technique	123
4.2.3	The Masson technique	125
4.2.3(a)	"Blank samples"	125
4.2.3(b)	Minerals	126
4.2.3(c)	Industrial slags	130
4.2.3(d)	Synthetic slags	131

	4.2.3(e) PbO-Al ₂ O ₃ -SiO ₂ slags	132
	4.2.3(f) Silica samples	134
<u>CHAPTER FIVE</u>	DISCUSSION	135
5.1	The Determination of Anionic Constitution in Silicate Materials	135
5.1.1	The trimethylsilylation of silicate minerals	135
5.1.2	The trimethylsilylation of industrial slags	139
5.1.3	The trimethylsilylation of synthetic slags	142
5.1.4	Summary of trimethylsilylation studies	148
5.2	The Decarburisation of Single Iron-Carbon Droplets	150
5.2.1	The effect of decarburisation on the physical properties of metal droplets	150
5.2.2	The identification of the decarburisation mechanisms operative during droplet-slag interaction	153
5.2.3	Explanation of the observed variation in decarburisation performance	158
5.2.4	Summary of the decarburisation process with respect to factors influencing slag-metal sulphur equilibria	161
	5.2.4(a) Conditions imposed by continuous phase control	162
	5.2.4(b) Conditions imposed by dispersed phase control	162
5.3	The Desulphurisation of Single Iron-Carbon-Sulphur Droplets	163
5.3.1	A hypothetical scenario for desulphurisation	163
	5.3.1(a) Conditions imposed during continuous phase controlled decarburisation	164

5.3.1(b)	Conditions imposed during dispersed phase controlled decarburisation	166
5.3.2	An appraisal of the observed desulphurisation behaviour	169
5.3.2(a)	Reactions involving slag KC1 (38.06 mass % CaO-30.88 mass % FeO -30.80 mass % SiO ₂ -0.27 mass % S)	169
5.3.2(b)	Reactions involving slag KC2 (27.67 mass % CaO-44.01 mass % FeO -28.17 mass % SiO ₂ -0.15 mass % S), KC3 (16.57 mass % CaO-55.08 mass % FeO-28.26 mass % SiO ₂ -0.09 mass % S), KC4 (10.21 mass % CaO-61.78 mass % FeO-27.69 mass % SiO ₂ -0.32 mass % S) and KC5 (0.86 mass % CaO-65.30 mass % FeO-33.54 mass % SiO ₂ -0.30 mass % S)	177
5.3.2(c)	Reactions involving slag KC6 (71.87 mass % FeO-27.81 mass % SiO ₂ -0.32 mass % S)	179
5.3.3	The prediction of slag-metal sulphur equilibria for the experimental conditions	181
5.3.3(a)	Application of the slag models	182
5.3.3(b)	An assessment of the predicted equilibrium sulphur concentrations of droplets	185
5.3.4	The applicability of mass transfer models to the results of the desulphurisation experiments	187
5.3.5	The applicability of the experimental results to LD steelmaking	198
<u>CHAPTER SIX</u>	CONCLUSIONS	203
<u>CHAPTER SEVEN</u>	SUGGESTIONS FOR FURTHER WORK	206
References		210
Tables		220
Figures		306
Plates		378
Appendix		A1

1. INTRODUCTION

The deleterious effects of sulphur in steel have stimulated a great deal of research into desulphurisation. Present day demands for low sulphur specifications create a need to investigate sulphur transfer based on oxygen steelmaking methods such as the LD process.

Many of the previous laboratory investigations into desulphurisation have employed graphite crucibles to contain quiescent layers of carbon-saturated iron and slag compositions omitting FeO. This has been necessary in order to overcome the problems of containing slags at high temperatures. Such systems have, however, borne a closer resemblance to iron blast furnace conditions than those encountered in LD steelmaking. There is clearly scope for the development of an experimental technique that can generate desulphurisation data based on conditions closer to oxygen steelmaking than previously employed. Such a technique must incorporate the use of CaO-FeO-SiO₂ slags to represent slag compositions produced in the LD process. Further, the metal phase composition to be desulphurised needs to include carbon so that decarburisation is occurring during metal-slag reaction. The ability to allow interaction between an iron-carbon-sulphur melt, in the form of a single droplet, and a slag phase is of particular significance as it provides a simple model of the droplet refining regime believed to exist in LD steelmaking.

The presence of SiO₂ in LD slags is of special interest as this component is considered detrimental to desulphurisation due

to the strong affinity of silicon for oxygen reducing the "free" oxygen anions. The slag models of Temkin and Flood have been reasonably successful in predicting slag-metal sulphur equilibria but are valid for basic slags only. In addition, SiO_2 is assumed to exist solely as the SiO_4^{4-} anion. These models are obviously restricted in use and do not accommodate the possibility of silicate polymerisation taking place in slag compositions in the basic slag region. Silicate polymerisation is believed to result in the formation of free oxygen anions and it is likely that such species exist in acid slag compositions. The involvement of free oxygen anions in silicate polymerisation and sulphur transfer processes suggests that the anionic constitution of a silicate slag has a major influence on sulphur equilibria. The Temkin and Flood Models cannot account for the possible effects of silicate polymerisation.

Newer silicate slag models have been proposed which consider silicate polymerisation and can be incorporated into the prediction of sulphur equilibria. These models are at present limited to binary metal oxide-silica systems but they suggest that, for a given SiO_2 concentration, greater silicate polymerisation and hence free oxygen anion concentration exists in the FeO-SiO_2 system compared with CaO-SiO_2 slags. The implication in slags containing silica, therefore, is that FeO can produce a higher free oxygen anion concentration than CaO and may be of greater benefit to sulphur removal.

To elucidate the effects of slag constitution on desulphurisation the current slag models need to be tested and

and developed beyond binary compositions. A great impediment in the assessment of silicate slag models is the inability to directly identify and evaluate the anionic constitution of a slag. However, novel techniques such as trimethylsilylation coupled with Gas Liquid Chromatography and Mass Spectrometry have become available which have allowed silicate species present in minerals and slags to be identified. The application of such techniques to simple synthetic slags provides an opportunity to further our understanding of silicate anion constitution in slags.

In view of the above factors, the present investigation was initiated with the aim of examining both sulphur transfer under conditions resembling LD steelmaking and the effect of slag composition on anionic constitution. These objectives were pursued by:-

1. Use of high temperature experimental techniques to investigate sulphur transfer during the decarburisation of single iron-carbon-sulphur droplets with liquid synthetic slags.
2. Investigation of trimethylsilylation techniques previously applied to silicate minerals of known structure with subsequent development of such techniques for the determination of the constitution of anions in steelmaking slags. Initially, such investigations were employed to study desulphurisation by utilising simple binary and ternary synthetic slags. It was believed that the use of similar slags for the droplet experiments and trimethylsilylation investigation would be useful in

explaining the effect of slag constitution on observed sulphur removal.

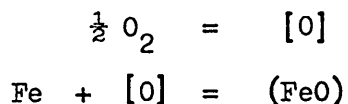
2.1 LD STEELMAKING

2.1.1 Introduction

The Linz-Donawitz (LD) steelmaking process was developed during the early 1950's. In 1983 basic oxygen steelmaking processes accounted for 67% of World steel output ¹. General reviews of LD steelmaking and other oxygen steelmaking processes are available in the literature ^{2, 3, 4, 5} and, therefore, it is proposed to confine the present review to those aspects of the process pertinent to this investigation.

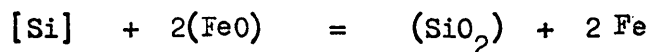
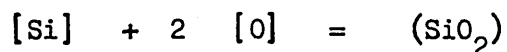
The process is characterised by the impingement of a jet of gaseous oxygen onto a bath of molten blast furnace metal and scrap contained in a converter vessel. Silicon, manganese, carbon and phosphorus are removed from the bath by an oxidation process, a basic slag also being a necessary requirement in order to achieve removal of phosphorus, and also sulphur. The shortness of the blow makes control of the process difficult and careful control of the composition of the charge is required. A suggested ideal hot metal analysis is 4.0 mass % C, 0.7-0.8 mass % Si, 0.7-0.8 mass % Mn, 0.01 mass % P max and 0.03 mass % S max ⁶.

Thermodynamic data for the reactions occurring in the LD are well documented and indicate that carbon, silicon and manganese should oxidise in preference to iron. The abundance of iron in the charge does, however, mean that the oxidation of these species often proceeds via the initial oxidation of iron ².



The theoretical order of removal of impurities as predicted by consideration of the equilibrium oxygen potentials at 1300°C is silicon, carbon, manganese ⁷. In LD steelmaking this sequence is not followed and the oxidation of different elements appears to be occurring simultaneously (Figure 1).

Silicon oxidises to form silica and is totally removed in about 6 to 7 minutes ³.



Similarly for manganese,

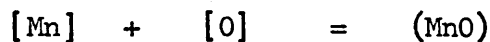


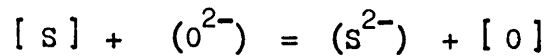
Figure 1 shows that the manganese content of the bath initially decreases but slight reversion occurs later in the blow. This has been attributed to two possible causes:

- (a) Melting of the scrap
- (b) Reduction of manganese oxide as a result of temperature changes and variations in slag composition which affect the activity of (MnO).

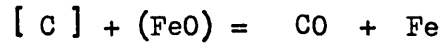
The oxidation of phosphorus in preference to iron requires that the activity of P_2O_5 in the slag be significantly lowered. This is achieved by using a highly basic slag.



Sulphur removal is favoured by reducing conditions and the presence of a highly basic slag.



The principal refining reaction is the removal of carbon as carbon monoxide.



The equilibrium relationship between the carbon and oxygen in the metal is well established. In the LD process, the oxygen concentration in the metal bath during the early stages of the blow reaches values in excess of that in equilibrium with the carbon present. As carbon is removed, the oxygen concentration in the metal approaches that at equilibrium with the carbon present, becoming close at less than 0.5 mass % C⁷.

Figure 2 is a typical decarburisation rate curve for the LD process showing that carbon removal exhibits three distinct phases. This is further illustrated in the idealised decarburisation rate curve shown in Figure 3. In stage one the decarburisation rate increases until a steady value is reached. This stage is related to slag formation since the plateau is attained more rapidly if a preformed slag is retained from the previous heat⁸. The second stage, a period of relatively steady decarburisation rate, although as shown in Figure 2 quite abrupt fluctuations can occur⁸, is believed to be controlled by the rate of introduction of oxygen into the system. The final stage shows a decrease in the decarburisation rate due to carbon transport control in the metal phase becoming rate controlling. Carbon transport control becomes dominant at compositions ranging from 1.2 to 0.2 mass % C⁹.

The decarburisation path may vary from cast to cast even for apparently identical conditions and this has also been observed when blowing onto simple iron-carbon melts ¹⁰. The process is metastable and much controversy surrounds the decarburisation mechanism.

2.1.2 Decarburisation in the LD Process

Early explanations for the rapid refining rates in the LD process were based on the presence of a localised high temperature region where the oxygen jet impinged on the metal bath ^{11, 12}. Criticisms arose due to the difficulty in reconciling the high refining rates with such a localised reaction site. Evidence by Meyer ^{8, 13} and Trentini ¹⁴, that the presence of a slag-metal emulsion in the converter may lead to large surface areas available for reaction, has provided a widely accepted explanation for the rapid refining rates.

Meyer working on a 230t LD converter and Trentini on an LDAC plant noted the presence of metal droplets in slag ejected from the converter. Meyer collected samples of taphole ejections on a metal tray positioned on the steelplant floor. It was estimated that 30% of the metallic charge could be dispersed in the slag. Determination of droplet sizes showed a size range from 3.4mm to less than 0.15mm diameter with 1.2mm to 0.6mm diameters being the most abundant. For a 230t converter the results suggested a very large specific surface area available for reaction, approaching 50,000m².

The droplets were of lower carbon content and impurity

levels compared with the bulk metal. The absence of very low carbon content droplets suggested that the supply of oxygen was rate controlling. Meyer considered that carbon transport control became effective when the carbon concentration in the bulk bath dropped to about 0.35 mass %. At the height of refining it was believed that up to two thirds of the total carbon present was removed via the emulsion.

The mechanism proposed by Meyer for decarburisation involved the unsteady state transfer of oxygen from the slag to the droplets surrounded by the carbon monoxide-slag foam. If the droplet was not contacted by a carbon monoxide bubble for some time then a high degree of supersaturation could be achieved with respect to the carbon-oxygen equilibria. Later work by Hazeldean has, however, shown that nucleation of CO bubbles from iron droplets is not as difficult as once thought ¹⁵.

A criticism which has been levelled at Meyer's work is that ejected samples are not typical of conditions inside the converter throughout most of the blow ². Sampling within the converter, involving the solidification of slag-metal emulsion on a chain attached to a weighted sample mould, was used by Price ¹⁶. For reasons of safety samples could only be taken during the second half of the blow which imposes limitations on the conclusions that can be drawn from the work. It was estimated that the maximum amount of metallic charge emulsified at any one time during the later stages of the blow was 15%. One third of the carbon initially present was considered to be removed in the emulsion whilst droplet sizes were predominately in the range of 1 to 2mm

diameter. The possibility that the technique may have underestimated the number of dispersed droplets has been expressed².

Results from experiments on a 6 tonne converter covering the maximum decarburisation rate period and with the bath deslagged prior to droplet sampling showed that droplets ejected from the melt by the impinging oxygen jet contained less carbon than that in the bulk bath¹⁷. It was suggested that 35-40% decarburisation was due to oxidation of droplets above the bath, thus raising doubts about the necessity of the emulsion. However, the necessity of having a fluid, basic slag was acknowledged in order to provide conditions conducive to sulphur and phosphorus removal.

Despite these reservations, the large surface area created by the dispersion of metal droplets in the slag and/or gaseous atmosphere above the bath still provides us with the most likely explanation for the fast refining rates encountered in the LD process. Meyer's work has identified the presence of foams and emulsions inside the converter with the resultant creation of large surface areas available for reaction.

2.1.3 Foams, Emulsions and Slag Formation

Extensive reviews of steelmaking foams and emulsions have been presented by Kozakevitch^{18, 19}.

The regime encountered in LD steelmaking is that of a continuous slag phase with dispersed phases comprising CO bubbles, solid oxide particles and metal droplets. The foam is dynamic in that its stability is dependent upon the continued evolution of

CO from the dispersed droplets and to a lesser extent from the bulk bath. Any significant reduction in the rate of CO evolution will cause the foam to collapse¹⁸.

The presence of metal droplets in the slag is primarily due to the action of the oxygen jet on the bulk metal bath¹⁹. Nucleation of CO bubbles within metal droplets may cause ejection of metal particles thus providing secondary emulsification¹⁵.

Although the slag-metal-gas emulsions in LD steelmaking are dynamic some stabilisation mechanisms have been proposed^{18, 19}. A high viscosity continuous phase will tend to encourage foam/emulsion stabilisation. The presence of long, complex anions is known to significantly increase slag viscosity²⁰. This mechanism appears unlikely to be important in the LD process where basic slags are used except possibly during the early stages of the blow when low slag temperatures and high silica contents prevail. The apparent viscosity of the slag may be increased by the presence of a dispersion of fine solid particles, which further encourage foam stabilisation by sticking to the surface of bubbles and inhibiting their coalescence.

Slag-metal-gas systems have relatively high interfacial energies and hence, due to their large surface area, foams and emulsions in steelmaking tend to be unstable. The adsorption of surface active solutes at interfaces may assist stabilisation by lowering the interfacial energy. The decay time for foams created in various CaO-SiO₂ melts has been shown to be relatively short²⁰. The addition of P₂O₅, which is surface active, improved stability only when the SiO₂ content exceeded 50 mole %, implying

that adsorption phenomena do not significantly contribute to foam stabilisation in LD slags except possibly in the early stages of the blow.

The evolution of the slag phase throughout the blow will influence the progress of refining. A complex mixture of oxides, sulphides and halide fluxes make up the slag, with no single component present in sufficient quantity to be considered the solvent. The early slag is rich in SiO_2 , FeO and MnO ^{16, 21}. The high silica content helps to flux lime introduced at the start of the blow, although there is a tendency to form a shell of dicalcium silicate around the lime particles which subsequently inhibits dissolution. Fluorspar additions may be introduced to aid dissolution. The use of dolomitic lime has become a feature of slag practice in recent years in an effort to increase lining life²².

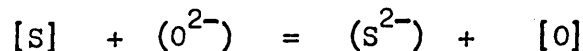
The principal oxides present in the LD slag are CaO , FeO and SiO_2 and the 1600°C isotherm of the CaO-FeO-SiO_2 ternary diagram has been used to identify the liquid phase fields²³ (Figure 4). Bardenheuer²⁴ has argued that the other oxides in the slag will increase the area of the liquid phase fields and has suggested the use of a pseudoternary $\text{CaO}'\text{-FeO}'\text{-SiO}_2'$ diagram where $\text{CaO} + \text{FeO} + \text{SiO}_2$ equals 80%. The pseudoternary diagram has been used to plot slag composition changes during the course of a blow (Figure 5)²⁵. The composition path indicated in Figure 5 shows the early siliceous slag initially increasing in iron oxide content with subsequent lime dissolution moving its composition towards the CaO' corner. The slag composition eventually enters

the (2CaO.SiO₂ + Liquid) phase field causing precipitation of 2CaO.SiO₂ crystals. This may cause slopping due to enhanced foam stabilisation associated with the resultant increase in the apparent viscosity of the slag. During the final stages of the blow an increase in the FeO content occurs as the decarburisation rate falls. Analysis of the Fe²⁺/Fe³⁺ ratio in slag samples suggests that the oxygen potential of the slag remains fairly constant through the middle portion of the blow¹³. The final FeO content of the slag is related to blowing parameters such as oxygen flow rate and lance height²⁶. Achieving the optimum slag composition path and hence control of a foam, may become an operational problem with the extremes being either slopping or production of a dry slag with poor sulphur and possibly phosphorus removal³.

Slag temperature rises rapidly during the first few minutes of blowing and can be 300°C above the metal temperature reflecting the extent to which refining is taking place as a droplet dispersion within the slag phase. The bath temperature rises gradually to reduce the difference to about 50°C on tapping²⁴.

2.1.4 Desulphurisation in the LD Process

Sulphur exists as sulphide ions in oxide melts where the partial pressure of oxygen is below 10⁻⁵ atmospheres and as sulphate ions for partial pressures greater than 10⁻³ atmospheres²⁷. For steelmaking conditions the sulphur in the slag is usually considered to exist as sulphide ions⁵. The sulphur transfer equation is



Sulphur removal is favoured by high oxygen anion concentration in the slag and high activity coefficient of sulphur in the metal. Carbon, silicon and phosphorus raise the activity coefficient of sulphur in iron ⁷ but as the blow proceeds and metalloids content is decreased, this effect will diminish. Sulphur transfer is accompanied by an increase in the metal oxygen content which inhibits the removal of sulphur. As the carbon content of the metal decreases the carbon-oxygen equilibrium will allow greater oxygen contents in the metal and sulphur reversion may occur ^{7, 28}.

The possibility of a gaseous desulphurisation mechanism occurring via the slag phase has been considered. It has been suggested that about 8% of the total sulphur charged is removed in this manner, slag-metal reaction playing the dominant role ^{29,30}.

Published work on sulphur removal in the LD process is in general agreement about the beneficial effect of lime and the need to achieve rapid dissolution ^{16, 30}. Conflicting evidence exists as to the effect of dolomitic lime on desulphurisation and more data is clearly required ^{31, 32}.

Work on a 90t converter showed that the bath sulphur level during the blow was virtually constant or increased slightly until the last few minutes of the blow ¹⁶. It was suggested that sulphur removal could occur without an emulsion provided the slag was sufficiently basic. A possible mechanism proposed for desulphurisation involved the dispersion of slag globules in the metal bath (an inverted emulsion) with bulk metal-

slag interface desulphurisation also contributing. The importance of the slag-bath interface as a site for desulphurisation has been emphasised by Nilles and Dauby²⁹ who point out that the high oxygen potential at the metal droplet-slag interface in the emulsion may inhibit sulphur transfer.

Russian workers³³ found that sulphur removal occurred during the initial 10 minutes of the blow followed by reversion to 15 minutes and resumption of desulphurisation until turndown. The possibility of scrap dissolution causing re-sulphurisation was mentioned but not discussed. An explanation based on free energy data and involving simultaneous reaction of manganese with oxygen and sulphur was proposed. When most of the manganese had been oxidised then sulphur removal could be retarded. Resulphurisation was associated with dry slag formation and as the blow continued, increase in bath temperature aided lime dissolution and promoted desulphurisation.

Yoshii and Ichinohe³⁰ have reported that about 50% of the total sulphur charged to the converter remained in the steel and in order to produce low sulphur steel a decrease of sulphur charged to the vessel was required.

Unlike carbon input which to a large extent is dependent on blast furnace practice, sulphur may be introduced from a number of sources. Ward has discussed the steelmaker's need for receiving hot metal of consistent analysis⁶. Up to 80% of sulphur in the blast furnace - LD process route is derived from coke but the attainment of low sulphur hot metal compositions

direct from the blast furnace incurs high ironmaking costs as shown in Figure 6 and Table 1^{6, 34}. Sulphur input to the vessel derived from scrap is difficult to quantify and practical difficulties in segregating low sulphur scrap can occur³⁴. The production and quality of lime for oxygen steelmaking has been discussed^{35, 36}. The use of extremely low sulphur content lime is not considered to be practically beneficial since it has been shown that an increase in lime sulphur content from 0.05 to 0.1% S contributes less than 0.001% increase to the final steel sulphur.

Desulphurisation performance in the LD is adversely affected by blast furnace slag being carried over into the vessel,^{6, 34} this being a source of both sulphur and acid slag components (Figure 7). Hot metal is usually delivered from the blast furnaces to the LD plant in torpedo shape containers and then transferred to a 'transfer ladle' for charging to the LD vessel. Reduced slag carry over may be achieved by discharging hot metal from the 'torpedo' car through a taphole³⁷ at the side of the vessel as opposed to the mouth positioned at the vessel top. In addition, benefits are gained by mechanically scraping slag off the surface of hot metal when contained in the transfer ladle. The introduction of nitrogen to the metal via the base of the ladle causing circulation of the metal can enhance this slag rabbling operation³⁸.

Many steelworks have introduced the practice of hot metal desulphurisation prior to charging to the converter. The use of a low flux blast furnace operation followed by external desulphurisation can be technically and economically favourable³⁹.

External desulphurisation agents include magnesium-impregnated coke ³⁹, calcium carbide ⁴⁰ and lime-magnesium mixtures ⁴¹.

Materials for desulphurisation by hot metal injection have been reviewed by Koros and Petrushka ⁴².

Conditions in the LD process are not favourable for desulphurisation. Data obtained from LD plants have not produced a coherent explanation of sulphur transfer mechanisms in the converter. Clearly, there is scope for a fundamental study of the desulphurisation behaviour of iron-carbon melts under oxidising slags. The investigation of sulphur removal from an iron-carbon droplet during decarburisation by reaction with a simple slag provides a logical starting point. Greater understanding of desulphurisation under oxidising conditions could assist in achieving optimum operating practice on LD plants with respect to sulphur removal and ultimately reduce the need, in some cases, for external desulphurisation.

2.2.1 Introduction

To evaluate the equilibrium distribution of sulphur between metal and slag requires knowledge of the reaction equilibrium constant and the relationship between the activity and the concentration of participating species. Equilibrium constants and thermodynamic data for iron base solutions are reasonably well documented. The main problem is lack of information about the activities of slag components and to overcome this, slag models have been developed which link slag composition with component activity.

In this section the experimental observations which have contributed to our understanding of sulphur transfer will firstly be described and then the application of ionic slag models to this problem will be considered.

2.2.2 Experimental Interpretation of Sulphur Transfer

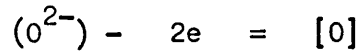
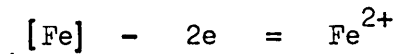
Early investigations indicated that the transfer of sulphur from the metal to the slag improved with increase in slag-metal interfacial area, slag basicity, temperature, sulphur content of the metal ^{43, 44, 45} and the presence of certain solute elements in the metal, such as carbon, silicon and phosphorus which increased the activity coefficient of sulphur ^{45, 46} (Figure 8). Many investigations into the solution thermodynamics of sulphur in liquid iron and iron alloys have been reported ^{47, 48, 49, 50}.

It is generally considered that the kinetics of slag-metal reactions at high temperature are controlled by mass transport processes ⁵¹. A number of workers have observed sulphur transfer to obey first order kinetics ^{43, 44, 52, 53, 54} with rate control being attributed to limiting diffusion of one of the reacting species across the boundary layer at the slag-metal interface ^{43, 44, 56}. Desulphurisation of liquid iron initially containing 1.62 and 0.64 mass % S by a CaO crucible has been described by radial diffusion of sulphur in the melt ⁵⁵. Sulphur removal from a 0.088 mass % S melt was achieved by CaO-saturated liquid iron oxide and gave enhanced reaction rates relative to diffusion predictions. Interfacial turbulence was considered as a possible reason.

Chemical reaction rate control was suggested by Ward and Salmon ⁵⁴ who studied desulphurisation with a range of CaO-MgO-SiO₂-Al₂O₃-CaF₂ slags. A mechanism for sulphur transfer, facilitated by silicon transfer from silicate anions to the metal leaving free oxygen anions at the slag-metal interface, was envisaged. The transfer of sulphur atoms across the interface with simultaneous transfer of metal atoms has been observed by other workers ^{44, 52, 53}. Sulphur transfer was considered as a partial electrochemical reaction with accompanying partial reactions required to maintain electroneutrality. The partial electrochemical equation for sulphur transfer becomes:-



Reactions to maintain electroneutrality could be:-



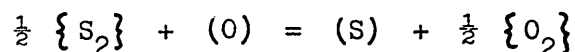
The rate of sulphur transfer is increased by the application of an electrical current (with the anode in the slag) but process efficiency is low, dismissing the possibility of industrial application⁵⁷. Electrochemical aspects of sulphur transfer and slag-metal reactions in general have been considered in the literature^{58, 59, 60, 61}.

The above observations have been based on the results of experiments involving quiescent slag-metal layers. In addition however, some information is available from the desulphurisation of dynamic metal droplets^{62, 63, 64, 65}. Carbon-saturated iron reacting with $\text{CaO-Al}_2\text{O}_3\text{-SiO}_2$ slags has been studied. Rate control by the convective mass transfer of sulphur in the slag was observed by Chon⁶² and Ishii⁶³. Other workers reported first order chemical kinetics and that free fall of the droplets through the slag precluded good desulphurisation because of insufficient reaction due to limited slag depth⁶⁴. Floating of the droplet was observed and provided a period of good desulphurisation believed to be related to an increase in slag-metal interfacial area⁶⁵. Sinking of the droplet was deemed to be related to FeO formation around the droplet. The slag compositions in these experiments are, however, not consistent with LD slags.

The effect of slag composition on the equilibrium sulphur distribution between liquid iron and slag has been investigated

by Rocca and co-workers⁶⁶. High slag basicity favoured sulphur removal, but the sulphur distribution ratio was decreased by increased FeO contents up to 1 mole %. This was attributed to the effect of FeO on the oxygen activity in the metal relative to the lesser and opposing effect it has upon the slag oxygen ion activity. With increasing FeO contents, at values greater than 1 mole % the oxygen activity in both the metal and the slag changed at similar rates and the sulphur distribution ratio became reasonably constant as shown in Figure 9. Fluorspar additions to slags have been found to increase the rate of sulphur transfer but not alter the slag-metal sulphur distribution ratio^{7, 67}.

The ability of a slag to hold sulphur has been defined in terms of its sulphide capacity, C_s ²⁷. For the equilibrium:-



$$K = \frac{(a_S) P_{O_2}^{\frac{1}{2}}}{(a_O) P_{S_2}^{\frac{1}{2}}}$$

assuming $(a_O) = \text{constant}$,

$$C_S = \frac{(\text{mass \% S}) P_{O_2}^{\frac{1}{2}}}{P_{S_2}^{\frac{1}{2}}}$$

The sulphide capacity was developed in relation to open hearth steelmaking conditions where a sulphur containing furnace atmosphere was present. The application of sulphide capacity to

sulphur removal in LD steelmaking is inappropriate and the use of slag models to predict sulphur distribution represents a more pertinent approach in assessing the effect of slag composition.

2.2.3 Ionic Slag Theories

The ionic nature of slags is now widely accepted. Early ionic slag models were proposed by Herasymenko⁶⁸ and Herasymenko and Speight⁶⁹ but the most successful models are those of Temkin⁷⁰ and Flood⁷¹.

(a) The Temkin Model

The principal features of the Temkin Model developed for basic slags are as follows:-

1. Molten slags were assumed to be ideal ionic solutions in which all like-charged ions exhibit the same interaction with nearest neighbours.
2. Ions existed separately on interpenetrating, independent cation and anion lattices, on each of which the ions of appropriate sign were randomly arranged.
3. Nearest neighbour ions were of opposite charge since due to repulsive forces between ions of like charge a cation could not replace an anion in a particular lattice site.

The entropy of mixing of cations or anions was determined

relative to the total respective amount of cations or anions assuming no cation-anion interaction. Temkin ionic fractions were defined for an oxide MO as:-

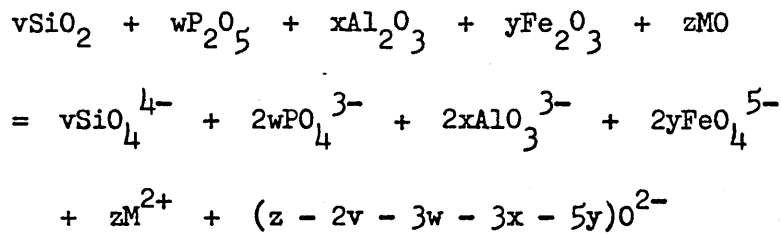
$$N_{M^{2+}} = \frac{n_{M^{2+}}}{\sum n_{\text{cations}}} \quad N_{O^{2-}} = \frac{n_{O^{2-}}}{\sum n_{\text{anions}}}$$

where $n_{M^{2+}}$, $n_{O^{2-}}$ = No. of M^{2+} and O^{2-} species respectively.

By combining the entropy of mixing terms for the cation and anion species, and obtaining an expression for the free energy of mixing, Temkin showed that the activity of, for example, a basic oxide in the slag could be defined by:-

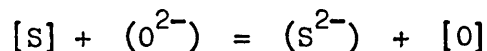
$$a_{MO} = N_{M^{2+}} \times N_{O^{2-}}$$

Temkin proposed that species such as Al, P and Si existed in basic slags as anions. A dissociation scheme was suggested:-



The slag was defined as basic when $(z - 2v - 3w - 3x - 5y)$ was positive so that free oxygen ions were present in the slag.

Temkin and co-workers⁷² went on to consider the application of the model to the slag-metal sulphur equilibria:-



$$K = \frac{(S^{2-})_{[mass \% O]}}{(O^{2-})_{[mass \% S]}}$$

Examination of laboratory and works' data gave an approximately constant value of $K = 0.017$.

The model was unsuccessful, however, when applied to the interpretation of the slag-metal phosphorus distribution. This is because no consideration is made of the effect of different cations present in the melt and does not take account of the strong interaction that exists between Ca^{2+} and PO_4^{3-} ions.

The assumptions that Al exists as AlO_3^{3-} and Fe_2O_3 as FeO_4^{5-} are reasonable for strongly basic slags ⁷. However, the silica level is high in the early LD slags and this leads to another shortcoming of the Temkin Model in that silica is assumed to exist exclusively as SiO_4^{4-} in basic slags. It is currently believed that polymerisation of silicate anions may occur in basic slags, the degree of this increasing as the acid-base transition is approached ⁷³.

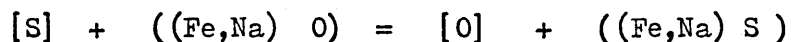
(b) The Flood Model

The Temkin model considered cations and anions as being replaceable by ions of like valency. However, the replacement of a cation by an anion is opposed by the repulsive forces from the anions surrounding the cation site and so purely random mixing is restricted. If a cation or anion is replaced by an ion of different valency then further restrictions are imposed

on purely random mixing. The substitution of a divalent cation for two monovalent cations (to maintain electro-neutrality) introduces a vacancy into the cation network. The entropy of the system increases giving rise to a different ionic fraction, known as the electrically equivalent ion fraction:-

$$N'_{B^{2+}} = \frac{2n_{B^{2+}}}{n_{A^+} + 2n_{B^{2+}} + 3n_{C^{3+}} + 4n_{D^{4+}} + \dots}$$

Flood and co-workers⁷¹ have used this type of ion fraction in addition to the Temkin anionic fraction in a model that considers the effect of the different cations present on slag-metal equilibria. The model permits the calculation of an equilibrium quotient for a complex slag by consideration of the equilibrium constants for simpler systems. Ward⁷⁴ has described the model by consideration of the desulphurisation reaction taking place via a simple mixed oxide slag (Figure 10):



The equilibrium quotient may be obtained from the free energy for the conversion of one mole of the mixed oxide to one mole of the mixed sulphide. Since the partial molar free energies of mixing of the sulphides and oxides of a common ion are similar the overall free energy change for the above reaction is given by:-

$$\Delta G_{Fe,Na} = N'_{Fe} \Delta G_{Fe} + N'_{Na} \Delta G_{Na}$$

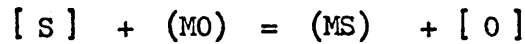
By substitution using the van't Hoff Isotherm,

$\Delta G^{\circ} = -RT \ln K$, an expression defining the mixed equilibrium quotient can be obtained:-

$$\log K' = N'_{Fe} \log K_{Fe} + N'_{Na} \log K_{Na}$$

where K_{Fe} and K_{Na} are the equilibrium constants for the reaction of sulphur with FeO and Na_2O respectively.

Assuming Henrian behaviour in the metal and utilising Temkin anionic fractions to describe activities in the slag, the equilibrium constant for the simple reaction,



may be written:-

$$K_M = \frac{(N_{M^{2+}}^{N_{S^{2-}}}) f_O^{[\text{mass \% O}]}}{(N_{M^{2+}}^{N_{O^{2-}}}) f_S^{[\text{mass \% S}]}} = \frac{(N_{S^{2-}}^{N_{O^{2-}}}) f_O^{[\text{mass \% O}]}}{(N_{O^{2-}}^{N_{S^{2-}}}) f_S^{[\text{mass \% S}]}}$$

The expression for the mixed equilibrium quotient may be described by an additive equation of the form:-

$$\log K' = \sum^i N' \log K_i + \sum^i (\gamma)$$

The first summation represents all the possible binary interchange reactions between the anion under consideration and a system of i species of cations. The term $\sum^i (\gamma)$ represents the activity coefficients in all the binary equilibria to account for the deviation from ideal ionic behaviour in the slag but is considered to cancel out, leaving only the first term of the equation 7.

Ward, using published data has presented the following expression for the mixed equilibrium quotient for the sulphur equilibria:-

$$\log K'_{1873} = -1.4N'_{Ca} - 1.9N'_{Fe} - 2.0N'_{Mn} - 3.5N'_{Mg}$$

The coefficients in the above expression representing the $\log K'_M$ terms may be used to compare the desulphurising abilities of the different cations relative to Ca^{2+} , as shown in Table 2. A coefficient for the Na^+ cation was included (+1.63) which suggested it was a powerful desulphuriser while the effect of Mg^{2+} was considered inferior to Ca^{2+} .

The Flood model was successful in the interpretation of both sulphur and phosphorus distribution. The development of the model has been the subject of recent debate ^{75, 76} but the principles employed have not fundamentally altered. The model in an adapted form has been used to estimate phosphorus equilibrium between liquid metal and basic slags at the end of refining hot metal with high and low phosphorus contents ⁷⁷.

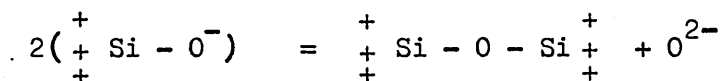
Despite the success of the Flood model and its ability to take account of the effect of the cations present in the slag, it does assume that only anions of the type O^{2-} , SiO_4^{4-} , AlO_3^{3-} ; PO_4^{3-} and FeO_4^{5-} exist in basic slags. The model is, therefore, not applicable to slag compositions where silicate polymerisation occurs.

2.3.1 The Classical Theory of Silicate Melts

In silica the silicon atom exhibits tetrahedral co-ordination with the oxygen atoms ^{7, 78}. The small size and high charge of the silicon cation provides a strong, mainly covalent bond with oxygen and precludes dissociation into simple ions in an oxide melt (Figure 11a). On melting it is supposed that almost all the oxygens remain shared but some regularity of the tetrahedral arrangement is lost as illustrated in Figure 11b.

Basic oxides such as CaO, FeO, MgO and MnO involve the respective cation in sixfold co-ordination with the oxygen in the ion lattice ⁷. Bonding is primarily electrovalent and dissociation into simple ionic species can occur in oxide melts.

The Network Theory postulated that the progressive addition of basic oxide to a silica melt results in oxygen anions breaking the Si-O-Si bridges between two tetrahedra. The added cations will, by charge effects, be located near these sites in holes in the structure as illustrated in Figure 12. Eventually, silicon is present only as discrete SiO_4^{4-} groups. Further basic oxide additions simply introduce more cations and anions into the melt. Thermal dissociation of silicate groups can occur and so oxygen anions can be present even in highly siliceous melts ⁷⁹:-

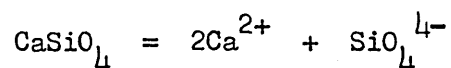


Viscosity - composition relationships for silicate melts have been used to provide structural interpretations⁸⁰. The first 10 to 15 mole % of basic oxide addition has the greatest effect in lowering the activation energy for viscous flow with subsequent additions having less effect on the viscosity of the melt as shown in Figure 13. The Network Theory was unable to explain this behaviour and a model involving the formation of discrete silicate ring ions was proposed^{81, 82}. The first 10 to 20 mole % basic oxide coincided with random breakdown of the silica network whilst retaining the three dimensional bonding in the melt. Cations were held in silicate cages as illustrated in Figure 14. Basic oxide additions from 12 to 50 mole % broke down the network to globular and ring ions of the type shown in Figure 15. The number of cations and ionic bonds associated with these ions varied little and explained the small change in the activation energy for viscous flow over this composition range. At greater than 50 mole % basic oxide the discrete ring anions degenerated into linear forms of progressively diminishing length until eventually only SiO_4^{4-} anions were present.

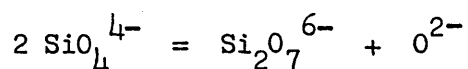
The Discrete Anion Model does not quantitatively account for the observed relative constancy of the partial molar volume of silica at compositions containing less than 33 mole % basic oxide. In addition there is no clear explanation for the immiscibility gap that occurs in some basic oxide-silica systems. This behaviour was explained in terms of the 'Iceberg' Theory of liquid silicates⁸³. The formation of silica rich regions, regarded as islets or icebergs, was believed to occur, separated

by thin films of liquid of $M_2O \cdot 2SiO_2$ composition in alkali-metal oxide-silica melts or $MO \cdot 2SiO_2$ composition in alkali earth metal oxide-silica melts. With increasing basic oxide in the range 12-33 mole % the size of the silica rich icebergs diminish until at 33 mole % they become indistinguishable from the discrete ring anions present at this composition.

The Discrete Anion and Iceberg Theories offer interpretations on silicate melt structures but the ion types suggested are based on simple stoichiometry with no account made of oxygen anions present due to thermal dissociation of silicate groups. Also, if the dissociation of the orthosilicate composition is considered to be represented by:-



then a zero activity for lime would be implied 74 . This contradicts the observed finite activity of lime in $CaO-SiO_2$ melts and so a polymerisation reaction of the following type is assumed:-



The inability of the classical theory to recognise different silicate polymers existing simultaneously in a given melt with the possibility of a significant oxygen anion concentration restricts the interpretation of the thermodynamics of silicate melts.

2.3.2 Thermodynamic Models of Silicate Melts

An early thermodynamic treatment of silicate melts was made by Toop and Samis⁸⁴. Later work by Masson et al applied the principles of polymer chemistry enabling a number of models to be developed. Statistical thermodynamic approaches have also been employed^{85, 86, 87, 88, 89} and reviewed by Gaskell⁹⁰. These models are complex and do not lead to simple analytical equations that can be directly applied to practical problems.

The work of Toop and Samis and Masson will be discussed but references should be consulted for details of the derivations of the respective models.

(a) The Toop and Samis Model

Toop and Samis used the concept of oxygen being able to exist in three different forms in silicate melts; doubly bonded (O^0), singly bonded (O^-) and free oxygen anions (O^{2-}).

The proposed equilibrium reaction was:-



An equilibrium constant K was defined that was assumed to be constant at constant temperature, characteristic of the cations present in any binary or ternary silicate melt and independent of composition:-

$$K = \frac{(O^0) (O^{2-})}{(O^-)^2} \quad 2.2$$

where (O) = moles of oxygen species per mole of slag.

Assuming that basic oxides are completely dissociated, to give one O^{2-} ion per molecule contributed, and that x_{SiO_2} moles of silica combine with $(1 - x_{SiO_2})$ moles of O^{2-} anions to form anions in one mole of melt, Toop and Samis showed from a charge balance:

$$2(O^{\circ}) + (O^{-}) = 4x_{SiO_2} = \text{No. of silicon bonds.}$$

The expression was rearranged to give the number of doubly bonded oxygen atoms in one mole of slag:-

$$(O^{\circ}) = \frac{4x_{SiO_2} - (O^{-})}{2} \quad 2.3$$

To obtain the number of free O^{2-} anions in the slag, a mass balance was used. x_{SiO_2} moles of silica combined with $(1 - x_{SiO_2})$ moles of oxygen to give $4x_{SiO_2}$ Si-O bonds, so,

$$\text{Final } (O^{2-}) = \text{No. of } (O^{2-}) \text{ initially} - \frac{1}{2} \text{ No. of } O^{-} \text{ formed.}$$

and hence

$$(O^{2-}) = (1 - x_{SiO_2}) - \frac{(O^{-})}{2} \quad 2.4$$

The terms for (O°) and (O^{2-}) given in 2.3 and 2.4 respectively were substituted into equation 2.2 to give:-

$$4K = \frac{[4x_{SiO_2} - (O^{-})][2 - 2x_{SiO_2} - (O^{-})]}{(O^{-})^2} \quad 2.5$$

A knowledge of the value of the equilibrium constant allows the above equation to be converted into quadratic form:-

$$a (O^-)^2 + b (O^-) + c = 0$$

Toop and Samis plotted the equilibrium concentrations of the oxygen types against silica composition for K equal to 0.06 and noted that the (O^-) curve resembled an integral free energy of mixing curve for a binary silicate melt.

By considering that 1 mole of oxygen ions (in pure liquid MO) reacts with 1 mole of doubly bonded oxygen atoms (in pure liquid SiO_2) forming 2 moles of singly bonded oxygen ions (pure liquid M_2SiO_4) then from consideration of equation 2.1 and use of the van't Hoff Isotherm, the standard free energy change (in calories) divided by $4.575T$ was written as:-

$$\frac{\Delta G^0}{4.575 T} = -\log \frac{1}{K} = \log K \quad 2.6$$

In general, the number of moles of (O^{2-}) reacting is equal to $\frac{1}{2} (O^-)$ per mole of liquid silicate formed so Toop and Samis considered that the free energy change due to equation 2.1 per mole of liquid silicate formed should be given approximately by:-

$$\frac{\Delta G^M}{4.575 T} = \frac{(O^-)}{2} \log K \quad 2.7$$

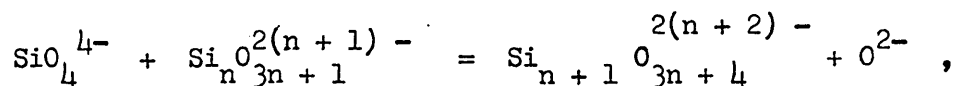
The above relationship was used to plot $\frac{\Delta G^M}{4.575 T}$ against x_{SiO_2} . Experimentally obtained values of ΔG^M for various systems were superimposed as shown in Figure 16. Similarity between calculated and experimental curves led Toop and Samis to suggest that the free energy of mixing for a binary silicate melt may arise entirely from the interaction of oxygen ions and

silica. The activity of the oxygen anions $a_{O^{2-}}$, was considered to be equal to the activity of the basic metal oxide in the expression for the binary integral molar free energy of mixing:-

$$(1 - x_{SiO_2}) \log a_{O^{2-}} + x_{SiO_2} \log a_{SiO_2} = \frac{\Delta G^M_{\text{binary}}}{4.575 T}$$

Thus, the effect of different cations in binary silicate melts would be to allow greater or less amounts of polymerisation and hence less or greater interaction between oxygen ions and silica. Toop and Samis proposed K values for various binary oxide-silica systems (Table 3).

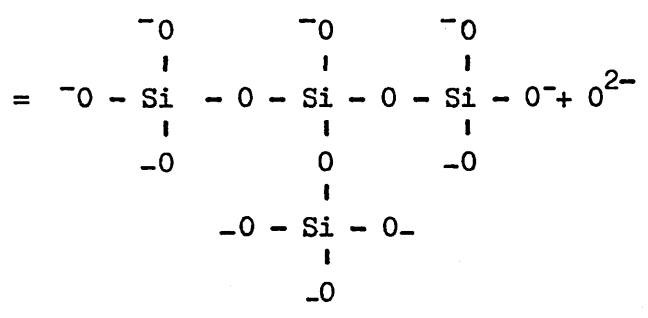
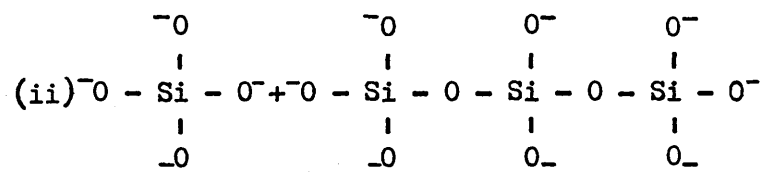
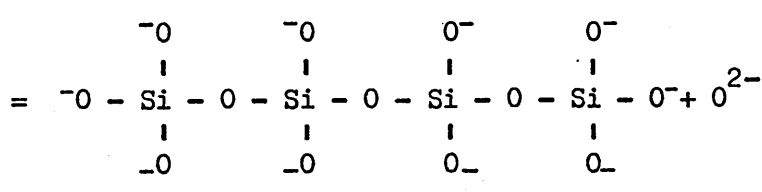
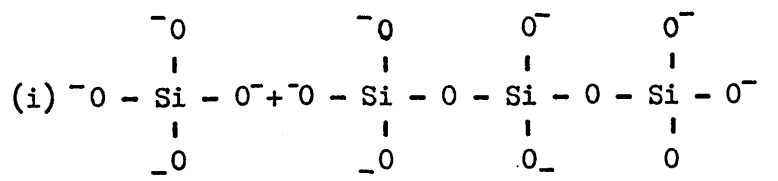
The model involves the assumption that K is independent of composition but this is incorrect because if it were, then for reactions of the type:-



K would be the same irrespective of chain length n.

(b) The Models of Masson

Masson⁹¹ initially considered the coefficient, K, used by Toop and Samis. From polymer theory the type of equilibrium ratio used by Toop and Samis would only be constant for cases where all polymer molecules have the same configuration. For the reactions:



there are two ways that reaction (i) may occur and three for reaction (ii). An equilibrium ratio $K_{1, n}$ will only be constant, regardless of chain length, for linear configurations.

Masson made three fundamental assumptions:-

1. Self-condensation of chains to yield ring structures or networks does not occur.
2. All functional groups are of equal reactivity. Thus,

all O^- groups are of equal reactivity regardless of the size of the polyion to which they are attached.

3. The activity of a component in the slag may be defined in terms of Temkin ionic fractions, i.e.

$$a_{MO} = N_{M^{2+}} \times N_{O^{2-}}$$

A model was formulated for linear chains only, in which Masson considered polycondensation reactions where SiO_4^{4-} could dimerise and then react with higher members of the silicate species. For a binary basic oxide-silica melt, the following expression was obtained:-

$$\frac{1}{x_{SiO_2}} = 2 + \frac{1}{(1 - a_{MO})} - \frac{1}{1 + a_{MO} \left(\frac{1}{K_{11}} - 1 \right)} \quad 2.8$$

which gives the activity of MO as a function of composition if K_{11} is known (Figure 17). The model gave some agreement with experimentally obtained activities of MO and enabled values of K_{11} to be designated to some binary MO- SiO_2 systems.

An expression was also derived to define the ionic fraction of a silicate species;

$$N_n = \left\{ \frac{1}{1 + \frac{a_{MO}}{K_{11} (1 - a_{MO})}} \right\}^{n-1} \left\{ \frac{1}{\frac{K_{11}}{a_{MO}} + \frac{1}{1 - a_{MO}}} \right\} \quad 2.9$$

where N_n is the ionic fraction of $Si_n O^{2(n+1)-}_{3n+1}$

and a_{MO} is given by equation 2.8.

Figure 18 shows the variation of the calculated ionic fraction of linear silicate anions of chain length $n = 1$ to $n = 6$ with mole fraction of SiO_2 for $\text{FeO} - \text{SiO}_2$ melts at $1257-1307^\circ\text{C}$.

Models based on polymer theory that pertain to branched chain configurations have been developed⁹². The three fundamental assumptions used previously were retained. The activity of MO was obtained from the following expressions:-

$$\frac{1}{x_{\text{SiO}_2}} = 2 + \frac{1}{(1 - a_{\text{MO}})} - \frac{3}{1 + a_{\text{MO}} \left(\frac{3}{K_{11}} - 1 \right)}, \quad 2.10$$

the resultant variation of a_{MO} with x_{SiO_2} being presented graphically in Figure 19.

The branched chain model gave good agreement with experimental data for the systems $\text{SnO}-\text{SiO}_2$, $\text{FeO}-\text{SiO}_2$, $\text{PbO}-\text{SiO}_2$ and $\text{MnO}-\text{SiO}_2$ with recent work further confirming agreement with the $\text{MnO}-\text{SiO}_2$ system⁹³. Figure 20 shows a comparison between experimental data for the $\text{CaO}-\text{SiO}_2$ system at 1600°C with the theoretical prediction for K equal to 0.0016. Table 4 records K_{11} for various systems.

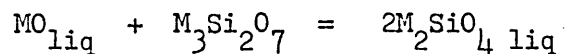
For branched chains the ionic fraction of a silicate species was given as:-

$$N_n = \frac{3n!}{(2n+1)!n!} \left\{ \frac{1}{1 + \frac{3a_{\text{MO}}}{K_{11}(1-a_{\text{MO}})}} \right\}^{n-1} \left\{ \frac{1}{1 + \frac{K_{11}(1-a_{\text{MO}})}{3a_{\text{MO}}}} \right\}^{2n+1} (1-a_{\text{MO}}) \quad 2.11$$

For the $\text{FeO}-\text{SiO}_2$ and $\text{CaO}-\text{SiO}_2$ systems (Figures 21, 22) the

SiO_4^{4-} anion is the most abundant species at all compositions up to $x_{\text{SiO}_2} = 0.5$. For the CaO-SiO₂ system the monomer is the sole species present below x_{SiO_2} equal to 0.3, but in the FeO-SiO₂ system longer chains exist at silica compositions below the orthosilicate composition.

Masson has suggested that the magnitude of the equilibrium constants K_{11} , K_{12} etc. provide a quantitative measure of polymerisation in binary silicate melts and that the tendency towards polymerisation is determined by the nature of the cation. The average chain length of a melt would, therefore, be governed by the difference in magnitude between cation-silicate and cation-oxygen ion attractions. Consequently, the extent of cation-oxygen attraction influences the degree of ionic bonding in silicon-oxygen linkages so that changes in bond strength can be reflected in standard free energies of formation of the various silicates from their constituent oxides. Masson showed that for the reaction:-



that,

$$RT \ln K_{11} = 2 \Delta G_{\text{ortho}}^{\circ} - \Delta G_{\text{pyro}}^{\circ}$$

This equation indicates that a tendency for polymerisation always exists in silicate melts because K_{11} may be small but can never be zero, unless the right hand side of the equation takes a value of minus infinity. Application of the equation is

limited as available thermodynamic data pertains to simple molecules thus restricting determination of K_{11} .

Criticisms of the Masson Models include doubts about the use of Temkin ionic fractions for a situation where different size silicate anions are present. Also, the linear chain model predicts zero MO activity at the metasilicate composition which is not observed experimentally⁸⁰. Since the development of the models, experimental evidence has indicated the existence of silicate rings in binary silicate melts and no provision has been made for this situation⁷³.

Application of polymer theory to ternary silicate melts incurs difficulties due to the competitive interactions between the anions and various cations. An attempt has been made to develop a model for a ternary silicate melt where a common cation exists, e.g. $\text{MO-MF}_2\text{-SiO}_2$ ⁹⁴. This work retained the assumptions of the previous models and although a new treatment was given to this type of melt, it served mainly to demonstrate the complexities of dealing with ternary systems.

2.3.3 Constitution of Silicate Melts

(a) Practical Attempts to Determine Silicate Melt Structures

At present, no technique has been found to directly observe and quantify the amounts of different silicate species in a melt. Workers have depended upon measurements of physical properties to provide structural interpretation of melts but the presence of immiscibility gaps in some systems can limit the

information obtainable.

Density measurements of CaO-FeO-SiO_2 melts have confirmed predictions ⁷³ that greater polymerisation occurs in iron silicate melts compared with calcium silicate melts and relates to the preferred association of Ca^{2+} cations with silicate anions thus releasing Fe^{2+} cations to associate with O^{2-} anions ⁹⁵, a phenomenon which increases the FeO activity in such melts ⁹⁶.

High temperature x-ray diffraction techniques, Raman spectroscopy and Mossbauer spectroscopy have all been used to examine silicate melts but no quantitative assessments of ionic distributions have been achieved ^{97, 98, 99, 100}. Mossbauer spectroscopy examinations of basic electric arc slags sampled during the oxygen blow has shown that Fe^{2+} cations can be present in a silicate phase or a 'mixed oxide' phase, the proportion taken up in the latter phase increasing with basicity ¹⁰¹. This tends to concur with Gaskell's comments on the preferred association of cations with silicate or oxygen anions ⁹⁶.

The distribution of silicate ions in a melt has been inferred from studies of phosphate glasses dissolved in water ⁸⁰. The dissolution technique cannot be applied to silicates as hydrolysis readily occurs in aqueous media producing indefinite polymers related to silica gel ¹⁰².

A technique has been developed where the blocking of O^- sites of the parent silicate structure of a mineral by

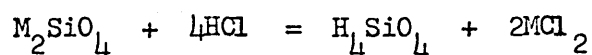
trimethylsilyl (TMS) groups, $(\text{CH}_3)_3\text{Si}-$, has been used to retain some of the original structure. Gas Liquid Chromatography (GLC) and Mass Spectrometry (MS) were used for respective separation and identification of the silicate derivatives ¹⁰³.

The trimethylsilylation of silicates is not always amenable to quantitative interpretation and attempts to improve this method by the formation of methyl and ethyl silicates has been unsuccessful ¹⁰². The trimethylsilylation of silicates has been developed by a number of workers and will be discussed in more detail.

(b) The Trimethylsilylation of Silicates

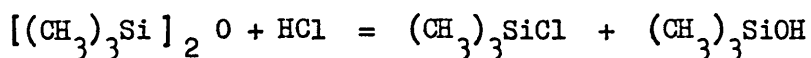
Trimethylsilylation is a pretreatment commonly applied to organic materials to improve their suitability for GLC analysis ¹⁰⁴. Inorganic anions other than silicates have been trimethylsilylated ^{105, 106}.

Lentz trimethylsilylated various silicate minerals using a reaction mixture of crushed ice, propan-2-ol, hexamethyldisiloxane and concentrated hydrochloric acid ¹⁰³. The process was completed by use of an ion exchange resin, Amberlyst 15. A proposed reaction scheme commenced with leaching of the metal cation portions of the mineral to produce metal chloride and silicic acid:-

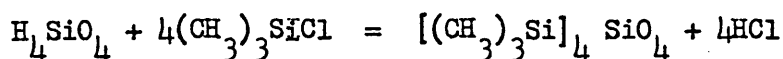


Interaction of HCl and hexamethyldisiloxane produced

trimethylchlorosilane (TMCS) and trimethylsilanol:



Either of the above products could be capable of reacting with silicic acid but Lentz considered trimethylchlorosilane and the trimethylsilylation reaction:-



where $[(\text{CH}_3)_3\text{Si}]_4\text{SiO}_4$ is the TMS derivative of the SiO_4^{4-} anion.

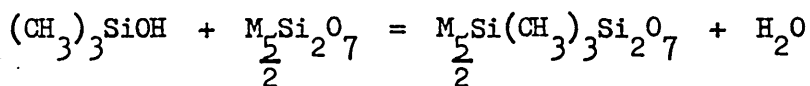
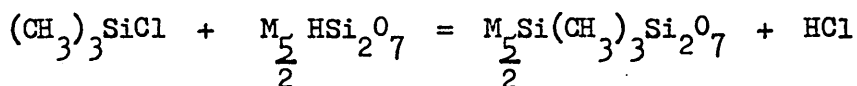
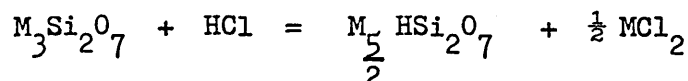
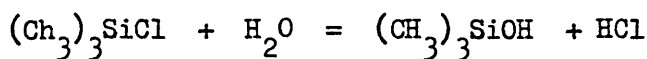
Unfortunately, side reactions can occur and have been attributed to polymerisation and depolymerisation reactions taking place during trimethylsilylation and by hydrolysis of the derivative itself ¹⁰⁷. Success of trimethylsilylation is related to both the type of metal cations ¹⁰⁸ and silicate anions present ¹⁰⁹. Leaching of the metal cation is undoubtedly influenced by the cation type present ^{110, 111} but the subject of acid attack on silicate minerals is still not fully understood ¹¹². The presence of certain cations such as iron was believed to aid leaching ¹¹² but increasing leachability by virtue of decreasing cation-oxygen bond strength for a given silicate group does not strictly confirm this ¹¹¹. Complex silicate structures may render cations inaccessible to acids and so retard leaching ^{111, 112}. For chain structures this appears to be of minimal importance ¹¹¹.

Trimethylsilylation of the mineral Natrolite, $\text{Na}_2\text{Al}_2\text{Si}_3\text{O}_{10} \cdot 2\text{H}_2\text{O}$, confirmed the presence of side reactions and

workers have published the chromatogram obtained ^{113, 114}

(Figure 23).

The development of 'direct' and 'unified' techniques based on reaction mixtures of hexamethyldisiloxane, trimethylchlorosilane, propan-2-ol and water followed by an Amberlyst 15 treatment have led to a reduction in side reactions ^{107, 108}. The direct technique produced excellent results for Hemimorphite $Zn_4(OH)_2Si_2O_7 \cdot 6H_2O$, with 97% of the chromatogram peak area due to the desired derivative ¹⁰⁷ and has been used to monitor the conversion of Hemimorphite to Willemite ($\alpha-ZnSiO_4$) ¹¹⁵. The success of this direct technique was attributed to the gradual leaching of the mineral by HCl formed from the reaction between trimethylchlorosilane and water followed by the almost instantaneous substitution of H groups by TMS groups:-

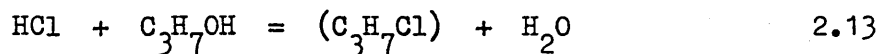
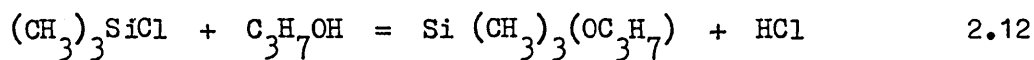


The method was not suitable for some anhydrous minerals and highly soluble silicates where it was found that water was required in the reaction mixture ^{108, 116, 117, 118}. The inclusion of water led to the technique described as the 'unified' method, which was claimed to be capable of reproducing silicate structures in the TMS derivatives with an

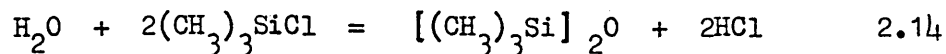
accuracy of 94% for the pyrosilicates and 82-88% for the orthosilicates. Despite some side reactions, the trimethylsilylation of mineral mixtures suggested that little anionic redistribution occurred during the reaction stir and the results were considered to be representative of the constitution of the original mixtures ¹¹⁹.

There is evidence that side reactions can result from Amberlyst 15 treatment particularly in minerals containing complex silicates ^{109, 120}. Work on Diopase, $\text{Cu}_6\text{Si}_6\text{O}_{18} \cdot 6\text{H}_2\text{O}$, produced a chromatogram with the desired derivative featured as three peaks corresponding to Si_6O_{18} ¹²⁻ isomers. Lengthy Amberlyst treatment interconverted the isomers.

A reaction scheme based on the direct and unified reaction mixtures has been proposed that also considers side reactions ¹⁰⁹. For the reaction mixture in the presence of a base, trimethylchlorosilane may react with propan-2-ol to produce HCl which itself may react with propan-2-ol:-

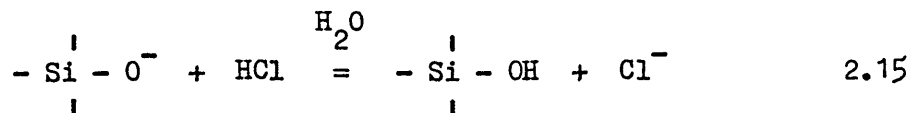


The water formed hydrolyses trimethylchlorosilane:-

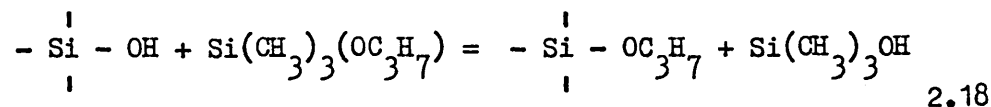
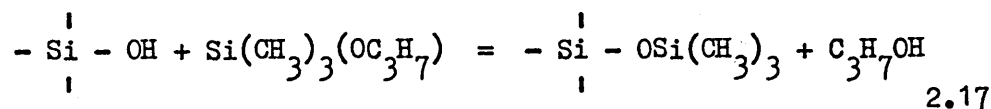
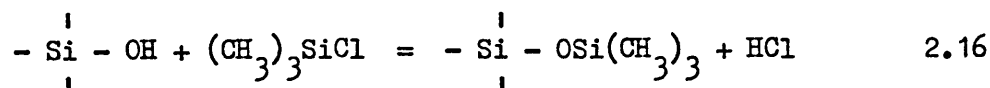


The O^- groups of the silicate portion of the mineral, say Ca_2SiO_4 , may be protonated by HCl in the presence of water to

give silicic acid groups:-

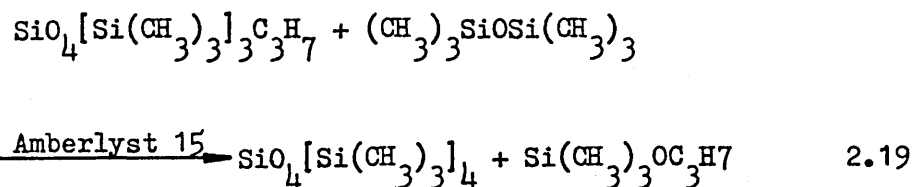


The silicic acid groups may react with trimethylchlorosilane and $\text{Si}(\text{CH}_3)_3\text{OC}_3\text{H}_7$ to yield various derivatives:-

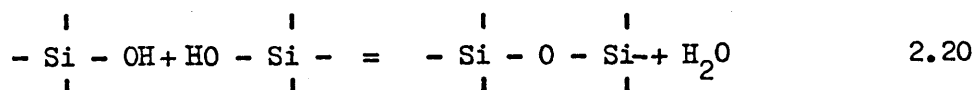


A subsequent array of mixed trimethylsilyl-isopropyl derivatives of general formula $\text{SiO}_4[(\text{CH}_3)_3]_x(\text{C}_3\text{H}_7)_{4-x}$, where x is 1 to 4 may be formed.

The replacement of isopropyl groups by TMS groups is catalysed by Amberlyst 15:-



The formation of higher anion derivatives by side reactions may be considered as the mutual interaction of silicic acids:-



Reaction 2.20 could compete with reactions 2.16, 2.17 and 2.18 and it was suggested that suppression of side reactions could be achieved by decreasing mineral concentration in 2.20 or by using excess propan-2-ol to increase the rates of reactions 2.17 and 2.18.

The use of the unified technique to identify silicate species in materials other than naturally occurring minerals has included work on PbO-SiO_2 ^{119, 121} and $\text{PbO-PbF}_2\text{-SiO}_2$ ¹²² melts. Results for the two melts were qualitatively in line with polymer theory predictions for the respective systems. For the simple PbO-SiO_2 melt, a small proportion of the Si_4O_{12} ⁸⁻ anion derivative was detected which is not accounted for by polymer theory.

For the metallurgist, the most interesting application of the unified technique must be the studies of open hearth and blast furnace slags¹²³ (Figures 24, 25). The most abundant silicate derivatives in both slag types were, in decreasing order, due to SiO_4 ⁴⁻, Si_2O_7 ⁶⁻, Si_3O_{10} ⁸⁻ and Si_4O_{12} ⁸⁻ anions, except for a slow cooled blast furnace slag where the Si_2O_7 ⁶⁻ anion derivative was predominant, although the presence of melilite type material (Si_2O_7 ⁶⁻ structure) was a possible explanation. The investigators did not establish whether other derivatives detected, which included ring structures up to nine silicon atoms, were representative of the slag structure or were side reaction products. It was clear, however, that trimethylchlorosilane required purification prior to use to prevent

interference peaks occurring for blank samples at SiO_4^{4-} and PO_4^{3-} derivative positions on the chromatogram.

From the literature reviewed it is clear that techniques for trimethylsilylation of silicates have been developed that are capable of suppressing, but not completely eliminating side reactions.

Application of the unified technique to slags is, unfortunately, limited. It is, therefore, considered that further work involving slags is required in order to assess the ability of the technique in providing a true representation of silicate species in slags.

2.4 SINGLE DROPLET STUDIES OF SLAG-METAL REACTION SYSTEMS

2.4.1 Hydrodynamic Behaviour of Falling Droplets

Liquid drops falling through a less dense, immiscible liquid deform to a degree dependent on size and interfacial tension^{124, 125, 126, 127}. A drop of one liquid falling through another will behave as a rigid sphere and obey Stokes' Law only when the Reynolds Number is less than unity. For steel in slag this corresponds to a diameter of less than 0.5mm. As the diameter is increased internal circulation is set up in the drop due to viscous forces operating at the interface. Further size increase causes the drop to deform to an oblate spheroid shape with the velocity falling below the Stokes' Law value. Vortices produced in the wake may cause oscillation of the drop. Finally, the drop velocity passes through a maximum and a size is reached where surface tension forces are insufficient to prevent droplet break-up.

In metallurgical processes where drops of interest have diameters of 1 to 5mm with Re 100-1000, then a wake is involved from which vortices are torn off. Well developed internal circulation patterns will also be established in the drop. A number of workers have attempted to relate the drop velocity to drop size for various types of circulation in the drop. Hu and Kintner¹²⁷ studied the terminal velocity of ten organic liquids falling through a stationary water phase covering the Reynolds Number range 0 to 2200. For nine of the ten systems the

following expression was obtained relating the drag coefficient (C_D), the Weber number (We), the Reynolds number (Re) and a physical property group (P):-

$$P = \frac{4 Re^4}{3 C_D We^3} = \frac{\rho_{con}^2 \sigma_i^3}{\epsilon \mu_{con}^4 (\rho_d - \rho_{con})}$$

This relationship has been confirmed by other workers¹²⁵ and appears to be the best correlation to date. The relationship has been applied to a drop of mercury in water as shown in Figure 26.

2.4.2 Mass Transfer Models

The rate at which the solute in the metal drop will react with the surrounding continuous phase will depend on¹²⁴:-

- (a) the rates at which reactants and products move between the bulk continuous phase and the metal interface
- (b) the rate of chemical reaction at the interface
- (c) the rate at which reactants and products move between the surface and interior of the drop.

It is generally recognised that at steelmaking temperatures the pertinent chemical reaction will proceed so rapidly that reaction rates will be transport controlled⁷. Mass transfer rates within a metal drop and the surrounding continuous phase will depend on flow conditions and it may be expected that a

stagnant, rigid drop with no internal circulation will be associated with low mass transfer rates. A droplet that is internally circulating and oscillating will produce stirring within the drop and enhance mass transfer rates.

Various workers have studied mass transfer within droplets for different fluid dynamic conditions. A rigid sphere treatment has been used by Vermulen¹²⁸ whilst Kronig and Brink¹²⁹ have considered the effect of simple circulation patterns in the absence of continuous phase resistance. The presence of internal circulation with oscillation in a drop has been considered in a model by Handlos and Baron¹³⁰. Rose and Kintner¹³¹ and Angelo et al¹³² have produced models for more violently oscillating drops. The results by Angelo agree well with experiments for aqueous-organic systems, but for small drops of metal in aqueous or molten phases, the model reduces to a form proposed by Rose and Kintner.

Mass transfer in the continuous phase has also been studied and Steinberger and Treybal developed a model for a rigid drop in the presence of mass transfer resistance in the continuous phase¹³³. Enhanced mass transfer rates are expected in the case of internally circulating drops and Griffiths¹³⁴ and Higbie¹³⁵ have proposed models.

The development of mass transfer models for droplets has mainly utilised aqueous and organic systems. This involves droplet surface tensions and densities that are very much smaller than in liquid metals and slags. To achieve greater

similarity with metal drop systems, mercury amalgams have been studied. Aeron and Crimes¹³⁶ have investigated the reaction of amalgam droplets with aqueous phases. For the experimentally obtained dispersed phase mass transfer coefficients, the Rose and Kintner model gave the best agreement. The obtained coefficients were about half that of the Handlos and Baron Model. For the continuous phase mass transfer coefficients, results fell between values predicted by the Higbie Model and for a stagnant sphere.

For metals, which have high surface tensions, it would appear that internal circulation is not as vigorous as compared with aqueous-organic systems on which the Handlos and Baron Models are successfully based. The inference, therefore, is that an accurate prediction of mass transfer coefficients in slag-metal systems is not possible. A further complication may arise when interfacial phenomena occur.

2.4.3 Surface Phenomena

Interfacial phenomena may retard or contribute to mass transfer rates in liquids¹³⁷.

Surface active solutes concentrate in the surface layer^{18, 19} and so it appears feasible that such surface active agents in a metal drop may interfere with circulation patterns or block surface reaction sites. The blocking effect of sulphur has been used to explain the decarburisation behaviour of certain iron-carbon alloy droplets^{15, 138}.

Transfer of a surface active agent from a droplet to the continuous phase can cause a change in interfacial tension ¹³⁹. It is possible that a variation in concentration, leading to a variation in interfacial tension, may occur at the droplet surface causing interfacial turbulence. Aeron ¹²⁶ has shown that during the oxidation of indium amalgam droplets by ferric nitrate solutions, interfacial turbulence significantly increased the rates of mass transfer both in the continuous and dispersed phases.

In iron and iron alloys the presence of both sulphur and oxygen can markedly lower surface tension ¹⁴⁰ and the possibility exists that during reactions where these solutes are transferred, interfacial turbulence may be set up ^{137, 141, 142}. Recent work has suggested that CO nucleation during the decarburisation of high sulphur iron-carbon droplets, may be made easier because of interfacial turbulence resulting from the transfer of sulphur from the metal to the slag ¹⁴³.

Little practical work has been reported on the effects of complex anions such as silicates at metal interfaces. Mechanisms have been presented for the stabilisation of metal droplets but are of a speculative nature and only appear feasible in acid slags ¹⁴⁴.

2.4.4 The Refining of Single Droplets

The majority of studies concerning the refining of single iron and iron alloy droplets has been directed towards the

decarburisation reaction. The need to achieve better sulphur transfer during steelmaking has initiated a number of laboratory investigations, but much of the work has involved slag-metal layers. Work reported on desulphurisation of metal droplets is, in comparison, rather limited. Droplet work investigating silicon transfer has been reported by Sano ¹⁴⁵ whilst Yavoiskii ¹⁴⁶ has studied the refining of high phosphorus pig iron droplets.

Many decarburisation experiments have involved levitated ^{147, 148, 149, 150} or free falling droplets ^{151, 152, 153, 154,} ¹⁵⁵ in flowing oxidising gases. Two possible mechanisms for decarburisation have been proposed. At high carbon concentrations a surface reaction between carbon and oxygen occurs and at lower carbon concentrations a subsurface reaction takes place with carbon monoxide bubbles nucleated within the drop. The latter mechanism was associated with the ejection of small metal particles from the drop.

The levitation work generally points to the surface reaction being controlled by countercurrent diffusion of the oxidant and product gases in the gaseous boundary layer. Distin ¹⁴⁸ found that an iron oxide film formed on the droplet surface when the carbon concentration at the surface was virtually zero. This allowed the bulk oxygen concentration in the droplet to rise and enabled the internal carbon boil to commence. The transition from surface to subsurface reaction behaviour could occur at various carbon concentrations down to 0.3 mass % carbon.

Results for the decarburisation of iron-carbon droplets during free fall through oxidising gas have shown that sub-surface nucleation of carbon monoxide occurred at higher carbon concentrations, compared with levitated droplets. This was attributed to the higher degree of induced stirring in the droplet produced by the levitation coil compared with that encountered during free fall. Baker ¹⁵¹ reported carbon transport control at almost all carbon levels up to 4.5 mass % carbon, whilst See and Warner ¹⁵⁴ suggested that internal nucleation of carbon monoxide began at about 3 to 4 mass % carbon. Roddis ¹⁵³ considered that gaseous diffusion control only occurred at carbon contents greater than 4 mass % carbon.

The decarburisation of iron-carbon droplets by oxidising slags has been investigated ¹³⁸. The work showed that decarburisation gave rise to significant foaming of the slag and that the decarburisation rate of an iron-carbon melt generally decreased at carbon contents below 0.3 to 0.5 mass % carbon. The overall removal of carbon was found to decrease with increase of FeO content of the slag. A mechanism for decarburisation rate control was not clear but Belton ¹⁵⁶ considered this work and suggested that interfacial chemical control was important.

A qualitative study of iron-carbon alloy droplet reactions with $\text{CaO-Fe}_2\text{O}_3\text{-FeO-Al}_2\text{O}_3\text{-SiO}_2$ slags has been reported by Hazeldean ¹⁵ who used an x-ray technique to observe the evolution of carbon monoxide from the reacting drop. For reactions involving slags containing iron oxide as Fe_2O_3 , it was noted that

when droplet surface reaction occurred, gas evolved from the metal-slag interface eventually formed a gas halo around the drop buoying it up. In the later stages of decarburisation the drop pulsated and increased in size due to the internal nucleation of carbon monoxide, this being capable of causing the droplet to fragment. With carbon saturated iron and high FeO content slags only small gas bubbles were observed and buoying up of the drop did not occur.

Hazeldean's work has recently been extended to include the determination of decarburisation rates by measurement of the pressure increase caused by evolution of gaseous products from the droplet-slag reaction ¹⁴³. To describe the most complex decarburisation behaviour five stages of reaction were suggested. An induction period reflected difficulties in the nucleation of carbon monoxide, but was followed by a fast decarburisation period where the droplet was surrounded by a gas halo. Carbon monoxide generated at the metal-gas interface was considered to diffuse across the gas halo and draw oxygen from the slag to form carbon dioxide, that could diffuse back and react with carbon dissolved in the iron to form carbon monoxide. The counter-diffusion of CO and CO₂ was believed to be rate controlling for this particular stage. An eventual collapse of the gas halo was associated with depletion of carbon at the droplet surface. A finite time was required to initiate internal CO nucleation thus producing what was described as a lull period. On release of a CO bubble from the droplet surface, disruption of the metal-slag interface could provide slag-metal mixing and was believed to

assist further CO nucleation. A period of external-internal decarburisation was envisaged with carbon and oxygen concentration gradients in the droplet and oxygen concentration gradient in the slag. The more likely nucleation of CO at the slag-metal interface would lead to denudation of carbon and oxygen at the interface and allow nucleation within the metal phase. The final internal nucleation stage was thought to be controlled by carbon and oxygen mass transfer in the metal phase.

This work confirmed the earlier x-ray observations of only small CO bubbles evolved from the droplet surface and the absence of a complete gas halo when slags of high FeO content were employed. The quantitative work confirmed the overall poor decarburisation achieved using such slags. The decarburisation stages taking place were regarded as the induction period followed by a fast decarburisation period where oxygen transport through the slag was considered important. The final stage of slow decarburisation was also related to the ability of oxygen to diffuse through the slag and achievement of the carbon-oxygen product for carbon monoxide nucleation at the slag-metal interface.

These results from the decarburisation of iron alloy droplets in slags have been used to explain reactions occurring in the LD converter. The synthetic slags do, however, contain alumina levels well in excess of those encountered in LD turndown slags. The reason for this was the difficulty in selection of a suitable slag container for high temperature laboratory work¹⁵⁷. The

experiments involved alumina crucibles and the deliberate inclusion of alumina in the slag reduced slag attack of the crucible.

Similar problems exist for experimental systems used to investigate sulphur transfer. The study of sulphur transfer has frequently employed quiescent slag-metal layers, contained in graphite crucibles. Carbon-saturated iron and $\text{CaO-Al}_2\text{O}_3\text{-SiO}_2$ slags have meant that blast furnace conditions are simulated, but the results have provided information about sulphur transfer as discussed in Section 2.2.2. The use of slags representing steelmaking compositions with an appreciable concentration of FeO , further narrows the choice of containers as graphite is rendered unsuitable.

Previous work on desulphurisation of iron-alloy droplets has also involved graphite crucibles, carbon-saturated iron and $\text{CaO-Al}_2\text{O}_3\text{-SiO}_2$ slags but the method of droplet production provides an additional practical consideration^{62, 63, 64, 65}. The melting of a notched sample rod above the slag has been used⁶² whilst Ishii⁶³ melted a droplet in a graphite nozzle arrangement and pushed the droplet into the slag by the slight increase of pressure in the nozzle. The simplest system appears to be that of Barger^{64, 65} who employed a stopper and seat arrangement.

Clearly the study of sulphur transfer by reaction of single metal droplets with slags representing steelmaking compositions poses practical difficulties. The successful development of a

technique that overcomes these difficulties, would provide more information on sulphur transfer and be based on conditions nearer to steelmaking systems than previous work has achieved.

CHAPTER THREE

EXPERIMENTAL PROCEDURE

3.1 PRELIMINARY SINGLE DROPLET WORK

3.1.1 Introduction

The requirements of a vertical tube furnace suitable for the study of molten iron droplets reacting with a liquid slag phase include:

1. An extensive stable hot zone with minimal temperature variation along the hot zone.
2. Adequate access to both the top and bottom of the tube.
3. The provision for a controlled atmosphere in the work tube.

The selection of a furnace for such work necessitated prior consideration of the technique for single droplet formation and subsequent transfer to a liquid slag. It was considered that the method of droplet production would be the main influence in the choice of furnace.

Preliminary work was undertaken to establish a droplet technique to produce droplets of about 3mm diameter. Such a size is slightly larger than the majority of droplets in LD steelmaking according to Meyer^{8, 13} and Trentini¹⁴ but the metal mass of 0.10 to 0.15g used was more convenient with respect to weighing and handling.

This preliminary work used Wood's metal. The low melting temperature of 71°C facilitated practical operations. It was

hoped that experience gained from the low temperature model would allow a more rapid establishment of the correct practical conditions for the higher temperature iron-carbon-sulphur system.

3.1.2 Low Temperature Droplet Model

(a) Components

The droplet production technique studied was a stopper and seat method similar to that of Bargeron et al ⁶⁴.

Components were made of Koss Cement (Purimachos Ltd.) with a maximum working temperature of 1250°C. The dimensions are given in figure 27a. The seat was produced by ramming the cement into a greased metal ring 30mm I.D. and 15mm high. A tapered orifice was formed by forcing a wooden cone into the cement when excess cement was displaced. The resulting orifice was smoothed after the cement had set. A central hole of 3mm diameter was drilled.

The stopper was produced by ramming cement into a copper tube. A mild steel rod was inserted into the drying cement to act as an operating lever. The dry rod was extracted from the tube and the stopper end finished to a point.

(b) Droplet Production

A piece of Wood's metal (0.10 to 0.15g) was placed in the seat of the assembled seat and stopper and heated by an air dryer. When the metal was liquid the dryer was removed and the stopper raised to release the metal.

The metal was photographed during fall in order to identify the droplet shape and possibility of droplet break-up. A reference marker (80mm from the seat base) in the field of view enabled calculation of distance travelled by the drop.

(c) Information from the Low Temperature Model

Seven droplets were photographed at different stages of fall and are shown in plates 1a to 1g.

The photographs indicated that metal break-up during fall had not occurred. At distances between 58mm to 80mm from the seat base apparently spherical shapes resulted. No data was obtained pertaining to droplets close to the seat base but the results suggested suitability of a stopper and seat method for producing single metal droplets.

3.1.3 Iron-Carbon-Sulphur Droplet Trial

Development of the work on droplet formation to the higher temperature system required first the replacement of the Koss cement used for stopper and seat components at low temperature.

(a) Stopper and Seat Components

Stopper and seat components were manufactured using graphite or alumina cement.

Graphite seats were prepared from 25mm diameter electrode material. The seat produced was 10mm high, 20mm diameter with a central hole of 5mm diameter. The tapered orifice had an included

angle of 75° , figure 27b. To produce the stopper rod graphite electrode material of 8mm diameter was tapered at one end by finishing and drilled at the other end to give a hole 1.5mm diameter and 10mm deep.

Alumina components were manufactured from C60 Alumina cement (Refractory Mouldings and Castings Ltd.).

Seat dimensions were identical to those described for the graphite component.

A perspex mould of the type depicted in plate 2a was constructed so that a slurry of C60 and water could be cast to shape. The perspex in contact with the slurry was greased prior to use. The slurry was allowed to dry for 16 hours, removed from the mould and fired in a muffle furnace at 950°C for 8 hours. A 5mm hole was drilled in the centre of the seat base and the base then finished flat. Firing at 1300°C for 16 hours in a vertical tube furnace completed the seat preparation.

Alumina slurry was cast into a greased, split perspex mould (plate 2a) to produce a rod of 9mm diameter and 50mm length. After drying for 16 hours the rod was fired at 950°C for 8 hours. As before the rod was tapered at one end and drilled (1.5mm diameter, 10mm deep) at the other. Firing at 1300°C completed the preparation.

(b) Stopper and Seat Arrangement

To hold the stopper and seat in a furnace hot zone the seat was attached by Alumina cement to a 1m long, 25mm O.D. and 20mm I.D. aluminous porcelain tube (Morgan Ltd.). The seat was

positioned in the tube with the base flush with the end of the tube.

The stopper was attached to a 1100mm length of 1.2mm diameter Kanthal A1 wire (Hall-Pickles, Sheffield) by Chromix adhesive (Fortafix Ltd.) and inserted down the tube until positioned in the seat. An aluminium alloy bung with central hole to allow the Kanthal A1 wire to protrude was placed in the top of the tube.

The stopper and seat were positioned in the furnace hot zone by suspension of the refractory tube with a Wilson seal fitting. Figure 28. A flange on the Wilson seal enabled it to rest on the furnace top fitting.

The stopper system was held at the desired position along the furnace tube and was introduced in stages to prevent cracking of the tube by thermal shock.

(c) Furnace Used for the Droplet Trial

A vertical tube furnace accommodating a 900mm long, 54mm O.D. and 45mm I.D. aluminous porcelain work tube (Morgan Ltd.) and heated by a helical silicon carbide element was used for melting metal at 1300°C. A watercooled Aluminium alloy sleeve was fitted at the top of the work tube. The bottom of the work tube was open and situated 5 ft above ground level.

A temperature profile of the furnace hot zone revealed a short linear hot zone 45mm long with 5°C variation. The use of a

sleeve on the work tube top effectively increased the work tube length by 30mm. The flange to hot zone centre distance was 485mm whilst hot zone centre to work tube base distance was 445mm.

An argon (99.999% purity) atmosphere was provided by inserting a copper tube carrying argon through a temporary plug of Kaowool refractory fibre positioned in the base of the work tube.

(d) Production of Droplets

Argon was passed into the furnace for 30 minutes to allow for temperature stabilisation. Temperature measurement was by a suspended Pt - Pt/13%Rh thermocouple inside the work tube.

The stopper and seat system was assembled with metal sample in position.

The Wilson seal was positioned on the refractory tube at a distance from the stopper seat that corresponded to the furnace top to hot zone centre distance of 485mm. The tube was slowly introduced to the furnace. Once the seat had reached the hot zone centre 15 minutes were allowed for uniform heating. The Kaowool plug and copper pipe were removed from the work tube base. The metal was released by raising the stopper rod and allowed to fall onto a metal tray beneath the furnace.

(e) Photography of Droplets

Photography was used to identify the shape of falling metal. The distance travelled by the metal prior to photographing was at least 445mm, due to metal being released from the hot zone and the

camera being positioned below the level of the work tube base. It was impractical to lower the stopper system to the base of the work tube immediately prior to releasing the metal. Manipulation difficulties created time delays and subsequent freezing of the metal in the seat occurred. In addition the possibility of cracking the aluminous porcelain tube was increased.

The photographic technique involved the use of a black revolving disc containing eight, equally spaced radial slits. The disc was placed between the path of falling metal and camera lens. The camera shutter was held open so that the revolving slits acted as shutters. Black cloth was placed beneath the four sides of the furnace housing to enclose the work tube base, camera and rotating disc. Illumination was provided solely by falling molten metal, thus being detectable on film.

The disc was rotated by a drill at 1420 r.p.m., the camera shutter held open and the metal released. The use of revolving slits meant a multiple image was caught on one frame. This represented one droplet at different stages of fall.

Plate 3a shows a droplet at seven stages of fall. A reasonable spherical shape has been obtained. Metal break up has not occurred. Plate 3b does not display as good a contrast between metal and background compared with 3a but a desirable shape of metal is featured.

(f) Implications of the Preliminary Work

The preliminary work with a melt similar to that to be used

for the research indicated the applicability of a stopper and seat technique. The small components used do not demand a furnace with an extremely large hot zone. The combined droplet studies suggested no metal break-up at distances over 60mm from the seat base.

The Fe-C-S droplet trials elucidated the problems inherent in high temperature work in terms of the stopper and seat performance. The main problem was failure of metal to fall through the graphite or alumina seat hole on raising the stopper rod. It was considered that the furnace atmosphere was not fully inert as graphite components displayed signs of oxidation after use. Thus, the trials were performed under rather severe conditions.

The preliminary work provided justification for developing a technique for single droplet work based on a stopper and seat technique. It was envisaged that modification of components to cope with operating temperatures of 1300°C would be necessary.

3.2. EXPERIMENTAL APPARATUS AND PROCEDURES FOR DROPLET
EXPERIMENTS

3.2.1 Metal Melt Preparation

(a) Melting Procedure

Iron-Carbon-Sulphur melts were prepared from Armco Iron (analysis, table 5a) using graphite and Iron Sulphide additions to attain the required carbon and sulphur levels. The aim mass of melt was 1.5kg.

Armco Iron and graphite powder (> 10 mesh) were melted in a graphite crucible by a 15kW high frequency induction furnace. The furnace atmosphere was controlled by a blast of argon into the top of the furnace at a flow rate of 0.5 l/min. When the charge was liquid the furnace power was switched off and the Iron Sulphide addition made. Heating was resumed for 5 minutes. Metal melt compositions are given in table 5a.

(b) Pin Sample Preparation for Experiments

Evacuated glass pin sampling tubes (Amalgams Ltd.) provided a method of collecting metal from the graphite crucible. The tube size 6mm O.D., 3.5mm I.D. and 150mm long meant that six lengths of metal (termed pin sections) each with mass greater than 1g could be cut from each pin.

Samples were collected from the metal bath until the metal temperature had dropped sufficiently to prevent successful sampling. If further samples were required the furnace was re-heated for 5 minutes and another batch of pins obtained. Poor

samples were discarded leaving only sound pins and were identified to signify order of sampling. For each melt a large number of pins was collected (at least 40 sound pins). About every fifth pin was analysed for carbon and sulphur. Some pins were cut in two and each half analysed. The large number of pins obtained enabled samples to be selected from batches within a melt that displayed minimal variation in analysis.

The sulphur and carbon contents were analysed by combustion techniques. The respective required sample masses were 1g and 0.2g. In view of this a decision was taken to study droplets of 1.0 to 1.2g mass.

A pin sample was selected to provide metal for five droplet reactions of varying reaction time, with a given slag composition. The pin sample was cut into six pin sections by a Servomet spark erosion machine. The mass of each pin section was checked to ensure a mass greater than 1g. Finishing was employed to effect any necessary decrease in mass. The pin section was then shot blasted, rinsed in acetone and dried.

One section was selected for sulphur or carbon analysis (depending on the reaction to be studied) whilst the other sections were sealed in an envelope and stored in a dessicator. Pin section compositions for particular reactions studied are given in tables 5b to 5e.

(c) High Sulphur Melts

Pin sampling to obtain a high sulphur melt (aim Fe-4.0 mass

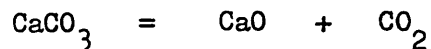
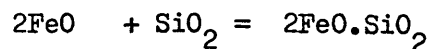
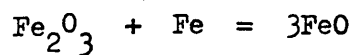
% C - 0.6 mass % S) was found unsuitable as sulphur was continually evolved from the bath during sampling. A repeat melt was made and the metal cast into three $\frac{5}{8}$ inch diameter metal moulds. Samples were taken along each bar to obtain average analyses for each bar.

To produce samples for droplet experiments, a groove was ground along the length of the bar to aid longitudinal fracture. The resulting half-round bars were sliced by the spark erosion machine and each slice identified. Lining was used to adjust the slice to the required mass.

3.2.2 Synthetic Slag Preparation

The synthetic slags chosen to model early LD slags were of compositions corresponding to points near the $2\text{FeO} \cdot \text{SiO}_2$ - $2\text{CaO} \cdot \text{SiO}_2$ tie line of the CaO - FeO - SiO_2 system, figure 29. The range of compositions were from fayalite ($2\text{FeO} \cdot \text{SiO}_2$) to 38 mass % CaO in fayalite (liquidus temperatures 1205°C and 1300°C respectively).

Slags were prepared according to the reactions ²²:-



Materials used were BDH-grade calcined ferric oxide (> 95% Fe_2O_3), BDH precipitated silica, electrolytic iron

powder (- 320 u) and Analar grade calcium carbonate.

The required mass of each material was weighed followed by thorough mixing. The mix was transferred to a graphite crucible for fusion in the Electroheating 15kw induction furnace. A flow rate of 0.75 l/min argon was maintained to provide a controlled atmosphere. The fused slag was furnace cooled under argon and the solid material placed on a 10 mesh B.S. sieve. This was to separate any carbon fines derived from abrasion of the crucible whilst breaking up the slag. The slag was then crushed in a percussion mortar in order to pass through the 10 mesh sieve. Any metallic iron was then removed by a hand magnet. Subsequent crushing for the slag to pass through 300 and 106 micron sieves followed. Removal of metallic iron was repeated after each sieving stage.

A maximum of 100g slag was produced from one melt and for each required composition a bulk of about 2.7kg was built up. Each bulk slag was thoroughly mixed and sampled by the cone and quartering technique. Slag compositions are given in table 7a.

3.2.3 Crucible Preparation

(a) Selection of Crucible

Slags used for reaction with a metal droplet had to be held in a container for both the melting period and the specified droplet-slag reaction time. The use of high temperatures (1300°C) and aggressive 'FeO' rich slags increased the difficulties of containment. Alumina crucibles have been used in previous studies

with necessary doping of the slag. For the present work this was considered unsuitable with respect to envisaged chromatographic work. The use of zirconia crucibles was prohibitive in view of the cost of a large number of crucibles. Work in the department by Ojeda¹⁵⁸ had involved the internal coating of iron crucibles with zirconia, ZrO_2 . Droplet experiments over a range of CaO - FeO - SiO_2 slags had been successful in terms of the coating preventing droplets welding to the crucible. This method of slag containment was, therefore, adopted.

(b) Preparation and Coating of Crucibles

Iron crucibles (0.06 mass % C) of 40mm diameter mouth, 28mm base diameter and 40mm high, were supplied by A. Brown, Sheffield.

Thorough degreasing of each crucible with acetone was performed prior to welding pairs of crucibles together, top to top. The end of a welded crucible was then sawn off to provide a mouth of about 30mm diameter. The welded crucible had a height of 75mm in order to prevent possible slag overflow should slag foaming occur during droplet-slag reaction. After smoothing the crucible mouth two diametrically opposed 1.5mm diameter holes were drilled at the top of the crucible, 70mm from the base. These holes accommodated wires for suspension of the crucible down a vertical tube furnace. The inside of the crucible was shot blast and the whole crucible degreased with acetone.

For coating the crucible, 5g of fused zirconia ($< 300 \mu$)

was placed in a prepared crucible and a slurry produced by stirring with 3cm³ of acetone. When the mixture was smooth the crucible was rotated and slightly tilted. As the acetone evaporated the zirconia formed a coating on the base and inside wall of the crucible. The coating was kept below the holes drilled in the crucible. Air drying of the coating was followed by inspection for cracking which if present required the coating stage to be repeated. If no cracking had occurred the crucible was positioned in the work tube of a vertical tube furnace (sections 3.1.3 (c) and 3.2.4) with an argon atmosphere. The crucible was introduced to the furnace hot zone of 1100°C over a period of 1 hr and held at 1100°C for 4 hrs. About 1 hr was taken to gradually remove the crucible from the furnace.

The firing resulted in a tenacious zirconia coating. Any cracked coatings were discarded. Coated crucibles were stored in dessicators.

3.2.4 Furnace Used for Droplet Experiments

The furnace selected for the droplet experiments was a Carbolite Vertical tube furnace with a 1.5m long, 54mm O.D. and 45mm I.D. recrystallised alumina work tube (Morgan Refractories). Six silicon carbide rods (Crusilite, Morgan Electroheat Ltd.) provided the heating source. Temperature control was by a Carbolite controller and Pt-Pt/13%Rh thermocouple.

Watercooled aluminium alloy sleeves were fitted over the top and bottom of the work tube with respective outlet and inlet for argon. Aluminium plates could be attached to each sleeve to

seal the tube. Plate 4 presents a view of the furnace rig whilst figure 30 is a schematic diagram.

A temperature profile was established for the furnace by suspending a Pt-Pt/13 % Rh thermocouple down the work tube. An argon flow rate of 1l/min through the tube was utilised to simulate experimental conditions. A typical profile is shown in figure 31. With the hottest part of the furnace at 1307°C a 5°C temperature variation existed over a hot zone of 67mm, whilst a 10°C variation occurred over 90mm.

3.2.5 The Stopper and Seat Technique

(a) Stopper and Seat Components

A change in the design of the stopper seat by increasing the taper of the orifice to an included angle of 60° and the use of a C60-40 mass % ZrO₂ mixture improved the stopper and seat performance used under conditions outlined in section-3.1.3 (d). Perspex moulds similar to those depicted in plate 2a were made to enable the components to be cast. Figure 27c shows the dimensions of the stopper and seat. Plate 2b shows the actual components.

The seat mould was essentially a 60° tapered cone of 19mm diameter base and 14mm height. A 20mm diameter ring, fitted over the cone stub, contained the material cast over the cone.

The stopper rod mould consisted of two 40mm x 75mm x 12mm pieces of perspex with the broad faces placed together and

secured by four bolts. A 9mm diameter hole was drilled centrally down the attached perspex to about 50mm depth. This provided a split mould for casting stopper rods. All mould faces were cleaned with perspex polish and lightly greased with silicone high vacuum grease.

60g of alumina cement was thoroughly mixed with water and an addition of 40g ZrO_2 made. More water was carefully added to obtain a consistency that facilitated pouring into the moulds. After pouring, the mould contents were compacted with a wire to displace any trapped air bubbles. The mould contents were left to dry overnight (16 hours). A decrease in this drying period (or increased ZrO_2 content) led to cracking of the components. If no cracks were detected the mould was gently warmed on a furnace housing for a couple of hours. Cooling followed and the mould contents carefully extracted.

After another inspection for cracks the stopper and seat were fired in a muffle furnace at $1000^{\circ}C$. On cooling a central 5mm diameter hole was drilled in the seat and the base finished flat. The rod was tapered by finishing at one end and a 1.5mm diameter hole, 10mm deep was drilled at the other end. Firing at $1300^{\circ}C$ in a horizontal tube furnace completed the stopper and seat manufacture.

(b) Stopper and Seat Assembly

The stopper and seat assembly were housed in an aluminous porcelain tube, the dimensions described in section 3.1.3 (b).

Two horizontal slits opposite one another were cut by a diamond cutting wheel 10mm from the tube base. Into each slit a length of alumina thermocouple sheath was cemented by alumina cement. The tube exterior was carefully finished to retain a circular profile. The inserts provided ledges for the seat to rest on and enabled easy removal of the seat for inspection purposes.

A seat was positioned on the ledges and a stopper rod to which a 1100mm length of 1.2mm diameter Kanthal A1 wire had been attached, was inserted in the seat. The Wilson seal was positioned on the tube and the aluminium alloy bung placed into the tube top with the stopper connecting wire protruding. The stopper was raised and a prepared pin section placed into the seat via the seat hole. The stopper rod was carefully lowered and repositioned in the seat.

950mm lengths of Kanthal A1 wire were attached to a coated crucible through the holes drilled in the crucible. The unattached ends of each wire were fed through 1.5mm holes drilled in the Wilson seal flange. The wires that emerged through the flange were gripped by bulldog clips. The flange surface to crucible base distance was 905mm where a heating temperature of $1300 \pm 2^{\circ}\text{C}$ was achieved in the furnace tube. 35g of slag was placed in the suspended crucible prior to insertion in the furnace work tube.

The Wilson seal was moved along the tube to a flange surface to tube base distance of 645mm. This corresponded to a heating temperature for the metal of 800°C . Figure 32 shows

the arrangement of apparatus for droplet experiments using the stopper and seat technique.

(c) Droplet Production Procedure

The furnace temperature was checked prior to each experimental run. An argon flow rate of 1l/min was maintained throughout temperature checks and experiments.

The crucible and tube was carefully fed down the work tube and the Wilson seal flange attached to the furnace sleeve. The crucible and contents commenced heating to 1300°C and a 10 minute period was allowed for metal heating to 800°C. The stopper system was then lowered further down the work tube for heating to 1000°C, (flange surface to tube base distance of 680mm) for 5 minutes. The final heating period for the metal was 5 minutes at 1300°C which involved careful movement of the stopper unit into the mouth of the crucible. The flange surface to tube base distance was 855mm and the estimated distance between slag and metal about 50mm. Figure 33 shows the relationship between the furnace hot zone temperature profile and position of slag and metal immediately prior to droplet transfer.

The droplet was transferred to the slag by raising the stopper. Timing of the reaction commenced simultaneously. The stopper system was then removed from the crucible mouth to a position just above the crucible. To complete a series of experiments for a given slag composition, reaction times of 2, 5, 10, 15 and 20 minutes were selected.

(d) Quenching and Droplet Collection

The reaction was stopped by quenching the crucible and contents. This was originally achieved by removal of the plate attached to the work tube bottom sleeve and dropping the crucible by releasing the support wire clamps. The crucible was dropped into a copper container containing an ice-water mixture. This was unsatisfactory since reaction between water and sulphur in slag occurred. An alternative quench into a copper container lined with ice where the crucible contents could be blasted with argon was adopted.

The cooled slag within the crucible was fractured to release the reacted metal droplet. The droplet was cleaned by shot blasting to remove adhering slag and followed by an acetone rinse and drying of the metal. Dimensions, appearance and mass of the reacted droplet were recorded prior to chemical analysis.

(e) Examination of Crucibles

The stopper and seat droplet experiments were successful for reactions between 38.31 mass % CaO-28.52 mass % FeO-1.90 mass % Fe₂O₃-31.00 mass % SiO₂-0.27 mass % S slag and varying metal compositions. It was discovered that experiments involving slags with lower lime contents (and increased FeO levels) resulted in droplets being welded to the crucible. A number of experiments were performed involving lower temperatures, smaller droplet sizes, greater slag mass, reduced droplet fall distance and slag doping with zirconia. Droplet

welding was a feature of all experiments with slag CaO levels less than 38 mass %. Inspection of crucibles revealed clean, bright surfaces that suggested the zirconia coating had failed and washed into the slag.

To confirm this effect the Scanning Electron Microscope (SEM) was used on a qualitative basis to study the effect of two slag compositions on the zirconia coating inside iron crucibles. Two coated iron crucibles were used for melting 35g of 38.31 mass % CaO-28.52 mass % FeO-1.90 mass % Fe_2O_3 -31.00 mass % SiO_2 -0.27 mass % S and 28.00 mass % CaO-40.20 mass % FeO-3.21 mass % Fe_2O_3 -28.50 mass % SiO_2 -0.15 mass % S slags respectively. The slags were heated at 1300°C for 20 minutes and quenched in argon. The end of the heating period represented the starting point of a droplet reaction. The crucibles with solidified contents were sectioned longitudinally by a diamond cutting wheel. The sectioned faces were ground sequentially on 240, 320, 400 and 600 grade silicon carbide papers. Polishing with 6 and 1 micron diamond paste followed. The polished surfaces were etched with 0.1% Nital and then coated with volatilised silver under vacuum.

Examination of the specimens was made by a Philips SEM with EDAX 711 analyser system (Sheffield Poly. Met. Dept.). An acceleration voltage of 25kv with spot size of 0.25 μm was employed with the sample inclined at 30° to the incident beam. For each sample an image of the crucible-slag interface was obtained. The EDAX facilities were used to obtain x-ray maps for detection of zirconium over the image. A transverse line scan across crucible-slag interface was used to indicate any

zirconium concentration gradient. An x-ray map of all detectable elements to indicate any topographical effects was also obtained. Photographs of each were recorded on 35mm Ilford Pan F.

3.2.6 The Suspended Droplet Technique

To study droplet reactions with slag less than 38 mass % CaO, an alternative technique was employed. This essentially involved the suspension of a metal drop into a slag by platinum wire ensuring that contact with the crucible was avoided.

(a) Suspended Droplet Experiment Equipment

The stopper and seat system was replaced by a 2.4mm diameter, 1m long Fe-Ni rod with a hook formed at one end. The free ends of a length of platinum wire looped around a pin section were attached to the hook. The pin section was suspended below the Fe-Ni rod.

A circular plate was used to seal the top of the furnace. Two holes were drilled to accommodate wires for crucible suspension. A 3mm diameter central hole was provided for the Fe-Ni rod. A periscope attachment was also included for viewing down the work tube. Figure 34 shows the arrangement of apparatus for droplet experiments using the suspended droplet technique.

(b) Suspended Droplet Experimental Procedure

The furnace temperature was monitored as described in sections 3.2.4 and 3.2.5(c).

Platinum wire 0.5mm diameter and 80mm long was looped three times around a pin section (1.0 to 1.2g). The free ends were attached to the Fe-Ni rod.

An uncoated iron crucible prepared as in section 3.2.3(b) was suspended by Kanthal A1 wires from the metal plate. The plate top to crucible base distance was 871mm in order to heat the slag to 1300°C. 50g of slag was placed in the crucible.

The Fe-Ni rod was positioned through the central hole of the plate and gripped by a bulldog clip. The suspended pin section was located 35mm from the crucible base, above the powdered slag level. A 120mm length of 0.5mm diameter Kanthal A1 wire was looped around the Fe-Ni rod and attached to the suspension wires at the crucible mouth. This was to maintain central positioning of the rod and pin section in the crucible. Figure 35 shows the apparatus and a temperature profile alongside indicates the temperature-position relationship.

The apparatus was carefully fed into the furnace hot zone. Once the metal plate was resting on the furnace top sleeve a heating period of 15 minutes was timed. The metal was liquid and had formed a drop shape within 5 minutes. The slag was liquid within 10 minutes. The metal droplet was gently suspended in the slag by lowering the Fe-Ni rod. A marker indicated the required position to achieve immersion without touching the crucible base. The metal was never positioned lower than 5mm from the crucible base. Once the metal was immersed timing of the reaction commenced.

On completion of the desired reaction time the metal droplet was carefully raised above the slag level. The apparatus was lifted out of the furnace and the metal and slag quenched by an argon blast. Reaction times of 2, 5, 10, 15 and 20 minutes were used to complete a series of reactions with given metal and slag compositions.

(c) Droplet Analysis

The reacted droplets and connected platinum wire were removed from the Fe-Ni rod and shot blast. The appearance and dimensions of the metal were noted.

The mass of metal and platinum was recorded and uncontaminated platinum subsequently cut off the droplet. The droplet was re-weighed. Knowledge of the original masses of metal and platinum enabled the determination of platinum mass remaining in the metal sent for analysis.

For combustion sulphur analysis, all the metal (with incorporated Pt) was used for one determination. The results received were corrected to allow for platinum present in the sample.

The carbon analysis involved splitting the metal and Pt droplet into three samples and combusting each. The three titres were totalled and carbon content calculated. This enabled the known amount of Pt to be present during metal combustion and so carbon analyses could be corrected accordingly for Pt present.

(d) Droplet and Platinum Examination

In order to check the behaviour of the platinum within the Fe-C-S melt a droplet test at 1300°C was performed in a slag for a reaction time of 35 minutes. The droplet was sectioned and mounted. After grinding, polishing and etching in 2% Nital, an optical photomicrograph was obtained.

3.3 TRIMETHYLSILYLATION-GLC; APPARATUS AND PROCEDURES

3.3.1 Materials

(a) Silicate Materials

Natrolite, $\text{Na}_2(\text{Al}_2\text{Si}_3\text{O}_{10}) \cdot 2\text{H}_2\text{O}$ was supplied by R.F.D. Parkinson Ltd., Somerset. Andradite, $\text{Ca}_3\text{Fe}_2(\text{SiO}_4)_3$ and Hemimorphite $\text{Zn}_4(\text{OH})_2\text{Si}_2\text{O}_7 \cdot \text{H}_2\text{O}$ were purchased from R. Tayler Minerals, Surrey.

In addition to the synthetic slags prepared for the droplet work, some FeO-SiO₂ slags were made by the procedure outlined in section 3.2.2. A blast furnace slag was supplied from B.S.C. Scunthorpe Works whilst some LD turndown slags were obtained through Steetley Minerals Ltd.

Lead Oxide-Silica melts were prepared by heating plumbic oxide and precipitated silica in an alumina crucible for 30 minutes at 1000°C. The melt was cast into a metal mould and then crushed to <106 μm when cool. The powder was re-melted (1000°C for 30 minutes), quenched in an ice-water mixture and crushed.

All materials selected for derivatisation were crushed to <106 μm. The analyses of synthetic melts and industrial slags are given in tables 7b, 7c and 7d.

(b) Reagents

Propan-2-ol (May and Baker Ltd.), Hexamethyldisiloxane (Hopkins and Williams), Trimethylchlorosilane (Hopkins and

Williams) and BDH Amberlyst 15 were supplied by Beecrofts, Sheffield. Another source of trimethylchlorosilane ("High Purity Grade") was Pierce and Warriner (UK), Cheshire.

3.3.2 Trimethylchlorosilane Purification

Both brands of trimethylchlorosilane had assays of 95% minimum but a purification process was required to remove the possible presence of SiCl_4 known to cause a peak corresponding to the SiO_4^{4-} derivative in the chromatogram of the blank sample. The purification method was suggested by Masson (private communication) ¹⁵⁹.

About 170 cm^3 of trimethylchlorosilane was placed in a separating funnel. 10 cm^3 of distilled water was carefully added and a ground glass stopper inserted in the funnel. The funnel was gently shaken and the mixture allowed to settle. The glass stopper was removed to release hydrogen chloride and trimethylchlorosilane vapours. The lower aqueous layer was removed via the separating funnel tap. This procedure was repeated four or five times. The use of safety goggles and fume cupboard was necessary due to trimethylchlorosilane being a suspected carcinogenic reagent and the possibility of mixing with water causing an explosive reaction.

The trimethylchlorosilane was left to dry overnight over anhydrous calcium chloride. Fractional distillation using a 20 inch column packed with glass helices followed. The middle cut was collected, corresponding to a constant temperature of 57°C at the distillation head. Plate 5 shows the distillation

unit.

Trimethylchlorosilane was used for trimethylsilylation immediately after distillation.

3.3.3 Trimethylsilyl Derivative Preparation

Two different methods of derivatisation were employed. The first, based on work by Wu et al¹¹³ is essentially the method developed by Lentz¹⁰³ and will be referred to as the Lentz technique. The other technique is that of Masson described as a unified method of trimethylsilylation¹²³.

(a) The Lentz Technique

The quantities of materials used were half that quoted by Wu¹¹³.

65g crushed ice, 75 cm³ concentrated hydrochloric acid, 150 cm³ propan-2-ol and 100 cm³ hexamethyldisiloxane were stirred for 1 hour at room temperature in a glass beaker. 10g Natrolite (<106 µm) was added to the reaction mixture and stirred for a further 16 hours at room temperature. The mixture was filtered and transferred to a separating funnel. The lower aqueous layer was removed and the retained organic layer washed with distilled water. The organic layer was stirred with 2.5g Amberlyst 15 for 1 hour and then distilled using a Dean and Stark trap. The vapour temperature of liquid in the distillation flask was raised to 115°C. The residue in the flask was retained for Gas Liquid Chromatography.

(b) The Masson Technique

1.5g. of silicate material was added to 90 cm³ hexamethyldisiloxane, 10 cm³ propan-2-ol and 2 cm³ distilled water contained in a Teflon jar equipped with tight-fitting screw cap. 20 cm³ of freshly distilled trimethylchlorosilane was added to the mixture and stirred for 5 hours. The mixture was filtered and transferred to a separating funnel. The upper (organic) layer was retained and placed in a small distillation flask. The liquid was distilled to a distillation head temperature of 98-99°C in order to remove unreacted trimethylchlorosilane. The residue was stirred in the capped Teflon jar with 1g Amberlyst 15 for 16 hours. After filtering the liquid was concentrated to about 3-6 cm³ by distillation in a Dean and Stark trap. The residue was retained for GLC analysis.

Plates 6 and 7 show the distillation equipment employed for trimethylsilylation.

(c) Internal Standard

Measured amounts of prepared derivatives were mixed with known volumes of an internal standard. The standard selected was a hydrocarbon Eicosane, C₂₀H₄₂, 15g dissolved in 50 cm³ of n-heptane.

For derivatives prepared by the Masson technique 0.25 cm³ of the internal standard was added to 1 cm³ of the derivative.

3.3.4 Gas Liquid Chromatography

(a) Principles of Chromatography

Chromatography is a separation technique involving some of the physical properties of molecules. The principal properties involved are ¹⁶⁰:-

1. The tendency of a molecule to dissolve in a liquid (solubility).
2. The tendency of a molecule to attach itself to a finely divided solid (adsorption).
3. The tendency for a molecule to enter the vapour state or evaporate (volatility).

Mixtures of substances to be separated by chromatography are placed in a dynamic experimental situation where they can exhibit two of the above properties. In GLC a volatile substance is distributed between a moving gas phase and a stationary liquid phase on an inert support. The support and liquid film is contained in a column and the moving phase termed carrier gas, passed through the column.

If a single component sample is considered, then on introduction to the system it will vaporise and be swept onto the column by the carrier gas. On reaching the stationary phase the major part of the sample will be adsorbed and an equilibrium established between adsorbed vapour and the amount remaining in the carrier gas. The carrier gas will move forward and the small

amount of unadsorbed vapour still in the gas will again achieve equilibrium with the stationary phase. Simultaneously, pure carrier gas will come into contact with the portion of sample originally adsorbed by the liquid. Some adsorbed vapour will then re-enter the gas to re-establish equilibrium. The movement of vapour to and from the carrier gas is the fundamental mechanism of GLC.

Applying the above to a two component sample, the properties of the liquid film are chosen such that the components differ in the extent adsorbed by the liquid and gas. This difference results in separation of the two phases because of different retention times in the column. The use of a detector and recorder will represent the sample components as two separate peaks on a graph.

(b) The Gas Liquid Chromatograph

A Pye 105 Chromatograph was used consisting of three distinct units - the analyser, programmer controller and ionisation amplifier.

The analyser consisted of four sub-units of oven, electrical control unit, gas connection bulkhead and flame ionisation detector head. The oven, powered by the electrical control unit accommodated the chromatographic column suspended from the flame ionisation detector head and injection head. The injection head was heated in order to instantly vaporise components injected through a rubber septum contained in the

injection port, Hydrogen and air were supplied to the flame ionisation detector and ignited by a removable glow plug ignitor. Nitrogen carrier gas was supplied to the column via the injector head. Figure 36 shows a plan view of the analyser unit whilst plate 8 shows the GLC equipment used.

The analyser oven temperature was controlled by a programmable controller. Temperature programming facilities provided a linear temperature increase with time with variable periods of initial and final isothermal operation. This mode of operation is employed for samples having components of widely different boiling points. The aim is to allow the resolution of low boiling point fractions at low temperature whilst gradual temperature increase permits resolution of high boiling point components.

The detector used on the 105 chromatograph was a flame ionisation detector (FID). The principle of operation relies on hydrogen being mixed with effluent gases from the column and burnt in a stream of air. Ions produced in the flame conduct a current from the flame jet, which serves as one electrode, to a second electrode above or around the flame. The elution of carrier gas only results in a background current. Any organic compounds eluted burn to form carbon dioxide (and water) and subsequent ionisation produces a greater current. A flame ionisation amplifier connected to the FID amplified the current and transmitted it to a chart recorder. The amplifier allowed correction of any base-line drift and an attenuation

control was employed during analysis to ensure all peaks fitted on the chart.

An FID is classed as a mass detector whereby the signal generated is proportional to the mass of component reaching the detector in unit time 10^4 . For mass detectors the area under a peak, A, is proportional to the mass, m, of the component.

$$A = fm$$

The proportionality factor, f, is called the detector response factor. The factor not only depends upon the type of detector but the chemical character of the component. Thus, different peak areas will be generated for equal amounts of different components. For closely related compounds an approximation may be made in assuming identical response factors.

(c) Operating Conditions

The Pye 105 Chromatograph was used with a stainless steel column 5 ft long, $\frac{1}{4}$ inch I.D., packed with 10% OV1 on acid washed Chromosorb W, 80-100 mesh. (Phase Separations Ltd.)

Nitrogen and hydrogen flow rates were $40 \text{ cm}^3/\text{min}$. each whilst the air supply registered a pressure of 10 p.s.i.

The temperature programme used was a temperature increase from 170°C to 320°C at 8°C per minute commencing from time of injection. The injection port was heated to $+50^\circ\text{C}$ of the initial column temperature.

A sample size of 1 μ l was obtained by a microsyringe (Terumo Ltd. or Hamilton Ltd.). The time of injection was marked on the recorder chart which moved at 40 inches per hour. During analysis the attenuation control was adjusted accordingly to fit peaks on the chart.

4.1 DROPLET EXPERIMENTS

4.1.1 The Determination of the Initial Composition of the Metal Droplets

An average composition was obtained from the results of three samples, for each high sulphur melt (melts 1, 2 and 3), from which the metal slices to provide the droplets for the refining experiments were to be obtained, Table 5a. The average compositions of melts 4 to 7 based on 14 to 15 samples for each melt are also included in Table 5a and in this case the metal to provide droplets was in the form of pin samples.

For desulphurisation experiments involving metal melts 4 to 7, the initial sulphur content of the droplet slug was assumed to be that of the pin sample from which the slug was taken. A short section of each pin sample was analysed for sulphur and each pin sample was used for only one series of desulphurisation experiments. The corresponding carbon content at zero reaction time was taken as the average carbon concentration of the appropriate melt. A similar approach was used for the decarburisation experiments whereby carbon contents were obtained by the analysis of a section from each pin sample used and the sulphur level taken to be that of the average melt composition. Results for the analyses of pin sections corresponding to droplet masses of 1.0 to 1.2 g are included in Tables 5b to 5e.

The single droplet refining studies were initiated by

performing a number of "blank runs" to determine whether sulphur loss from the droplet occurred during the heating and melting of the metal prior to reaction with the liquid slag. For each "blank run" two adjacent pin sections or metal slices in the case of melts 1, 2 and 3, were involved, one of which was analysed in the original condition. The other metal sample was heated according to the heating cycle used for the stopper and seat technique (see section 3.2.5 (c)) or the suspended droplet technique (see section 3.2.6 (b)). The use of the stopper and seat apparatus involved transfer of the melted pin sample from the stopper and seat into an empty iron crucible internally coated with zirconia. The crucible and contents were dropped to the base of the furnace work tube and allowed to cool in the argon atmosphere. With the suspended droplet apparatus the metal was gently raised to the top of the furnace work tube thus freezing the metal at a time that corresponds to commencement of the slag-metal reaction. Initial and final sulphur contents from the "blank runs" are shown in Tables 6a and 6b.

Greatest sulphur loss was encountered with droplets obtained from the high sulphur melts 1, 2 and 3. The variation of sulphur content for samples from melt 1 showed a decrease of sulphur content. Melt 2 samples showed sulphur pick-up whilst loss and gain was described by melt 3 samples. Variations in sulphur content may be partly attributed to segregation effects in the metal samples not detected in the original melt analyses. For melt 1 samples some sulphur may be driven from the metal during heating and melting. For each high sulphur melt,

therefore, the average value of the two sulphur analyses obtained after the "blank runs" was used as an estimate of the initial sulphur content of the metal droplet at the commencement of slag-metal reaction for the desulphurisation experiments. The carbon content at zero reaction time was taken as the average carbon composition of the relevant melt.

The droplets from the lower sulphur content melts, 4 to 7, used extensively for the suspended droplet technique experiments, gave only slight changes in sulphur content as indicated in Table 6b. For these experiments the sulphur content of the droplet at the start of slag-metal reaction was assumed to be the same as that of the analysed section of the pin sample from which it was taken. The same assumption was made when these lower sulphur melts were used in the stopper and seat experiments.

Droplet masses permitted one sulphur determination only, but reproducibility of the combustion technique using standard samples, was checked and found to be ± 0.002 mass % S. The results presented in Table 6b, with one exception, are in this range. This suggested that the pin samples from which droplet slugs were taken did not exhibit unacceptable chemical inhomogeneity.

Slag samples were also subjected to "blank runs" by heating them at 1300°C for 20 minutes and then cooling by dropping the crucible containing slag to the base of the furnace work tube. No change in the sulphur content occurred as the results coincided with those presented in Table 7a.

4.1.2 The Stopper and Seat Technique

(a) Desulphurisation Results

The experiments performed using the stopper and seat technique, described in Section 3.2.5, involved the use of only one slag composition, designated KCl and which contained 38.31 mass % CaO-28.52 mass % FeO-1.90 mass % Fe₂O₃-31.00 mass % SiO₂-0.27 mass % S. Desulphurisation results were obtained for droplets obtained from pin samples or metal slices taken from each of the melts listed in Table 5a and are presented in Figures 37 to 43 and Tables 8a to 8e. The initial sulphur content of the droplets studied essentially fell into seven groups, these being approximately: 0.51, 0.44, 0.30, 0.12, 0.08, 0.05 and 0.03 mass % S. Investigations commenced with 0.12 mass % S iron and proceeded to the 0.08, 0.05 and 0.03 mass % S levels, since these are reasonably compatible with sulphur concentrations encountered in U.K. L.D. steelmaking practice. The results obtained, which will be described in more detail below, indicated that resulphurisation of the droplet could occur under certain conditions, and it was thought that this might be attributable to the relatively high sulphur content of 0.27 mass %, in the initial slag. A second group of experiments were performed in which the sulphur content of the droplet was increased so as to maintain an initial bulk metal-slag sulphur differential closer to that encountered in LD practice and thereby suppress the reversion phenomena.

For a "0.512 mass % S" droplet sulphur loss was rapid

during the first 5 minutes of reaction in which time the sulphur content fell to 0.123 mass % (Figure 37, Table 8a). Results for longer reaction times exhibited some scatter but a general levelling off in the rate of sulphur removal occurred with the final sulphur content achieved after 20 minutes being 0.065 mass % S. The value obtained for the 15th minute of reaction, 0.028 mass % S, was considered to be anomalous and not an indication of sulphur reversion at 20 minutes reaction. This may be justified by the desulphurisation behaviour shown by droplets of melts 2 and 3 described below.

Desulphurisation of a "0.440 mass % S" droplet (Figure 38, Table 8a) gave the lowest final sulphur level of the three high sulphur melts, achieving 0.020 mass % S after 20 minutes. Sulphur removal was rapid during the initial 5 minutes of reaction and became less rapid in the 5 to 10 minute period. From the slope of the curve obtained, desulphurisation of the droplet appeared to have virtually ceased by 20 minutes reaction time.

A more gradual loss of sulphur was observed from a "0.302 mass % S" droplet (Figure 39, Table 8a) compared with the other high sulphur droplets. The 0 to 10 minutes reaction period brought about a reduction in sulphur content to 0.069 mass % S followed by a subsequent fall to 0.048 mass % S over the 10 to 20 minutes reaction time.

The first experiments were performed using metal droplets initially containing 0.123 mass % S and 0.120 mass % S (Figure 40,

Table 8b). A single line was used to describe the two sets of data. The similarity of these results at their respective reaction times suggested reasonable reproducibility for the overall technique. Desulphurisation was effective during the first 10 minutes of reaction, whilst the results for the 10 to 20 minutes period indicated a decrease in sulphur removal rate. The mean sulphur concentration of the droplets from both sets of data after 20 minutes was 0.022 mass % S.

For a "0.076 mass % S" droplet, sulphur pick-up occurred during the initial 5 minutes of reaction, Figure 41, Table 8c. Desulphurisation then commenced and during the 5 to 15 minute period the droplet sulphur content fell from 0.100 mass % S to 0.034 mass % S. The 15 to 20 minute period gave a very small decrease in sulphur content with the final sulphur level given as 0.033 mass % S.

A further three experiments involved droplets with sulphur contents of 0.057, 0.054 and 0.057 mass % S as shown in Figures 42a, b and c respectively and Table 8d. Reproducibility between these results was not as good as for the "0.12 mass % S" droplet experiments. However, the form of the three desulphurisation graphs was similar. Two of the runs (Figures 42a, b) showed a pick-up of sulphur by the metal droplet during the first 2 minutes of reaction whilst the third run (Figure 42c) involved sulphur pick-up for the initial 5 minutes. After this initial period desulphurisation commenced for a period of 10 to 12 minutes and then levelled off. Final sulphur

contents of 0.037 mass % S and 0.030 mass % S (Figures 42a, b) were achieved. The third run (Figure 42c) had a final sulphur level of 0.038 mass % S (Table 8d).

Desulphurisation of a "0.034 mass % S" droplet commenced after 2 minutes when sulphur pick up had finished (Figure 43, Table 8e). The sulphur content at 2 minutes was 0.068 mass % S and fell to 0.026 mass % S at 20 minutes. This reaction period was described by a straight line of negative slope.

If the sulphur content remaining in the droplet after 20 minutes is taken as an indication of refining efficiency we can define the percentage degree of desulphurisation as:-

$$\% \text{ desulphurisation} = \frac{[\text{mass \% S}]_{\text{Initial}} - [\text{mass \% S}]_{\text{final}}}{[\text{mass \% S}]_{\text{Initial}}} \times 100$$

For the results obtained, the percentage degree of desulphurisation decreased with decrease of initial droplet sulphur content. The best results were obtained with the high initial sulphur droplets with percentage desulphurisations of 87, 95 and 84% for the 0.512, 0.440 and 0.302 mass % S droplets respectively. A high percentage desulphurisation was also recorded for the 0.12 mass % S droplets at 82%. The "0.076 mass % S" droplet gave a figure of 57% desulphurisation whilst the average for the three runs with 0.057, 0.054 and 0.057 mass % S droplets was 37%. The poorest percentage desulphurisation of 23% resulted for the "0.034 mass % S" droplet.

(b) Decarburisation Results

The stopper and seat technique was employed to produce the droplets for two sets of decarburisation experiments the results of which are presented in Figures 44 and 45 and Tables 9a and 9b.

Decarburisation of a 4.35 mass % C - 0.111 mass % S droplet in slag KC1 achieved a final carbon content of 0.66 mass % C after 20 minutes as shown in Figure 44. The first 10 minutes of reaction provided the greatest degree of decarburisation down to 1.35 mass % C at an almost constant decarburisation rate. The rate of decarburisation diminished after 15 minutes reaction time and from the results obtained decarburisation had virtually ceased by 20 minutes reaction time, the respective carbon contents for the 15 and 20 minute droplets being 0.74 and 0.66 mass %.

The second decarburisation experiment involved the reaction of a 4.60 mass % C - 0.050 mass % S droplet, with slag KC1, the results obtained being shown in Figure 45. The most effective decarburisation at an almost constant rate was again attained in the 0 to 10 minute period. The final carbon level after 20 minutes reaction was 0.55 mass % C.

(c) Condition of Reacted Droplets

The crucible containing the slag and droplet was quenched into water or rapidly cooled in an argon jet at the end of the

desired reaction time in order to terminate the slag-metal droplet reaction. After removal from the slag, the droplet was examined and its appearance noted, and in some cases it was photographed, prior to subjecting it to chemical analysis.

Plates 9a to 9e show the appearance of typical droplets for 2, 5, 10, 15 and 20 minutes reaction respectively. These droplets were of initial 4.20 mass % C - 0.123 mass % S composition reacted with slag KCl and the desulphurisation results are featured in Figure 40 and Table 8b. The method of quench had no effect on appearance, but change in droplet appearance did result with length of reaction with the slag. The initial sulphur or carbon contents of the droplets did not indicate any effect on droplet appearance.

Droplets after 2 minutes reaction time had not developed a spherical shape and possessed an ellipsoidal form (plate 9a). It is possible that the impact of the metal on entering the slag was the cause for this since the shape of the droplets for longer reactions were much more regular. A near spherical shape generally resulted after 5 minutes reaction time as shown in plate 9b. The droplet often exhibited a flat area on its surface suggesting that at the time of quenching it had been lying on the bottom of the crucible. This was confirmed in some cases by carefully removing the slag in order to ascertain the position of the droplet within the crucible. The droplet appearance changed markedly for reactions of 10 minutes and longer. The 10 minutes reacted droplet was reasonably spherical

but the surface was covered with craters as a consequence of CO evolution, (Plate 9c). Some droplets showed evidence of metal ejection having occurred in the form of small metal globules attached to the main droplet. These ejection sites were also a feature of 15 minute reacted droplets and caused some distortion of the essentially spherical shape, (Plate 9d). Craters also covered the metal surface but were smaller than for the droplets which had reacted for 10 minutes. Droplets of 20 minutes reaction time also exhibited surface craters and metal ejection sites were more predominant than for other samples, (Plate 9e).

The distortion of the droplets arising from surface craters, ejection sites and subsurface blowholes, all of which are attributable to CO evolution, made it difficult to measure their dimensions. For the majority of experiments three diameters were measured for each clean droplet. Table 10a summarises the droplet diameters for each reaction time by use of mean and standard deviation values. The populations used to calculate these figures involved every droplet diameter recorded for the particular reaction time irrespective of initial composition or reaction studied. The measurement of droplet diameters involved locating a flat area on the droplet. From this 'base' a 'height' measurement was recorded (designated d_1), then 'width' and 'depth' readings were taken (designated d_2 and d_3 dimensions). A breakdown of these dimensions is included in Tables 10b to 10m and covers nearly all the droplets at different reaction times for each desulphurisation and

decarburisation series performed with the stopper and seat technique.

Referring to Table 10a the standard deviation for the 2 minute reaction specimens indicated a large spread of diameters as a consequence of their non-spherical shape as illustrated by Plate 9a. The mean diameter assigned to droplets of 2 minutes reaction is difficult to reconcile with the usual ellipsoidal shape of specimen obtained. However, the mean diameter with associated large standard deviation was employed in order to provide some notion of a characteristic dimension. The 10, 15 and 20 minutes reaction specimens produced more uniformly sized droplets with respect to their mean diameters and associated standard deviations. The mean diameter for the 5 minute reacted droplets was slightly less than those of longer reaction times. The presence of surface craters and subsurface blowholes affected measurement despite efforts made to take dimensions from the distinguishable mother drop and this in part could explain the slightly smaller diameter of the 5 minute reacted droplet.

A comparison of initial and final droplet masses is made in Tables 11a to 11l and it will be noted that both increases and decreases of droplet mass were observed illustrating the difficulty of interpretation of such results. The instances of increased mass suggested possible slag entrainment despite careful droplet preparation prior to analysis. Decreased droplet mass could not be related exclusively to carbon and sulphur removal and in such instances metal ejection was deemed to have occurred. The reacted slag was examined in order to collect metal

ejections but the absence of small metal droplets indicated that no major break up of droplets had occurred. The mean reduction in droplet mass was 7% whilst the mean value for increased droplet mass was about 4%.

(d) Slag-Crucible Examination

The ZrO_2 coated crucibles performed well in the experiments carried out with slag containing 38.31 mass % CaO - 28.52 mass % FeO - 1.90 mass % Fe_2O_3 - 31.00 mass % SiO_2 - 0.27 mass % S; the ZrO_2 coating being effective in preventing welding of the droplet to the iron crucible. However, in experiments with slags of lower lime and higher iron oxide contents the droplet welded to the crucible wall even at reaction times of less than 2 minutes, (Plate 10). The problem of welding could not be solved by variation of the experimental conditions, e.g. changing the slag mass, metal mass, temperature etc. Visual examination of the welded droplet-crucible interface suggested that failure of the ZrO_2 coating had occurred. Interaction between ZrO_2 and iron silicate melts has been encountered by Williams²² who found that iron silicate melts, contained in ZrO_2 crucibles, at temperatures similar to the operating temperatures used in the present work, picked up about 14 mass % ZrO_2 .

A full investigation of ZrO_2 dissolution was beyond the scope of the present work but the interaction between the ZrO_2 coating and two slags, one containing 38.31 mass % CaO - 28.52 mass % FeO - 1.90 mass % Fe_2O_3 - 31.00 mass % SiO_2 - 0.27 mass % S and the other 28.00 mass % CaO - 40.20 mass % FeO - 3.21 mass %

Fe_2O_3 - 28.50 mass % SiO_2 - 0.15 mass % S, was studied using scanning electron microscopy augmented by an EDAX analysis technique. Plates 11a to 12d show the results of such studies, the samples having been obtained from crucibles which had been held containing slag at 1300°C for 20 minutes thus representing the starting point condition of the coating for the slag-droplet reaction.

Plate 11a is a view of the area in the vicinity of the crucible-coating-slag interface where the bulk slag composition was 38.31 mass % CaO - 28.52 mass % FeO - 1.90 mass % Fe_2O_3 - 31.00 mass % SiO_2 - 0.27 mass % S. Plate 11b shows the zirconium distribution for the same field of view. The zirconium is clearly present at the slag-crucible interface. A zirconium concentration profile (Plate 11c) obtained from a line scan perpendicular to the crucible wall confirmed that the ZrO_2 coating had remained intact. Plate 11d, a map for all detectable elements, indicated no major inhomogeneity in the slag phase.

Plates 12a to 12d are corresponding results for the much higher FeO content slag KC2, (28.00 mass % CaO - 40-20 mass % FeO - 3.21 mass % Fe_2O_3 - 28.50 mass % SiO_2 - 0.15 mass % S). The Zr map, Plate 12b, showed no localised regions of Zr and the line scan confirmed this (Plate 12c). Plate 12d showed no major inhomogeneity in the slag phase. The ZrO_2 coating had clearly fully dissolved and been assimilated into the slag. Introduction of an iron droplet would, therefore, have resulted in direct

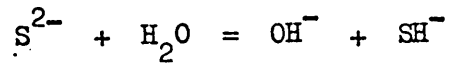
droplet-crucible contact thus explaining the observed tendency for welding to occur.

The SEM work offered qualitative evidence that a significant change in the dissolution rate of ZrO_2 existed between the two slags. For droplet experiments that utilised slags KC2 to KC6 an alternative experimental technique had to be developed, namely the suspended droplet technique.

(e) Reacted Slag Analyses

A number of slags were analysed for ZrO_2 and/or sulphur after reaction with a metal droplet. The results of ZrO_2 analyses for two desulphurisation series are given in Tables 12a and 12b. The details featured in Table 12a show variable ZrO_2 concentrations with low concentrations at longer reaction times. The higher concentrations at 2 and 5 minutes reaction could be due to mechanical break up of the coating and inadvertent mixing into the slag. The concentrations shown in Table 12b showed a maximum value of 0.137 mass % ZrO_2 . It was considered that only a small degree of ZrO_2 dissolution into the liquid slag resulted over the duration of the experiment for this particular slag.

The sulphur content of the slag for crucibles quenched into water was determined and found to be virtually zero. This was attributed to hydrogen sulphide formation, which occurs by hydrolysis of an alkaline earth metal sulphide, e.g. CaS. The reactions involved are:



On boiling, $SH^- + H_2O = OH^- + H_2S \uparrow$

The use of argon quenching caused more sulphur to be retained in the slag (Table 12b) but erratic results were obtained.

4.1.3 The Suspended Droplet Technique

(a) Desulphurisation Results

Desulphurisation experiments were performed using five different slag compositions designated KC2 to KC6 (Table 7a) and each being reacted with droplets from metal melts 4 to 7 (average compositions of melts in Table 5a) of varying initial sulphur content (Table 5d). Analytical results are recorded in Tables 13a to 17 whilst the corresponding desulphurisation graphs are given in Figures 46a to 50d.

Slag KC2 (28.00 mass % CaO - 40.20 mass % FeO -
3.21 mass % Fe₂O₃ - 28.50 mass % SiO₂ - 0.15 mass % S)

The variation with time of the sulphur content of droplets of initially different sulphur content, as a result of interaction with slag KC2 are presented graphically in Figures 46a to 46d and in a tabular form in Tables 13a and 13b.

The results illustrated in Figures 46a to 46c exhibit an initial short period of effective desulphurisation followed by slow or virtual cessation of sulphur removal. The initial rate of desulphurisation decreased as the initial sulphur content

decreased. The behaviour of the 0.034 mass % S droplets illustrated in Figure 46d differed in that sulphur pick up occurred during the initial 2 minutes of reaction.

The series of droplets initially containing 0.120 mass % S displayed very rapid sulphur removal over the initial 5 minutes of reaction (Figure 46a). The longer reaction time results could be considered to exhibit a significant amount of scatter and so involve difficulty in the interpretation of such results. However, the line plotted on this desulphurisation graph highlighted the general trend of the analytical results in that a slow rate of sulphur removal occurred. A final sulphur content after 20 minutes reaction was 0.014 mass % S which gave a percentage degree of desulphurisation of 88%.

A similar form of curve was obtained for the series of droplets initially containing 0.083 mass % S, (Figure 46b). Most rapid desulphurisation was observed during the initial 5 minutes of reaction and slow sulphur removal was indicated to have taken place for reaction times from about 10 to 20 minutes. The final result was 0.026 mass % S which represented 69% desulphurisation.

The three series of experiments involving droplets initially containing sulphur levels of 0.054 mass % S (2 off) and 0.055 mass % S were used to examine the reproducibility of the experimental technique, Figure 46c, Table 13b. Results for the experiments of duplicated reaction times were with one exception in good agreement and had fallen within the standard deviation for sulphur content of the parent melt (0.005 mass % S). The

exception was the 20 minute reacted droplet where sulphur contents of 0.011 and 0.037 mass % S had resulted. Additional results pertained to reaction times of 1, 7.5, 12.5 and 17.5 minutes and with the exception of the latter contributed to the general pattern of the desulphurisation curve. Desulphurisation during the initial period of reaction was not as rapid as for the 0.120 and 0.083 mass % S droplets but occurred over a slightly longer time of 7.5 minutes. The desulphurisation rate during this stage appeared to be almost constant as indicated by the linearity of this part of the curve in Figure 46c. The line ascribed to the results indicated the virtual cessation of sulphur removal from about 10 minutes onwards despite the observed scatter in results for the longer reaction times. The mean of the analytical results at 20 minutes was 0.024 mass % S and represented 56% desulphurisation.

The reaction of slag KC2 with droplets initially containing 0.030 mass % S commenced with sulphur pick up by the droplet increasing its sulphur content to 0.042 mass % S, (Figure 46d). Desulphurisation occurred during the 2 to 20 minute period at an approximately constant rate reducing the sulphur content of the droplet to 0.022 mass %.

Slag KC3 (17.01 mass % CaO - 46.10 mass % FeO -
7.72 mass % Fe₂O₃ - 29.00 mass % SiO₂ - 0.09 mass % S

The results of experiments that involved slag KC3 are given in Table 14 and presented graphically in Figures 47a to 47d. For droplets initially containing 0.100 mass % S and

0.085 mass % S the results show an initial period of rapid desulphurisation followed by a period of slower, more gradual sulphur loss. Fast initial desulphurisation did not take place for the 0.046 mass % S droplet which displayed only the gradual removal of sulphur. The 0.030 mass % S droplet behaved similarly after an initial period of sulphur pick up.

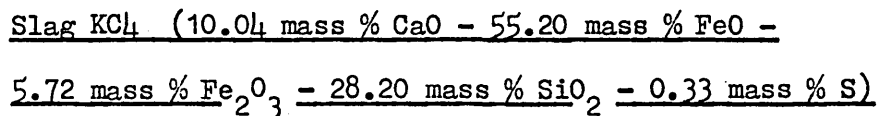
Desulphurisation of the droplets initially containing 0.100 mass % S was most effective during the initial 2 minutes of reaction, during which time the sulphur content of the droplets fell to 0.053 mass % S, (Table 14, Figure 47a). Removal of sulphur began to slow down during the 2 to 7.5 minute period with the 7.5 to 20 minute period showing the slowest rate of desulphurisation. The sulphur levels observed after 15 and 20 minutes was 0.024 mass % S which represents an overall desulphurisation of 76%.

The behaviour of the droplets initially containing 0.085 mass % S was very similar to that for the 0.100 mass % S droplet series, (Table 14, Figure 47b). The most rapid desulphurisation was during the initial 2 minutes reducing the sulphur level to 0.051 mass % S. The 5 to 20 minutes reaction period (although represented as a curve was almost a straight line of negative slope) gave a final sulphur content of 0.018 mass % S, giving a percentage desulphurisation of 79%.

The initial rapid desulphurisation period was absent for the reaction of a 0.046 mass % S droplet, Figure 47c. The 0 to 15 minute period produced desulphurisation down to 0.024 mass % S

and the final 5 minutes represented a virtual constant sulphur level with an endpoint sulphur result of 0.023 mass % S, giving 50% desulphurisation.

The behaviour of the droplets initially containing 0.030 mass % S differed from the others in this group by virtue of sulphur reversion occurring during the initial 5 minutes of reaction, (Figure 47d, Table 14). Gradual desulphurisation from 5 to 20 minutes gave a final sulphur content of 0.015 mass % S (50% desulphurisation).



The results obtained with slag KCl₄ were similar to those obtained with slag KC₃ in that they exhibited a rapid initial rate of desulphurisation with the higher initial sulphur droplets, longer gradual desulphurisation with the "0.056 mass % S" droplets and initial sulphur pick up with the "0.027 mass % S" droplets, (Figure 48a to 48d, Table 15).

The rate of desulphurisation of the "0.110 mass % S" droplets was rapid during the initial 3 minutes, (Figure 48a). The curve describing the general trend was based on consideration that the result for 5 minutes (0.053 mass % S) was anomalous and not an indication of reversion. The sulphur content implied by the curve at 3 minutes was about 0.052 mass % S. For the 5 to 20 minutes period a slow rate of sulphur removal was indicated by an almost horizontal plot with a final sulphur level of 0.034 mass % S, (69% desulphurisation).

"Levelling off" of the desulphurisation curve was not as marked for the droplets initially containing 0.085 mass % S, (Figure 48b, Table 15). For these droplets, most of the sulphur removal occurred in the first 5 minutes and thereafter proceeded steadily until after 20 minutes 0.032 mass % S remained (62% desulphurisation). The final sulphur level was close to that attained for the droplets initially containing 0.110 mass % S.

Results for the droplets initially containing 0.056 mass % S exhibited some scatter, (Figure 48c, Table 15), but produced an essentially straight line of negative slope. A very slow rate of sulphur removal was indicated with no apparent initial fast sulphur removal stage. The final analytical result was 0.040 mass % S and was a slightly higher level than the final values obtained from the initially higher sulphur droplets. The degree of desulphurisation was low at 29%.

The final sulphur content after reaction of the droplets initially containing 0.027 mass % S showed an increase to 0.039 mass % S, (Figure 48d, Table 15). The increase resulted from an initial period of sulphur pick up during the first 2 minutes of reaction resulting in a maximum sulphur content of 0.049 mass % S. The subsequent period of sulphur removal produced an almost linear relationship (Figure 48d), the desulphurisation rate being very similar to that for the "0.056 mass % S" droplets.

Slag KC5 (0.87 mass % CaO - 62.80 mass % FeO -
2.23 mass % Fe₂O₃ - 33.80 mass % SiO₂ - 0.30 mass % S)

The desulphurisation data obtained from droplet interaction

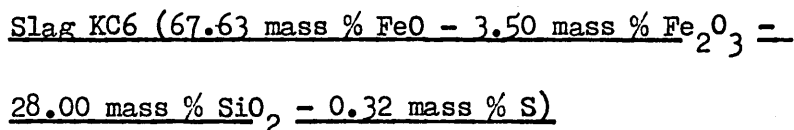
with slag KC5 are presented graphically in Figures 49a to 49d and in tabular form in Table 16. The form of the curves resembled those obtained for the experiments with slag KC4.

Desulphurisation of droplets initially containing 0.102 mass % S and 0.070 mass % S gave similar shaped curves (Figures 49a and 49b). The principal difference between the two was that the higher initial sulphur content droplets exhibited a greater desulphurisation rate during the initial stages of reaction. After 5 minutes reaction the sulphur content had fallen to 0.049 mass % and 0.045 mass % for the "0.102 mass % S" and "0.070 mass % S" droplets respectively which is remarkably close. Little further desulphurisation appeared to occur beyond 5 minutes. For the droplet initially containing 0.102 mass % S the percentage desulphurisation calculated from the sulphur analysis result at 20 minutes of 0.026 mass % S was 74% and from the line plotted (0.038 mass % S) was 63%. The sulphur analysis result of 0.036 mass % S for the droplets initially containing 0.070 mass % S gives 49% desulphurisation whilst the line of best fit gives a final sulphur level of 0.041 mass % S equivalent to 41% desulphurisation.

A straight line of negative slope described the data for the "0.046 mass % S" droplet reaction with slag KC5, (Figure 49c, Table 16). The data was scattered around the line and an initial fast desulphurisation period did not occur. The final sulphur analysis coincided with the line of the graph and was 0.037 mass % S (20% desulphurisation). The sulphur levels

encountered are similar to those for the higher initial sulphur content droplets for reaction times greater than 5 minutes.

The droplets initially containing 0.030 mass % S exhibited sulphur pick up for a 5 minute period at the end of which the sulphur content had risen to 0.059 mass %, (Figure 49d, Table 16). The 5 to 20 minute period showed a steady decrease of sulphur to 0.043 mass % S.



Desulphurisation results for the slag KC6 are given in Table 17, and presented graphically in Figures 50a to 50d.

The droplets initially containing 0.110 mass % S were observed to desulphurise most rapidly during the first 2 minutes. The reaction slowed appreciably during the 2 to 6 minute period and virtually ceased from 6 to 20 minutes, (Figure 50a, Table 17). The final sulphur concentration was 0.028 mass % S (74 % desulphurisation).

A cessation of sulphur removal over the 5 to 20 minute period was also evident from the reaction of droplets initially containing 0.080 mass % S, (Figure 50b, Table 17). Most rapid desulphurisation occurred during the initial 3.5 minutes whilst the final sulphur level was 0.032 mass % S (60% desulphurisation).

Slight sulphur reversion from 0.056 mass % S to 0.058 mass % S occurred in the first 2 minutes of reaction with droplets

initially containing 0.056 mass % S, (Figure 50c, Table 17). Desulphurisation commenced from the second minute and continued to 20 minutes. The sulphur level at the end of this period was 0.027 mass % S, (36% desulphurisation).

Reaction of droplets initially containing 0.030 mass % S showed sulphur reversion for the first 5 minutes to give a maximum sulphur content of 0.043 mass % S, (Figure 50d, Table 17). Subsequent desulphurisation to the 20 minutes reaction time was described by a straight line plot. The final sulphur level was 0.027 mass % S (10% desulphurisation).

(b) Decarburisation Results

Seven series of decarburisation experiments utilised slags KC2 to KC6 with droplets of various compositions (Table 5e) to provide information about carbon levels during droplet-slag reaction. The results are presented in Figures 51 to 55 and Tables 18 to 22.

All the decarburisation curves were characterised by relatively good initial carbon removal during the first 2 minutes. The decarburisation rate decreased thereafter and the 5 to 20 minute reaction period exhibited a slow rate of removal of carbon. The variation of carbon content with time during this period produced almost straight relationships of negative slope. Of the 5 slags used, slag KC2 was the only slag capable of achieving droplet carbon concentrations of less than 1 mass % C after a 20 minutes reaction period.

The best degree of decarburisation was 79% achieved by the reaction of slag KC2 with a droplet initially containing 4.00 mass % C - 0.050 mass % S, (Figure 51, Table 18). The carbon content dropped to 2.20 mass % after 2 minutes and achieved a value of 0.85 mass % C after 20 minutes.

The reaction of slag KC3 with a 4.23 mass % C - 0.111 mass % S droplet produced 55% decarburisation after 20 minutes, (Figure 52, Table 19). The 2 minute carbon level was 3.17 mass % C and the final value 1.90 mass % C.

Three droplets of different initial composition were decarburised by slag KC4 with results presented graphically in Figures 53a to 53c and in tabular form, Tables 20a to 20c. The droplets differed only slightly in carbon content (4.41, 4.72 and 4.10 mass % C) but the variation of the nominal sulphur contents was more significant (0.111, 0.083 and 0.030 mass % S respectively) with the intention of determining the effect on decarburisation. No difference was observed between the decarburisation of 4.41 mass % C - 0.111 mass % S and 4.72 mass % C - 0.083 mass % S droplets, these producing similar results, (Figures 53a and 53b respectively). The percentage decarburisations after 20 minutes reaction were 51 and 52% respectively. Decarburisation of the 4.10 mass % C - 0.030 mass % S droplet (Figure 53c) was not dissimilar to the other two but during the 5 to 20 minute period a near cessation of carbon removal was observed. 40% decarburisation resulted after 20 minutes.

Slag KC5 was reacted with droplets initially containing 4.53 mass % C - 0.083 mass % S and produced a final carbon content of 2.65 mass % representing 41% decarburisation. The results are featured in Figure 54 and Table 21.

Decarburisation of a 4.26 mass % C - 0.111 mass % S droplet by an FeO-SiO₂ slag (KC6) gave the poorest carbon removal (36%) with a final carbon content after 20 minutes of 2.74 mass % C, (Figure 55, Table 22). Compared with decarburisation of a droplet of initially similar composition in slag KC3 (Figure 52, Table 19), reaction with slag KC6 exhibited a more gradual initial decarburisation period (3.42 mass % C at 2 minutes cf 3.14 mass % C) and a slower carbon removal over the 5 to 20 minute period (2.74 mass % C at 20 minutes cf. 1.90 mass % C).

(c) Condition of Reacted Droplets

After a droplet had been allowed to react with the slag for the desired length of time, the experiment was terminated by removing the droplet suspended on the Pt wire from the slag, lifting the crucible and suspended droplet from the furnace tube and quenching the droplet in an argon blast. Plates 13a to 13e show droplet appearances for 2, 5, 10, 15 and 20 minutes reaction respectively, whilst Plates 14a and 14b show general views of reacted droplets. These droplets were of initial composition 4.01 mass % C - 0.027 mass % S and were reacted with slag KC4, the desulphurisation results being shown in Table 15, Figures 48a to 48d. Plates 13a to 13e highlight the typical surface appearances of the droplets at the various reaction times. Initial

sulphur or carbon composition of the droplet did not exhibit any influence on surface character of the droplets. The surface of the 2, 5 and 10 minute reacted droplets did not display any significant differences (Plates 13a, 13b and 13c). The 15 minute reacted droplet was similar but some potential metal ejection sites are apparent in Plate 13d. The appearance of the 20 minute reacted droplet was quite different from that of the other droplets, Plate 13e. Potential metal ejection sites were observed in addition to surface cratering and blowholes.

The plates also illustrate that some metal had migrated up the platinum wire but it is not clear whether this is due to metal being buoyed up during reaction possibly as a result of CO evolution or that on removal of the droplet from the slag, surface tension and inertial forces had partially allowed the wire to be pulled out of the droplet. If the removal of the droplet from the slag does contribute to metal migration and hence a change in droplet shape, it is possible that surface character of the droplets are also affected. In addition, a time delay from removing the droplet from the slag to argon blasting of about 10 seconds was usually incurred which could also influence the final droplet appearance. However, each reacted droplet was examined visually and it was judged that Plates 13a to 13e show a good representation of droplet surface appearance. It was also clear that the presence of surface blowholes was generally associated with droplets reacted for periods of 10 minutes and longer.

The droplets obtained using the suspended droplet technique often assumed an approximate spherical shape or, in most cases an ellipsoidal shape. This latter form was adopted due to the presence of the platinum wire. In order to assign some characteristic dimension to these droplets a mean diameter was calculated for each droplet of a particular reaction time, based on three measurements taken from each droplet. The three measurements taken off every droplet were as near as possible perpendicular to each other to balance out the effects of droplet distortion. The results, used as a summary, are shown in Table 23. Included in Table 23 are the corresponding standard deviation values and are very large, reflecting the distortion encountered. The dimensions recorded for each droplet included in the populations to calculate mean and standard deviation values are given in Tables 24a to 32.

The initial and final masses of reacted droplets are recorded in Tables 33a to 42. The initial mass of the droplet was simply the mass of the section of pin sample used to produce the droplet. The final mass was calculated as the difference between the mass of both the metal droplet with the incorporated Pt wire after reaction and the mass of Pt wire used for the particular experiment. The results show that some droplets had increased in mass while others had decreased. Slag entrainment and metal ejection, respectively, are the most likely explanations for these observations. The mean change in mass of the droplets ranged from +2% to -6% of the droplet mass. The break up of droplets during reaction in the slag never occurred and

subsequent slag examination did not reveal the presence of any small droplets.

(d) Droplet Metal - Pt Wire Examination

Throughout the course of experiments no failure of the platinum wire occurred. A droplet was suspended in liquid slag for 35 minutes and after removal from the slag and quenching in argon the Fe-Pt region of the sectioned droplet was examined. Plate 15 shows the Fe-Pt interface.

The photomicrograph allowed a distinction to be made between the Fe-C-S droplet and the Pt wire. There is an indication of a slight interaction between the iron and platinum, possibly due to dissolution. This is in the form of a small "bands" appearing on the Fe-C-S surface and also at Fe-C-S droplet - Pt interfaces. This band was about 6 μm wide. The ability of the droplet to be suspended for a period in excess of the reaction times of interest suggests minimal Fe-Pt interaction.

(e) Reacted Slag Analyses

Twenty reacted slags (comprising four series of de-sulphurisation experiments) were analysed to obtain sulphur contents (Tables 4.3 to 4.6). The results were erratic. High sulphur levels could not be accounted for by sulphur transferred from the droplet. The reason for such "excessive" sulphur contents is not clear. Low sulphur values could have possibly resulted from the delay incurred in quenching the slag in argon, so that sulphur may have escaped to the atmosphere. Analysis of

furnace cooled slags, in an argon atmosphere, had produced consistent sulphur levels. Only the sulphur analysis data for the metal droplets were, therefore, used in studying the desulphurisation behaviour of the various slag-droplet systems.

4.2 TRIMETHYLSILYLATION - GLC EXPERIMENTS

4.2.1 Treatment of Results

Data from the trimethylsilylation - GLC work were in the form of chromatograms (Figures 56 to 86). The chromatograms featured a number of peaks each representing a component present in the injected sample. Trimethylsilylated silicates of the parent ions SiO_4^{4-} , $\text{Si}_2\text{O}_7^{6-}$, $\text{Si}_3\text{O}_9^{6-}$, $\text{Si}_4\text{O}_{12}^{8-}$ and $\text{Si}_3\text{O}_{10}^{8-}$ are labelled 1 to 5 respectively in Figures 56 to 86. The solvent is labelled 'Sol' and 'IS' signifies the internal standard peak. In order that each peak could fit on the chromatogram the attenuation level had to be adjusted appropriately, the value being indicated opposite each chromatogram.

The retention times (RT) of each silicate derivative peak and the internal standard peaks were determined from a knowledge of the point of injection and chart speed. The retention times obtained from the chromatograms are presented in Tables 47a to 53b. To allow for possible changes in operating conditions during GLC analysis a relative retention time (RRT) defined as the ratio of silicate derivative retention time to internal standard retention time, has been calculated for each silicate derivative and these too are presented in Tables 47a to 53b. The values quoted are to 2 decimal places although such accuracy is not claimed, but the purpose of this is to highlight that slight differences exist between the RRT values of the $\text{Si}_2\text{O}_7^{6-}$ and $\text{Si}_3\text{O}_9^{6-}$ derivatives and also the $\text{Si}_4\text{O}_{12}^{8-}$ and $\text{Si}_3\text{O}_{10}^{8-}$

derivatives.

A quantitative analysis of the silicate derivatives produced from a mineral or slag requires knowledge of the detector response factor for each silicate derivative and that of the internal standard. To determine the response factor of a trimethylsilylated silicate involves producing a chromatogram showing only one peak which is due solely to the trimethylsilylated silicate. Given the mass of silicate used in the trimethylsilylation reaction and the peak area obtained, the detector response factor can be calculated (see Section 3.3.4 (b)). In the present work it is seen that the trimethylsilylation process produces a liquor containing a mixture of silicate derivatives. GLC facilities capable of collecting separated derivatives after elution from the chromatographic column were not available and so individual silicate derivative samples could not be obtained. Consequently, detector response factors are not known. The response factors of the silicate derivatives will, however, be related to the combustible (CH_3 -) portion of the TMS groups attached to each silicate. The ratio of the molecular mass of CH_3 - groups incorporated in the TMS groups attached to the silicate to the total molecular mass of the silicate derivative provide a measure of the amount of combustible portion in each derivative. For the 5 derivatives of interest, the ratio does not vary significantly (0.41 to 0.47) and infers that the response factors may not exhibit large differences. However, in the absence of known values of response factors, the analysis of the

GLC results can, at best, only be considered semi-quantitative.

A semi-quantitative assessment of the relative proportions of silicate derivatives present in a sample was obtained from peak area measurement. Peak area was calculated from:-

$$\text{Peak Area} = \text{Peak height} \times \text{Peak width at half Peak height.}$$

Silicate derivative peak areas were expressed as relative peak areas, i.e. relative to the internal standard peak area. The product of the relative peak area and the derivative liquor volume (i.e. the liquid obtained after the final distillation stage of trimethylsilylation) provides a measure of the proportion of a particular silicate anion present, thus permitting a comparison to be made between different sample materials. Knowing the relative peak area - derivative liquor volume product values for all the silicate anions in a particular sample, the proportion of each respective silicate derivative may be calculated as a percentage of the total of the silicate derivatives detected and could be compared directly with similar terms of other samples. The derivative liquor volume could be measured to an accuracy of 0.05 cm^3 and so the values for percentage of total silicate derivatives detected were quoted to the nearest 0.05%. The peak area, relative peak area and the relative peak area - derivative liquor volume product for each silicate derivative peak in each chromatogram are presented in Tables 47a to 53b.

4.2.2 The Lentz Technique

The Lentz technique was employed primarily for silicate

derivative peak identification. Results are quoted in Figures 56 and 57 and Tables 47a and 47b.

Results of a "blank sample" (Figure 56, Table 47a), where the trimethylsilylation procedure is followed but no slag or mineral is added to the reaction mixture, showed that the material injected into the chromatograph was essentially solvent, hexamethyldisiloxane. Some material was designated as SiO_4^{4-} derivative (peak 1) but the peak was small despite the most sensitive attenuation level that avoided 'noise' problems being used (i.e. 20×10^2 attenuation). The volume of derivative liquor (3.25 cm^3) that resulted from this "blank sample" was small compared to the volume obtained after trimethylsilylation of the mineral, Natrolite (20.30 cm^3). This further suggests that the liquor remaining after trimethylsilylation was solvent as the small volume was a result of the distillation stage removing much of the solvent.

Results for the mineral Natrolite, $\text{Na}_2(\text{Al}_2\text{Si}_3\text{O}_{10}) \cdot 2\text{H}_2\text{O}$, (Figure 57, Table 47b), provided peak retention time and peak area data. Five types of silicate anion derivative were detected by comparing the positions of peaks featured in a published chromatogram of Natrolite¹¹³ with those in the obtained chromatogram. The most abundant anion derivative was attributed to $\text{Si}_3\text{O}_{10}^{8-}$, which in the case of Natrolite is the desired result^{103, 114}, and accounted for 45.50% of the total detected anion derivatives present. Side reactions had occurred resulting with the formation of SiO_4^{4-} , $\text{Si}_2\text{O}_7^{6-}$,

$\text{Si}_3\text{O}_9^{6-}$ and $\text{Si}_4\text{O}_{12}^{8-}$ derivatives to the extent, 23.95, 18.75, 8.30 and 3.50% respectively, of the total anion derivatives present.

4.2.3 The Masson Technique

The Masson technique of trimethylsilylation was applied to a range of silicate-containing materials. Chromatograms from subsequent GLC analysis of derivatives are presented in Figures 58 to 86. Retention and peak area data are given in Tables 48a to 53b.

(a) "Blank Samples"

The term "blank sample" refers to a liquor produced by the trimethylsilylation process but no mineral or slag was added to the reaction mixture. Figure 58 and Table 48a give details of a "blank sample" result where untreated TMCS was employed in the trimethylsilylation reaction mixture. A dominant peak was detected that corresponded to the position of the SiO_4^{4-} anion derivative (relative retention time 0.23). The peak was labelled 'peak 1' and was recorded at an attenuation level of 2×10^4 . The component had a relative peak area - derivative liquor volume product value of 0.56 and was considered to be of significant proportion of the material produced by the trimethylsilylation technique. In addition to the solvent, internal standard and the SiO_4^{4-} derivative peak, a fourth peak appeared on the chromatogram prior to peak 1. The source of this peak could not be

identified but did not interfere with the peaks of interest.

For a "blank sample" where trimethylsilylation was performed using pretreated TMCS, different results emerged (Figure 59, Table 48b). The peak that corresponded to the SiO_4^{4-} derivative position was barely distinguishable at the lowest attenuation level of 20×10^2 . The relative retention time was 0.20 and the relative peak area - derivative liquor volume product was 0.0003. The designated peak 1 was considered as insignificant and no other peaks appeared that could interfere with silicate derivative peaks.

The results for the "blank samples" prepared by the Masson technique clearly show that TMCS must be purified prior to use in the trimethylsilylation reaction mixture to ensure that an interference peak corresponding to the SiO_4^{4-} derivative in the chromatogram does not appear. The problem occurs due to SiCl_4 impurity in the TMCS which under the experimental conditions hydrolyses to form orthosilicic acid and eventually, trimethylsilylated SiO_4^{4-} anions 118, 159.

(b) Minerals

Three types of mineral were trimethylsilylated by the Masson technique. The trimethylsilylation of Natrolite was performed to determine whether similar chromatograms to those from Natrolite trimethylsilylated by the Lentz technique were produced. The peak area information permitted a direct comparison of the accuracy of the two trimethylsilylation

techniques to be made, i.e. to identify the technique which produces the largest percentage of the $\text{Si}_3\text{O}_{10}^{8-}$ derivative. The trimethylsilylation of Hemimorphite $\text{Zn}_4(\text{OH})_2\cdot\text{Si}_2\text{O}_7\cdot\text{H}_2\text{O}$ and Andradite $\text{Ca}_3\text{Fe}_2(\text{SiO}_4)_3$ should provide chromatograms with the main peaks being due to the $\text{Si}_2\text{O}_7^{6-}$ derivative and SiO_4^{4-} derivative respectively. The peak retention time data confirms the peak identifications made initially (section 4.2.1). Peak area information allows an assessment of the accuracy of the trimethylsilylation technique in producing trimethylsilylated silicates that should retain the respective $\text{Si}_2\text{O}_7^{6-}$ and SiO_4^{4-} structures of the minerals.

The results for Natrolite show relative retention times similar to those obtained using the Lentz technique (Figures 60 and 61, Tables 49a and 49b). Peak area results however (Tables 49a and 49b) differed from the results obtained using the Lentz technique. The two sets of results for Natrolite involved two separate trimethylsilylation (Masson technique) - GLC exercises performed at different times. The similarity of the results are indicative of the reproducibility of the Masson trimethylsilylation technique. The dominant derivative peak was due to the $\text{Si}_3\text{O}_{10}^{8-}$ anion that accounted for 67.70% and 69.10% of the fully trimethylsilylated silicate anion derivatives detected for the two respective experiments (Tables 49a and 49b). The presence of peaks 1 to 4 in the two chromatograms (Figures 60 and 61) indicate that side reactions must have taken place during the trimethylsilylation process to produce silicate anions not present in Natrolite which should

only contain $\text{Si}_3\text{O}_{10}^{8-}$. The trimeric ring derivative was the main side reaction product and accounted for about 12.50% of the silicate anion derivatives detected. The amount of SiO_4^{4-} derivative present was about 10% and for the $\text{Si}_4\text{O}_{10}^{8-}$ derivative about 4%. The results for Natrolite showed that the Masson trimethylsilylation technique was more accurate than the Lentz technique.

Duplicate trimethylsilylation - GLC experiments performed at different times for the Hemimorphite mineral, $\text{Zn}_4(\text{OH})_2\text{Si}_2\text{O}_7 \cdot \text{H}_2\text{O}$, showed the desired peak, for the $\text{Si}_2\text{O}_7^{6-}$ derivative, to be the most prominent (Figures 62 and 63, Tables 49c and 49d). Reasonable reproducibility of the trimethylsilylation technique was achieved between the two experiments, the respective amounts of the $\text{Si}_2\text{O}_7^{6-}$ derivative being 76.40% and 83.00%. The difference of about 7% appeared to be largely accounted for by the amount of the tetrameric derivative, $\text{Si}_4\text{O}_{12}^{8-}$, formed by side reaction, the corresponding values being 15.30% and 9.45%. The proportions for the SiO_4^{4-} , $\text{Si}_3\text{O}_9^{6-}$ and $\text{Si}_4\text{O}_{12}^{8-}$ derivatives were low at 4.15 and 3.75%, 1.40 and 1.90% and 2.80 and 1.90% respectively.

GLC analysis of the trimethylsilylated mineral Andradite, $\text{Ca}_3\text{Fe}_2(\text{SiO}_4)_3$ (Figure 64, Table 49e) produced a chromatogram with the main silicate derivative being of the SiO_4^{4-} anion which is the expected result with this mineral. The SiO_4^{4-} derivative accounted for 66.65% of the total silicate derivatives present. Very sensitive attenuation levels had to

be employed in order to produce reasonably high peaks which suggested a poor yield of trimethylsilyl derivatives. The amounts of the $\text{Si}_3\text{O}_9^{6-}$, $\text{Si}_4\text{O}_{12}^{8-}$ and $\text{Si}_3\text{O}_{10}^{8-}$ derivatives were barely detectable but the amount of the $\text{Si}_2\text{O}_7^{6-}$ derivative present was 33.35%. A number of unidentified peaks were present on the chromatogram (Figure 64) and these probably only appeared by virtue of the sensitive attenuation level employed. These peaks did not in any case interfere with the silicate derivative peaks.

Mixtures of Hemimorphite and Natrolite were trimethylsilylated and analysed by GLC in order to determine whether the trimethylsilylation of a silicate mixture could accurately reproduce silicate derivative proportions based on those obtained from the individual minerals. Results for a 0.75g Hemimorphite + 0.75g Natrolite mixture are presented in Figure 65, Table 49f. Included in Table 49f is the predicted percentage silicate derivative proportions based on the results for Hemimorphite (Table 49d) and Natrolite (Table 49b). The most abundant silicate derivative was due to the $\text{Si}_2\text{O}_7^{6-}$ anion accounting for 61.95% of total derivative detected. This figure exceeds the predicted value by a difference of approximately 19%. The $\text{Si}_3\text{O}_{10}^{8-}$ anion derivative accounted for 19.70% of total derivative detected which is, approximately, a difference of 16% lower than that predicted. A mixture of 0.5g Hemimorphite + 1.0g Natrolite indicated the proportions of the $\text{Si}_2\text{O}_7^{6-}$ and $\text{Si}_3\text{O}_{10}^{8-}$ derivatives to be 39.30% and 41.05% respectively (Figure 66, Table 49g). In this

instance the $\text{Si}_2\text{O}_7^{6-}$ anion derivative proportion exceeded the predicted value by approximately 10% whilst the amount of $\text{Si}_3\text{O}_{10}^{8-}$ derivative was about 6% lower than predicted. Results for both mixtures indicated that SiO_4^{4-} , $\text{Si}_3\text{O}_9^{6-}$ and $\text{Si}_4\text{O}_{12}^{8-}$ derivatives were the products of side reactions occurring during the trimethylsilylation treatment. Each of these species accounted for about 5 to 7% of the total silicate derivative detected. The trimethylsilylation of mineral mixtures will be discussed in more detail in Section 5.1.1. However, the results for Natrolite only did prove that the Masson technique involved less side reactions than the Lentz technique. On this basis, the Masson technique was adopted to study a range of industrial and synthetic slags.

(c) Industrial Slags

Results obtained for a trimethylsilylated iron blast furnace slag are presented in Figure 67, Table 50a. Figure 68 and Table 50b present data obtained for an LD slag.

For both slags the chain anion derivatives of SiO_4^{4-} , $\text{Si}_2\text{O}_7^{6-}$ and $\text{Si}_3\text{O}_{10}^{8-}$ were the most abundant species.

The blast furnace slag (34.02 mass % SiO_2 - 0.78 mass % FeO - 41.00 mass % CaO - 7.95 mass % MgO - 0.95 mass % MnO - 13.90 mass % Al_2O_3 - 1.29 mass % S) showed the derivative of the $\text{Si}_2\text{O}_7^{6-}$ chain to be the main component (41.20%) and the SiO_4^{4-} anion derivative to be the second most abundant (29.40%). The trimer chain derivative accounted for 17.65% of the total

derivative detected whilst the two ring species were present in similar amounts of 5.90% each.

The main anion derivative of the LD slag (13.00 mass % SiO_2 - 30.90 mass % FeO - 42.70 mass % CaO - 4.70 mass % MgO - 0.45 mass % Al_2O_3 - 1.87 mass % P_2O_5), was that of the SiO_4^{4-} anion (61.55%) with the dimeric derivative present at 23.10%. The $\text{Si}_3\text{O}_{10}^{8-}$ chain derivative and $\text{Si}_4\text{O}_{12}^{8-}$ ring derivative were both detected and present at 7.70% each. The $\text{Si}_3\text{O}_9^{6-}$ ring derivative was detected but was considered insignificant with respect to the other species.

(d) Synthetic Slags

Results pertaining to binary FeO-SiO_2 synthetic slags are presented in Figures 69 to 76, Tables 51a to 51h, whilst Figures 77 to 81, Tables 51i to 51m refer to CaO-FeO-SiO_2 synthetic slags.

Relative retention times (Tables 51a to 51m) for the peaks labelled 1 to 5 (Figures 69 to 81) compared well with those for the mineral results and industrial slags and provided the basis for silicate derivative peak identification.

Despite the wide range of slag compositions studied the percentage proportions of each particular silicate anion derivative were found to be similar (Tables 51a to 51m). For the binary slags the proportion of the SiO_4^{4-} derivative fell into the 66 to 76% range whilst the proportions in the ternary

melts were around 62 to 70%. The second most abundant derivative in all cases was that of the $\text{Si}_2\text{O}_7^{6-}$ anion. In the binary slag it accounted for 18 to 27% of the total silicate anion derivative detected and 22 to 26% in the ternary slags. For both binary and ternary slags the trimeric chain derivative was present at 2 to 8% whilst derivatives of the silicate rings $\text{Si}_3\text{O}_9^{6-}$ and $\text{Si}_4\text{O}_{12}^{8-}$ were, in all cases, a very small proportion of the total derivative detected. The proportion of the ring anion derivatives did not exceed 2.5%.

Two binary slags (slag BF3 : $\text{FeO}-0.39\text{xSiO}_2$ and slag 4 : $\text{FeO}-0.46\text{xSiO}_2$) both in a quenched condition and a slow cooled condition, were trimethylsilylated. Results for each slag (Figures 72 to 75, Tables 51d to 51g) indicated that the thermal history of the slag had no effect on the proportions of silicate anion derivatives detected.

(e) $\text{PbO}-\text{Al}_2\text{O}_3-\text{SiO}_2$ Slags

The trimethylsilylation work on synthetic slags of the $\text{FeO}-\text{SiO}_2$ and $\text{CaO}-\text{FeO}-\text{SiO}_2$ systems produced the SiO_4^{4-} anion derivative as the major component irrespective of SiO_2 composition of the slag. It was decided to perform a series of trimethylsilylation experiments on a different type of synthetic slag to determine whether different proportions of silicate anion derivatives could be achieved from synthetic slags of different SiO_2 compositions. The system $\text{PbO}-\text{SiO}_2$ was selected and three slag compositions were made. The production

of two of these slags involved Al_2O_3 contamination from the Al_2O_3 crucible during melting of the slag-making materials. A third slag, however, involved very little Al_2O_3 pick up (0.20 mass % Al_2O_3). Analyses of these $\text{PbO-Al}_2\text{O}_3\text{-SiO}_2$ slags are presented in Table 7d.

Results from the trimethylsilylation of three $\text{PbO-Al}_2\text{O}_3\text{-SiO}_2$ slags of slightly differing composition are presented in Figures 82 to 84, and Tables 52a to 52c.

The chromatographic results indicated that different proportions of the silicate anion derivatives were present in each case. In all three the most abundant was that of the SiO_4^{4-} anion. The proportion of monomeric derivative decreased as the amount of silica in the slag increased.

For a $\text{PbO-0.14xAl}_2\text{O}_3\text{-0.25xSiO}_2$ slag (Figure 82, Table 52a) only the monomeric and dimeric derivatives were present in any significant amounts, and had relative proportions of 71.45% and 28.55% respectively.

A $\text{PbO-0.11xAl}_2\text{O}_3\text{-0.32xSiO}_2$ slag revealed the presence of monomeric and dimeric silicate anion derivatives in the proportions of 50.00% and 30.00% respectively (Figure 83, Table 52b). The tetramic ring and chain derivatives each accounted for 10.00% of the total derivative detected.

The proportion of SiO_4^{4-} anion derivative further decreased in the PbO-0.36xSiO_2 slag which contained less than

$0.01xAl_2O_3$ (Figure 84, Table 52c), to a level of 42.85%. The $Si_2O_7^{6-}$ and $Si_3O_{10}^{8-}$ derivatives had increased to respective proportions of 35.70% and 21.45%. The ring species were present in insignificant amounts.

(f) Silica Samples

Further trimethylsilylation experiments employed the use of silica in the trimethylsilylation process. This was to determine whether the presence of "free" silica in the trimethylsilylation reaction mixture could produce 'interference' peaks and thus provide some explanation for results of the FeO-SiO₂ and CaO-FeO-SiO₂ synthetic slags. Two forms of silica were used. Firstly, precipitated SiO₂ (BDH grade) which is the material used in preparation of the synthetic slags (see Section 3.2.2) and secondly the use of a sample of fused SiO₂ rod, crushed prior to use. Results are presented in Figures 85 and 86 and Tables 53a and 53b.

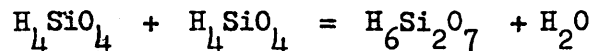
In both cases very small peaks (labelled 1) were found at the position corresponding to the SiO₄⁴⁻ derivative. Both had relative retention times of 0.21. The relative peak area - derivative liquor volume products were small for each sample at 0.003 and 0.008 (Tables 53a and 53b). In comparison with values obtained from silicate containing minerals and slags the results of the experiments on the silica samples did not suggest that significant trimethylsilylation had occurred nor that the silica was capable of undergoing side reactions during the trimethylsilylation process to generate ionic species.

5.1 THE DETERMINATION OF ANIONIC CONSTITUTION IN SILICATE MATERIALS

5.1.1 The Trimethylsilylation of Silicate Minerals

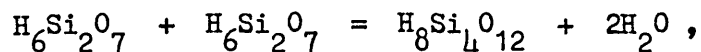
The trimethylsilylation of a mineral of known silicate structure allows an assessment of the accuracy of the trimethylsilylation technique to be made. Results for Natrolite confirmed that the Masson unified technique involved less side reactions than the Lentz technique, but as expected the trimethylsilylation of minerals namely Andradite, Hemimorphite and Natrolite, by the Masson technique, still involved some side reactions ¹⁰⁸.

Trimethylsilylation of Andradite and Hemimorphite highlighted some particular side reactions found by previous workers ¹⁰⁸. Derivatisation of Andradite involved a polymerisation side reaction to produce some $\text{Si}_2\text{O}_7^{6-}$ anion derivative which is probably attributable to the high reactivity of the (expected) SiO_4^{4-} anion. This makes quantitative trimethylsilylation of orthosilicate structures difficult ¹⁰⁸, ¹⁰⁹. The following equation involving silicic acids may be used to describe the polymerisation reaction:-



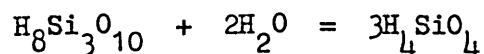
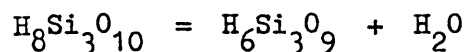
Subsequent replacement of the -H groups on the disilicic acid by TMS groups produce the TMS derivative. With Hemimorphite the major side reaction, also observed by other workers ¹⁰⁸, was the formation of the $\text{Si}_4\text{O}_{12}^{8-}$ anion derivative. The

polymerisation reaction may be represented by:-



with substitution of TMS groups for -H groups on the cyclic tetramer forming the derivative.

Data is not available in the literature for Natrolite, trimethylsilylated by the Masson technique, but the main side reactions observed in the present work were the formation of the $\text{Si}_3\text{O}_9^{6-}$ and SiO_4^{4-} anion derivatives. Possible reactions are:-



Again, replacement of -H groups by TMS groups produces the trimethylsilyl derivatives.

The ability of the trimethylsilylation technique to retain the original silicate structure in the form of trimethylsilyl derivatives was, in the present work, not as good as the claims made by other workers¹⁰⁸. However, the observed reproducibility of results for both Hemimorphite (Tables 49c and 49d) and Natrolite (Tables 49a and 49b) allowed the technique to be used to make interpretations of chromatograms for materials of unknown silicate structures.

The results for Hemimorphite and Natrolite mixtures, however, imply that the technique is not able to trimethylsilylate a silicate mixture to produce silicate derivatives in

proportions that are representative of the mineral mixture (Tables 49f and 49g). The results suggest that the $\text{Si}_3\text{O}_{10}^{8-}$ anion derivative is depolymerised during the trimethylsilylation process and boosts the proportion of $\text{Si}_2\text{O}_7^{6-}$ anion derivative. The combined effects of the different side reactions from each mineral in a mixture during trimethylsilylation may make assessment of the original silicates present virtually impossible. The results are not in agreement with the work of Gotz and Masson ¹¹⁹ on the trimethylsilylation of Olivine, Hemimorphite and Laumontite mixtures where experimental determinations were in good agreement with the predicted silicate anion distributions based on results for the individual minerals. The published results are reproduced in Tables 54 and 55 and it is assumed that the calculated values in Table 55 were based on the data in Table 54. Using the information from both these tables, a silicon balance has been used to check the 'calculated' values in Table 56. The results in Table 56 highlight some inconsistencies. The trimethylsilylation behaviour from the silicon balance infers that breakdown of the $\text{Si}_4\text{O}_{12}^{8-}$ anion derivative occurs resulting in less $\text{Si}_4\text{O}_{12}^{8-}$ anion derivative, but more SiO_4^{4-} anion derivative than expected. These discrepancies may be due to the data in Tables 54 and 55 taking account of the absolute yields of the trimethylsilylated species despite no reference being made to such details. The absolute yield can depend upon the amounts of mineral and water included in the reaction mixture ^{108, 116} and the leachability of the cations present ^{108, 112}. Differences in leachability can

lead to a situation of preferential leaching¹¹¹ and may be very important where mineral mixtures are concerned due to the various cations present.

With reference to the present work, the use of data from Hemimorphite (Table 49d) and Natrolite (Table 49b) should be suitable to permit an estimation of the relative yields of the two minerals. The experiments for the individual minerals employed 1.5g of mineral with similar reagent quantities and produced identical volumes of derivative liquor. For a mineral mass of 1.5g, Hemimorphite contains 0.52g of silicate and Natrolite 0.96g. The greater mass of silicate available for trimethylsilylation in Natrolite compared with Hemimorphite should be reflected on the chromatogram by their total peak areas due to silicate anion derivatives. This will also be indicated by the totals of the relative peak area - derivative liquor volume product term. The latter values are 2.65 for Hemimorphite and 2.75 for Natrolite. Similarity of these values and the difference in respective amounts of silicates available for trimethylsilylation suggest that the yield of silicate anion derivatives from Natrolite is less than that for Hemimorphite. A difference in yields does not fully explain the discrepancies between the calculated and observed silicate anion derivative proportions for Hemimorphite and Natrolite. However, the lack of a precise assessment of absolute yields does contribute to the discrepancies. A further consideration is that the calculated silicate anion derivative proportions for the mixtures (Tables 49f and 49g) were based on data from

individual minerals where different mineral masses were employed compared with those in the mixtures. The amount of mineral can affect yield and it has been reported¹¹⁶ that as silicate quantity in the reaction mixture is increased, higher TMS derivatives may form by polymerisation and not be detected on the chromatogram. In the present work the mineral quantities in the reaction mixture were decreased relative to their individual trimethylsilylations. This may have altered yields and caused differences between observed and calculated results. One possible effect could be an enhanced trimethylsilylation of Hemimorphite which would account for the high proportions of the $\text{Si}_2\text{O}_7^{6-}$ anion derivative.

The trimethylsilylation of mineral mixtures in the absence of data on absolute yields may be misleading. The dependence of yield on factors such as cation leaching and mineral quantities is extremely relevant to mineral mixtures. It is, therefore, very difficult to determine whether the chromatographic results are due to anionic redistribution or whether yield effects are chiefly responsible. The reproducibility of the trimethylsilylation technique when applied to individual minerals, given that some side reactions occur, may be a better indicator of the potential of the technique to provide details of silicate structures in simple slag systems.

5.1.2 The Trimethylsilylation of Industrial Slags

Results from trimethylsilylated slags, unlike minerals, cannot be compared with a "reference" structure.

The iron blast furnace slag used in the present investigation is very similar in composition to a blast furnace slag trimethylsilylated by other workers¹²³ (Table 57a). The chromatographic results were compared by converting the peak area data obtained by these workers into percentage proportions of the SiO_4^{4-} , $\text{Si}_2\text{O}_7^{6-}$, $\text{Si}_3\text{O}_9^{6-}$, $\text{Si}_4\text{O}_{12}^{8-}$ and $\text{Si}_3\text{O}_{10}^{8-}$ anion derivatives relative to their total peak area. Table 57b shows the converted values obtained and the results of the present experiments.

The comparison shows quite close agreement between the proportions of the three chain anion derivatives. The main differences arise in the results for the $\text{Si}_3\text{O}_9^{6-}$ and $\text{Si}_4\text{O}_{12}^{8-}$ ring anion derivatives although the total proportions of the two species are close.

If the blast furnace slag composition used in this investigation (Table 57a) is considered to consist essentially of CaO , MgO and SiO_2 then conversion of their mole fractions to total unity shows that the mole fraction of MgO remains relatively low at 0.13. Assuming MgO to be "equivalent" to CaO and adding their mole fraction values together, the slag composition considered in terms of a binary system approximates to $\text{CaO}-0.39\text{xSiO}_2$ (Table 57a). Silicate anionic fractions based on the Masson Branched Chain Model (Section 2.3.2 (b)) where k_{11} equals 0.0016 can be calculated for this binary slag composition giving 0.62, 0.20 and 0.08 for the SiO_4^{4-} , $\text{Si}_2\text{O}_7^{6-}$ and $\text{Si}_3\text{O}_{10}^{8-}$ species respectively. These values clearly

show that the main species expected is the SiO_4^{4-} and is characteristic of the model predictions for the CaO-SiO_2 system up to the metasilicate composition as shown in Figure 22. The corresponding anionic fractions calculated from the GLC data (Appendix 1a) are 0.36, 0.28 and 0.08 which suggests that there is a larger amount of the $\text{Si}_2\text{O}_7^{6-}$ anion than predicted by the Masson Branched Chain Model and certainly less SiO_4^{4-} . Discrepancies between the observed and predicted results will arise from adjusting the blast furnace slag composition to that of a binary system in order to use the model. The assumption of MgO being "equivalent" to CaO is not strictly valid and in addition the slag actually contained 10.5 mass % Al_2O_3 (0.08 mole fraction). The effect of this component on the silicate structure in the slag and the trimethylsilylated structures cannot be accounted for.

Despite the observed results not following the trends predicted by the Branched Chain Model the similarity with earlier chromatographic work¹²³ is interesting. A comparison with this work shows that for similar slag compositions trimethylsilylated under similar experimental conditions, the main chromatographic peak was due to the $\text{Si}_2\text{O}_7^{6-}$ anion derivative (Tables 57a and 57b). The earlier work mentioned the possibility of Melilite type materials ($\text{Ca}_2\text{MgSi}_2\text{O}_7$) being present in the slag thus boosting the proportion of dimeric derivative. This would provide an explanation why the obtained results differ to the Branched Chain Model predictions.

The trimethylsilylation of the LD slag showed the predominance of the SiO_4^{4-} anion derivative. The LD slag is basic (Table 57c) and so the results are qualitatively in line with what would be expected. Tables 57c and 57d give a comparison with published results¹²³ for an open hearth furnace slag, as converted in a manner similar to that used for the blast furnace slag. The LD slag is more oxidising than the open hearth slag (Table 57c) but a degree of similarity exists in the silicate anion derivative proportions for each slag.

The trimethylsilylation of industrial slags by the unified technique compares well with the data of other workers. Although no definitive structure can be used as a "reference" the technique gives, on a qualitative basis, the results to be expected, i.e. higher anion derivatives present in acid compositions and a predominance of monomeric derivative in a basic slag.

5.1.3 The Trimethylsilylation of Synthetic Slags

The results for trimethylsilylated FeO-SiO_2 and CaO-FeO-SiO_2 slags (Tables 51a to 51m, Figures 69 to 81) exhibit very similar proportions of each anion derivative present. The SiO_4^{4-} anion derivative was always the dominant species and this appeared to be the case irrespective of the silica concentration of the slag. For FeO-SiO_2 slags, oxygen balances were constructed from the GLC data assuming that oxygen anions in the slag were derived from complete dissociation of FeO and that the amount of oxygen

"consumed" was determined by the proportions of each silicate anion detected. (Method of calculation is illustrated in Appendix 1a). Only those slags of basic composition satisfied the balance in that there was sufficient oxygen available from the basic oxide to form the various silicate anions present in the proportions suggested by GLC. The similarity of results for the CaO-FeO-SiO₂ slags made it impossible to establish whether or not a variation in the relative proportions of CaO and FeO affected silicate constitution.

Data obtained for these synthetic slags imply a radical departure from accepted ideas on slag structure. The indication of a very high SiO₄⁴⁻ anion content even in acid slag compositions requires that factors involving both the trimethylsilylation technique and the slag itself be examined to determine the reason for this trend.

Slags were melted twice to ensure complete fusion. For samples in quenched and slow-cooled conditions a second re-fusion was performed but this gave no significant difference in the GLC results. Incomplete fusion would have retained some "free" SiO₂ yielding a fused portion more basic than the overall chemical composition suggests. This in turn would be reflected in the resultant trimethylsilyl derivatives as it was established that "free" SiO₂ did not respond to trimethylsilylation (Tables 53a and 53b, Figures 85 and 86). However, in practice, all slags appeared to be completely fused. Small amounts of incompletely fused material are in any case unlikely to

compensate and cause the similarity of the obtained derivative proportions.

The results raise doubts as to the usefulness of the present trimethylsilylation and GLC technique in assessing the ionic constitution of these synthetic slags. The presence of higher anion derivatives were, however, detected in the blast furnace slag suggesting that depolymerisation processes giving a predominance of SiO_4^{4-} anion derivative, had not occurred in this case. The major difference in composition between the blast furnace and synthetic slags was the FeO content, with the former having an almost insignificant concentration. The LD slag studied had an FeO concentration close to some of the synthetic slags giving better agreement between the GLC results.

The results indicate the possibility that the FeO or rather the presence of the Fe^{2+} cation, may be capable of affecting the trimethylsilylation process in some way. Minerals containing iron have been trimethylsilylated but those involving the Fe^{2+} cation were usually of the orthosilicate structure¹⁰⁸. In this situation the overriding problem has been considered to be a polymerisation side reaction due to high reactivity of the SiO_4^{4-} anion^{108, 109}. Currell et al¹¹² have cited the work of Petzold¹⁶¹ which suggests that the presence of iron can aid cation leaching. They went on to prove this for the mineral Hedenburgite, $\text{CaFe}(\text{Si}_2\text{O}_6)$, which involves the ferrous cation.

Good cation removal would mean that silicic acids

presumably corresponding in structure to the original silicates present, would be readily formed. The success of the unified technique of trimethylsilylation is attributed to gradual leaching of the cation followed by almost instantaneous substitution of the -H groups of the silicic acids by TMS groups. If cation leaching is, therefore, enhanced by virtue of iron contained in a silicate, it is possible that a more rapid generation of silicic acid occurs. This may provide more favourable circumstances for depolymerisation/polymerisation equilibria to compete with the trimethylsilylation reaction.

The mechanism suggested above places emphasis on the Fe^{2+} cation. An iron cation can exist in solution in three different oxidation states with the 2+ and 3+ states being the most common. It is necessary to establish that the existence of two types of iron cation in solution via a redox mechanism, does not interfere with trimethylsilylation. Fe^{2+} in aqueous solution can oxidise to Fe^{3+} but in an acidic solution this process is slow. The trimethylsilylation reaction mixture was acid and the aqueous layer that formed was a pale green colour. This would suggest the presence of Fe^{2+} ions. It is likely, therefore, that under these conditions conversion to Fe^{3+} with any subsequent interference with the derivatisation of the silicate groups is prevented. This does not, however, eliminate the possibility of interference by the Fe^{2+} cation.

Three PbO-SiO_2 synthetic slags were also studied as an alternative example of a system from which FeO was excluded

(Tables 52a to 52c, Figures 82 to 84). Unfortunately, two of these samples proved to be contaminated by Al_2O_3 . The presence of this component creates complications in the interpretation of the results obtained because the precise effect on silicate constitution is not known. From the viewpoint of trimethylsilylation it is possible that any aluminosilicate structures present will be trimethylsilylated to yield derivatives of the silicate portions only and, therefore, distort the overall pattern of the obtained chromatogram ¹²³.

The only true binary slag produced in this group was of composition $PbO-0.36xSiO_2$ and for this a reliable interpretation of the GLC results can be made. Firstly, the proportion of the SiO_4^{4-} anion derivative is less than that encountered with $FeO-SiO_2$ and $CaO-FeO-SiO_2$ slags and suggests that the trimethylsilylation process has responded in a different manner in the absence of FeO . On the basis that this GLC analysis represents the true silicate structure of the slag, the results can be used to test the predictions of the various silicate slag models.

From the GLC data for the $PbO-0.36xSiO_2$ slag, an oxygen balance gives a free oxygen anion concentration of 0.05 moles O^{2-} per mole of slag. Substituting this value into equation 2.4, Section 2.3.2 (a), to determine the (O^-) concentration and then using this term in equation 2.5, Section 2.3.2 (a), a value for the Toop and Samis equilibrium constant, K , can be evaluated. The value obtained for the slag was 0.005 compared with 0.04 quoted

by Toop and Samis⁸⁴. The inference is that the model predicts a greater degree of polymerisation than that shown by the trimethylsilylation - GLC analysis. Toop and Samis have also suggested a scheme for determining which ions are most likely to be present in binary oxide-silica systems⁸⁴. For the $\text{PbO}-0.36\text{xSiO}_2$ composition then, the most likely anionic species would contain 3 Si atoms per anion corresponding to the $\text{Si}_3\text{O}_{10}^{8-}$ chain anion (Appendix 1b). The GLC results disagree with this prediction although a reasonable proportion of the $\text{Si}_3\text{O}_{10}^{8-}$ anion derivative (21.5%) was detected.

The most abundant derivative for this slag was that of the SiO_4^{4-} anion. The Masson Slag Models⁷³ applied to binary oxide-silica systems where K_{11} data is available always predict that up to the metasilicate composition, the SiO_4^{4-} anion will be the predominant species. The Branched Chain Model predicts that the ionic fractions of the SiO_4^{4-} , $\text{Si}_2\text{O}_7^{6-}$ and $\text{Si}_3\text{O}_{10}^{8-}$ anions for this slag are 0.45, 0.14 and 0.06 respectively. The corresponding ionic fractions based on the GLC results are 0.50, 0.23 and 0.10, which is considered to be in reasonable agreement with the theoretical prediction. The experimental data tends to indicate slightly more polymerisation than that predicted by the Masson Model but better agreement exists with this model compared with that of Toop and Samis.

The trimethylsilylation technique applied to synthetic slags containing FeO clearly requires modification in order to ensure reliable and accurate derivatisation. On the basis that

the presence of the ferrous ion facilitates cation leaching and gives a rapid generation of silicic acids, the following two approaches warrant investigation. Firstly, the effect of adjusting reagent quantities and the amount of slag in the reaction mixture needs to be examined. If small amounts of slag are employed then the concentration of silicic acids produced will be low and may prevent depolymerisation and polymerisation side reactions occurring prior to the trimethylsilylation reaction. This approach has been successful in the derivatisation of soluble silicates where it was found that large quantities of silicate used was associated with a high degree of side reactions ¹¹⁶.

A second approach could incorporate the use of a trimethylsilylating agent stronger than trimethylchlorosilane. In this case silicic acids produced from the leaching operation could undergo a rapid substitution of the -H groups by TMS groups thus precluding side reactions. The reagent Bistrimethylsilylacetamide, $\text{CH}_3\text{CNO}[\text{Si}(\text{CH}_3)_3]_2$, is a more powerful trimethylsilylating agent than trimethylchlorosilane and its use in derivatising soluble silicates has led to a decrease in side reactions ¹⁶². However, the applicability of this reagent in trimethylsilylating solid silicates such as slags or minerals where a leaching stage is required, has yet to be investigated.

5.1.4 Summary of Trimethylsilylation Studies

The trimethylsilylation work indicated that use of the unified technique provided scope for making structural interpretations from chromatograms of slags of hitherto unknown

silicate constitution. Results for an iron blast furnace slag were particularly encouraging in relation to previous work¹²³. However, FeO in synthetic FeO-SiO₂ and CaO-FeO-SiO₂ slags and real LD slags is clearly detrimental to successful trimethylsilylation.

The results obtained for slags containing FeO suggest that the presence of this species causes massive anionic re-distribution such that the slags apparently exhibit an identical silicate constitution irrespective of the silica concentration. If FeO is excluded from the silicate, as illustrated by using a PbO-SiO₂ synthetic slag and iron blast furnace slag, the GLC results are altered. At present it is not possible to verify that these are reliable interpretations of the silicate constitution.

The inability to trimethylsilylate FeO containing slags so that the results obtained reliably respond to slag composition changes, is a great impediment to the development of our understanding of slag systems such as those encountered in LD steelmaking. Clearly, further work is necessary in the area of trimethylsilylating slags of appreciable FeO content in order to identify the reasons for the observed behaviour and to modify the technique to obtain accurate derivatisation of these slags.

The trimethylsilylation work has been applied to a different system, PbO-SiO₂, to examine slag model predictions on silicate constitution and on the basis of this limited study it appears that the Masson Branched Chain Model provides a better prediction than the Toop and Samis Model.

Introduction

The droplet refining experiments enabled both the decarburisation and desulphurisation processes to be monitored. The observed decarburisation behaviour suggested that at least two decarburisation mechanisms were operative and this could affect sulphur equilibria and sulphur transfer kinetics. For this reason the decarburisation process is examined first in order to identify the decarburisation mechanisms and to consider their effect on desulphurisation. The desulphurisation results will be discussed in the next section taking into account the implications of the decarburisation process.

5.2.1 The Effect of Decarburisation on the Physical Properties of Metal Droplets

The decarburisation process can cause variations in the physical properties of both the metal and slag phases. The effects concerning the slag phase will be dealt with in Section 5.2.3.

Carbon removal from the droplet can be responsible for changes in viscosity and lowering of the liquidus temperature so that solidification of the droplet could occur within the 20 minute period of observed droplet-slag reactions.

Data regarding the effect of carbon concentration on the viscosity of iron-carbon melts is somewhat conflicting. A decrease from 4 to 1 mass % C has been reported to give an increase in viscosity ¹⁶³ while other work ¹⁶⁴ shows a very

narrow viscosity range with a minima at 2 to 3 mass % C. It has also been reported ⁸⁰ that the influence of carbon is only substantial at high concentrations (>4 mass % C), which is outside the range employed in this work. The variation in droplet viscosity due to carbon removal is, therefore, not likely to be sufficient to exert an overriding effect on the results of the droplet-slag reactions.

An assessment of the metal liquidus temperatures of droplets where carbon concentrations were determined experimentally can be made by reference to the Fe-C equilibrium diagram ¹⁶⁵, Figure 87a. From the liquidus line for the (γ + liquid) phase field, the composition Fe-2.65 mass % C has a liquidus temperature of 1300°C which corresponds to the temperature used for droplet-slag experiments. Knowledge of the bulk carbon contents at different reaction times makes it possible to estimate the time for which the droplet is fully liquid. Superior carbon removal resulted for droplets decarburised by slags KC1 and KC2 (Figures 44, 45 and 51) with the reaction times available before solidification commenced being estimated as 5 and 2 minutes respectively. The remaining slags which produced poorer decarburisation gave longer reaction times of about 10 minutes for slag KC3 (Figure 52), about 7 to 15 minutes for three series of decarburisation experiments with slag KC4 (Figures 53a, b and c) and 20 minutes for slags KC5 and KC6 (Figures 54 and 55 respectively).

The reaction time available before solidification commences

may have been increased by the presence of sulphur and oxygen. Unfortunately, no data were available for the Fe-C-O-S system. However, it was noted that for the simple binary systems with iron ^{166, 167} (Figures 87b, c), the addition of sulphur and oxygen lower the liquidus temperature albeit by a very small extent over the concentration ranges applicable to this work. The Fe-O-S ternary system has been studied by other workers ¹⁶⁸ (Figure 87d) but the compositions investigated did not include those pertinent to the present work.

From the estimate of reaction time based on the Fe-C equilibrium diagram, it would appear that the droplets may be solid after 5 and 2 minutes respectively for reactions involving slags KC1 and KC2. However, carbon removal by slag KC1 occurs up to 15 minutes and this is well in excess of the estimated period of 5 minutes for which the droplet is fully liquid. With slag KC2 the initial 5 minutes of reaction exhibited rapid decarburisation and subsequently continued at a slower rate up to 20 minutes reaction time despite the estimated time for which the droplet was fully liquid being 2 minutes. It would have been expected that as solidification initiated and proceeded to completion as the carbon content fell that there would be a corresponding significant retardation in the decarburisation rate. Clearly, this does not appear to have occurred. In addition, the droplet appearance altered with reaction time (see Sections 4.1.2 (c) and 4.1.3 (c)) with longer reaction times being associated with cratering and subsurface blowholes. The development of 'potential' metal ejection sites was often at a

maximum at 20 minutes reaction time again suggesting that droplet solidification had not occurred.

Although no data pertinent to the droplet-slag compositions studied could be found to quantify the effects, the removal of carbon from iron is an exothermic reaction. The implication of this is that heat generated at the droplet-slag interface should maintain a liquid metal and slag. Thus, the study of droplet reactions can be interpreted in terms of the droplets being fully liquid over the 20 minutes reaction time and range of carbon concentrations encountered.

5.2.2 The Identification of the Decarburisation Mechanisms Operative During Droplet-Slag Interaction

The appearance of quenched droplets was observed to change with reaction time (Plates 9a to 9e, 12a to 12e). A smooth droplet surface was produced from reaction times of 5 minutes and less. Craters on the droplet surface and subsurface blow-holes were associated with reaction times of 10 minutes and longer. This trend was clearly exhibited for droplets reacted with slag KC1 (38.31 mass % CaO-28.52 mass % FeO -1.90 mass % Fe_2O_3 - 31.00 mass % SiO_2 - 0.27 mass % S) where the stopper and seat technique was used. Cratering was not as distinct for suspended droplet specimens and was considered to be due to delays in quenching the droplet after removal from the slag. A distinction could still be made, however, between the appearance of droplets reacted up to 5 minutes and those of longer reaction times.

The transition in droplet appearance suggested that two distinct decarburisation mechanisms were operative. Smooth surface droplets indicated that surface nucleation of CO had occurred. The formation of craters and subsurface blowholes were manifestations of internal CO nucleation.

Previous workers ^{147, 148, 149, 150, 151, 152, 153, 154,}
¹⁵⁵ using levitated and free falling droplets in oxidising gases have also proposed a two stage mechanism involving surface C-O reaction at higher carbon concentrations and internal CO nucleation at lower carbon concentrations. The latter mechanism resulted in metal being ejected from the droplet due to internal CO nucleation. A comparison can be made with observations in the present work where, after long reaction times, small globules of metal were noted at the droplet surface.

The formation of craters and subsurface blowholes during the present experimental work could be a quenching effect due to the equilibrium constant for the C-O reaction being increased by a decrease in temperature ⁷. However, as will be discussed below, the kinetic data suggests that dispersed phase control of the decarburisation kinetics becomes dominant at longer reaction times and that this would be consistent with internal nucleation of CO at 1300°C.

The kinetic data obtained for decarburisation (Tables 9a, 9b and 18 to 22, Figures 44, 45 and 51 to 55) showed an initial efficient period of carbon removal followed by a period of slow decarburisation rate. This is consistent with a two stage

mechanism. The change in decarburisation rate was not, however, coincident with the change in droplet appearance except for decarburisation experiments involving slag KC1. The general trend was for the decarburisation rate to decrease prior to the onset of cratering.

The initial efficient decarburisation period exhibited a constant rate of carbon removal indicative of a continuous phase control condition. In this situation the rate of transport of FeO in the slag phase controls the decarburisation rate. For a large value of the equilibrium constant for the decarburisation reaction (649 at 1300°C⁷) and assuming that equilibrium is established at the droplet-slag interface, the interfacial concentration of FeO becomes zero under conditions of continuous i.e. slag, phase control. The molar rate of transport can be defined by:-

$$\dot{n}_{\text{FeO}} = \dot{n}_{\text{C}} = \gamma_{\text{Sl}} A_d (k_{\text{FeO}})_{\text{Sl}} (C_{\text{FeO}})_{\text{Sl}}^b$$

where \dot{n}_{FeO} , \dot{n}_{C} = molar rate of transport of FeO and C respectively

γ_{Sl} = fraction of droplet surface in contact with slag phase

A_d = surface area of droplet

$k_{\text{FeO},\text{Sl}}$ = mass transfer coefficient of FeO in slag phase

$(C_{\text{FeO}})_{\text{Sl}}^b$ = bulk concentration of FeO in slag

The large amount of slag employed in the experiments relative to that of the metal droplet means that the FeO concentration remains relatively constant giving a constant decarburisation rate during the period that this mechanism is dominant.

The slow decarburisation period can be attributed to a dispersed phase control mechanism. The depletion of carbon in the droplet creates a carbon concentration gradient which ultimately produces a surface concentration of zero. The FeO concentration of slag at the interface becomes that of the bulk slag composition. The rate of decarburisation is now dependent upon the rate of carbon transport in the metal and can be expressed by:-

$$\dot{n}_C = \gamma_{Sl} A_d [k_C]_d [C_C]_d^b$$

where $k_{C,d}$ = mass transfer coefficient of carbon in the droplet

$C_{C,d}^b$ = bulk carbon concentration in droplet.

The decarburisation rate is, therefore, dependent upon the bulk carbon concentration in the droplet and since this will decrease with time, the rate of carbon removal will decrease with time.

It has been noted (Section 2.4.4) that other workers¹⁵,
¹⁴³ interpretations of the decarburisation process have included mechanisms in addition to those considered above. The presence

of an induction period has been reported to exist over the initial few seconds of droplet-slag reaction. The basis of such a mechanism is that a barrier to CO nucleation exists. A delay is then incurred until the oxygen concentration of the droplet has increased to give a C-O product sufficiently high for CO nucleation to occur.

The present experimental work could not obtain data over such a short timescale to confirm the existence or otherwise, of an induction period. It is clear from all the present decarburisation results that carbon removal has certainly commenced within the initial 2 minutes of droplet-slag interaction.

A further mechanism proposed by other workers¹⁴³ has been described as "external-internal decarburisation". This is essentially a mixed transport control mechanism and represents the consequence of concentration gradients of FeO in the slag and carbon in the droplet. With respect to the present work a transition period obviously exists between the two dominant mechanisms of continuous and dispersed phase control. The transition could be a manifestation of mixed transport control. Progressive removal of carbon under mixed transport conditions would eventually lead to domination of the dispersed phase control mechanism as was observed experimentally.

In droplet refining systems not involving gas evolution the transition from continuous to dispersed phase control is more distinct. The extended mixed period of control observed by other workers studying decarburisation may be as a consequence of the

change of state associated with the formation of the reaction product CO. It could be envisaged that the onset of internal CO nucleation might increase turbulence within the drop and, therefore, increase the local mass transfer coefficient of carbon in the drop, $[k_C]_d$. This might be sufficient to create a finite carbon concentration at the droplet surface thereby temporarily restoring slag phase controlling. The transition region observed by the other workers may, therefore, be visualised possibly as a period of oscillation between the two mechanisms until finally the carbon concentration in the droplet falls so low as to be totally dominating. With respect to the present work this behaviour would provide an explanation for the observed time-lag between the decrease in decarburisation rate and change in droplet appearance.

It is considered from the present experimental work that two dominant decarburisation mechanisms were operative. An initial continuous phase controlled mechanism resulted in the surface reaction of carbon and oxygen whilst a subsequent dispersed phase control condition produced internal CO nucleation. The presence of a third type of mechanism, mixed transport control, could not be discounted and would operate during the transition from continuous phase to dispersed phase control.

5.2.3 Explanation of the Observed Variation in Decarburisation Performance

The experimental results clearly showed that decarburisation

efficiency was, as expected, related to the duration of the continuous phase control mechanism. This was well illustrated for decarburisation reactions involving slag KC1 (38.31 mass % CaO - 28.52 mass % FeO - 1.90 mass % Fe₂O₃ - 31.00 mass % SiO₂ - 0.27 mass % S) where a 10 minute period of continuous phase control was identified. Droplets decarburised by slag KC1 contained 0.55 to 0.66 mass % C after 20 minutes reaction (Tables 9a and 9b, Figures 44 and 45). For slag KC2 (28.00 mass % CaO - 40.20 mass % FeO - 3.21 mass % Fe₂O₃ - 28.50 mass % SiO₂ - 0.15 mass % S) the continuous phase control mechanism was slightly shorter than for slag KC1 (approximately 5 minutes) and gave a final droplet carbon concentration of 0.85 mass % after 20 minutes reaction. The briefest periods of continuous phase control were encountered with slags KC3 to KC6 (approximately 2 minutes). This was reflected in the high carbon concentrations 1.90 to 2.74 mass % after 20 minutes reaction time.

The sustained period of continuous phase control exhibited by the decarburisation data for slag KC1-droplet reactions suggested that the rate of FeO transport in slag KC1 was slow relative to that in the other slags.

A feature of CaO-FeO-SiO₂ slags is the greater interaction between silicate anions with Ca²⁺ cations than with Fe²⁺ cations producing a preferred association between Ca²⁺ and silicate groups and Fe²⁺ cations and O²⁻ anions^{95, 96}. The strong interaction of Ca²⁺ with silicate anions could, therefore, be expected to result in an increase in Fe²⁺ mobility¹⁶⁹. If the

CaO concentration is increased and, therefore, available to associate with more silicate, the diffusivity of FeO could be expected to increase. However, the experimental results do not conform to a decarburisation mechanism being solely dependent upon FeO diffusivity. It follows that the observed decarburisation is regulated by convective mass transfer processes.

It has already been noted (Section 5.2.2) that the conditions for slag phase control are related to the bulk concentration of FeO. This parameter is at a minimum for slag KC1 relative to the other slag compositions employed and can, therefore, contribute to a comparatively longer period of continuous phase control. However, the mass transfer coefficient must also be considered and will depend upon a number of factors such as FeO diffusivity, slag viscosity and slag liquidus temperature.

An increase in slag viscosity could decrease the mass transfer coefficient⁸⁰. It has been shown²² that an increase in slag viscosity occurs through the composition range fayalite to fayalite - 32 mass % CaO at 1300°C. Following from this, slag KC1 containing 38.31 mass % CaO would be expected to represent the most viscous slag employed in the present work. In addition, the liquidus temperature reported for this slag composition²³ corresponds to the experimental temperature of 1300°C. The slag was observed to be liquid at this temperature but must be considered to be viscous. For the other slags employed, the decrease in CaO concentration will produce lower

slag viscosities. A differential between the experimental and liquidus temperatures is also established ranging from 80°C for slag KC2 to 140°C for slag KC4. The results tend to suggest that the duration of the continuous phase controlled decarburisation period is increased with increase of slag viscosity.

In summary, the present results confirm that the efficiency of decarburisation is related to the duration of continuous phase control. Superior decarburisation of droplets by slag KC1 was achieved by a sustained period of continuous phase control. This is connected to the relatively high viscosity of slag KC1 compared with the other compositions employed.

5.2.4 Summary of the Decarburisation Process With Respect to Factors Influencing Slag-Metal Sulphur Equilibria

The transition from a continuous phase controlled decarburisation mechanism to conditions of dispersed phase control brings about changes at the droplet-slag interface. The sulphur transfer reaction also takes place at the interface and any change at this site imposed by the decarburisation process may affect the sulphur equilibria and sulphur transfer kinetics. A summary of the characteristics of the decarburisation rate controlling mechanisms which might affect desulphurisation is given below. The ramifications of the interfacial conditions listed below in terms of desulphurisation kinetics, are discussed in Section 5.3.

(a) Conditions Imposed by Continuous Phase Control

- (i) The concentration of FeO at the droplet-slag interface is zero producing an interfacial slag consisting of CaO, SiO₂ and S.
- (ii) A finite concentration of carbon exists at the droplet interface.
- (iii) A surface reaction between carbon and oxygen takes place. This can be considered to maintain the oxygen concentration at the droplet surface at a relatively low value.

(b) Conditions Imposed by Dispersed Phase Control

- (i) The concentration of FeO at the droplet-slag interface is equal to that of the bulk slag composition.
- (ii) The concentration of carbon at the droplet surface is zero.
- (iii) CO is being nucleated internally and as carbon concentration decreases oxygen concentration within the droplet increases to maintain the C-O product. In addition, oxygen concentration gradients may exist in the droplet from the slag-metal interface to internal nucleation sites.

5.3 THE DESULPHURISATION OF SINGLE IRON-CARBON-SULPHUR

DROPLETS

Introduction

The slag compositions used in the droplet experiments have been referred to in previous sections as containing some Fe_2O_3 (Table 7a). However, under the experimental conditions employed, i.e. slag contained in an iron crucible, argon atmosphere and high initial carbon concentration droplets, it is considered that iron oxide will be present as FeO. For the purposes of discussing desulphurisation, the slags are considered in terms of CaO-FeO-SiO₂-S compositions. The converted compositions assuming iron oxide solely as FeO are given in Table 58. This allows a more realistic representation of slag composition under the experimental conditions. In addition, slags KC1 to KC4 and KC6 correspond to basic compositions and allow slag-metal sulphur equilibria to be considered in terms of the Temkin and Flood slag models.

5.3.1 A Hypothetical Scenario for Desulphurisation

The scenario is developed from the conditions imposed at the reaction interface by the decarburisation process. Account is taken of the desulphurisation reaction being rate controlled by mass transfer processes and that equilibrium must be maintained at the droplet-slag interface.

(a) Conditions Imposed During Continuous Phase Controlled

Decarburisation

During continuous phase controlled decarburisation a finite carbon concentration exists at the droplet surface. This will increase the activity coefficient of sulphur at the surface and lower that of oxygen¹⁶⁶. Both factors provide thermodynamic impetus for sulphur transfer from metal to slag⁷. Carbon at the droplet surface will react with oxygen arriving at the interface from the bulk slag. This reaction will maintain a relatively low oxygen concentration at the droplet surface. In addition, any oxygen transferred to the droplet by virtue of the sulphur transfer reaction may be removed by the carbon at the interface. The maintenance of a low oxygen concentration at the droplet surface will favour desulphurisation.

The interfacial slag composition during this decarburisation mechanism will have a zero concentration of FeO. For bulk slag compositions of CaO-FeO-SiO₂-S an interfacial slag of CaO-SiO₂-S will be produced. This represents an increase in the Ca²⁺ concentration relative to the bulk slag composition and can result in a more favourable equilibrium quotient for sulphur transfer. However, as can be seen in Table 59, for the slags used in this investigation the complete denudation of FeO produces acid slag compositions which precludes application of the Flood model.

The modified slag composition also has implications with respect to the concentration of free O²⁻ anions at the droplet-

slag interface. The interpretation by Temkins Model ⁷⁰ of acid slag compositions is that free O^{2-} anions do not exist. This would suggest that sulphur transfer could not take place. The silicate slag models accommodate the presence of O^{2-} anions in an acid slag near the acid-base transition by virtue of silicate polymerisation reactions ^{73, 84}. However, for the case of CaO-SiO₂ slags in the present work, small O^{2-} anionic fractions are predicted by the Masson Model ⁷³ (0.002 and 0.001) and the Toop and Samis Model ⁸⁴ (0.032 and 0.021) for slags KC1 and KC2 where, despite complete denudation of FeO, their silica contents are still below the metasilicate composition, Table 59. This is due to the small degree of polymerisation occurring in the CaO-SiO₂ system reflected by low K_{11} values of 0.0016 (Masson) and 0.0017 (Toop and Samis).

A limiting case exists for slag KC6 of bulk composition 71.87 mass % FeO-27.81 mass % SiO₂-0.32 mass % S (Table 58) when considering complete FeO denudation at the droplet-slag interface. The period of continuous phase controlled decarburisation would correspond with the presence of a silica film at the droplet surface (Table 59). Consequently, no desulphurisation could be expected.

Provided an acid slag composition is not formed at the droplet-slag interface, it is clear that during continuous phase controlled decarburisation interfacial conditions are established that favour metal to slag sulphur transfer. However, in the case of acid interfacial slags of the CaO-SiO₂ system the low O^{2-} anion concentrations would tend to negate the effects of the metal

phase solutes [C] and [O] and their effect on the activity coefficient of sulphur. Thus, efficient sulphur transfer would not be expected.

(b) Conditions Imposed During Dispersed Phase Controlled Decarburisation

Dispersed phase controlled decarburisation produces a carbon concentration of zero at the droplet surface. Consequently, the activity coefficient of sulphur at the surface is lowered and that of oxygen raised. Both variations are detrimental to good sulphur removal⁷. An increase in the oxygen concentration of the droplet can also be expected due to the need to supply oxygen, [O], to satisfy the needs for the internal nucleation of CO and will also detract from good desulphurisation conditions.

The interfacial slag composition during this mechanism will correspond to that of the bulk slag. For the CaO-FeO-SiO₂-S compositions employed, the presence of Fe²⁺ according to Flood⁷¹ will decrease the equilibrium quotient for sulphur transfer relative to that established during continuous phase controlled decarburisation. For the binary slag KC6, the equilibrium quotient will increase by virtue of FeO-SiO₂ present at the interface instead of SiO₂.

Slags KC1 to KC4 and KC6 are all basic with respect to Temkin's Model and should provide a higher interfacial concentration of O²⁻ anions compared with that established when slag phase control decarburisation is operative. Slag KC5 (0.86 mass % CaO-65.30 mass % FeO-33.54 mass % SiO₂ - 0.30 mass

% S, Table 58) is slightly acid. If this slag is considered in terms of silicate slag theory it may be construed as containing O^{2-} anions. This reasoning is based on the effect of adding FeO to the CaO-SiO₂ system⁷³. The presence of FeO will increase the degree of polymerisation because the value of K_{11} for FeO-SiO₂ is greater than that for CaO-SiO₂. This polymerisation will produce free O^{2-} anions. The trend may be, therefore, that as FeO concentrations increase from slag KC1 (30.88 mass %, Table 58) to KC5 (65.30 mass %, Table 58) the concentration of O^{2-} anions also increases.

The implication of dispersed phase decarburisation is that the interfacial [O] and [C] respond in a manner that detract from good desulphurisation while the O^{2-} anion concentration produced in the slag appears to be favourable for desulphurisation. This latter factor must be capable of suppressing the other effects in order for sulphur transfer from metal to slag to continue at the droplet-slag interface.

The hypothetical desulphurisation mechanisms, based on two dominant decarburisation mechanisms, highlight the importance of O^{2-} anions at the reaction interface in the desulphurisation process. If O^{2-} anions are present during continuous phase controlled decarburisation transfer of sulphur from metal to slag is to be expected. The equilibrium interfacial sulphur concentration of the droplet will be low and will create a concentration gradient relative to the bulk sulphur concentration of the droplet. This will ensure that sulphur in the droplet will be transported to the interface for reaction.

When the dispersed phase control decarburisation mechanism becomes dominant the O^{2-} anion concentration of the slag must be sufficient to override the accompanying interfacial conditions that do not favour desulphurisation. If this is achieved the resulting interfacial equilibrium sulphur concentration of the droplet will maintain a concentration gradient relative to the bulk composition. This gradient will allow the continued transport of sulphur in the droplet to the interface for eventual transfer to the slag phase. On the basis that the interfacial conditions establish concentration gradients that allow metal to slag sulphur transfer throughout droplet-slag interaction, then the effect of mass transfer processes can be considered. It may, therefore, be expected that if the initial sulphur concentration in the droplet is sufficiently high, then the desulphurisation rate may be determined by conditions of continuous phase control, i.e. O^{2-} anion transport control to the reaction interface, especially if the decarburisation process is controlling the availability of O^{2-} anions at the reaction interface. This is similar to the situation discussed earlier (section 5.2.2) and would be expected to produce a constant desulphurisation rate. At lower sulphur concentrations in the droplet, dispersed phase control, i.e. S transport control in the droplet, would be expected to govern the rate of removal and a decreasing desulphurisation will be observed with reaction time. This situation is further encouraged if O^{2-} anions at the surface increase as the decarburisation mechanism changes to one of carbon transport control.

5.3.2 An Appraisal of the Observed Desulphurisation Behaviour

The ensuing discussion refers to the desulphurisation results given in Tables 8a to 8e and 13a to 17 and expressed diagrammatically in Figures 37 to 43 and 46a to 50d. The appraisal considers the observed desulphurisation behaviour with respect to factors considered in the scenario developed in the previous section. Explanations are given to account for any differences between the hypothetical desulphurisation mechanisms and observed desulphurisation behaviour.

(a) Reactions Involving Slag KC1 (38.06 Mass % CaO - 30.88
Mass % FeO - 30.80 Mass % SiO₂ - 0.27 Mass % S)

Droplets of Initial Sulphur Concentrations 0.512 Mass %, 0.440
Mass %, 0.302 Mass %, 0.120 Mass %

The desulphurisation results for these higher initial sulphur concentration droplets are presented in Figures 37 to 40, Tables 8a and 8b.

Results for the "0.512 mass % S" droplet showed a linear change in sulphur content with time for about 2 minutes (Figure 37). Thereafter, the sulphur removal rate decreased with time. An identical scale was used to plot Figures 38 and 39 for the "0.440 mass % S" and "0.302 mass % S" droplets. In both cases there was no initial linear change of sulphur concentration with time. The reaction rate decreased with time to a very slow desulphurisation rate at 20 minutes. The "0.120 mass % S" droplet desulphurisation curve (Figure 40) was plotted using a different

scale and an exaggerated initial desulphurisation rate was evident relative to the higher sulphur concentration droplet results. It was clear, however, that in this experiment also, desulphurisation rate decreased with reaction time.

If the results discussed above had exhibited a well defined linear change of sulphur concentration with time, i.e. constant desulphurisation rate, then a period of slag phase controlled desulphurisation could have been interpreted. With the exception of the "0.512 mass % S" droplet for a very short period at the high initial sulphur concentration, it is difficult to envisage that such a mechanism was operative.

The general trend for the above results, i.e. decreasing desulphurisation rate with time, suggests at a first inspection that dispersed phased control conditions existed. In such a case the desulphurisation rate falls as a response to decreasing sulphur content of the droplet.

For the four sets of results, the best desulphurisation occurred within the 10 minute period of continuous phase controlled decarburisation observed for this slag (Figures 44 and 45). During this decarburisation process the slag composition at the droplet-slag interface assuming zero FeO concentration, would be $\text{CaO}-0.43\text{xSiO}_2-0.01\text{xS}$. This composition is in the acid region but for the observed sulphur removal to have occurred, O^{2-} anions must have been present at the interface. Clearly, this situation is anomalous with respect to the hypothetical mechanisms proposed for the continuous phase

controlled decarburisation period. The actual desulphurisation achieved was too good to be accounted for by silicate polymerisation in the CaO-SiO_2 system. This suggests that the interfacial slag was not completely denuded in FeO and that during the first few minutes of reaction when desulphurisation rates were quite high, the interfacial composition must have been close to the bulk composition.

Retardation of sulphur removal also took place within the continuous phase controlled decarburisation period. This could be an indication of sulphur transport control in the droplet with the desulphurisation rate falling due to the sulphur content of the droplet decreasing.

After 10 minutes reaction the decarburisation process becomes dispersed phase controlled. The desulphurisation results at longer reaction times show some scatter but it is considered that a slow sulphur removal rate is evident. The hypothetical desulphurisation mechanisms discussed earlier for this decarburisation period suggest that the interfacial slag composition becomes that of the bulk composition. In addition, the slag O^{2-} anion concentration must negate the effects of decreasing $[\text{C}]$ and increasing $[\text{O}]$ levels in the droplet to allow metal to slag sulphur transfer to continue. The observed sulphur removal over this period fits the hypothetical discussion. The interfacial equilibrium sulphur concentration of the droplet must still be less than the bulk composition in order that sulphur can be transported to the reaction interface

with subsequent transfer to the slag.

The results for slag KC1 reacted with droplets of initial sulphur concentration 0.440 mass % were found to contain 0.020 mass % S after 20 minutes. In comparison, the droplets initially containing 0.512 mass % S and 0.302 mass % S were found to contain 0.065 and 0.048 mass % S respectively after 20 minutes. There is no reason apparent why the "0.440 mass % S" droplet should have exhibited superior desulphurisation. The probable explanation is a variation in the initial sulphur concentration as considered in Section 4.1.1.

Droplets of Initial Sulphur Concentration ≤ 0.076 Mass %

Results for reactions of slag KC1 with droplets of initial sulphur concentrations of 0.076 mass % and lower are given in Tables 8c to 8e and Figures 41 to 43. An initial transfer of sulphur from slag to metal followed by a period of desulphurisation is a feature common to the results of these lower initial sulphur concentration droplets.

The initial sulphur reversion phenomenon is clearly inconsistent with the hypothetical scenario discussed in the previous section. The reversion was observed for up to 2 to 5 minutes, well within the 10 minute period of continuous phase controlled decarburisation. A situation, therefore exists where sulphur reversion has occurred under conditions apparently favourable for desulphurisation as implied from the results of the higher initial sulphur concentration droplets.

A possible explanation for the initial sulphur reversion

is that an instantaneous denudation of FeO from the interfacial slag does not occur. Consequently, the early stages of droplet-slag interaction involve a gradual depletion of FeO via the continuous phase controlled decarburisation mechanism. During this time the slag close to the droplet surface is moving towards an acid composition and will culminate in a situation of minimum O^{2-} anion concentration and maximum S^{2-} anion concentration at the droplet-slag interface. This latter point can be seen from a comparison of the mass % S values presented in Tables 58 and 59. The consequence of slag composition moving towards an acid composition in the CaO-SiO₂ system will be to reduce O^{2-} anion concentration. This effect, in conjunction with S^{2-} anion concentration and low initial sulphur concentrations of droplets provides a basis for slag to metal sulphur transfer to occur.

In view of the gradual depletion of FeO at the droplet-slag interface, it is appropriate to make a retrospective comment on the observed desulphurisation behaviour of the higher sulphur content droplets. At high initial sulphur concentrations in the droplet a greater potential exists for metal to slag sulphur transfer. During the period of FeO depletion in the slag, thereby lowering O^{2-} anion concentration, no sulphur reversion took place but a decrease in desulphurisation rate occurred within the initial 5 minutes reaction time. The retardation of desulphurisation rate in response to a decrease in O^{2-} anion concentration in the slag, if strict continuous phase control is discounted, suggests that a mixed transport control

desulphurisation mechanism was operative. Thus, at the very early stages of reaction the high initial sulphur concentration of the droplet and high O^{2-} anion concentration at the droplet surface created a strong potential for metal to slag sulphur transfer. Indeed, quite high desulphurisation rates were observed over the early reaction period. When the sulphur concentration in the droplet had fallen to a low enough level for sulphur reversion to be a possibility, the decarburisation mechanism had fortuitously changed to one of dispersed phase control resulting in an increase of O^{2-} anion concentration. The rising O^{2-} anion concentration would, therefore, suppress sulphur reversion.

The presence of mixed transport controlled desulphurisation can be justified by other features of the lower sulphur concentration droplet desulphurisation results. Firstly, sulphur reversion itself is indicative of the equilibrium quotient for sulphur transfer not being extreme in magnitude. In addition, it would be expected that lower sulphur levels in the metal would be conducive to sulphur transport control in the droplet. Under strict dispersed phase control the sulphur concentration at the droplet surface would be zero and consequently, insensitive to the O^{2-} anion concentration of the interfacial slag. This behaviour did not apply to the results obtained for the lower sulphur content droplets because sulphur transfer clearly responded to changes in slag composition. For the higher sulphur concentration droplets, therefore, desulphurisation was controlled by a mixed transport

mechanism with a possible transition to dispersed phase control conditions as the sulphur content in the droplet decreased.

Returning to the sulphur reversion phenomenon observed with the lower sulphur content droplets, it has already been mentioned (Section 5.2.2) that an induction period may play a role in the decarburisation process. This involves an increase in metal oxygen concentration prior to the initial nucleation of CO¹⁴³. The length of this induction period is of the order of seconds and if it is applicable to the present work, will terminate before sulphur reversion finishes. The time-lag between the completion of these two phenomena precludes the possibility that the induction period is the major factor in sulphur reversion at the commencement of droplet-slag reaction. However, the occurrence of an induction period can make a limited contribution to sulphur reversion due to the build up of metal oxygen concentration prior to CO nucleation. This will take place during the period of increasing slag acidity and S²⁻ anion concentration. Thus, another feature is added to the conditions which favour slag to metal sulphur transfer.

A further factor in the occurrence of sulphur reversion could be the surface active nature of sulphur in iron and in slag^{80, 140}. It is possible that the surface active effects cause higher sulphur concentrations in the metal and slag at the interface than in the bulk phases. A high S²⁻ anion concentration at the slag surface would further help to create conditions

favourable for sulphur reversion.

Following initial sulphur reversion, desulphurisation of droplets of initial sulphur concentration 0.076 mass % and lower commenced within the continuous phase controlled decarburisation period of 10 minutes. In view of the preceding increase in droplet sulphur concentration, it is difficult to envisage that desulphurisation is initiated by the eventual attainment of an interfacial CaO-SiO_2 slag coupled with a high concentration of sulphur at the droplet surface. The hypothetical desulphurisation mechanisms discussed in the previous section do not account for this phase of the observed behaviour.

It has been proposed (Section 5.2.2) that the decarburisation process may involve a period of mixed transport control prior to the domination of dispersed phase control conditions. The onset of such a mechanism will result in the gradual increase in slag FeO concentration at the interface re-establishing a more basic slag composition. When dispersed phase controlled decarburisation becomes dominant, the interfacial slag will correspond to the bulk slag composition. Thus, if mixed transport controlled decarburisation occurs then conditions are created for sulphur removal to occur. These conditions are sustained albeit at a lower desulphurisation potential due to increasing oxygen and decreasing carbon levels in the droplet when dispersed phase controlled decarburisation dominates. During the sulphur removal periods of the lower sulphur concentration droplets, the desulphurisation rate is governed by a mixed transport control mechanism with a possible

transition to dispersed phase controlled conditions as the sulphur concentration of the droplet decreases.

(b) Reactions Involving Slag KC2 (27.67 Mass % CaO-44.01 Mass % FeO-28.17 Mass % SiO₂-0.15 Mass % S), KC3 (16.57 Mass % CaO-55.08 Mass % FeO-28.26 Mass % SiO₂-0.09 Mass % S), KCl₄ (10.21 Mass % CaO-61.78 Mass % FeO-27.69 Mass % SiO₂-0.32 Mass % S) and KC5 (0.86 Mass % CaO-65.30 Mass % FeO-33.54 Mass % SiO₂-0.30 Mass % S)

Results for droplet desulphurisation experiments using the above slags are given in Tables 13a to 16 and Figures 46a to 49d.

The desulphurisation of droplets of approximate initial sulphur concentrations of 0.10, 0.080 and 0.050 mass % by the above slags all exhibited initial removal of sulphur. This period was coincident with the continuous phase controlled decarburisation period observed for each slag, approximately 5 minutes for KC2 and 2 minutes for the remainder.

The initial sulphur removal can be explained by the reasons given in the previous section to account for desulphurisation of the higher sulphur concentration droplets by slag KC1. The hypothetical desulphurisation mechanisms are again inapplicable due to the gradual removal of FeO from the interfacial slag. Desulphurisation rate can be considered as mixed transport controlled and at long reaction times a dispersed phase controlled mechanism may be operative due to

falling sulphur levels in the droplets.

In contrast to the desulphurisation results obtained with slag KC1, sulphur reversion of droplets of approximate initial sulphur contents 0.080 and 0.050 mass % S was not observed after reaction with slags KC2 to KC5. The relatively higher FeO concentrations of the latter slags compared with slag KC1, produce a greater concentration of O^{2-} anions at the droplet-slag interface enabling sulphur removal to occur despite the low sulphur concentration of the droplet.

The reactions of droplets initially containing about 0.030 mass % S with slags KC2, KC3, KC4 and KC5 exhibited the initial sulphur reversion phenomenon. This feature existed for 2 minutes with slags KC2 and KC4 and 5 minutes for slags KC3 and KC5. The results for KC3 and KC5 indicated that the time over which reversion occurred appeared to exceed that of slag phase controlled decarburisation. These two examples do not, therefore, follow the trend observed for the instances of reversion discussed earlier. It may be possible that the continuous phase controlled decarburisation mechanism was operative for a period greater than the 2 minutes interpreted from Figures 52 and 54. It is considered that the explanations presented in Section 5.3.2 (a) to account for sulphur reversion can be applied to reversion occurring in droplet-slag reactions involving slags KC2 to KC5.

(c) Reactions Involving Slag KC6 (71.87 Mass % FeO-27.81 Mass %

SiO₂-0.32 Mass % S)

Initial desulphurisation preceded a period of very slow sulphur removal for the reaction involving a droplet of initial sulphur concentration 0.110 mass % (Figure 50a, Table 17). For the "0.080 mass % S" droplet, desulphurisation occurred for approximately 3 minutes and then ceased (Figure 50b, Table 17). An initial period of sulphur reversion was observed for the lower sulphur concentration droplets of 0.056 and 0.030 mass % (Figures 50c and 50d, Table 17). Reversion took place for 2 minutes for the "0.056 mass % S" droplet resulting in a very small increase in sulphur concentration to a value of 0.058 mass % S. Re-sulphurisation was more pronounced in the "0.030 mass % S" droplet which occurred over 5 minutes giving a sulphur content of 0.043 mass % S.

The hypothetical desulphurisation mechanisms proposed in Section 5.3.1(a) highlighted an interesting feature of the continuous phase controlled decarburisation process involving FeO-SiO₂ slags. The complete removal of FeO at the droplet-slag interface would produce a film of silica and sulphur at the droplet surface. Silica has a melting point of 1722°C and would be solid at the experimental temperature employed, i.e. 1300°C. With respect to slag-metal sulphur equilibria, desulphurisation would not be possible. For the results obtained with the "0.110" and "0.080 mass % S" droplets however, sulphur removal has clearly occurred suggesting the availability of O²⁻ anions for

reaction. Free O^{2-} anions must have been derived from the presence of FeO at the interface. Credence is, therefore, given to the proposal that FeO is not instantaneously depleted at the droplet-slag interface.

The results obtained demonstrate that the presence of FeO at the interface can provide conditions for desulphurisation. This is the case for droplets of higher initial sulphur concentrations (0.110 and 0.080 mass %). For reactions involving the lower initial sulphur concentration droplets (0.056 and 0.030 mass %) the movement towards an acid slag composition dominates the interfacial conditions and sulphur reversion occurs.

The onset of dispersed phase controlled decarburisation, which boosts the FeO concentration of the interfacial slag, takes place at approximately the same time that the "0.110 mass % S" and "0.080 mass % S" droplets have almost ceased desulphurisation. The insensitivity towards increasing O^{2-} anion concentration of the slag suggests that conditions of mixed transport controlled desulphurisation have given way to dispersed phase control. The "0.056 mass % S" and "0.030 mass % S" droplets commenced desulphurisation at about the same time that dispersed phase controlled decarburisation occurred indicating that mixed transport controlled desulphurisation was operative.

The consideration of reactions with an FeO-SiO₂ slag justifies the explanation given earlier (Section 5.3.2(b)) for sulphur reversion having occurred in reactions involving lower

initial sulphur concentration droplets (~ 0.050 mass % and lower) with slags KC2 to KC6 compared with slag KC1 (0.076 mass % S droplets and lower). With the extreme case of slag KC6, of FeO-SiO₂ composition, the bulk FeO concentration is at a maximum relative to the other slags. It may be considered, therefore, that total depletion of FeO is least likely to occur in this slag. As initial bulk FeO concentration is decreased to a minimum value of 30.88 mass % FeO in slag KC1, the possibility of total interfacial depletion increases. If a given degree of depletion is considered then the resultant slag acidity will increase with decreasing initial bulk FeO concentration. Thus, KC1 relative to the other slags could achieve the most acid slag composition during continuous phase controlled decarburisation. This could be reflected in the extent of sulphur reversion and a comparison of the desulphurisation results for droplets of approximate initial sulphur content 0.030 mass % S reacted with slags KC1 to KC6 (Tables 8e, 13a and 14 to 17) shows that the greatest reversion ($+0.034$ mass % S) resulted from slag KC1.

5.3.3 The Prediction of Slag-Metal Sulphur Equilibria for the Experimental Conditions

The equilibrium sulphur content of a metal droplet after reaction with a slag may be calculated from ⁷²:-

$$[S] = \frac{(N_{2-})_S [O] [f]_O}{(N_{2-})_K [f]_S} \quad 5.1$$

where,

[S] = Sulphur concentration in the metal phase [mass %]

[f_S] [f_O] = Henrian activity coefficients of sulphur and oxygen respectively, in the metal phase

K = Equilibrium "constant" for sulphur transfer

($N_{S^{2-}}$) = Anionic fraction of sulphur in slag

($N_{O^{2-}}$) = Anionic fraction of oxygen in slag

It has been established (Section 5.2.2) that dispersed phase control decarburisation is operative at the longer reaction times. Predictions of slag-metal sulphur equilibria must take into account that the interfacial slag composition is that of the bulk composition and that a zero concentration of carbon exists at the droplet surface. This allows a prediction to be made of the interfacial sulphur equilibrium concentration. However, the conditions also apply to absolute equilibrium and can, therefore, be compared with the results obtained after 20 minutes reaction to assess whether the reaction has achieved equilibrium.

(a) Application of the Slag Models

The Temkin ⁷⁰ and Flood ⁷¹ Models were developed to predict an equilibrium constant for sulphur transfer. To obtain an equilibrium sulphur concentration of metal as defined in equation 5.1, the equilibrium constant of the particular model must be identified.

The equilibrium "constant" for sulphur transfer according to Temkin is 0.017 ⁷². This value was obtained by Temkin using

other workers' data ¹⁷⁰ but the assumption was made that both f_0 and f_S were unity. Using the interaction parameters selected for the present work (Table 60) this data was checked and the Temkin equilibrium "constant" confirmed as 0.017.

For calculations involving the Flood Model a mixed equilibrium quotient may be determined for each slag using the relationship ⁷⁴:-

$$\log K^{\ddagger} = -1.4 N'_{Ca^{2+}} - 1.9 N'_{Fe^{2+}},$$

the values being presented in Table 61.

The Temkin and Flood Models can be applied to all the slags employed in the present work with the exception of KC5 which is acid.

Additional predictions for reactions involving slag KC6 (71.87 mass % FeO-27.81 mass % SiO₂-0.32 mass % S) can be made using the silicate slag models of Masson ⁷³ and Toop and Samis ⁸⁴. Their use is strictly applicable to binary slags. However, these models derive values of oxygen anion fraction only (see Sections 2.3.2(b) and 2.3.2(c)) and do not yield an equilibrium quotient for sulphur transfer. Thus, the predicted anionic fractions from these models were used in equation 5.1 in conjunction with the Temkin equilibrium "constant" and, for comparison, the Flood equilibrium quotient calculated for slag KC6.

Temkin ionic fractions, based on bulk slag compositions given in Table 58, were calculated for slags KC1 to KC4 and KC6 (see Section 2.2.3(a)), and the values are given in Table 62.

Electrically equivalent cation fractions based on the Flood Model (Section 2.2.3(b)) for the same slags are recorded in Table 61. Oxygen anion fractions for slag KC6 derived from the Masson and Toop and Samis Models are presented in Table 63.

Equation 5.1 requires that values are assigned to the activity coefficients of sulphur and oxygen in the metal droplet. The following relationships may be used ⁷:-

$$\log f_S = e_S^S \text{ mass \% S} + e_S^O \text{ mass \% O}$$

$$\log f_O = e_O^O \text{ mass \% O} + e_O^S \text{ mass \% S}$$

Values of interaction parameters employed are given in Table 60. The activity coefficients were calculated using the initial droplet sulphur concentrations of the particular droplet-slag reaction. However, in the absence of experimentally obtained metal oxygen concentrations no specific oxygen value could be used. The oxygen concentration of the droplet is obviously influenced by the desulphurisation and decarburisation processes. An estimate of oxygen pick up due to desulphurisation alone can be obtained from a consideration of the stoichiometry of the sulphur transfer equation. Desulphurisation by slag KC1 of a droplet initially containing 0.110 mass % S resulted in a final sulphur concentration of 0.028 mass % after 20 minutes reaction. For an initial droplet mass of 1.1950g, then the mass of sulphur removed was 0.0010g which corresponded to 0.0005g of oxygen transferred to the droplet, giving an oxygen concentration of

0.042 mass %. This is incompatible with the Vacher-Hamilton isotherm¹⁷¹ which predicts, for the experimentally determined bulk carbon concentration of 0.6 mass % C at 20 minutes reaction time, an oxygen concentration of 0.004 mass %. Other workers predict a similar oxygen concentration at this carbon level¹⁷². In order to allow for the effect of metal oxygen content on sulphur equilibria, calculations were performed for each specific droplet-slag interaction for a range of oxygen concentrations. A value of f_0 and f_S was generated for each oxygen concentration. The range selected was from zero to 0.06 mass % O.

(b) An Assessment of the Predicted Equilibrium Sulphur Concentrations of Droplets

The equilibrium sulphur concentrations of droplets predicted by the various slag models are given in Tables 64 to 66.

For a given slag composition, equilibrium quotient and metal oxygen concentration the predicted droplet sulphur concentration did not alter significantly with initial droplet sulphur content. This is due to the ratio f_0/f_S being the only factor in equation 5.1 which is related to metal composition at a given oxygen concentration. However, for different sulphur concentrations this term did not change sufficiently in order to produce a variation in predicted equilibrium sulphur concentration with initial droplet composition.

The response of the sulphur predictions to different slag compositions was obviously related to the variation of the ratio N_{S_2} / N_{O_2} . The smallest value of this term was obtained for slag KC3 (0.024) and led to the lowest predictions for the Temkin and Flood Models.

A comparison between the predictions of the Temkin, Flood, Masson and Toop and Samis Models for reactions involving slag KC6 shows that lower predictions result from the silicate slag models (Tables 64 to 66).

The predictions of equilibrium sulphur concentration for a given slag show a wide variation over the metal oxygen concentration range considered. The lack of a precise value for oxygen concentration makes it very difficult to interpret the predicted sulphur levels against those obtained experimentally. The analytical determination of the oxygen concentration of droplets may have allowed the considered oxygen range to be modified but no information would be obtained on interfacial concentrations.

The concentration of oxygen dissolved in iron, considered to be in equilibrium with carbon levels corresponding to the bulk concentrations after 20 minutes reaction in the present work, has been reported as 0.004 mass %¹⁷². Using this value as a guideline, a comparison can be made between the predictions at an oxygen concentration of 0.005 mass % and the experimental results at 20 minutes reaction time. The data is summarised in Tables 64 to 66. This may provide an indication of whether

sulphur equilibrium has actually been achieved. However, from Tables 64 to 66 it can be seen that some predictions are lower than the experimental result and vice-versa. The data generated by the slag models does not allow a straightforward assessment to be made of the difference in droplet sulphur concentration between droplets reacted for 20 minutes and droplets at equilibrium. This is clearly affected by the lack of data on oxygen concentration. Another complication may exist in that the slags employed in the present work approach the acid-base transition and, therefore, the models of Temkin and Flood may be unreliable.

5.3.4 The Applicability of Mass Transfer Models to the Results of the Desulphurisation Experiments

Desulphurisation has been considered with respect to thermodynamic predictions and kinetics explained in terms of mass transfer processes. It is also possible to predict sulphur removal rates by the use of mass transfer models. This can serve to test the validity of theoretical models by comparison with experimentally measured data. If sulphur removal is adequately described by such a model then there is potential for incorporating the information into a steelmaking control system.

The experimental results for the "0.512 mass % S" droplet reacted with slag KC1 showed that the desulphurisation rate could be considered constant during the first few minutes of reaction. This would be consistent with continuous phase control. Therefore, models based on this regime will be considered first.

For a rigid drop in a continuous phase, the following relationship has been proposed for conditions of continuous phase control ¹³³:-

$$Sh = 2 + 0.57 (Gr.Sc)^{0.25} + 0.35Re^{0.62} Sc^{0.31} \quad 5.2$$

$$\text{for } Gr.Sc < 10^8$$

The equation is additive in that the three terms represent contributions for diffusion, natural convection and forced convection respectively.

If sulphur removal is controlled exclusively by the diffusion of O^{2-} anions in the slag phase, then the Sherwood Number, Sh, is equal to 2:-

$$Sh = 2$$

but,

$$Sh = \frac{k_{Sl} \times d_d}{D_{Sl}}$$

where,

k_{Sl} = Mass transfer coefficient of reacting species in slag phase

D_{Sl} = Diffusivity of reacting species in slag phase

d_d = Diameter of drop

If the mass transfer coefficient is known then the molar rate of transfer of the reactant can be determined:-

$$\dot{n} = k_{Sl} A (C_{Sl}^b - C_{Sl}^i)$$

where,

\dot{n} = Molar rate of transfer of considered species

C_{Sl}^b = Bulk concentration of reacting species in slag phase

C_{Sl}^i = Interfacial concentration of reacting species in slag phase

A = Area for reaction

Assuming that the reacting slag phase species is immediately consumed on arrival at the interface, then C_{Sl}^i is zero; from the experimental work, however, this situation may only be valid for a very short time of reaction between an "0.512 mass % S" droplet and slag KC1:-

$$\dot{n} = k_{Sl} A C_{Sl}^b$$

In the present work, the reacting species can be considered to be O^{2-} and, therefore, the above equation becomes:-

$$\dot{n}_{O^{2-}} = k_{O^{2-}} A C_{O^{2-}}^b$$

where,

A = Surface area of droplet

$C_{O^{2-}}^b$ = Bulk concentration of O^{2-} anions in slag = molar density of slag x moles O^{2-} per mole of slag

One mole of O^{2-} reacts with one mole of sulphur so if the

molar rate of transport of O^{2-} is known, then the molar quantity of sulphur reacted can be determined. This can be presented graphically as plots of sulphur concentration remaining in the droplet versus reaction time.

To make predictions for diffusion control in the slag phase a diffusivity value for oxygen anions in the slag is required. Data available on diffusion in slags is both scarce and conflicting⁸⁰. Experimental problems associated with the containment of slags at high temperatures have restricted the number of investigations carried out and the amount of data obtained. The interpretation of results is difficult in the absence of structural knowledge of the slag and, therefore, not knowing how the species of interest is interacting with other slag components. For the present analysis a value of $1.2 \times 10^{-6} \text{ cm}^2/\text{s}$ was taken as the diffusivity of oxygen¹⁷³. The limited data available on oxygen diffusivity suggests that oxygen diffuses faster than calcium⁸⁰. This is surprising in that the calcium cation is smaller than the oxygen anion. The value selected for this work, based on CaO-SiO_2 melts, gives an oxygen diffusivity lower than that for calcium but close to that for silicon.

For diffusion control:-

$$\text{Sh} = 2 = \frac{k_{O^{2-}} x d}{D_{O^{2-}}}$$

$$k_{O^{2-}} = \frac{1.2 \times 10^{-6} \times 2}{0.8}$$

$$k_{O^{2-}} = 3 \times 10^{-6} \text{ cm/s}$$

The above treatment indicates that the molar flux of the O^{2-} species will vary as the value of $C_{O^{2-}}^b$ alters with slag composition. The molar concentration of the O^{2-} anion cannot be determined directly and requires that assumptions are made regarding the anionic constitution of the slag. For basic slags, Temkins Model ⁷⁰ utilised a dissociation scheme that assumed free O^{2-} anions were present, provided sufficient oxygen had been contributed by basic oxides to allow silicon to exist solely as SiO_4^{4-} anions. Using this dissociation scheme a value can be obtained for the molar concentration of O^{2-} anions in the slag and multiplied by the molar density of the slag (calculated from density values proposed by Gaskell ⁹⁵) will give a value of $C_{O^{2-}}^b$. Temkin's dissociation scheme, when applied to the basic slags in this work, gave small and similar values of O^{2-} anion concentration due to slag compositions being close to the acid-base transition. However, molar rates of transport of O^{2-} anions and hence sulphur removal rates were calculated for some droplet interactions involving slag KC1 (38.06 mass % CaO-30.88 mass % FeO-30.80 mass % SiO_2 -0.27 mass % S) which represented a typical molar O^{2-} anion concentration of 0.003 moles O^{2-} /mole slag and slag KC2 (27.67 mass % CaO-44.01 mass % FeO-28.17 mass % SiO_2 -0.15 mass % S) which gave the highest value of 0.005 moles O^{2-} /mole slag. Also considered was slag KC6 (71.87 mass % FeO-

27.81 mass % SiO_2 -0.32 mass % S) of O^{2-} molar concentration 0.003 moles O^{2-} per mole of slag.

For the above slags, with Sh equal to two, the values of $\dot{n}_{\text{O}^{2-}}$ were calculated:-

$$\text{Slag KC1} , \dot{n}_{\text{O}^{2-}} = 2 \times 10^{-8} \text{ mole/s}$$

$$\text{Slag KC2} , \dot{n}_{\text{O}^{2-}} = 3 \times 10^{-8} \text{ mole/s}$$

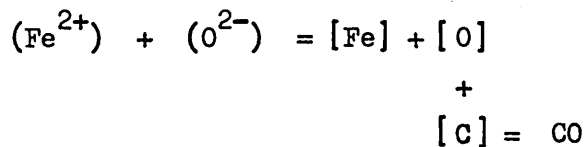
$$\text{Slag KC6} , \dot{n}_{\text{O}^{2-}} = 2 \times 10^{-8} \text{ mole/s}$$

For slag KC1 the predicted sulphur removal was calculated for the examples of initial droplet sulphur concentrations 0.512 and 0.120 mass % S. The results are plotted in Figures 88a and 88b, with the experimental results included. The predictions and experimentally obtained results for slag KC2 reacted with a droplet of initial sulphur concentration 0.120 mass % S and slag KC6 reacted with a "0.110 mass % S" droplet are given in Figures 89 and 90 respectively.

The above examples all predict a lower sulphur removal rate than that measured experimentally. The main reason for this is the very low O^{2-} concentrations calculated from the Temkin dissociation scheme. The effect of this term can be further examined by application of the Toop and Samis slag Model to the binary slag KC6 (71.87 mass % FeO-27.81 mass % SiO_2 -0.32 mass % S). This model will allow an oxygen anion

concentration to be evaluated which takes into account O^{2-} anions contributed to the slag by silicate polymerisation. The model predicts an oxygen concentration of 0.328 moles O^{2-} /mole slag which gives a molar concentration of 0.017 moles O^{2-}/cm^3 slag. The value of $\dot{n}_{O^{2-}}$ becomes 10.5×10^{-8} mole/s compared with 2×10^{-8} mole/s derived from the Temkin dissociation scheme. Predicted sulphur removal is given in Figure 90 with the high O^{2-} anion concentration having increased the desulphurisation rate. However, the predicted rate of removal is still lower than the experimental data obtained for the first 2 minutes of reaction.

It is clear that the predictions for diffusion control even when accounting for O^{2-} concentration due to silicate polymerisation, show a lower sulphur removal rate than those actually obtained in the experiments. It has been mentioned earlier in this section that the data available for oxygen diffusivity in slags could be a source of error. Further, the treatment of mass transfer in the calculations has employed an area term equal to the surface area of the droplet which assumes maximum droplet-slag contact. This cannot be correct due to the evolution of CO. In addition, not all the O^{2-} anions in the slag are available for the sulphur transfer reaction because some will be involved in a coupled reaction with Fe^{2+} for decarburisation to occur,



Unfortunately, the latter two factors cannot be quantified. The

present analysis is, therefore, based on conditions which will increase the predicted rate of sulphur removal. As the predictions give lower sulphur removal rates than actually observed it must be concluded that conditions of diffusion control do not govern the early stages of sulphur removal,

The predicted rates of sulphur removal can be increased by use of the terms for natural convection given in equation 5.2. For conditions of natural convection the following relationship has been proposed ¹³³:-

$$Sh = 2 + 0.57 (Gr.Sc)^{0.25} \quad 5.3$$

It has already been noted that the present experimental system involves CO evolution which will produce slag stirring. The contribution to mass transfer rates by a mechanism of natural convection is considered inapplicable.

If mass transfer rates are controlled by conditions of forced convection, the following relationship applies ¹³³:-

$$Sh = 2 + 0.35 Re^{0.62} Sc^{0.31} \quad 5.4$$

Unfortunately, this equation cannot be used to predict sulphur removal rates based on the experimental conditions because a value of slag velocity, required for the Reynolds Number, is not known. If the experimental results for slag KC1 reacted with a "0.512 mass % S" droplet are considered, the desulphurisation rate over the first 2 minutes of reaction corresponds to a Sherwood Number of 75 (Figure 88a). Substitution of this value into equation 5.4 will allow a value

for the slag velocity to be calculated. Using a slag viscosity of $1\text{g/cm}\cdot\text{s}$ ¹⁷⁴ and a density of 3.06g/cm^3 ⁹⁵ the Schmidt Number is:-

$$Sc = \frac{\mu_{Sl}}{\rho_{Sl} D_o^2}$$

$$Sc = 272 \times 10^3$$

from

$$Sh = 75 = 2 + 0.35 Re^{0.62} Sc^{0.31}$$

then

$$Re = 10.5$$

$$Re = 10.5 = \frac{\rho_{Sl} u_{Sl} d_d}{\mu_{Sl}}$$

$$u_{Sl} = 4.3 \text{ cm/s}$$

Thus, to achieve the observed initial rate of sulphur removal, a slag velocity of 4.3 cm/s is required. It has been mentioned (Section 2.4.4) that x-ray studies by other workers^{15, 143} have indicated limited slag stirring during decarburisation of iron alloy droplets by slags of high FeO contents. The calculated slag velocity may, therefore, be greater than that achieved experimentally. In addition, no account has been made for CO evolution reducing the metal-slag contact area. If bubbles cover a large proportion of the droplet surface, then in order to achieve the observed desulphurisation rate, slag velocity will have to be greater than that calculated.

The experimental results for slag KC1 reacted with "0.512 mass % S" droplets showed a linear rate of sulphur removal followed by a decreasing desulphurisation rate suggesting a transition to dispersed phase control. Models dealing with mass transfer control within the dispersed phase will be applied to the observed periods of decreasing sulphur removal rate.

The slowest mass transfer rates within the droplet are predicted for a non-circulating, non-oscillating drop or rigid drop. The analysis simplifies to a consideration of radial diffusion of the solute within the drop assuming a constant surface concentration equal to zero. This diffusion problem has been considered by Crank¹⁷⁵ who provides a number of graphical solutions but these can be accurately represented by the empirical equation of Vermulen¹²⁸ :-

$$f = \left[1 - \exp\left(\frac{-4D\pi^2 t}{d^2}\right) \right]^{\frac{1}{2}} \quad 5.5$$

where

- f = fraction of solute extracted
- D = Diffusivity of solute in droplet
- t = reaction time
- d = diameter of droplet

From the above equation, employing a value for the diffusivity of sulphur in carbon-saturated iron of $2.9 \times 10^{-5} \text{ cm}^2/\text{s}$ ¹⁶⁶, values of f have been evaluated.

Dispersed phase control did not start at zero time and for the purpose of calculations was considered to correspond to the reaction time at which the experimentally measured de-sulphurisation graph deviated from linearity. The predictions are presented in graphical form shown as sulphur concentration [mass %] in the droplet against reaction time. Figures 91a, 91b, 92 and 93 show the predictions for the respective reactions of KC1 with the "0.512 mass % S" droplet, KC1 with "0.120 mass % S" droplet, KC2 with the "0.120 mass % S" droplet and KC6 with the "0.110 mass % S" droplet. Each figure includes the curve obtained from the experimental results.

The examples considered show that the predicted rates of sulphur removal are greater than the experimentally measured data. This tends to rule out the possibility of the droplets behaving as stagnant spheres. However, the calculations assume that the complete droplet surface is in contact with slag which as pointed out earlier, cannot be true because of CO evolution. The predictions, therefore, over-estimate the fractions of sulphur extracted from the droplet.

Qualitatively, it is difficult to envisage that the droplet will behave as a stagnant sphere when internal nucleation of CO occurs. Thus, internal circulation of the droplet should be expected. The fraction of solute extracted from a fully circulating droplet can be calculated using the following relationship proposed by Kronig and Brink¹²⁹ :-

$$f = \left[1 - \exp \left(\frac{-2.25 \times 4 \times D \pi^2 t}{d^2} \right) \right]^{\frac{1}{2}} \quad 5.6$$

The predictions based on this model are included in Figures 91a to 93. As the model takes account of internal circulation an increase in sulphur removal rate relative to the rigid drop model predictions, is produced. This widens the difference between experimental and predicted rates but as in the previous situations the calculated results assume maximum slag-metal contact.

The applicability of mass transfer models to slag-metal systems such as the one studied is clearly very limited. The models themselves were developed mainly from aqueous and organic systems with attendant physical properties far removed from those of metals and slags. However, if data is available for metal-slag systems it is often of suspect accuracy. The data for slags, particularly diffusivity values, is clearly a problem area because no precise account can be made for anionic constitutions. Finally, the practical difficulties involved in working with high temperature slag-metal systems makes it difficult to obtain the information required for the models.

5.3.5 The Applicability of the Experimental Results to LD Steelmaking

Initial metal sulphur levels encountered in LD steel-making depend upon blast furnace practice and whether external desulphurisation techniques have been used. Assuming no

external desulphurising treatment, a typical sulphur level of blast furnace metal is about 0.050 mass % S³⁴. As indicated, this can vary with blast furnace practice and levels as high as 0.100 mass % S are not unknown. The majority of droplet experiments in the present work have employed droplet sulphur concentrations of about 0.030 to 0.100 mass % and, therefore, correspond to the industrial situation.

A consideration of slag compositions in U.K. LD steelmaking practice shows that turndown sulphur levels are around 0.28 mass % S³⁴. The experimental slags ranged from 0.09 to 0.32 mass % S. By careful control of charge compositions, slag sulphur levels would be expected to be reasonably low at the early stages of the LD blow. The experimental work, therefore, represented with respect to slag sulphur concentration, severe conditions for desulphurisation.

The first few minutes of the LD blow produces a slag rich in FeO, MnO and SiO₂. Early formation of a high SiO₂ content slag produces rapid fluxing of CaO^{16, 21}. During this period the slag refining path moves towards the CaO' corner of the CaO'-FeO'-SiO₂' pseudoternary diagram²⁵ (Figure 5). Lime concentration increases at the expense of FeO and because the SiO₂ concentration is high the slag is close to the acid-base transition. The slags employed for the droplet experiments, therefore, provide a simple representation of those present during the early stages of the LD blow. The starting point is modelled by a 71.87 mass % FeO

-27.81 mass % SiO_2 -0.32 mass % S composition (KC6, Table 58) with progressive substitution of CaO for FeO up to a composition of 38.06 mass % CaO-30.88 mass % FeO-30.80 mass % SiO_2 -0.27 mass % S (slag KC1, Table 58).

If refining in the LD process is proceeding by the reaction of metal droplets with the slag phase, then the experimental results indicate that droplets of sulphur concentrations 0.050 mass % and higher will be desulphurised by slags containing up to 28 mass % CaO (slags KC6 to KC2, Table 58). A slag composition containing 38 mass % CaO (slag KC1) will desulphurise droplets of 0.100 mass % S and higher. The desulphurisation commences at the start of droplet-slag interaction due to the availability of O^{2-} anions which are derived from the presence of FeO at the droplet-slag interface. The FeO prevents formation of a CaO- SiO_2 interfacial slag of low O^{2-} anion activity. In addition, the removal of carbon under conditions of slag phase control maintains a finite carbon and low oxygen content at the droplet surface creating conditions favourable for sulphur removal. The extent of desulphurisation will, however, be limited by the onset of sulphur removal being governed by conditions of dispersed phase control.

The observations referred to above show that conditions can exist for sulphur removal to occur early in the blow which can result in lowering of the bulk metal bath sulphur content. This does refer to a situation of reasonably high initial metal

sulphur levels reacted with high sulphur concentration slags. The experiments involving "0.512 mass % S" droplets reacted with the 38.06 mass % CaO-30.88 mass % FeO-30.80 mass % SiO₂-0.27 mass % S slag (KC1) shows that good desulphurisation can be expected when a differential exists between the bulk sulphur concentrations of the metal and slag phases. Again, the onset of dispersed phase controlled desulphurisation will prevent a protracted period of efficient desulphurisation.

For a situation of low initial sulphur concentration droplets and slag sulphur levels similar to those employed in the experiments, a possibility of sulphur reversion exists. This was demonstrated by reactions between "0.030 mass % S" droplets with slags up to 28 mass % CaO (KC6 to KC2) and droplets containing 0.076 mass % S and lower with a slag of 38 mass % CaO (KC1). As the slag increases in CaO concentration, the depletion of interfacial FeO becomes more pronounced. This causes the interfacial slag composition to become progressively more acidic and if a CaO-SiO₂ acid slag is produced then O²⁻ anion availability is very low. Conditions are, therefore, established for sulphur reversion to occur. An eventual change in the ongoing decarburisation mechanism from continuous to mixed or dispersed phase control will re-create a more basic interfacial slag composition allowing desulphurisation to commence. The effect on the bulk metal bath will be either an increase in sulphur content assuming droplets return to the bath during the reversion

phenomenon or a small decrease in sulphur concentration due to droplets re-entering the bath during the delayed desulphurisation period.

Conditions surrounding the initial reversion phenomenon may be of limited applicability to LD steelmaking with respect to early slag and metal sulphur levels. The presence of low, initial sulphur concentration metal (~ 0.020 mass % S) would be assured if external desulphurisation processes have been used which tends to be standard practice nowadays. Control of charge compositions should provide low sulphur concentrations of slags at the early stages of the blow. However, it is possible that blast furnace slag introduced into the metal transfer car on casting, and slag from the external desulphurising operation, are not removed from the hot metal prior to charging into the LD vessel. These materials provide a source of acid slag components and sulphur. The time required to dilute these components depends upon the development of the slag during the early stages of the LD blow. Thus, a period is created where a high sulphur concentration slag is present. If this situation occurs then on the basis of the experimental results, the possibility of sulphur reversion is very high.

6. CONCLUSIONS

1. The anionic constitution of silicate minerals and slags was investigated by trimethylsilylation and GLC techniques. For minerals of known silicate structure the main product of trimethylsilylation was always the TMS derivative of the parent anion.
2. Trimethylsilylation of industrial and synthetic slags containing appreciable amounts of FeO produced similar chromatographic results irrespective of the silica concentration of the slag. Different chromatographic responses were obtained from slags of low or zero FeO concentrations.
3. The influence of FeO or Fe²⁺ cation on the trimethylsilylation process employed prevents structural interpretations being made from chromatograms of trimethylsilylated slags of steelmaking compositions.
4. A limited study on a PbO-SiO₂ synthetic slag gave chromatographic results that were best described by the Masson Branched Chain Slag Model.
5. Techniques have been developed to investigate the desulphurisation of single iron-carbon droplets by a range of oxidising slag compositions. The techniques were also employed to monitor the decarburisation process.

6. The decarburisation of single metal droplets involved two dominant mechanisms. An initial period of efficient carbon removal was indicative of continuous phase control and a subsequent slow decarburisation rate was attributed to dispersed phase control.
7. Slag containing up to 28 mass % CaO reacted with droplets of about 0.050 mass % S and higher, showed an initial efficient period of desulphurisation followed by a transition to a slow sulphur removal rate. A similar trend occurred for droplets of 0.120 mass % S and higher reacted with a 38 mass % CaO slag.
8. The initial efficient desulphurisation period always occurred during the continuous phase controlled decarburisation process which established a finite carbon and low oxygen concentration at the droplet surface. It is believed that these conditions, in conjunction with the presence of FeO at the droplet-slag interface, provide circumstances favourable for sulphur removal.
9. An initial period of sulphur reversion occurred for droplets of about 0.030 mass % S reacted with slag containing up to 28 mass % CaO and droplets of 0.076 mass % S and lower with slag containing 38 mass % CaO. Reversion was operative for 2 to 5 minutes after which desulphurisation commenced.

10. Sulphur reversion was attributed to the development of an acid interfacial slag via progressive denudation of FeO during the continuous phase controlled decarburisation process. Subsequent desulphurisation was initiated by the replenishment of FeO to the interfacial slag by virtue of a transition to mixed transport or dispersed phase controlled decarburisation.
11. The observed desulphurisation of droplets by an FeO-SiO₂ slag during continuous phase controlled decarburisation confirmed that instantaneous denudation of FeO at the droplet-slag interface did not occur.
12. For the range of slags studied, the availability of free oxygen anions for the sulphur transfer reaction during continuous phase controlled decarburisation was related to the presence of FeO. This species inhibits the formation of an interfacial CaO-SiO₂ acid slag of low oxygen anion concentration.

CHAPTER SEVEN

SUGGESTIONS FOR FURTHER WORK

7. SUGGESTIONS FOR FURTHER WORK

1. In view of the lack of data on silicate slag structures and the need to test and extend existing slag models, the trimethylsilylation technique represents an important approach to this area of research. The following points are considered:-

(a) The use of a chromatogram with sample collection facilities will allow TMS derivatives of silicate anions to be separated and collected. These samples can be used to determine detector response factors from which a re-appraisal of the accuracy of the trimethylsilylation technique can be made using minerals of known structure.

(b) Modification of the trimethylsilylating process is required in order to study slags containing FeO. The effect of adjusting the relative quantities of reagents and slag needs to be investigated in addition to the possibility of employing trimethylsilylating agents other than trimethylchlorosilane. The determination of the optimum conditions of trimethylsilylation of the orthosilicate mineral Fayalite, Fe_2SiO_4 or Akermanite $\text{Ca}_2\text{FeSi}_2\text{O}_7$, provides a starting point from which synthetic FeO-SiO_2 and CaO-FeO-SiO_2 slags can be investigated.

(c) Trimethylsilylation of CaO-SiO₂ synthetic slags would provide information on a system relevant to steelmaking slags and allow comparison with available silicate slag model data.

2. With respect to the single metal droplet techniques, information on desulphurisation could be augmented by:-

(a) An investigation of reactions between slags of very low sulphur concentrations and droplets similar to those already employed. The high sulphur concentrations of the slags used were primarily derived from the graphite crucible in which the slags were initially fused. Sulphur can be removed by water quenching small quantities of re-fused slag but this lengthens the slag preparation procedure.

(b) The modification of apparatus to achieve quenching of reacted droplet and slag in an inert atmosphere that will permit data to be collected on reacted slag sulphur levels. This information coupled with experimental data of droplet oxygen concentrations at intervals during the reaction period will improve the predictions of equilibrium sulphur concentrations based on slag models.

(c) The development of alternative crucibles for the stopper and seat technique particularly, that will permit higher experimental temperatures and a wider

range of slag compositions.

3. The following points are considered as areas of future research relevant to the study of desulphurisation of single metal droplets:-

- (a) The investigation of sulphur transfer between iron-carbon droplets and slags should always be complemented by a study of the simultaneous decarburisation process. Further elucidation of the effect of slag composition on decarburisation is required including a study of carbon removal behaviour at very short reaction times.
- (b) The effect of different metal solutes on the desulphurisation (and decarburisation) of metal droplets by oxidising slags needs identifying. Choice of solutes should be governed by typical iron blast furnace metal compositions but the droplet analyses used in the present work with around a 1 mass % Si addition seems a logical starting point.
- (c) LD steelmaking practice now commonly features the use of dolomitic lime additions to the slag but the effect on desulphurisation is not clear. There is scope for single droplet desulphurisation studies employing slags used in the present investigation with about 5 mass % MgO addition. Again, the

decarburisation process should be monitored to
identify any effects relative to carbon removal.

REFERENCES

1. Data published in Iron and Steelmaker, July 1984
2. Walker R.D. and Anderson D. Iron and Steel
Part I 1972, June p271
Part II 1972, August p403
Part III 1972, October p497
3. Lange K.W. International Conference On Physical Chemistry and Steelmaking, Versaille, October, 1978. SFM, IRSID, ATS. Pre-print.
4. Pehlke R.D. Met. Trans. B., 1980, 11B, p539
5. Gaines et al (Eds) BOF Steelmaking, 5 volume Monograph Series ISS-AIME, 1977, Ed. J.M. Gaines
6. Ward M.D. Ironmaking and Steelmaking Quarterly, 1975, No. 2, p89
7. Bodsworth C. and Bell H.B. Physical Chemistry of Iron and Steel Manufacture. Longmans, 1972 2nd Edition
8. Meyer H.W. J.I.S.I., 1969, June, p781
9. Szekely J. and Todd M.R. Trans. Met. Soc. AIME, 1967, 239, p1664
10. Li K., Dukelow A. and Smith G.C. Trans. Met. Soc. AIME, 1964, 230, p71
11. Oeters F. B.I.S.I. Translation 5505
12. Kawakami K. J. Met., 1966, July, p836
13. Meyer H.W. et al J. Met., 1968, July, p35
14. Trentini B. Trans. Met. Soc. AIME, 1968, 242, p2377
15. Mulholland E.W., Hazeldean G.S.F. and Davies M.W. J.I.S.I., 1973, September, p632
16. Price D.J. Ph.D. Thesis, Brunel University, 1972
17. Chaterjee A. et al Ironmaking and Steelmaking Quarterly, 1976, No. 1, p21
18. Kozakevitch P. J. Met., 1969, July, p57
19. Kozakevitch P. Physical Chemistry of Steelmaking The Chipman Conference, 1958, Ed. J.F. Elliott M.I.T. Press and Wiley

20. Cooper C.F. and Kitchener J.A. J.I.S.I., 1959, September, p48
21. Van Hoorn A.I. and Van Konynenburg J.I. Symposium External Desulphurisation of Hot Metal, Ed. W-K Lu, McMaster University, Canada, May 1975
22. Williams P. Ph.D. Thesis, Sheffield City Polytechnic, 1980
23. Muan A. and Osborn E.F. Phase Equilibria Among Oxides in Steelmaking, Addison-Wesley Comp. Inc., 1965
24. Bardenheuer F. et al Blast Furnace and Steel Plant, 1970, June, p401
25. Baker R. British Steel Corporation Report CAPL/SM/A/31/74
26. Marinin A.V. and Bolshakov V.A. Stal in English, 1968, October, p826
27. Richardson F.D. and Fincham C.J.B. J.I.S.I., 1954, September, p4
28. Riboud P.V. et al B.I.S.I. Translation, 8990
29. Nilles P., Dauby P. and Claes J. Met. Soc. Conf., London, 1978
30. Yoshii M. and Ichinohe M. B.I.S.I. Translation, 8854
31. Harhai J.G. and Dukelow D.A. J. Met., 1966, July, p833
32. Obst. K-H Stahl u. Eisen 100, 1980, p20
33. Starov R.V. et al Steel in the USSR, 1974, February, p106
34. Cavaghan N.J., Ford D. and Woodhead A. Ironmaking and Steelmaking Quarterly, 1981, No. 2, p66
35. Anderson L.C. and Vernon J. J.I.S.I., 1970, April, p239
36. Leonard L.A. J.I.S.I., 1970, April, p324
37. McMulkin F.J. Ironmaking and Steelmaking Quarterly, 1981, No. 2, p76
38. Recknagel W. and Hater M. Ibid., 1981, No. 2, p81

39. Potocic R.F. and Leewis K.G. Symposium. External Desulphurisation of Hot Metal. Details as Ref. 21
40. Meichsner W. et al J. Met., 1974, April, p55
41. Koros P.J. et al Ironmaking and Steelmaking, 1977, June, p34
42. Koros P.J. and Petrushka R.G. Symposium. External Desulphurisation of Hot Metal. Details as Ref. 21
43. Chang L. and Goldman K. Trans. (AIME), 1948, 176, p309
44. Derge G., Philbrook W.O. and Goldman K. Ibid, 1950, 188, p1111
45. Derge G., Philbrook W.O. and Goldman K. Ibid, 1954, May, p534
46. Turkdogan E.T., Hancock R.A. and Pearson J. J.I.S.I., 1955, April, p338
47. Morris J.P. and Buehl R.C. Trans. (AIME), 1950, 188, p317
48. Sherman C.W., Elvander H.I. and Chipman J. Ibid, 1950, 188, p334
49. Sherman C.W. and Chipman J. Ibid, 1952, 194, p597
50. Ban-ya S. and Chipman J. Trans. Met. Soc. AIME, 1969, 245, p133
51. Mitchell A. International Conference On Physical Chemistry and Steelmaking. Details as Ref. 3
52. Ramachandran S., King T.B. and Grant N.J. Trans. (AIME), 1956, 206, p1549
53. King T.B. and Ramachandran S. Physical Chemistry of Steelmaking. The Chipman Conference, p125. Details as Ref. 19.
54. Ward R.G. and Salmon K.A. J.I.S.I., 1960, December, p393
55. Saelim A. and Gaskell D.R. Met. Trans. B., 1983, 14B, p259

56. Fulton J.C. and Chipman J. Physical Chemistry of Steelmaking. The Chipman Conference, p113. Details as Ref. 19.
57. Ward R.G. and Salmon K.A. J.I.S.I., 1963, March, p222
58. Froberg M.G., Kapoor M.L. and Nilas A. Chemical Metallurgy of Iron and Steel, ISI, 1973, p139
59. Tokuda M. and Ohtani M. Ibid, p93
60. Niwa K. and Yokokawa T. Ibid, p77
61. Froberg M.G., Nilas A. and Kapoor M.L. Trans. I.S.I.J., Vol. 11, 1971, p495
62. Chon M. et al Ibid, p500
63. Ishii K. et al Ibid, p506
64. Bargeron W.N., Trojan P.K. and Flinn R.A. Trans. Am. Fndrymn. Soc., 1969, 77, p303
65. Bargeron W.N., Trojan P.K. and Flinn R.A. AFS. Cast Metals Res. Jnl., 1970, 6, p129
66. Rocca R., Grant N.J. and Chipman J. Trans. (AIME), 1951, 3, p319
67. Kor. G.J.W. Met. Trans. B., 1977, 8B, p107
68. Herasymenko P. Trans. Farad. Soc., 1938, 34.2, p1245
69. Herasymenko P. and Speight G.E. J.I.S.I. Part I 1950, November, p169
Part II 1950, December, p289
70. Temkin M. Acta. Physicochemica URSS, 1945, XX, p411
71. Flood H. and Grjotheim K. J.I.S.I., 1952, May, p64
72. Temkin M. et al Acta. Physicochemica URSS, 1945, XX, p421
73. Masson C.R. Chemical Metallurgy of Iron and Steel ISI, 1973, p3
74. Ward R.G. An Introduction to the Physical Chemistry of Iron and Steelmaking, Arnold, 1962

75. Elliott J.F.,
Lynch D.C. and
Braun T.B. . Met. Trans. B., 1975, 6B, p495
76. Blander M. Ibid, 1977, 8B, p529
77. Gaye H.,
Grosjean J.C.
and Riboud P.V. C.E.C.A. Research Project No. 7210,
CA/3/303
78. Coudurier L.,
Hopkins D.W.
and Wilkomersky I. Fundamentals of Metallurgical Processes.
Pergamon 1st Ed., 1978
79. Richardson F.D. Physical Chemistry of Steelmaking,
The Chipman Conference, 1958, p55.
Details as Ref. 19
80. Richardson F.D. Physical Chemistry of Melts in Metallurgy,
Vols. 1&2, Academic Press Inc.(London)Ltd.,
1974
81. Bockris J. O'M.,
Mackenzie J.D.
and Kitchener J. Trans. Farad. Soc., 1955, 51, p1734
82. Bockris J.O'M.,
and Lowe D.C. Proc. Roy. Soc., 1954, 226, p423
83. Bockris J.O'M.,
Tomlinson J.W.
and White J.L. Trans. Farad. Soc., 1956, 52, p299
84. Toop G.W. and
Samis C.S. Trans. Met. Soc. AIME, 1962, 224, p878
85. Kapoor M.L. and
Frohberg M.G. Chemical Metallurgy of Iron and Steel,
ISI, 1973, p17
86. Yokokawa and Niwa Trans. Jap. Inst. Met., 1969, 10
87. Borgianni C. and
Granati P. Met. Trans. B., 1977, 8B, p147
88. Borgianni C. and
Granati P. Ibid, 1979, 10B, p21
89. Lin P.L. and
Pelton A.D. Ibid, 1979, 10B, p667
90. Gaskell D.R. Inter. Symp. Metall. Slags, Halifax,
Canada, 1980, August. Pre-print
91. Masson C.R. Proc. Roy. Soc., 1965, A227, p201

92. Masson C.R.,
Smith I.B. and
Whiteway S.G. Can. J. Chem., 1970, 48, p1456
93. Rao B.K.D.P. and
Gaskell D.R. Met. Trans. B., 1981, 12B, p311
94. Masson C.R. and
Caley W.F. J.C.S. Faraday I., 1978, 74, p2942
95. Lee Y.E. and
Gaskell D.R. Met. Trans., 1974, 5, p853
96. Gaskell D.R. Iron and Steelmaker, 1983, July, p49
97. Waseda Y. and
Toguri J.M. Met. Trans. B., 1977, 8B, p563
98. Waseda Y. and
Toguri J.M. Ibid, 1978, 9B, p595
99. Kashio S. et al Trans. I.S.I., Jap., 1980, 20, p251
100. Bowker J.C.,
Lupis C.H.P. and
Flinn P.A. Inter. Symp. Metall. Slags, Halifax,
Canada, 1980, August. Pre-print
101. Ramous E. et al Met. Trans. B., 1981, 12B, p403
102. Jeffes J.H.E. Inter. Symp. Metall. Slags, Halifax,
Canada, 1980, August. Pre-print
103. Lentz C.W. Inorg. Chem., 1964, 3, 4, p574
104. Jones A.R. An Introduction to Gas Liquid
Chromatography, Academic Press, 1970
105. Butts W.C. Analyt. Letters, 1970, 3, p29
106. Butts W.C. and
Rainey W.T. Analyt. Chem., 1971, 43, p538
107. Gotz J. and
Masson C.R. J. Chem. Soc. (A), 1970, p2683
108. Gotz J. and
Masson C.R. Ibid, 1971, p686
109. Calhoun H.P. and
Masson C.R. J.C.S. Dalton, 1980, p1282
110. Terry B. and
Monhemius A.J. Met. Trans. B., 1983, 14B, p335
111. Terry B. Hydrometallurgy, 1983, 10, p135

112. Currell B.R.,
Midgley H.G.,
Seaborne M.A. and
Thakur C.P. Br. Polym. J., 1974, 6, p229
113. Wu F.F.H. et al J. Chromatog., 1970, 48, p515
114. Eglinton G. et al Chem. Geol., 1974, 13, p125
115. Gotz J. and
Masson C.R. J.C.S. Dalton, 1978, p1342
116. Sharma S.K.,
Glasser L.S.D.
and Masson C.R. Ibid, 1973, p1324
117. Masson C.R. Jnl. Non-Cryst. Solids, 1977, 25, p1
118. Glasser L.S.D.
and Sharma S.K. Br. Polym. J., 1974, 6, p283
119. Gotz J. and
Masson C.R. Proc. 9th Inter. Congress, Glass, Paris.
Institut du Verre, 1971
120. Garzo G. et al J.C.S. Dalton, 1980, p2068
121. Gotz J.,
Masson C.R. and
Castelliz L.M. Amorphous Materials, Ed. Douglas R.W. and
Ellis B., New York, Wiley, 1972, p317
122. Calhoun H.P.,
Jamieson W.B.
and Masson C.R. J.C.S. Dalton, 1979, p454
123. Masson C.R.,
Jamieson W.D.
and Mason F.G. Physical Chemistry of Process Metallurgy.
The Richardson Conference, IMM, 1974, p223
124. Richardson F.D. Trans. I.S.I., Japan, 1973, 13, p369
125. Richardson F.D. Met. Trans. B., 1971, 2B, p2747
126. Aeron S.M. Ph.D. Thesis, University of London, 1971
127. Hu S. and
Kintner R.C. A.I.Ch.E.Jnl., 1955, March, p42
128. Vermulen T. Ind. Eng. Chem., 1953, 45, p1664
129. Kronig R. and
Brink J.C. Appl. Sci. Res. A2, p142
130. Handlos A.E. and
Baron T. A.I.Ch.E.Jnl., 1957, 3, p127

131. Rose P.M. and Kintner R.C. Ibid, 1966, 12, p530
132. Angelo J.B. et al Ibid, 1966, 12, p198
133. Steinberger R.L. and Treybal R.E. Ibid, 1960, 6, p327
134. Griffith R.M. Ch. Eng. Sci., 1960, 12, p198
135. Higbie R. Trans. Am. Inst. Chem. Engrs., 1935, 31, p365
136. Aeron S.M., Crimes P.B. and Richardson F.D. Trans. Inst. Min. Met., 1974 [C] , 83, p168
137. Richardson F.D. Trans. I.S.I., Jap., 1974, 4, p1
138. Gaye H. and Riboud P.V. Met. Trans. B., 1977, 8B, p409
139. Kozakevitch P., Urbain G. and Sage M. Coal Trade Rev., 1955, 170, p963
140. Kozakevitch P. Surface Phenomena of Metals, Soc. Ch. Ind. Monograph 28, 1968, p223
141. Richardson F.D. Chemical Metallurgy of Iron and Steel, ISI, 1973, p82
142. Lu W-K and Hamielec A.E. Ibid, p110
143. Gare T. and Hazeldean G.S.F. Ironmaking and Steelmaking Quarterly, 1981, No. 4, p169
144. Urquhart R.C. and Davenport W.G. J. Met., 1970, June, p36
145. Sano N. and Matsushita Y. Trans. I.S.I. Japan, 1971, 11, p232
146. Yavoiskii V.I. et al Steel in the USSR, 1978, Sept., p502
147. Baker L.A., Warner N.A. and Jenkins A.E. Trans. Met. Soc. AIME, 1967, 239, p857
148. Distin P.A., Hallett G.D. and Richardson F.D. J.I.S.I., 1968, August, p821

149. Kaplan R.S. and Philbrook W.O. Trans. Met. Soc. AIME, 1969, 245, p2195
150. El-Kaddah N.H. and Robertson D.G.C. Met. Trans. B., 1978, 9B, p191
151. Baker R. J.I.S.I., 1967, June, p637
152. Baker L.A. and Ward R.G. Ibid, 1967, July, p714
153. Roddis P.G. Ibid, 1973, January, p53
154. See J.B. and Warner N.A. Ibid, 1973, January, p44
155. Vig S.K. and Lu W-K Ibid, 1971, August, p630
156. Belton G.R. Met. Trans. B., 1979, 10B, p118
157. Grieveson P. and Pomfret R.J. Inter. Symp. Metall. Slags, Halifax, Canada, 1980, August, Pre-print
158. Ojeda M. Ph.D. Thesis, Sheffield City Polytechnic
159. Masson C.R. Private Communication
160. Bobbit, Schwarting and Gritter Introduction to Chromatography, Reinhold Science Studies, 1968
161. Petzold A. Wiss. Zeit. Hoch. Arch. Bauwesen. Weimer, 1966, 13 (3), p343
162. Garbo G. et al J. Chromatog., 1978, 167, p321
163. Kawai Y. Trans. I.S.I.J., Vol. 11, 1971, p387
164. Narita K. and Onoye T. Ibid, p400
165. Smithells C.J. Metals Reference Book, 5th Edition, Butterworths, 1976
166. Elliot J.F., Gleiser M. and Ramakrishna V. Thermochemistry for Steelmaking, 1963, Vol. II, Addison Wesley
167. Levin E.M., Robbins C.R. and McMurdie H.F. Phase Diagrams for Ceramists, The American Ceramic Society, Inc., 1964
168. Hilty D.C. and Crafts W. Trans. A.I.M.E. (J. Metals), December, 1952, p1307

169. Johnston R.F., Stark R.A. and Taylor J. Ironmaking and Steelmaking Quarterly, 1974, No. 4, p220
170. Fettters K.L. and Chipman J. Trans. Amer. Inst. Min. (Metall) Engrs., 1941, 145, p95
171. Vacher H.C. and Hamilton E.H. Trans. A.I.M.E., 1931, 95, p124
172. Turkdogan E.T., Davies L.S., Leake L.E. and Stevens G.S. J.I.S.I., 1955, October, p123
173. Keller H. et al Met. Trans. B., 13B, 2, 1982, p237
174. Rontgen P. et al B.I.S.I.T., Translation 2475
175. Crank J. The Mathematics of Diffusion, Oxford Clarendon Press, 5th Edn., 1970

Table 1

Effect of Iron Sulphur Specification on Coke Rate, Output and Cost for Base Case Hot Metal Sulphur Content 0.045 Mass % S, Coke Sulphur 1.0 Mass % (34)

Iron Sulphur Mass %	Coke Rate (kg/t)	Production (t/day)	Cost Increase
0.045		10000	
0.025	16	9610	1.8
0.020	38	9110	4.3
0.015	78	8290	8.9
0.010	183	6745	20.9

Table 2

Relative Desulphurising Powers of the Basic Oxides (74)

Cation i	Ca ²⁺	Fe ²⁺	Mn ²⁺	Mg ²⁺	Na ⁺
log K' _i	-1.4	-1.9	-2.0	-3.5	+1.63
K' _i	0.040	0.013	0.01	0.0003	42.6
Desulphurising Power Relative to Calcium as Unity	1.0000	0.325	0.25	0.0075	1070

Table 3

Proposed Values of the Toop and Samis Equilibrium
Constant K for Various Binary Oxide-Silica Melts (84)

System	K	Melt Temperature °C
Cu ₂ O-SiO ₂	0.35	1100
FeO-SiO ₂	0.17	1600
ZnO-SiO ₂	0.06	1300
PbO-SiO ₂	0.04	1100
CaO-SiO ₂	0.0017	1600

Table 4

Values of K₁₁ for Various Binary Oxide-Silica Melts
from the Masson Branched Chain Model (73)

System	K ₁₁	Melt Temperature °C
FeO-SiO ₂	1.0	1600
FeO-SiO ₂	0.70	1300
PbO-SiO ₂	0.196	1000
CaO-SiO ₂	0.0016	1600

Tables 5a to 5e : Metal Melt Details

Table 5a

Metal Melts; Average Compositions

Melt No.	Mass % Fe	Mass % C	Mass % S	st. dev. Mass % S	No. of Samples
1	95.02	4.38	0.598	0.003	3
2	94.87	4.71	0.415	0	3
3	95.13	4.60	0.294	0.021	3
4	95.69	4.20	0.111	0.007	15
5	95.37	4.55	0.083	0.007	15
6	95.94	4.01	0.050	0.005	15
7	95.96	4.01	0.030	0.003	14

Armco Iron Base Metal Analysis

C	Si	Mn	S	P	Ni	Cr
0.012	<0.01	0.04	0.013	0.008	0.065	0.015
V	Cu	Sn	Nb	Ti	Al	N
<0.01	0.14	0.015	<0.01	<0.01	0.004	0.004

Table 5b

Initial Metal Sulphur Contents from Pin Sections and Metal Slices for Droplet Desulphurisation Experiments Using The Stopper and Seat Technique

Slag	Melt No.	Mass % S
KC1	1	0.512
"	2	0.440
"	3	0.302
"	4 (I)	0.123
"	4 (II)	0.120
"	5	0.076
"	6 (I)	0.057
"	6 (II)	0.054
"	6 (III)	0.057
"	7	0.034

Table 5c

Initial Metal Carbon Contents from Pin Sections for Droplet
Decarburisation Experiments Using the Stopper and Seat

Technique

Slag	Melt No.	Mass % C
KC1	4	4.35
"	6	4.60

Table 5d

Initial Metal Sulphur Contents from Pin Sections for Droplet
Desulphurisation Experiments Using The Suspended Droplet

Technique

Slag	Mass % Sulphur			
	Metal Melt No.			
	4	5	6	7
KC2	0.120	0.083	0.054	0.030
KC2			0.055	
KC2			0.054	
KC3	0.100	0.085	0.046	0.030
KC4	0.110	0.085	0.056	0.027
KC5	0.102	0.070	0.046	0.030
KC6	0.110	0.080	0.056	0.030

Table 5e

Initial Metal Carbon Contents from Pin Sections for Droplet
Decarburisation Experiments Using The Suspended Droplet

Technique

Slag	Mass % Carbon			
	Metal Melt No.			
	4	5	6	7
KC2			4.00	
KC3	4.23			
KC4	4.41	4.72		4.01
KC5		4.53		
KC6	4.26			

Tables 6a and 6b

"Blank Run" Sulphur Compositions For The Metal Droplets

Table 6a

Stopper and Seat Technique

Melt No.	Initial Mass % S	Final Mass % S	Difference Mass % S	Difference %
1	0.600	0.505	-0.095	-16
1	0.595	0.520	-0.075	-13
2	0.415	0.440	+0.025	+ 6
2	0.415	0.440	+0.025	+ 6
3	0.306	0.307	+0.001	+ 0.3
3	0.306	0.298	-0.008	- 3
4	0.106	0.112	+0.006	+ 6

Table 6b

Suspended Droplet Technique

Melt No.	Initial Mass % S	Final Mass % S	Difference Mass % S	Difference %
4	0.106	0.107	+0.001	+ 1
5	0.083	0.083	0.000	0
5	0.083	0.083	0.000	0
6	0.060	0.055	-0.005	- 8
7	0.030	0.032	+0.002	+ 7
7	0.030	0.028	-0.002	- 7

Tables 7a to 7d

Slag Melt Details

Table 7a

Synthetic Slag Compositions : Droplet and GLC Experiments

Slag	Mass % CaO	Mass % FeO	Mass % Fe ₂ O ₃	Mass % SiO ₂	Mass % S
KC1	38.31	28.52	1.90	31.00	0.27
KC2	28.00	40.20	3.21	28.50	0.15
KC3	17.01	46.10	7.72	29.00	0.09
KC4	10.04	55.20	5.72	28.20	0.33
KC5	0.87	62.80	2.23	33.80	0.30
KC6	-	67.63	3.50	28.00	0.32

Table 7b

Synthetic Slag Compositions : GLC Experiments

Slag	Mass % CaO	Mass % FeO	Mass % Fe ₂ O ₃	Mass % SiO ₂	Mole Frac'n SiO ₂
1	-	82.61	9.27	8.12	0.10
2	-	76.93	7.13	15.84	0.19
3	-	68.44	2.39	29.10	0.33
BF3	-	62.85	1.66	34.80	0.39
4	-	57.00	2.13	40.70	0.46
5	-	50.57	1.61	47.82	0.53
6	1.29	61.44	1.34	35.93	0.40

Slag making materials:

1. Electrolytic Iron = 0.002 mass % S
2. BDH Calcined Fe₂O₃ = 0.467 mass % S
3. H & W Calcined Fe₂O₃ = 0.400 mass % S

Table 7c

Industrial Slags. GLC Experiments

Slag	Mass % SiO ₂	Mass % FeO	Mass % CaO	Mass % MgO	Mass % MnO	Mass % Al ₂ O ₃	Mass % P ₂ O ₅	Mass % S
Iron Blast Furnace	34.02	0.78	41.00	7.95	0.95	13.9		1.29
LD Slag	13.00	30.90	42.70	4.70		0.45	1.87	

Table 7d

PbO-Al₂O₃-SiO₂ Slags : GLC Experiments

Melt	Mass % PbO	Mass % Al ₂ O ₃	Mass % SiO ₂	Mole fraction Al ₂ O ₃	Mole fraction SiO ₂
1	84.00	8.31	7.40	0.14	0.25
2	78.0	6.80	9.70	0.11	0.32
3	86.4	0.20	13.20	< 0.01	0.36

Tables 8a to 8e

Droplet Desulphurisation Results Using the Stopper and Seat
Technique for Slag KC1, 38.31 Mass % CaO - 28.52 Mass % FeO
- 1.90 Mass % Fe₂O₃ - 31.00 Mass % SiO₂ - 0.27 Mass % S

Table 8a

Droplets Obtained From Metal Slices Taken From Melts 1, 2
and 3 With Initial Respective Carbon Contents of
4.38, 4.71 and 4.60 Mass %

Reaction Time (mins)	S Conc'n of Droplet Mass % S		
	Melt 1	Melt 2	Melt 3
0	0.512	0.440	0.302
2	0.254	0.205	0.165
5	0.123	0.107	0.125
10	0.090	0.033	0.069
15	0.028	0.027	0.058
20	0.065	0.020	0.048

Table 8b

Droplets Obtained From Pin Samples Taken From Melt 4
Initially Containing 4.20 Mass % C

Reaction Time (mins)	S conc'n of Droplet Mass % S	
	Run No.	
	I	II
0	0.123	0.120
2	0.095	0.093
5	0.077	0.079
10	0.041	0.056
15	0.050	0.047
20	0.021	0.024

Table 8c

Droplets Obtained From Pin Samples Taken From Melt 5

Initially Containing 4.55 Mass % C

Reaction Time (mins)	S Conc'n of Droplet Mass % S
0	0.076
2	0.092
5	0.100
10	0.048
15	0.034
20	0.033

Table 8d

Droplets Obtained From Pin Samples Taken From Melt 6

Initially Containing 4.01 Mass % C

Reaction Time (mins)	S Conc'n of Droplet Mass % S		
	Run No.		
	I	II	III
0	0.057	0.054	0.057
2	0.070	0.072	0.073
5	0.056	0.044	0.086
10	0.055	0.040	0.064
15	0.024	0.020	0.042
20	0.037	0.030	0.038

Table 8e

Droplets Obtained From Pin Samples Taken From Melt 7

Initially Containing 4.01 Mass % C

Reaction Time (mins)	S Conc'n of Droplet Mass % S
0	0.034
2	0.068
5	0.051
10	0.050
15	0.029
20	0.026

Tables 9a and 9b

Droplet Decarburisation Results Using the Stopper and Seat
Technique For Slag KC1 38.31 Mass % CaO - 28.52 Mass % FeO
- 1.90 Mass % Fe₂O₃ - 31.00 Mass % SiO₂ - 0.27 Mass % S

Table 9a

Droplets Obtained From Pin Samples Taken from Melt 4
Initially Containing 0.111 Mass % S

Reaction Time (mins)	C Conc'n of Droplet Mass % C
0	4.35
2	3.72
5	2.73
10	1.35
15	0.74
20	0.66

Table 9b

Droplets Obtained From Pin Samples Taken From Melt 6
Initially Containing 0.050 Mass % S

Reaction Time (mins)	C Conc'n of Droplet Mass % C
0	4.60
2	3.42
5	2.61
10	1.92
15	0.99
20	0.55

Tables 10a to 10m

Droplet Diameter Results For Desulphurisation and
Decarburisation Experiments Using the Stopper and
Seat Technique For Slag KC1 38.31 Mass % CaO
- 28.52 Mass % FeO - 1.90 Mass % Fe₂O₃
- 31.00 Mass % SiO₂ - 0.27 Mass % S

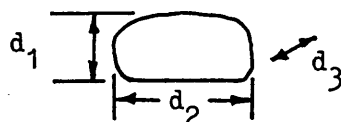
Table 10a

Summary Table. The Mean and Standard Deviation
Values of Droplet Diameters For All Stopper and
Seat Experiments

Reaction Time (mins)	Mean Diameter (cms)	Standard Deviation (cms)	n
2	0.7837	0.2609	32
5	0.7287	0.1721	31
10	0.8219	0.1649	34
15	0.8624	0.1526	34
20	0.8503	0.1842	34

Definition of droplet diameters:-

If a flat area was detected on sample, then



thus,

d_1 = "height"

d_2 = "width"

d_3 = "depth"

as the flat area provides the only 'reference' point for a direction of measurement, then d_2 and d_3 are 'interchangeable'.

$$\text{Mean diameter} = \frac{\sum d}{n}$$

where n = No. of d readings taken.

Table 10b

Droplet Diameters Resulting From the Desulphurisation

Experiment Involving Melt 1, 4.38 Mass % C

- 0.512 Mass % S With Slag KC1

Reaction Time (mins)	Dimension in cms		
	d ₁	d ₂	d ₃
2	-	-	-
5	0.4415	0.9701	0.0678
10	0.8712	0.9679	0.6720
15	0.8850	0.8757	0.7501
20	0.6540	0.8768	0.7738

Table 10c

Droplet Diameters Resulting From the Desulphurisation

Experiment Involving Melt 2, 4.71 Mass % C

- 0.440 Mass % S With Slag KC1

Reaction Time (mins)	Dimension in cms		
	d ₁	d ₂	d ₃
2	0.4610	0.8505	0.7344
5	-	-	-
10	0.8440	0.7800	0.7343
15	0.9056	0.9150	0.7880
20	0.8146	0.9759	0.8504

Table 10d

Droplet Diameters Resulting From the Desulphurisation

Experiment Involving Melt 3, 4.60 Mass % C

- 0.302 Mass % S With Slag KC1

Reaction Time (mins)	Dimension in cms		
	d ₁	d ₂	d ₃
2	0.5975	1.0125	0.5395
5	0.5375	0.6895	0.6900
10	0.9106	0.8309	0.6017
15	0.8706	0.7988	0.7513
20	0.5020	0.9905	0.8219

Table 10e

Droplet Diameters Resulting From the Desulphurisation

Experiment Involving Melt 4, 4.20 Mass % C

- 0.123 Mass % S With Slag KC1

Reaction Time (mins)	Dimension in cms		
	d ₁	d ₂	d ₃
2	0.3590	1.2640	-
5	0.5270	0.8030	-
10	0.7340	0.8720	-
15	0.5810	0.7960	-
20	0.8325	0.8510	-

Table 10f

Droplet Diameters Resulting From the Desulphurisation

Experiment Involving Melt 4, 4.20 Mass % C

- 0.120 Mass % S With Slag KC1

Reaction Time (mins)	Dimension in cms		
	d ₁	d ₂	d ₃
2	0.4619	1.0061	1.0430
5	0.4858	1.0210	0.8086
10	0.6197	1.0030	0.8356
15	1.0383	1.0960	0.5183
20	0.8170	1.0430	1.0231

Table 10g

Droplet Diameters Resulting From the Desulphurisation

Experiment Involving Melt 5, 4.55 Mass % C

- 0.076 Mass % S With Slag KC1

Reaction Time (mins)	Dimension in cms		
	d ₁	d ₂	d ₃
2	0.3677	1.0664	1.0442
5	0.5128	0.8140	0.7821
10	0.6160	1.0055	0.8480
15	0.7190	1.0740	0.8984
20	0.6052	1.1796	0.8702

Table 10h

Droplet Diameters Resulting From the Desulphurisation

Experiment Involving Melt 6, 4.01 Mass % C

- 0.057 Mass % S With Slag KC1. (Run I)

Reaction Time (mins)	Dimension in cms		
	d ₁	d ₂	d ₃
2	0.4702	1.1539	0.8720
5	0.6341	0.8656	0.7485
10	0.6363	1.3046	0.7880
15	0.8665	1.0412	0.8589
20	1.0419	0.8187	0.5650

Table 10i

Droplet Diameters Resulting From the Desulphurisation

Experiment Involving Melt 6, 4.01 Mass % C

- 0.054 Mass % S With Slag KC1. (Run II)

Reaction Time (mins)	Dimension in cms		
	d ₁	d ₂	d ₃
2	0.5245	1.0522	1.0250
5	0.5740	0.8530	0.7410
10	0.5756	1.0730	0.8385
15	0.8082	0.9828	0.6885
20	0.6761	1.1030	0.7115

Table 10j

Droplet Diameters Resulting From the Desulphurisation

Experiment Involving Melt 6, 4.01 Mass % C

- 0.057 Mass % S With Slag KC1. (Run III)

Reaction Time (mins)	Dimension in cms		
	d ₁	d ₂	d ₃
2	0.4479	0.8290	0.8487
5	0.4808	0.9037	0.8279
10	0.7355	0.9694	0.7825
15	0.6190	0.8397	0.7476
20	0.5050	0.9900	0.8284

Table 10k

Droplet Diameters Resulting From the Desulphurisation

Experiment Involving Melt 7, 4.01 Mass % C

- 0.034 Mass % S With Slag KC1

Reaction Time (mins)	Dimension in cms		
	d ₁	d ₂	d ₃
2	0.6665	1.0335	0.7329
5	0.5605	0.8807	0.7756
10	0.5545	1.0035	0.7810
15	0.7830	1.0653	1.0051
20	1.0327	1.0166	0.7339

Table 10l

Droplet Diameters Resulting From the Decarburisation

Experiment Involving Melt 4, 4.35 Mass % C

- 0.111 Mass % S With Slag KC1

Reaction Time (mins)	Dimension in cms		
	d ₁	d ₂	d ₃
2	0.5670	0.9840	0.8445
5	0.5495	1.0155	-
10	0.8180	1.0635	-
15	0.8550	1.2205	-
20	0.7775	1.2000	-

Table 10m

Droplet Diameters Resulting From the Decarburisation

Experiment Involving Melt 6, 4.60 Mass % C

- 0.050 Mass % S With Slag KC1

Reaction Time (mins)	Dimension in cms		
	d ₁	d ₂	d ₃
2	0.4673	1.0406	0.7110
5	0.5724	0.8392	1.0069
10	0.6350	0.8442	0.7960
15	0.8102	1.0130	0.8560
20	0.5860	1.0325	0.8104

Tables 11a to 11l

Droplet Masses For the Desulphurisation and Decarburisation
Experiments Using The Stopper and Seat Technique For
Slag KC1 38.31 Mass % CaO - 28.52 Mass % FeO
- 1.90 Mass % Fe₂O₃ - 31.00 Mass % SiO₂ - 0.27 Mass % S

Table 11a

Droplet Masses in the Desulphurisation
Experiments Involving Melt 1, 4.38 Mass % C
- 0.512 Mass % S With Slag KC1

Reaction Time (mins)	Droplet Mass (g)		Mass Difference (g)
	Initial	Final	
2	1.0106	0.8920	-0.1186
5	1.0200	0.8508	-0.1692
10	1.1661	-	-
15	1.1510	0.9604	-0.1906
20	1.1065	1.0444	-0.0621

Table 11b

Droplet Masses in the Desulphurisation
Experiments Involving Melt 2, 4.71 Mass % C
- 0.440 Mass % S With Slag KC1

Reaction Time (mins)	Droplet Mass (g)		Mass Difference (g)
	Initial	Final	
2	1.1488	1.0620	-0.0868
5	1.1101	0.8912	-0.2189
10	1.0682	0.9964	-0.0718
15	1.0890	1.0527	-0.0363
20	1.1349	1.0841	-0.0508

Table 11c

Droplet Masses in the Desulphurisation
Experiments Involving Melt 3, 4.60 Mass % C
- 0.302 Mass % S With Slag KC1

Reaction Time (mins)	Droplet Mass (g)		Mass Difference (g)
	Initial	Final	
2	1.1960	0.9255	-0.2705
5	1.1518	1.0898	-0.0620
10	1.1407	1.0872	-0.0535
15	1.0930	1.0571	-0.0359
20	1.1012	1.0709	-0.0303

Table 11d

Droplet Masses in the Desulphurisation
Experiments Involving Melt 4, 4.20 Mass % C
- 0.123 Mass % S With Slag KC1 (Run I)

Reaction Time (mins)	Droplet Mass (g)		Mass Difference (g)
	Initial	Final	
2	1.1661	1.1285	-0.0376
5	1.1401	1.0970	-0.0431
10	1.1716	1.1265	-0.0451
15	1.1658	1.0017	-0.1641
20	1.1683	1.1000	-0.0683

Table 11e

Droplet Masses in the Desulphurisation
Experiments Involving Melt 4, 4.20 Mass % C
- 0.120 Mass % S With Slag KC1. (Run II)

Reaction Time (mins)	Droplet Mass (g)		Mass Difference (g)
	Initial	Final	
2	1.0486	1.0313	-0.0173
5	1.1694	1.1954	+0.0260
10	1.1766	1.1468	-0.0298
15	1.1902	1.2115	+0.0213
20	1.1725	1.1864	+0.0139

Table 11f

Droplet Masses in the Desulphurisation
Experiments Involving Melt 5, 4.55 Mass % C
- 0.076 Mass % S With Slag KC1

Reaction Time (mins)	Droplet Mass (g)		Mass Difference (g)
	Initial	Final	
2	1.1757	1.1248	-0.0509
5	1.0713	1.0683	-0.0030
10	1.1193	1.1685	+0.0492
15	1.1533	1.1872	+0.0339
20	1.1743	1.0725	-0.1018

Table 11g

Droplet Masses in the Desulphurisation
Experiments Involving Melt 6, 4.01 Mass % C
- 0.057 Mass % S With Slag KC1. (Run I)

Reaction Time (mins)	Droplet Mass (g)		Mass Difference (g)
	Initial	Final	
2	1.1862	1.1978	+0.0116
5	1.1815	1.1908	+0.0093
10	1.1777	1.2307	+0.0530
15	1.1926	1.2662	+0.0736
20	1.1971	0.9164	-0.2807

Table 11h

Droplet Masses in the Desulphurisation
Experiments Involving Melt 6, 4.01 Mass % C
- 0.054 Mass % S With Slag KC1. (Run II)

Reaction Time (mins)	Droplet Mass (g)		Mass Difference (g)
	Initial	Final	
2	1.1560	1.0821	-0.0739
5	1.1841	1.2154	+0.0313
10	1.1595	1.2098	+0.0503
15	1.1440	1.1132	-0.0308
20	1.1828	0.9786	-0.2042

Table 11i

Droplet Masses in the Desulphurisation
Experiments Involving Melt 6, 4.01 Mass % C
- 0.057 Mass % S With Slag KC1. (Run III)

Reaction Time (mins)	Droplet Mass (g)		Mass Difference (g)
	Initial	Final	
2	1.1881	1.2064	+0.0183
5	1.1812	1.2168	+0.0356
10	1.1851	1.1603	-0.0248
15	1.1691	1.0478	-0.1213
20	1.1625	1.2079	+0.0454

Table 11j

Droplet Masses in the Desulphurisation
Experiments Involving Melt 7, 4.01 Mass % C
- 0.034 Mass % S With Slag KC1

Reaction Time (mins)	Droplet Mass (g)		Mass Difference (g)
	Initial	Final	
2	1.1353	1.1272	-0.0081
5	1.1396	1.1244	-0.0152
10	1.1441	1.1547	+0.0106
15	1.0763	1.0760	-0.0003
20	1.1795	1.2017	+0.0222

Table 11k

Droplet Masses in the Decarburisation
Experiments Involving Melt 4, 4.35 Mass % C
- 0.111 Mass % S With Slag KC1

Reaction Time (mins)	Droplet Mass (g)		Mass Difference (g)
	Initial	Final	
2	1.0486	1.0313	-0.0173
5	1.1694	1.1954	+0.0260
10	1.1766	1.1468	-0.0298
15	1.1902	1.2115	+0.0213
20	1.1725	1.1864	+0.0139

Table 111

Droplet Masses in the Decarburisation
Experiments Involving Melt 6, 4.60 Mass % C
- 0.050 Mass % S With Slag KC1

Reaction Time (mins)	Droplet Mass (g)		Mass Difference (g)
	Initial	Final	
2	1.1751	1.1752	+0.0001
5	1.1730	1.1380	-0.0350
10	1.1494	1.1739	+0.0245
15	1.1932	1.1023	-0.0909
20	1.1523	1.2004	+0.0481

Tables 12a and 12b

Sulphur and Zirconia Concentrations of Slag KC1

Initial Composition 38.31 Mass % CaO - 28.52 Mass % FeO
- 1.90 Mass % Fe₂O₃ - 31.00 Mass % SiO₂ - 0.27 Mass % S,
After Desulphurisation Experiments Using The Stopper and
Seat Technique

Table 12a

Zirconia Concentrations in Slag KC1 After Reaction

With Melt 4, 4.20 Mass % C - 0.123 Mass % S

Reaction Time (mins)	ZrO ₂ Conc'n of Slag (Mass %)
0	0
2	7.69
5	2.55
10	0.35
15	0.59
20	0.72

Table 12b

Sulphur and Zirconia Concentrations in Slag KC1 After

Reaction With Melt 7, 4.01 Mass % C - 0.034 Mass % S

Reaction Time (mins)	ZrO ₂ Conc'n of Slag (Mass %)	S Conc'n of Slag (Mass %)
0	0	0.27
2	0.016	0.40
5	0.137	0.22
10	0.014	0.40
15	0.028	0.10
20	0.109	-

Tables 13a and 13b

Droplet Desulphurisation Results Using the Suspended Droplet
Technique for Slag KC2, 28.00 Mass % CaO - 40.20 Mass % FeO
- 3.21 Mass % Fe₂O₃ - 28.50 Mass % SiO₂ - 0.15 Mass % S

Table 13a

Droplets Obtained From Pin Samples Taken From Melts
4, 5 and 7 Initially Containing 4.20, 4.55 and 4.01
Mass % C Respectively

Reaction Time (mins)	S Conc'n of Droplet Mass % S		
	Melt 4	Melt 5	Melt 7
0	0.120	0.083	0.030
2	0.054	0.049	0.042
5	0.034	0.027	0.034
10	0.013	0.025	0.033
15	0.036	0.031	0.017
20	0.014	0.026	0.022

Table 13b

Droplets Obtained From Pin Samples Taken From Melt 6
Initially Containing 4.01 Mass % C

Reaction Time (mins)	S Conc'n of Droplet Mass % S		
	Run No.		
	I	II	III
0	0.054	0.055	0.054
1			0.042
2	0.046	0.046	
5	0.040	0.037	
7.5			0.021
10	0.026	0.019	
12.5			0.022
15	0.035	0.035	
17.5			0.010
20	0.037	0.011	

Tables 14 to 17

Droplet Desulphurisation Results Using The
Suspended Droplet Technique

Table 14

Droplet Desulphurisation Results Using the Suspended Droplet
Technique For Slag KC3, 17.01 Mass % CaO - 46.10 Mass % FeO
- 7.72 Mass % Fe₂O₃ - 29.00 Mass % SiO₂ - 0.09 Mass % S
Reacted With Droplets Obtained From Pin Samples Taken From
Melts 4, 5, 6 and 7 Initially Containing 4.20, 4.55, 4.01
and 4.01 Mass % C Respectively

Reaction Time (mins)	S Conc'n of Droplet Mass % S			
	Melt 4	Melt 5	Melt 6	Melt 7
0	0.100	0.085	0.046	0.030
2	0.053	0.051	0.043	0.030
5	0.049	0.043	0.034	0.046
10	0.034	0.040	0.030	0.030
15	0.024	0.026	0.024	0.020
20	0.024	0.018	0.023	0.015

Table 15

Droplet Desulphurisation Results Using the Suspended Droplet
Technique for Slag KCl, 10.04 Mass % CaO - 55.20 Mass % FeO
- 5.72 Mass % Fe₂O₃ - 28.20 Mass % SiO₂ - 0.33 Mass % S
Reacted With Droplets Obtained From Pin Samples Taken From
Melts 4, 5, 6 and 7 Initially Containing 4.20, 4.55, 4.01
and 4.01 Mass % C Respectively

Reaction Time (mins)	S Conc'n of Droplet Mass % S			
	Melt 4	Melt 5	Melt 6	Melt 7
0	0.110	0.085	0.056	0.027
2	0.046	0.058	0.048	0.049
5	0.053	0.052	0.058	0.040
10	0.038	0.043	0.047	0.049
15	0.036	0.039	0.052	0.043
20	0.034	0.032	0.040	0.039

Table 16

Droplet Desulphurisation Results For the Suspended Droplet
Technique For Slag KC5, 0.87 Mass % CaO - 62.80 Mass % FeO
- 2.23 Mass % Fe₂O₃ - 33.80 Mass % SiO₂ - 0.30 Mass % S
Reacted With Droplets Obtained From Pin Samples Taken From
Melts 4, 5, 6 and 7 Initially Containing 4.20, 4.55, 4.01
and 4.01 Mass % C Respectively

Reaction Time (mins)	S Conc'n of Droplet (Mass % S)			
	Melt 4	Melt 5	Melt 6	Melt 7
0	0.102	0.070	0.046	0.030
2	0.048	0.045	0.045	0.055
5	0.049	0.045	0.047	0.059
10	0.049	0.048	0.043	0.057
15	0.041	0.042	0.034	0.050
20	0.026	0.036	0.037	0.043

Table 17

Droplet Desulphurisation Results For the Suspended Droplet
Technique For Slag KC6, 67.63 Mass % FeO - 3.50 Mass % Fe₂O₃
- 28.00 Mass % SiO₂ - 0.32 Mass % S Reacted With Droplets
Obtained From Pin Samples Taken From Melts 4, 5, 6 and 7
Initially Containing 4.20, 4.55, 4.01
and 4.01 Mass % C Respectively

Reaction Time (mins)	S Conc'n of Droplet Mass % S			
	Melt 4	Melt 5	Melt 6	Melt 7
0	0.110	0.080	0.056	0.030
2	0.044	0.031	0.058	0.043
5	0.035	0.032	0.050	0.045
10	0.038	0.028	0.038	0.039
15	0.031	0.032	0.029	0.035
20	0.028	0.032	0.027	0.027

Tables 18 to 22

Droplet Decarburisation Results Using The
Suspended Droplet Technique

Table 18

Droplet Decarburisation Results Using The Suspended Droplet
Technique For Slag KC2, 28.00 Mass % CaO - 40.20 Mass % FeO
- 3.21 Mass % Fe₂O₃ - 28.50 Mass % SiO₂ - 0.15 Mass % S,
Reacted With Droplets Obtained From Pin Samples Taken From
Melt 6, Initially Containing 0.050 Mass % S

Reaction Time (mins)	C Conc'n of Drop Mass % C
0	4.00
2	2.20
5	1.70
10	1.32
15	1.08
20	0.85

Table 19

Droplet Decarburisation Results Using The Suspended Droplet
Technique For Slag KC3, 17.01 Mass % CaO - 46.10 Mass % FeO
- 7.72 Mass % Fe₂O₃ - 29.00 Mass % SiO₂ - 0.09 Mass % S,
Reacted With Droplets Obtained From Pin Samples Taken From
Melt 4, Initially Containing 0.111 Mass % S

Reaction Time (mins)	C Conc'n of Drop Mass % C
0	4.23
2	3.17
5	2.93
10	2.76
15	2.23
20	1.90

Tables 20a to 20c

Droplet Decarburisation Results Using The Suspended Droplet
Technique For Slag KCl, 10.04 Mass % CaO - 55.20 Mass % FeO
- 5.72 Mass % Fe₂O₃ - 28.20 Mass % SiO₂ - 0.33 Mass % S

Table 20a

Droplets Obtained From Pin Samples Taken From Melt 4,
Initially Containing 0.111 Mass % S

Reaction Time (mins)	C Conc'n of Drop Mass % C
0	4.41
2	3.32
5	3.08
10	2.85
15	2.16
20	2.14

Table 20b

Droplets Obtained From Pin Samples Taken From Melt 5,
Initially Containing 0.083 Mass % S

Reaction Time (mins)	C Conc'n of Drop Mass % C
0	4.72
2	3.50
5	3.28
10	3.03
15	2.75
20	2.24

Table 20c

Droplets Obtained From Pin Samples Taken From Melt 7.
Initially Containing 0.030 Mass % S

Reaction Time (mins)	C Conc'n of Drop Mass % C
0	4.10
2	3.30
5	2.95
10	2.76
15	2.62
20	2.47

Table 21

Droplet Decarburisation Results Using The Suspended Droplet
Technique For Slag KC5, 0.87 Mass % CaO - 62.80 Mass % FeO
- 2.23 Mass % Fe₂O₃ - 33.80 Mass % SiO₂ - 0.30 Mass % S
Reacted With Droplets Obtained From Pin Samples Taken From
Melt 5, Initially Containing 0.083 Mass % S

Reaction Time (mins)	C Conc'n of Drop Mass % C
0	4.53
2	-
5	3.37
10	3.23
15	2.59
20	2.65

Table 22

Droplet Decarburisation Results Using The Suspended Droplet
Technique For Slag KC6, 67.63 Mass % FeO - 3.50 Mass % Fe₂O₃
- 28.00 Mass % SiO₂ - 0.32 Mass % S, Reacted With Droplets
Obtained From Pin Samples Taken From Melt 4, Initially Contain-
ing 0.111 Mass % S

Reaction Time (mins)	C Conc'n of Drop Mass % C
0	4.26
2	3.42
5	3.51
10	3.17
15	2.87
20	2.74

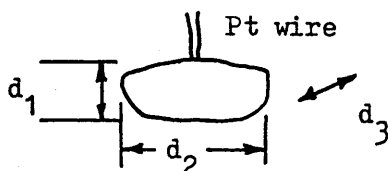
Droplet Diameter Results For Desulphurisation and
Decarburisation Experiments Using The Suspended
Droplet Technique

Table 23

Summary Table. The Mean and Standard
Deviation Values of Droplet Diameters
For All Suspended Droplet Experiments

Reaction Time (mins)	Mean Diameter (cms)	St. Dev. (cms)	n
2	0.7839	0.2654	75
5	0.8064	0.2854	77
10	0.8171	0.2968	78
15	0.8308	0.2972	76
20	0.8336	0.3048	78

Definition of droplet diameters:-



thus, d_1 = "height"
 d_2 = "width"
 d_3 = "depth"

$$\text{Mean diameter} = \frac{\sum d}{n}$$

where n = No. of readings taken.

Tables 24a to 24d

Droplet Diameter Results For Desulphurisation Experiments
Using the Suspended Droplet Technique With Slag KC2,
28.00 Mass % CaO - 40.20 Mass % FeO - 3.21 Mass % Fe₂O₃
- 28.50 Mass % SiO₂ - 0.15 Mass % S

Table 24a

Droplets Obtained From Pin Samples Taken From Melt 4,
Initially Containing 4.20 Mass % C - 0.120 Mass %S

Reaction Time (mins)	Dimension in cms		
	d ₁	d ₂	d ₃
2	1.0220	0.6970	0.5855
5	0.6870	1.2044	0.5362
10	0.6070	1.2465	0.6168
15	0.6600	0.9503	0.6305
20	1.5748	0.7076	0.6450

Table 24b

Droplets Obtained From Pin Samples Taken From Melt 5,
Initially Containing 4.55 Mass % C - 0.083 Mass %S

Reaction Time (mins)	Dimension in cms		
	d ₁	d ₂	d ₃
2	0.5629	1.1460	0.4950
5	0.5750	1.2650	0.5895
10	0.5041	1.2005	0.4969
15	0.5139	1.1691	0.5520
20	0.5354	1.1635	0.5045

Table 24c

Droplets Obtained From Pin Samples Taken From Melt 6,
Initially Containing 4.01 Mass % C - 0.054 Mass % S (Run I)

Reaction Time (mins)	Dimension in cms		
	d ₁	d ₂	d ₃
2	0.8361	0.8658	0.6540
5	0.9760	0.6798	0.7619
10	0.8790	0.9000	0.7232
15	0.8695	0.8700	0.6860
20	1.0440	0.7761	0.7390

Table 24d

Droplets Obtained From Pin Samples Taken From Melt 7,
Initially Containing 4.01 Mass % C - 0.030 Mass % S

Reaction Time (mins)	Dimension in cms		
	d ₁	d ₂	d ₃
2	0.6525	0.8551	0.6775
5	-	0.8095	0.5610
10	0.8839	0.7880	0.5705
15	-	0.7085	0.6515
20	0.6705	0.7695	0.6705

Tables 25a to 25d

Droplet Diameter Results For Desulphurisation Experiments

Using The Suspended Droplet Technique With Slag KC3

17.01 Mass % CaO - 46.10 Mass % FeO - 7.72 Mass % FeO₂₋₃
- 29.00 Mass % SiO₂ - 0.09 Mass % S

Table 25a

Droplets Obtained From Pin Samples Taken From Melt 4.

Initially Containing 4.20 Mass % C - 0.100

Mass % S

Reaction Time (mins)	Dimension in cms		
	d ₁	d ₂	d ₃
2	0.5538	1.0135	0.5429
5	0.6220	0.8418	0.5456
10	0.5407	1.1141	0.5182
15	0.5069	1.0079	0.5079
20	0.5623	1.1229	0.5642

Table 25b

Droplets Obtained From Pin Samples Taken From Melt 5.

Initially Containing 4.55 Mass % C - 0.085

Mass % S

Reaction Time (mins)	Dimension in cms		
	d ₁	d ₂	d ₃
2	1.2121	1.0501	0.5312
5	1.2583	0.9304	0.5207
10	1.0075	0.7939	0.5796
15	0.9832	1.2021	0.5706
20	1.2787	1.2359	0.5128

Table 25c

Droplets Obtained From Pin Samples Taken From Melt 6.

Initially Containing 4.01 Mass % C -0.046

Mass % S

Reaction Time (mins)	Dimension in cms		
	d ₁	d ₂	d ₃
2	0.5891	1.1100	0.5822
5	0.5220	1.1923	0.5278
10	0.5815	1.1008	0.4900
15	0.5734	1.2191	0.5155
20	0.5429	1.1367	0.5551

Table 25d

Droplets Obtained From Pin Samples Taken From Melt 7.

Initially Containing 4.01 Mass % C -0.030

Mass % S

Reaction Time (mins)	Dimension in cms		
	d ₁	d ₂	d ₃
2	0.9459	0.9208	0.5404
5	1.6114	1.0983	0.4941
10	1.6040	1.0580	0.5340
15	1.6275	1.1101	0.5500
20	1.6429	1.1492	0.4962

Tables 26a to 26d

Droplet Diameter Results For Desulphurisation Experiments

Using the Suspended Droplet Technique With Slag KCl,
10.04 Mass % CaO - 55.20 Mass % FeO - 5.72 Mass % Fe₂O₃
- 28.20 Mass % SiO₂ - 0.33 Mass % S

Table 26a

Droplets Obtained From Pin Samples Taken From Melt 4,
Initially Containing 4.20 Mass % C - 0.110 Mass % S

Reaction Time (mins)	Dimension in cms		
	d ₁	d ₂	d ₃
2	0.7624	0.8919	0.6770
5	0.6419	0.9235	0.5460
10	0.6880	0.9611	0.5592
15	0.8009	0.0782	-
20	0.7198	1.0645	0.5961

Table 26b

Droplets Obtained From Pin Samples Taken From Melt 5,
Initially Containing 4.55 Mass % C - 0.085 Mass % S

Reaction Time (mins)	Dimension in cms		
	d ₁	d ₂	d ₃
2	0.5326	1.3450	0.5301
5	0.4963	1.1470	0.4805
10	0.5879	1.2420	0.4890
15	0.7401	1.1804	0.5492
20	0.5972	1.0430	0.5149

Table 26c

Droplets Obtained From Pin Samples Taken From Melt 6.
Initially Containing 4.01 Mass % C - 0.056 Mass % S

Reaction Time (mins)	Dimension in cms		
	d ₁	d ₂	d ₃
2	0.4785	1.2324	0.4911
5	0.5511	1.1460	0.5155
10	0.5805	1.0539	0.5371
15	0.6890	1.0721	0.5755
20	0.5320	1.0831	0.5329

Table 26d

Droplets Obtained From Pin Samples Taken From Melt 7.
Initially Containing 4.01 Mass % C - 0.027 Mass % S

Reaction Time (mins)	Dimension in cms		
	d ₁	d ₂	d ₃
2	0.7845	0.7858	0.5742
5	0.8018	0.7958	0.6027
10	0.7462	0.7254	0.5389
15	0.8079	0.8220	0.5608
20	0.6901	0.9670	0.5985

Tables 27a to 27c

Droplet Diameter Results For Desulphurisation Experiments

Using The Suspended Droplet Technique With Slag KC5

0.87 Mass % CaO - 62.80 Mass % FeO - 2.23 Mass % Fe₂O₃
- 33.80 Mass % SiO₂ - 0.30 Mass % S

Table 27a

Droplets Obtained From Pin Samples Taken From Melt 4.

Initially Containing 4.20 Mass % C - 0.102 Mass % S

Reaction Time (mins)	Dimension in cms		
	d ₁	d ₂	d ₃
2	0.5838	1.1030	0.5188
5	0.5405	1.1552	0.5196
10	0.5229	1.0680	0.5506
15	0.6080	1.2266	0.5138
20	0.5725	1.2015	0.5190

Table 27b

Droplets Obtained from Pin Samples Taken From Melt 5.

Initially Containing 4.55 Mass % C-0.070 Mass % S

Reaction Time (mins)	Dimension in cms		
	d ₁	d ₂	d ₃
2	0.5315	1.2420	0.4857
5	0.6080	1.0191	0.5041
10	0.5561	1.2206	0.5120
15	0.5055	1.3355	0.4883
20	0.5836	1.0540	0.5713

Table 27c

Droplets Obtained From Pin Samples Taken From Melt 6.
Initially Containing 4.01 Mass % C - 0.046 Mass % S

Reaction Time (mins)	Dimensions in cms		
	d ₁	d ₂	d ₃
2	0.5553	1.1245	0.5423
5	0.5777	1.0409	0.5490
10	0.5696	1.3296	0.5592
15	0.6707	1.2077	0.5627
20	0.6448	1.2152	0.6022

Table 27d

Droplets Obtained From Pin Samples Taken From Melt 7.
Initially Containing 4.01 Mass % C - 0.030 Mass % S

Reaction Time (mins)	Dimension in cms		
	d ₁	d ₂	d ₃
2	1.1421	0.6167	0.6506
5	1.1783	0.6741	0.6368
10	1.2038	0.7673	0.6057
15	1.1074	0.6465	0.5530
20	1.1651	0.7103	0.5975

Tables 28a to 28d

Droplet Diameter Results For Desulphurisation Experiments

Using The Suspended Droplet Technique With Slag KC6,
67.63 Mass % FeO - 3.50 Mass % Fe₂O₃ - 28.00 Mass % SiO₂
- 0.32 Mass % S

Table 28a

Droplets Obtained From Pin Samples Taken From Melt 4,
Initially Containing 4.20 Mass % C - 0.110 Mass % S

Reaction Time (mins)	Dimension in cms		
	d ₁	d ₂	d ₃
2	0.6529	1.0423	0.5424
5	0.9150	0.6885	0.6368
10	0.7610	1.0261	0.6075
15	0.6840	1.1090	0.5821
20	0.8123	0.8240	0.6546

Table 28b

Droplets Obtained From Pin Samples Taken From Melt 5,
Initially Containing 4.55 Mass % C - 0.080 Mass % S

Reaction Time (mins)	Dimension in cms		
	d ₁	d ₂	d ₃
2	0.7084	1.1305	0.6381
5	0.6560	1.1450	0.6295
10	0.4270	1.2189	0.4940
15	0.7975	1.0689	0.6120
20	0.6780	1.1120	0.5240

Table 28c

Droplets Obtained From Pin Samples Taken From Melt 6.
Initially Containing 4.01 Mass % C - 0.056 Mass % S

Reaction Time (mins)	Dimension in cms		
	d ₁	d ₂	d ₃
2	0.6980	0.6919	0.5376
5	0.9165	0.7229	0.6000
10	0.5655	1.0751	0.5269
15	0.5631	1.1665	0.5031
20	0.5472	1.0811	0.5195

Table 28d

Droplets Obtained From Pin Samples Taken From Melt 7.
Initially Containing 4.01 Mass % C - 0.030 Mass % S

Reaction Time (mins)	Dimension in cms		
	d ₁	d ₂	d ₃
2	0.5340	1.2020	0.5025
5	0.5099	1.2690	0.5150
10	0.4755	1.3060	0.4990
15	0.4570	1.2340	0.5081
20	0.5328	1.0819	0.4955

Table 29

Droplet Diameter Results For the Decarburisation
Experiments Using The Suspended Droplet Technique
For Slag KC3, 17.01 Mass % CaO - 46.10 Mass % FeO
- 7.72 Mass % Fe₂O₃ - 29.00 Mass % SiO₂ - 0.09 Mass % S.
Reacted With Droplets Obtained From Pin Samples Taken From
Melt 4, Initially Containing 4.23 Mass % C - 0.111 Mass%S

Reaction Time (mins)	Dimension in cms		
	d ₁	d ₂	d ₃
2	1.3220	1.0903	0.5318
5	1.0072	0.8034	0.5913
10	1.3729	1.1831	0.5686
15	1.1422	1.1731	0.6104
20	1.4892	1.2643	0.5798

Tables 30a to 30c

Droplet Diameter Results From The Decarburisation Experiments

Using The Suspended Droplet Technique With Slag KCl₄,
10.04 Mass % CaO - 55.20 Mass % FeO - 5.72 Mass % Fe₂O₃
- 28.20 Mass % SiO₂ - 0.33 Mass % S

Table 30a

Droplets Obtained From Pin Samples Taken From Melt 4,
Initially Containing 4.41 Mass % C - 0.111 Mass % S

Reaction Time (mins)	Dimension in cms		
	d ₁	d ₂	d ₃
2	1.1084	1.1338	0.5325
5	1.5271	1.0128	0.5973
10	1.3710	1.0368	0.6536
15	0.9861	1.5792	1.0380
20	1.1098	1.1206	0.5832

Table 30b

Droplets Obtained From Pin Samples Taken From Melt 5,
Initially Containing 4.72 Mass % C - 0.083 Mass % S

Reaction Time (mins)	Dimension in cms		
	d ₁	d ₂	d ₃
2	0.7370	1.3038	0.4851
5	1.2081	1.2683	0.4842
10	1.0820	1.1512	0.5744
15	1.0943	1.3023	0.5468
20	1.1516	1.0490	0.5492

Table 30c

Droplets Obtained From Pin Samples Taken From Melt 7,
Initially Containing 4.10 Mass % C - 0.030 Mass % S

Reaction Time (mins)	Dimension in cms		
	d ₁	d ₂	d ₃
2	0.8791	0.6061	0.5195
5	1.1880	0.6309	0.6154
10	1.0720	1.0633	0.5875
15	1.3291	0.5770	0.7079
20	1.4775	0.8000	0.5669

Table 31

Droplet Diameter Results For The Decarburisation Experiments

Using The Suspended Droplet Technique For Slag KC5,
0.87 Mass % CaO - 62.80 Mass % FeO - 2.23 Mass % Fe₂₋₃O₃
- 33.80 Mass % SiO₂ - 0.30 Mass % S Reacted With Droplets
Obtained From Pin Samples Taken From Melt 5, Initially
Containing 4.53 Mass % C - 0.083 Mass % S

Reaction Time (mins)	Dimension in cms		
	d ₁	d ₂	d ₃
2	-	-	-
5	1.0799	1.1142	0.5143
10	1.2560	1.0031	0.6129
15	0.8455	1.2119	0.5196
20	1.0649	1.0939	0.6098

Table 32

Droplet Diameter Results For The Decarburisation Experiments

Using The Suspended Droplet Technique For Slag KC6,
67.63 Mass % FeO - 3.50 Mass % Fe₂₋₃O₃ - 28.00 Mass % SiO₂
- 0.32 Mass % S, Reacted With Droplets Obtained From Pin
Pin Samples Taken From Melt 4, Initially Containing 4.26 Mass
% C - 0.111 Mass % S

Reaction Time (mins)	Dimension in cms		
	d ₁	d ₂	d ₃
2	1.0665	1.1651	0.6102
5	1.0093	1.0870	0.6885
10	1.0774	1.0081	0.6185
15	0.9615	1.0614	0.5313
20	0.8462	1.2438	0.5836

Tables 33a to 33f

Droplet Masses For The Desulphurisation Experiments
Using The Suspended Droplet Technique For The Slag KC2,
28.00 Mass % CaO - 40.20 Mass % FeO - 3.21 Mass % Fe₂O₃
- 28.50 Mass % SiO₂ - 0.15 Mass % S

Table 33a

Droplet Masses Obtained From Pin Samples Taken From Melt 4,
Initially Containing 4.20 Mass % C - 0.120 Mass % S

Reaction Time (mins)	Droplet Mass (g)		Mass Difference (g)
	Initial	Final	
2	1.1484	1.1180	-0.0304
5	1.0645	1.1083	+0.0438
10	1.1141	1.1889	+0.0748
15	1.1481	1.2143	+0.0662
20	1.1835	1.2672	+0.0837

Table 33b

Droplet Masses Obtained From Pin Samples Taken From Melt 5,
Initially Containing 4.55 Mass % C - 0.083 Mass % S

Reaction Time (mins)	Droplet Mass (g)		Mass Difference (g)
	Initial	Final	
2	1.1745	1.1797	+0.0052
5	1.0304	1.0476	+0.0172
10	1.0235	1.0684	+0.0449
15	1.1602	1.2216	+0.0614
20	1.0816	1.1687	+0.0871

Table 33c

Droplet Masses Obtained From Pin Samples Taken From Melt 6,
Initially Containing 4.01 Mass % C - 0.054 Mass % S (Run I)

Reaction Time (mins)	Droplet Mass (g)		Mass Difference (g)
	Initial	Final	
2	1.1743	1.2133	+0.0390
5	1.0643	1.0829	+0.0186
10	-	-	-
15	1.1877	1.0030	-0.1847
20	1.1076	0.7317	-0.3759

Table 33d

Droplet Masses Obtained From Pin Samples Taken From Melt 6,
Initially Containing 4.01 Mass % C - 0.055 Mass % S (Run II)

Reaction Time (mins)	Droplet Mass (g)		Mass Difference (g)
	Initial	Final	
2	1.0294	1.0316	+0.0022
5	1.0813	1.1068	+0.0255
10	1.1376	1.1474	+0.0098
15	1.1676	1.1851	+0.0175
20	1.0877	1.0951	+0.0074

Table 33e

Droplet Masses Obtained From Pin Samples Taken From Melt 6,
Initially Containing 4.01 Mass % C - 0.054 Mass % S (Run III)

Reaction Time (mins)	Droplet Mass (g)		Mass Difference (g)
	Initial	Final	
1	1.1616	0.8875	-0.2741
7.5	1.1541	1.1800	+0.0259
12.5	1.1923	1.2214	+0.0291
17.5	1.1374	1.1839	+0.0465

Table 33f

Droplet Masses Obtained From Pin Samples Taken From Melt 7.
Initially Containing 4.01 Mass % C - 0.030 Mass % S

Reaction Time (mins)	Droplet Mass (g)		Mass Difference (g)
	Initial	Final	
2	1.0386	1.0021	-0.0365
5	1.1578	1.1452	-0.0126
10	1.1693	1.1955	+0.0262
15	1.1605	1.2037	+0.0432
20	1.1824	1.2158	+0.0334

Tables 34a to 34d

Droplet Masses For The Desulphurisation Experiments
Using The Suspended Droplet Technique For The Slag KC3,
17.01 Mass % CaO - 46.10 Mass % FeO - 7.72 Mass % Fe₂O₃
- 29.00 Mass % SiO₂ - 0.09 Mass % S

Table 34a

Droplet Masses Obtained Using Pin Samples Taken From Melt 4,
Initially Containing 4.20 Mass % C - 0.100 Mass % S

Reaction Time (mins)	Droplet Mass (g)		Mass Difference (g)
	Initial	Final	
2	1.1855	1.1322	-0.0533
5	1.1516	1.0761	-0.0755
10	1.1731	1.1521	-0.0210
15	1.1782	0.8710	-0.3072
20	1.1655	1.1918	+0.0263

Table 34b

Droplet Masses Obtained Using Pin Samples Taken From Melt 5,
Initially Containing 4.55 Mass % C - 0.085 Mass % S

Reaction Time (mins)	Droplet Mass (g)		Mass Difference (g)
	Initial	Final	
2	1.0861	0.9454	-0.1407
5	1.0509	0.9710	-0.0799
10	1.1010	0.9965	-0.1045
15	1.1192	1.0223	-0.0969
20	1.1784	1.1623	-0.0161

Table 34c

Droplet Masses Obtained Using Pin Samples Taken From Melt 6.

Initially Containing 4.01 Mass % C - 0.046 Mass % S

Reaction Time (mins)	Droplet Mass (g)		Mass Difference (g)
	Initial	Final	
2	1.1643	1.1702	+0.0059
5	1.1559	1.1738	+0.0179
10	1.1638	1.1746	+0.0108
15	1.1342	1.1709	+0.0367
20	1.1271	1.1149	-0.0122

Table 34d

Droplet Masses Obtained Using Pin Samples Taken From Melt 7.

Initially Containing 4.01 Mass % C - 0.030 Mass % S

Reaction Time (mins)	Droplet Mass (g)		Mass Difference (g)
	Initial	Final	
2	1.1932	1.1002	-0.0930
5	1.1810	1.1679	-0.0131
10	1.1758	1.2031	+0.0273
15	1.1875	1.2034	+0.0159
20	1.0484	1.0320	-0.0164

Tables 35a to 35d

Droplet Masses For The Desulphurisation Experiments
Using the Suspended Droplet Technique For The Slag KCl,
10.04 Mass % CaO - 55.20 Mass % FeO - 5.72 Mass % Fe₂O₃
- 28.20 Mass % SiO₂ - 0.33 Mass % S

Table 35a

Droplet Masses Obtained Using Pin Samples Taken From Melt 4,
Initially Containing 4.20 Mass % C - 0.110 Mass % S

Reaction Time (mins)	Droplet Mass (g)		Mass Difference (g)
	Initial	Final	
2	1.1850	1.1126	-0.0724
5	1.1803	1.1021	-0.0782
10	1.1876	1.2028	+0.0152
15	1.1755	1.1589	-0.0166
20	1.1876	1.1845	-0.0031

Table 35b

Droplet Masses Obtained Using Pin Samples Taken From Melt 5,
Initially Containing 4.55 Mass % C - 0.085 Mass % S

Reaction Time (mins)	Droplet Mass (g)		Mass Difference (g)
	Initial	Final	
2	1.1586	1.0144	-0.1442
5	1.0800	0.9765	-0.1035
10	1.1510	1.1198	-0.0312
15	1.1574	1.1624	+0.0050
20	1.1664	1.1774	+0.0110

Table 35c

Droplet Masses Obtained From Pin Samples Taken From Melt 6,
Initially Containing 4.01 Mass % C - 0.056 Mass % S

Reaction Time (mins)	Droplet Mass (g)		Mass Difference (g)
	Initial	Final	
2	1.1565	1.1175	-0.0390
5	1.1946	1.1567	-0.0379
10	1.1808	1.1693	-0.0115
15	1.1573	1.1167	-0.0406
20	1.1422	1.1380	-0.0042

Table 35d

Droplet Masses Obtained From Pin Samples Taken From Melt 7,
Initially Containing 4.01 Mass % C - 0.027 Mass % S

Reaction Time (mins)	Droplet Mass (g)		Mass Difference (g)
	Initial	Final	
2	1.1425	1.1198	-0.0227
5	1.0836	1.0793	-0.0043
10	1.1514	1.1646	+0.0132
15	1.1612	1.1732	+0.0120
20	1.1408	1.1528	+0.0120

Tables 36a to 36d

Droplet Masses For The Desulphurisation Experiments
Using The Suspended Droplet Technique For The Slag KC5,
0.87 Mass % CaO - 62.80 Mass % FeO - 2.23 Mass % Fe₂O₃
- 33.80 Mass % SiO₂ - 0.30 Mass % S

Table 36a

Droplet Masses Obtained From Pin Samples Taken From Melt 4,
Initially Containing 4.20 Mass % C - 0.102 Mass % S

Reaction Time (mins)	Droplet Mass (g)		Mass Difference (g)
	Initial	Final	
2	1.1691	1.1888	+0.0197
5	1.1725	1.2004	+0.0279
10	1.1566	1.1800	+0.0234
15	1.1704	1.2402	+0.0698
20	1.1617	1.2509	+0.0892

Table 36b

Droplet Masses Obtained From Pin Samples Taken From Melt 5,
Initially Containing 4.55 Mass % C - 0.070 Mass % S

Reaction Time (mins)	Droplet Mass (g)		Mass Difference (g)
	Initial	Final	
2	1.1344	1.1328	-0.0016
5	1.1025	1.1272	+0.0247
10	1.1023	1.1106	+0.0083
15	1.1237	1.1745	+0.0508
20	1.0455	1.0999	+0.0544

Table 36c

Droplet Masses Obtained From Pin Samples Taken From Melt 6,
Initially Containing 4.01 Mass % C - 0.046 Mass % S

Reaction Time (mins)	Droplet Mass (g)		Mass Difference (g)
	Initial	Final	
2	1.1426	1.1480	+0.0054
5	1.1322	1.1463	+0.0141
10	1.1816	1.2204	+0.0388
15	1.1903	1.2380	+0.0477
20	1.1903	1.2530	+0.0627

Table 36d

Droplet Masses Obtained From Pin Samples Taken From Melt 7,
Initially Containing 4.01 Mass % C - 0.030 Mass % S

Reaction Time (mins)	Droplet Mass (g)		Mass Difference (g)
	Initial	Final	
2	1.1555	1.1653	+0.0098
5	1.1331	1.1421	+0.0090
10	1.1954	1.2248	+0.0294
15	1.1785	1.2193	+0.0408
20	1.1614	1.2226	+0.0612

Tables 37a to 37d

Droplet Masses For The Desulphurisation Experiments
Using The Suspended Droplet Technique For The Slag KC6
67.63 Mass % FeO - 3.50 Mass % Fe₂O₃ - 28.00 Mass % SiO₂
- 0.32 Mass % S

Table 37a

Droplet Masses Obtained From Pin Samples Taken From Melt 4,
Initially Containing 4.20 Mass % C - 0.110 Mass % S

Reaction Time (mins)	Droplet Mass (g)		Mass Difference (g)
	Initial	Final	
2	1.1735	1.0278	-0.1457
5	1.1688	1.0456	-0.1232
10	1.1739	1.1586	-0.0153
15	1.1900	1.1997	+0.0097
20	1.1950	1.0989	-0.0961

Table 37b

Droplet Masses Obtained From Pin Samples Taken From Melt 5,
Initially Containing 4.55 Mass % C - 0.080 Mass % S

Reaction Time (mins)	Droplet Mass (g)		Mass Difference (g)
	Initial	Final	
2	1.1344	1.0501	-0.0843
5	1.1004	1.0112	-0.0892
10	1.0130	0.9520	-0.0610
15	1.1327	1.0328	-0.0999
20	1.1556	0.9898	-0.1658

Table 37c

Droplet Masses Obtained From Pin Samples Taken From Melt 6,
Initially Containing 4.01 Mass % C - 0.056 Mass % S

Reaction Time (mins)	Droplet Mass (g)		Mass Difference (g)
	Initial	Final	
2	1.1984	0.7919	-0.4065
5	1.1521	1.1129	-0.0392
10	1.1958	1.2027	+0.0069
15	1.0320	0.9816	-0.0504
20	1.1793	1.2055	+0.0262

Table 37d

Droplet Masses Obtained From Pin Samples Taken From Melt 7,
Initially Containing 4.01 Mass % C - 0.030 Mass % S

Reaction Time (mins)	Droplet Mass (g)		Mass Difference (g)
	Initial	Final	
2	1.0962	1.1076	+0.0114
5	1.1668	1.1725	+0.0057
10	1.1822	1.1864	+0.0042
15	1.1369	1.1444	+0.0075
20	1.0174	1.0405	+0.0231

Tables 38 to 42

Droplet Masses For The Decarburisation Experiments
Using The Suspended Droplet Technique

Table 38

Droplet Masses Obtained From Pin Samples Taken From Melt 6,
Initially Containing 4.00 Mass % C - 0.050 Mass % S,
Reacted With Slag KC2, 28.00 Mass % CaO - 40.20 Mass % FeO -
3.21 Mass % Fe₂O₃ - 28.50 Mass % SiO₂ - 0.15 Mass % S

Reaction Time (mins)	Droplet Mass (g)		Mass Difference (g)
	Initial	Final	
2	1.1902	1.1995	+0.0093
5	1.1995	1.2166	+0.0171
10	1.1414	1.1344	-0.0070
15	1.1565	1.1609	+0.0044
20	1.1791	1.2413	+0.0622

Table 39

Droplet Masses Obtained From Pin Samples Taken From Melt 4,
Initially Containing 4.23 Mass % C - 0.111 Mass % S,
Reacted With Slag KC3, 17.01 Mass % CaO - 46.10 Mass % FeO -
7.72 Mass % Fe₂O₃ - 29.00 Mass % SiO₂ - 0.09 Mass % S

Reaction Time (mins)	Droplet Mass (g)		Mass Difference (g)
	Initial	Final	
2	1.1753	1.1626	-0.0127
5	1.1577	1.0828	-0.0749
10	1.1595	1.0618	-0.0977
15	1.0533	1.0292	-0.0241
20	1.1802	1.1887	+0.0085

Tables 40a to 40c

Droplet Diameter Results For The Decarburisation Experiments
Using The Suspended Droplet Technique With Slag KCl,
10.04 Mass % CaO - 55.20 Mass % FeO - 5.72 Mass % Fe₂O₃
- 28.20 Mass % SiO₂ - 0.33 Mass % S

Table 40a

Droplet Masses Obtained From Pin Samples Taken From Melt 4,
Initially Containing 4.41 Mass % C - 0.111 Mass % S

Reaction Time (mins)	Droplet Mass (g)		Mass Difference (g)
	Initial	Final	
2	1.1927	1.1297	-0.0630
5	1.0855	1.0685	-0.0170
10	1.1980	1.1909	-0.0071
15	1.1038	1.0506	-0.0532
20	1.1565	1.1527	-0.0038

Table 40b

Droplet Masses Obtained From Pin Samples Taken From Melt 5,
Initially Containing 4.72 Mass % C - 0.083 Mass % S

Reaction Time (mins)	Droplet Mass (g)		Mass Difference (g)
	Initial	Final	
2	1.1713	1.0184	-0.1529
5	1.1125	1.0867	-0.0258
10	1.1271	1.0618	-0.0653
15	1.1192	1.1514	+0.0322
20	1.0223	0.9907	-0.0316

Table 40c

Droplet Masses Obtained From Pin Samples Taken From Melt 7.
Initially Containing 4.01 Mass % C - 0.030 Mass % S

Reaction Time (mins)	Droplet Mass (g)		Mass Difference (g)
	Initial	Final	
2	1.1506	0.5591	-0.5915
5	1.1818	1.0926	-0.0892
10	1.1951	1.1633	-0.0318
15	1.0240	0.9933	-0.0307
20	1.1803	1.1924	+0.0121

Table 41

Droplet Masses Obtained From Pin Samples Taken From Melt 5,
Initially Containing 4.55 Mass % C - 0.083 Mass % S
Reacted With Slag KC5, 0.87 Mass % CaO - 62.80 Mass % FeO -
2.23 Mass % Fe₂O₃ - 33.80 Mass % SiO₂ - 0.30 Mass % S

Reaction Time (mins)	Droplet Mass (g)		Mass Difference (g)
	Initial	Final	
2	-	-	-
5	1.1651	1.0987	-0.0664
10	1.1787	1.1908	+0.0121
15	1.1611	1.1160	-0.0451
20	1.1192	1.1316	+0.0124

Table 42

Droplet Masses Obtained From Pin Samples Taken From Melt 4,
Initially Containing 4.20 Mass % C - 0.111 Mass % S
Reacted with Slag KC6, 67.63 Mass % FeO - 3.50 Mass % Fe₂O₃ =
28.00 Mass % SiO₂ - 0.32 Mass % S

Reaction Time (mins)	Droplet Mass (g)		Mass Difference (g)
	Initial	Final	
2	1.1547	1.1622	+0.0075
5	1.1922	1.2230	+0.0308
10	1.1643	1.1340	-0.0303
15	1.1203	1.1565	+0.0362
20	1.1411	1.1293	-0.0118

Tables 43 to 46

Sulphur Concentrations of Slags After Desulphurisation Experiments
Using The Suspended Droplet Technique

Table 43

Sulphur Concentration of Slag KC2, Initial Composition
28.00 Mass % CaO - 40.20 Mass % FeO - 3.21 Mass % Fe₂O₃ =
28.50 Mass % SiO₂ - 0.15 Mass % S, After Reaction With Metal
Droplets, Initially Containing 4.20 Mass % C - 0.120 Mass % S

Reaction Time (mins)	S Conc'n of Slag (Mass %)
0	0.15
2	0.43
5	0.29
10	0.11
15	0.11
20	0.10

Table 44

Sulphur Concentration of Slag KC2, Initial Composition
28.00 Mass % CaO - 40.20 Mass % FeO - 3.21 Mass % Fe₂O₃ =
28.50 Mass % SiO₂ - 0.15 Mass % S, After Reaction With Metal
Droplets Initially Containing 4.01 Mass % C - 0.054 Mass % S

Reaction Time (mins)	S Conc'n of Slag (Mass %)
0	0.15
2	0.25
5	0.24
10	0.47
15	0.44
20	0.44

Table 45

Sulphur Concentration of Slag KC5, Initial Composition
0.87 Mass % CaO - 62.80 Mass % FeO - 2.23 Mass % Fe₂O₃ -
33.80 Mass % SiO₂ - 0.30 Mass % S, After Reaction With Metal
Droplets Initially Containing 4.01 Mass % C - 0.030 Mass % S

Reaction Time (mins)	S Conc'n of Slag (Mass %)
0	0.30
2	0.46
5	0.42
10	0.24
15	0.11
20	0.35

Table 46

Sulphur Concentration of Slag KC6, Initial Composition
67.63 Mass % FeO - 3.50 Mass % Fe₂O₃ - 28.00 Mass % SiO₂ -
0.32 Mass % S, After Reaction With Metal Droplets Initially
Containing 4.55 Mass % C - 0.080 Mass % S

Reaction Time (mins)	S Conc'n of Slag (Mass %)
0	0.32
2	0.45
5	0.71
10	0.55
15	0.58
20	0.59

Tables 47a to 47b

Chromatogram Data From Trimethylsilylation Experiments

Using The Lentz Technique

Table 47a

Blank Sample

Peak	RT (mins)	RRT	Peak Area	R. Peak Area	R.Pk. Area x deriv. liq. vol.
SiO ₄ ⁴⁻	2.94	0.22	0.01	0.003	0.01
IS	13.39	1.00	3.31	1.00	-

derivative liquor volume = 3.25 cm³

Table 47b

Natrolite

Peak	RT (mins)	RRT	Peak Area	R. Peak Area	R.Pk. Area x deriv. liq. vol.	%
SiO ₄ ⁴⁻	3.01	0.22	6.37	1.71	34.70	23.95
Si ₂ O ₇ ⁶⁻	9.54	0.68	4.99	1.34	27.20	18.75
Si ₃ O ₉ ⁶⁻	10.59	0.76	2.18	0.59	12.00	8.30
IS	13.95	1.00	3.72	1.00	-	-
Si ₄ O ₁₂ ⁸⁻	16.93	1.21	0.94	0.25	5.05	3.50
Si ₃ O ₁₀ ⁸⁻	17.56	1.26	12.09	3.25	65.95	45.50

derivative liquor volume = 20.30 cm³

Tables 48a to 53b

Chromatogram Data From Trimethylsilylation Experiments

Using The Masson Technique

Table 48a

Masson Technique Blank Sample : Untreated TMCS

Peak	RT (mins)	RRT	Peak Area	R. Peak Area	R. Pk. Area x deriv. liq. vol.
SiO ₄ ⁴⁻	3.13	0.23	0.66	0.20	0.56
IS	13.66	1.00	3.32	1.00	-

derivative liquor volume = 2.80cm³

Table 48b

Masson Technique Blank Sample : Pretreated TMCS

Peak	RT (mins)	RRT	Peak Area	R. Peak Area	R. Pk. Area x deriv. liq. vol.
SiO ₄ ⁴⁻	2.53	0.20	0.0004	0.0001	0.0003
IS	12.69	1.00	4.03	1.00	-

derivative liquor volume = 3.50 cm³

Tables 49a to 49g

Chromatogram Data : Minerals

Table 49a

Natrolite

Peak	RT (mins)	RRT	Peak Area	R. Peak Area	R. Pk. Area x deriv. liq. vol.	%
SiO ₄ ⁴⁻	2.85	0.22	0.34	0.11	0.35	9.25
Si ₂ O ₇ ⁶⁻	8.88	0.67	0.13	0.04	0.15	4.60
Si ₃ O ₉ ⁶⁻	9.82	0.75	0.40	0.13	0.40	12.30
IS	13.06	1.00	3.04	-	-	-
Si ₄ O ₁₂ ⁸⁻	15.72	1.20	0.12	0.04	0.15	4.60
Si ₃ O ₁₀ ⁸⁻	16.27	1.24	2.09	0.69	2.20	67.70

derivative liquor volume = 3.20 cm³

Table 49b

Natrolite

Peak	RT (mins)	RRT	Peak Area	R. Peak Area	R. Pk. Area x deriv. liq. vol.	%
SiO ₄ ⁴⁻	3.04	0.22	0.32	0.10	0.30	10.90
Si ₂ O ₇ ⁶⁻	9.37	0.68	0.14	0.04	0.10	3.65
Si ₃ O ₉ ⁶⁻	10.33	0.76	0.39	0.12	0.35	12.75
IS	13.59	1.00	3.33	-	-	-
Si ₄ O ₁₂ ⁸⁻	16.32	1.20	0.11	0.03	0.10	3.65
Si ₃ O ₁₀ ⁸⁻	16.84	1.23	2.15	0.65	1.90	69.10

derivative liquor volume = 2.95 cm³

Table 49c

Hemimorphite

Peak	RT (mins)	RRT	Peak Area	R. Peak Area	R.Pk.Area x deriv. liq.vol.	%
SiO ₄ ⁴⁻	2.76	0.21	0.15	0.04	0.15	4.15
Si ₂ O ₇ ⁶⁻	8.73	0.67	2.40	0.67	2.75	76.40
Si ₃ O ₉ ⁶⁻	9.69	0.75	0.02	0.01	0.05	1.40
IS	12.88	1.00	3.57	-	-	-
Si ₄ O ₁₂ ⁸⁻	15.52	1.20	0.45	0.13	0.55	15.30
Si ₃ O ₁₀ ⁸⁻	16.06	1.24	0.10	0.03	0.10	2.80

derivative liquor volume = 4.10 cm³

Table 49d

Hemimorphite

Peak	RT (mins)	RRT	Peak Area	R. Peak Area	R.Pk.Area x deriv. liq. vol.	%
SiO ₄ ⁴⁻	2.76	0.21	0.13	0.04	0.10	3.75
Si ₂ O ₇ ⁶⁻	9.07	0.68	2.58	0.76	2.20	83.00
Si ₃ O ₉ ⁶⁻	10.03	0.76	0.02	0.01	0.05	1.90
IS	13.23	1.00	3.38	-	-	-
Si ₄ O ₁₂ ⁸⁻	15.97	1.21	0.29	0.09	0.25	9.45
Si ₃ O ₁₀ ⁸⁻	16.50	1.25	0.07	0.02	0.05	1.90

derivative liquor volume = 2.95 cm³

Table 49e

Andradite

Peak	RT (mins)	RRT	Peak Area	R. Peak Area	R.Pk.Area x deriv. liq. vol.	%
SiO ₄ ⁴⁻	2.92	0.22	0.08	0.02	0.10	66.65
Si ₂ O ₇ ⁶⁻	0.16	0.69	0.02	0.01	0.05	33.35
Si ₃ O ₉ ⁶⁻	10.15	0.76	0	0	0	0
IS	13.33	1.00	3.50	-	-	-
Si ₄ O ₁₂ ⁸⁻	16.17	1.21	0	0	0	0
Si ₃ O ₁₀ ⁸⁻	16.59	1.25	0.01	0	0	0

derivative liquor volume = 4.20 cm³

Table 49f

Hemimorphite (0.75g) + Natrolite (0.75g)

Peak	RT (mins)	RRT	Peak Area	R.Peak Area	R.Pk.Area x deriv. liq. vol.	%	Pred.% *
SiO ₄ ⁴⁻	3.06	0.23	0.23	0.08	0.25	7.05	7.40
Si ₂ O ₇ ⁶⁻	9.25	0.69	2.03	0.69	2.20	61.95	42.60
Si ₃ O ₉ ⁶⁻	10.18	0.76	0.18	0.06	0.20	5.65	7.40
IS	13.36	1.00	2.93	-	-	-	-
Si ₄ O ₁₂ ⁸⁻	16.11	1.21	0.21	0.07	0.20	5.65	6.50
Si ₃ O ₁₀ ⁸⁻	16.62	1.24	0.64	0.22	0.70	19.70	36.10

derivative liquor volume = 3.20 cm³

* Predicted % based on results for Hemimorphite and Natrolite given in Tables 48d and 48b respectively.

Table 49g

Hemimorphite (0.5g) + Natrolite (1.0g)

Peak	RT (mins)	RRT	Peak Area	R. Peak Area	R.Pk.Area x deriv. liq. vol.	%	Pred. % *
SiO ₄ ⁴⁻	2.68	0.21	0.28	0.07	0.20	7.15	8.60
Si ₂ O ₇ ⁶⁻	8.80	0.68	1.43	0.36	1.10	39.30	29.45
Si ₃ O ₉ ⁶⁻	9.78	0.76	0.28	0.07	0.20	7.15	9.20
IS	12.93	1.00	3.92	-	-	-	-
Si ₄ O ₁₂ ⁸⁻	15.67	1.21	0.18	0.05	0.15	5.35	5.50
Si ₃ O ₁₀ ⁸⁻	16.18	1.25	1.45	0.37	1.15	41.05	47.25

derivative liquor volume = 3.20 cm³

* Predicted % based on results for Hemimorphite and Natrolite given in Tables 48d and 48b respectively.

Tables 50a to 50b

Chromatogram Data : Industrial Slags

Table 50a

Iron Blast Furnace Slag (B.S.C. Scunthorpe)

(34.02 Mass % SiO₂ - 0.78 Mass % FeO - 41.00 Mass % CaO
- 7.95 Mass % MgO - 0.95 Mass % MnO - 13.90 Mass % Al₂O₃
- 1.29 Mass % S)

Peak	RT (mins)	RRT	Peak Area	R. Peak Area	R.Pk.Area x deriv. liq.vol.	%
SiO ₄ ⁴⁻	2.79	0.21	0.27	0.08	0.25	29.40
Si ₂ O ₇ ⁶⁻	9.01	0.68	0.41	0.12	0.35	41.20
Si ₃ O ₉ ⁶⁻	10.03	0.76	0.03	0.01	0.05	5.90
IS	13.20	1.00	3.36	-	-	-
Si ₄ O ₁₂ ⁸⁻	15.93	1.21	0.04	0.01	0.05	5.90
Si ₃ O ₁₀ ⁸⁻	16.44	1.24	0.16	0.05	0.15	17.65

derivative liquor volume = 3.05 cm³

Table 50b

LD Slag (B.S.C. Appleby-Frodingham)

(13.00 Mass % SiO₂ - 30.90 Mass % FeO - 42.70 Mass % CaO
- 4.70 Mass % MgO - 0.45 Mass % Al₂O₃ - 1.87 Mass % P₂O₅)

Peak	RT (mins)	RRT	Peak Area	R. Peak Area	R.Pk.Area x deriv. liq. vol.	%
SiO ₄ ⁴⁻	2.76	0.21	0.43	0.13	0.40	61.55
Si ₂ O ₇ ⁶⁻	8.86	0.68	0.12	0.04	0.10	23.10
Si ₃ O ₉ ⁶⁻	9.85	0.75	<0.01	0	0	0
IS	13.06	1.00	3.24	-	-	-
Si ₄ O ₁₂ ⁸⁻	15.79	1.21	0.02	0.01	0.05	7.70
Si ₃ O ₁₀ ⁸⁻	16.33	1.25	0.03	0.01	0.05	7.70

derivative liquor volume = 3.20 cm³

Tables 51a to 51m

Chromatogram Data : Synthetic Slags

Table 51a

Slag 1 (FeO-0.10x SiO₂)

Peak	RT (mins)	RRT	Peak Area	R. Peak Area	R.Pk.Area x deriv. liq. vol.	%
SiO ₄ ⁴⁻	2.79	0.21	0.49	0.15	0.50	66.65
Si ₂ O ₇ ⁶⁻	8.94	0.69	0.21	0.06	0.20	26.65
Si ₃ O ₉ ⁶⁻	9.91	0.76	0.01	0	0	0
IS	13.03	1.00	3.25	-	-	-
Si ₄ O ₁₂ ⁸⁻	15.73	1.21	0.02	0.01	0	0
Si ₃ O ₁₀ ⁸⁻	16.26	1.25	0.07	0.02	0.05	6.65

derivative liquor volume = 3.20 cm³

Table 51b

Slag 2 (FeO-0.19x SiO₂)

Peak	RT (mins)	RRT	Peak Area	R. Peak Area	R.Pk.Area x deriv. liq. vol.	%
SiO ₄ ⁴⁻	2.64	0.21	1.66	0.44	1.95	73.60
Si ₂ O ₇ ⁶⁻	8.56	0.67	0.49	0.13	0.60	22.65
Si ₃ O ₉ ⁶⁻	9.58	0.75	0.02	0	0	0
IS	12.76	1.00	3.74	-	-	-
Si ₄ O ₁₂ ⁸⁻	15.51	1.21	0.02	0	0	0
Si ₃ O ₁₀ ⁸⁻	16.02	1.25	0.08	0.02	0.10	3.75

derivative liquor volume = 4.45 cm³

Table 51c

Slag 3 (FeO-0.33x SiO₂)

Peak	RT (mins)	RRT	Peak Area	R.Peak Area	R.Pk.Area x deriv. liq. vol.	%
SiO ₄ ⁴⁻	2.95	0.22	2.58	0.52	2.55	68.90
Si ₂ O ₇ ⁶⁻	9.18	0.69	0.95	0.19	0.95	25.65
Si ₃ O ₉ ⁶⁻	10.17	0.76	0.04	0.01	0.05	1.35
IS	13.36	1.00	5.00	-	-	-
Si ₄ O ₁₂ ⁸⁻	16.06	1.20	0.02	0	0	0
Si ₃ O ₁₀ ⁸⁻	16.54	1.24	0.14	0.03	0.15	4.05

derivative liquor volume = 4.90 cm³

Table 51d

Slag BF3 Quenched (FeO-0.39x SiO₂)

Peak	RT (mins)	RRT	Peak Area	R.Peak Area	R.Pk.Area x deriv. liq. vol.	%
SiO ₄ ⁴⁻	2.76	0.21	2.73	0.80	2.80	70.0
Si ₂ O ₇ ⁶⁻	8.91	0.68	0.88	0.26	0.90	22.5
Si ₃ O ₉ ⁶⁻	9.91	0.75	0.04	0.01	0.05	1.25
IS	13.17	1.00	3.39	-	-	-
Si ₄ O ₁₂ ⁸⁻	15.91	1.21	0.05	0.01	0.05	1.25
Si ₃ O ₁₀ ⁸⁻	16.44	1.25	0.19	0.06	0.20	5.00

derivative liquor volume = 3.50 cm³

Table 51e

Slag BF3 Slow Cooled (FeO-0.39x SiO)

Peak	RT (mins)	RRT	Peak Area	R. Peak Area	R.Pk.Area x deriv. liq. vol.	%
SiO ₄ ⁴⁻	2.86	0.21	2.67	0.86	3.00	68.20
Si ₂ O ₇ ⁶⁻	9.19	0.68	0.93	0.30	1.05	23.85
Si ₃ O ₉ ⁶⁻	10.18	0.76	0.04	0.01	0.05	1.15
IS	13.41	1.00	3.12	-	-	-
Si ₄ O ₁₂ ⁸⁻	16.18	1.21	0.05	0.02	0.05	1.15
Si ₃ O ₁₀ ⁸⁻	16.66	1.24	0.22	0.07	0.25	5.70

derivative liquor volume = 3.50 cm³

Table 51f

Slag 4 Quenched (FeO-0.46x SiO)

Peak	RT (mins)	RRT	Peak Area	R. Peak Area	R.Pk.Area x deriv. liq. vol.	%
SiO ₄ ⁴⁻	2.74	0.21	2.17	0.62	3.05	72.60
Si ₂ O ₇ ⁶⁻	8.92	0.68	0.60	0.17	0.85	20.25
Si ₃ O ₉ ⁶⁻	9.93	0.75	0.03	0.01	0.05	1.20
IS	13.17	1.00	3.49	-	-	-
Si ₄ O ₁₂ ⁸⁻	15.99	1.21	0.02	0.01	0.05	1.20
Si ₃ O ₁₀ ⁸⁻	16.45	1.25	0.13	0.04	0.20	4.75

derivative liquor volume = 4.90 cm³

Table 51g

Slag 4 Slow Cooled (FeO-0.46x SiO₂)

Peak	RT (mins)	RRT	Peak Area	R. Peak Area	R.Pk.Area x deriv. liq. vol.	%
SiO ₄ ⁴⁻	2.64	0.20	2.84	0.91	4.05	74.30
Si ₂ O ₇ ⁶⁻	8.70	0.67	0.82	0.26	1.15	21.10
Si ₃ O ₉ ⁶⁻	9.70	0.75	0.03	0.01	0.05	0.90
IS	12.91	1.00	3.11	-	-	-
Si ₄ O ₁₂ ⁸⁻	15.67	1.21	0.01	0	0	0
Si ₃ O ₁₀ ⁸⁻	16.15	1.25	0.14	0.04	0.20	3.65

derivative liquor volume = 4.45 cm³

Table 51h

Slag 5 (FeO-0.53x SiO₂)

Peak	RT (mins)	RRT	Peak Area	R. Peak Area	R.Pk.Area x deriv. liq. vol.	%
SiO ₄ ⁴⁻	2.94	0.22	2.31	0.72	2.80	75.70
Si ₂ O ₇ ⁶⁻	9.12	0.68	0.57	0.18	0.70	18.90
Si ₃ O ₉ ⁶⁻	10.09	0.76	0.03	0.01	0.05	1.35
IS	13.33	1.00	3.20	-	-	-
Si ₄ O ₁₂ ⁸⁻	16.08	1.21	0.02	0.01	0.05	1.35
Si ₃ O ₁₀ ⁸⁻	16.59	1.24	0.10	0.03	0.10	2.70

derivative liquor volume = 3.90 cm³

Table 51i

Slag 6 (1.29 Mass % CaO - 61.44 Mass % FeO - 35.93 Mass % SiO₂)

Peak	RT (mins)	RRT	Peak Area	R. Peak Area	R.Pk.Area x deriv. liq. vol.	%
SiO ₄ ⁴⁻	2.83	0.21	2.94	0.81	2.90	68.25
Si ₂ O ₇ ⁶⁻	8.97	0.68	1.02	0.28	1.05	24.70
Si ₃ O ₉ ⁶⁻	9.96	0.76	0.04	0.01	0.05	1.20
IS	13.17	1.00	3.62	-	-	-
Si ₄ O ₁₂ ⁸⁻	15.94	1.21	0.05	0.01	0.05	1.20
Si ₃ O ₁₀ ⁸⁻	16.47	1.25	0.23	0.06	0.20	4.70

derivative liquor volume = 3.55 cm³

Table 51j

Slag KC1 (38.31 Mass % CaO - 28.52 Mass % FeO - 1.90 Mass % Fe₂O₃
- 31.00 Mass % S)

Peak	RT (mins)	RRT	Peak Area	R. Peak Area	R.Pk.Area x deriv. liq. vol.	%
SiO ₄ ⁴⁻	2.83	0.21	1.29	0.41	1.27	62.85
Si ₂ O ₇ ⁶⁻	9.04	0.68	0.51	0.16	0.50	24.75
Si ₃ O ₉ ⁶⁻	10.02	0.76	0.04	0.01	0.05	2.50
SI	13.26	1.00	3.17	-	-	-
Si ₄ O ₁₂ ⁸⁻	16.00	1.21	0.05	0.02	0.05	2.50
Si ₃ O ₁₀ ⁸⁻	16.51	1.24	0.16	0.05	0.15	7.50

derivative liquor volume = 3.10 cm³

Table 51k

Slag KC2 (28.00 Mass % CaO - 40.20 Mass % FeO - 3.21 Mass % Fe₂O₃
- 28.50 Mass % SiO₂)

Peak	RT (mins)	RRT	Peak Area	R.Peak Area	R.Pk.Area x deriv. liq. vol.	%
SiO ₄ ⁴⁻	2.68	0.21	1.45	0.43	1.55	68.90
Si ₂ O ₇ ⁶⁻	8.71	0.67	0.47	0.14	0.50	22.20
Si ₃ O ₉ ⁶⁻	9.73	0.75	0.03	0.01	0.05	2.20
IS	12.97	1.00	3.34	-	-	-
Si ₄ O ₁₂ ⁸⁻	15.72	1.21	0.04	0.01	0.05	2.20
Si ₃ O ₁₀ ⁸⁻	16.21	1.25	0.12	0.03	0.10	4.45

derivative liquor volume = 3.60 cm³

Table 51l

Slag KC3 (17.01 Mass % CaO - 46.10 Mass % FeO - 7.72 Mass % Fe₂O₃
- 29.00 Mass % SiO₂)

Peak	RT (mins)	RRT	Peak Area	R. Peak Area	R.Pk.Area x deriv. liq. vol.	%
SiO ₄ ⁴⁻	2.88	0.22	1.53	0.38	1.65	64.70
Si ₂ O ₇ ⁶⁻	9.04	0.68	0.58	0.15	0.65	25.50
Si ₃ O ₉ ⁶⁻	10.03	0.76	0.04	0.01	0.05	2.00
IS	13.23	1.00	3.97	-	-	-
Si ₄ O ₁₂ ⁸⁻	15.97	1.21	0.05	0.01	0.05	2.00
Si ₃ O ₁₀ ⁸⁻	16.47	1.24	0.16	0.04	0.15	5.90

derivative liquor volume = 4.30 cm³

Table 51m

Slag KCl (10.04 Mass % CaO - 55.20 Mass % FeO - 5.72 Mass % Fe₂O₃
- 28.20 Mass % SiO₂)

Peak	RT (mins)	RRT	Peak Area	R.Peak Area	R.Pk.Area x deriv. liq. vol.	%
SiO ₄ ⁴⁻	2.65	0.21	2.31	0.60	2.95	69.40
Si ₂ O ₇ ⁶⁻	8.67	0.67	0.76	0.20	1.00	23.55
Si ₃ O ₉ ⁶⁻	9.64	0.75	0.04	0.01	0.05	1.20
IS	12.85	1.00	3.83	-	-	-
Si ₄ O ₁₂ ⁸⁻	15.45	1.20	0.04	0.01	0.05	1.20
Si ₃ O ₁₀ ⁸⁻	16.08	1.25	0.17	0.04	0.20	4.70

derivative liquor volume = 4.90 cm³

Tables 52a to 52c

PbO - Al₂O₃ - SiO₂ Melts

Table 52a

PbO - 0.14x Al₂O₃ - 0.25x SiO₂ (84.00 Mass % PbO - 8.31 Mass %

Al₂O₃ - 7.40 Mass % SiO₂)

Peak	RT (mins)	RRT	Peak Area	R. Peak Area	R.Pk.Area x deriv. liq. vol.	%
SiO ₄ ⁴⁻	2.85	0.21	0.44	0.11	0.25	71.45
Si ₂ O ₇ ⁶⁻	9.09	0.68	0.17	0.04	0.10	28.55
Si ₃ O ₉ ⁶⁻	10.05	0.76	0.01	0	0	0
IS	13.26	1.00	3.81	-	-	-
Si ₄ O ₁₂ ⁸⁻	16.06	1.21	0	0	0	0
Si ₃ O ₁₀ ⁸⁻	16.59	1.25	0.05	0.01	0	0

derivative liquor volume = 2.10 cm³

Table 52b

PbO-0.11xAl₂O₃-0.32xSiO₂ (78.00 Mass % PbO-6.80 Mass % Al₂O₃-9.70

Mass % SiO₂)

Peak	RT (Mins)	RRT	Peak Area	R. Peak Area	R.Pk. Area x deriv. liq. vol.	%
SiO ₄ ⁴⁻	2.95	0.22	0.42	0.11	0.25	50.00
Si ₂ O ₇ ⁶⁻	9.27	0.69	0.24	0.06	0.15	30.00
Si ₃ O ₉ ⁶⁻	10.23	0.76	0.02	0	0	0
IS	13.50	1.00	3.73	-	-	-
Si ₄ O ₁₂ ⁸⁻	16.24	1.20	0.06	0.02	0.05	10.00
Si ₃ O ₁₀ ⁸⁻	16.77	1.24	0.10	0.03	0.05	10.00

derivative liquor volume = 2.10 cm³

Table 52c

$\text{PbO} - <.01 \times \text{Al}_2\text{O}_3 - 0.36 \times \text{SiO}_2$ (86.40 Mass % PbO - 0.20 Mass %

$\text{Al}_2\text{O}_3 - 13.20$ Mass % SiO_2)

Peak	RT (Mins)	RRT	Peak Area	R. Peak Area	R.Pk.Area x deriv. liq. vol.	%
SiO_4	2.74	0.21	0.47	0.13	0.30	42.85
Si_2O_7	8.71	0.67	0.42	0.12	0.25	35.70
Si_3O_{10}	9.69	0.75	0.03	0.01	0	0
IS	12.91	1.00	3.49	-	-	-
Si_4O_{12}	15.61	1.21	0.01	0	0	0
Si_3O_{10}	16.15	1.25	0.24	0.07	0.15	21.45

derivative liquor volume = 2.20 cm³

Tables 53a to 53b

Silica Samples

Table 53a

Precipitated Silica (BDH Reagent)

Peak	RT (mins)	RRT	Peak Area	R. Peak Area	R. Pk. Area x Deriv. Liq. Vol.
SiO ₄ ⁴⁻	2.77	0.21	0.003	0.0009	0.003
IS	13.15	1.00	3.31	1.00	-

derivative liquor volume = 3.50 cm³

Table 53b

Fused SiO₂ Rod Sample

Peak	RT (mins)	RRT	Peak Area	R. Peak Area	R.Pk.Area x Deriv. Liq. Vol.
SiO ₄ ⁴⁻	2.77	0.21	0.01	0.0028	0.008
IS	13.15	1.00	3.53	1.00	-

derivative liquor volume = 2.95 cm³

Table 54

Results For The Trimethylsilylation Of Various Minerals
Reported By Masson ¹¹⁹

Silicate	% Si, by weight in the products as			
	SiO ₄ ⁴⁻	Si ₂ O ₇ ⁶⁻	Si ₃ O ₁₀ ⁸⁻	Si ₄ O ₁₂ ⁸⁻
Andradite	83.0	11.6	5.4	-
Olivine	88.0	9.7	2.3	-
Hemimorphite	1.1	93.6	-	5.3
Laumontite	3.8	-	-	96.2

Table 55

Comparison Between Calculated and Measured Anionic
Distribution In Synthetic Samples (Masson ¹¹⁹)

Composition of mixture in grams				Wt % of Si, present as			
Olivine	Hemi-Morphite	Laumon-tite		SiO ₄ ⁴⁻	Si ₂ O ₇ ⁶⁻	Si ₃ O ₁₀ ⁸⁻	Si ₄ O ₁₂ ⁸⁻
0.03	0.03	0.03	calculated	37.4	24.0	0.4	38.2
			measured	40.8	21.8	0.7	36.7
0.04	0.02	0.04	calculated	41.4	15.1	0.4	43.1
			measured	42.5	17.7	0.9	38.9
0.02	0.05	0.02	calculated	29.5	41.7	0.3	28.5
			measured	31.9	43.8	0.7	23.6

Table 56

Comparison Between Measured Anionic Distributions In Table 55
And Recalculated Distributions Based On A Si Balance
Using Information From Tables 54 and 55

Composition of mixture in grams				Wt of Si, present as			
Olivine	Hemi-morphite	Laumontite		SiO ₄ ⁴⁻	SiO ₂₇ ⁶⁻	SiO ₃₁₀ ⁸⁻	SiO ₄₁₂ ⁸⁻
0.03	0.03	0.03	recalculated	33.5	23.1	0.8	42.5
			measured	40.8	21.8	0.7	36.7
0.04	0.02	0.04	recalculated	33.3	15.3	0.8	50.6
			measured	42.5	17.7	0.9	38.9
0.02	0.05	0.02	recalculated	22.4	41.7	0.5	35.4
			measured	31.9	43.8	0.7	23.6

Tables 57a to 57d

Comparison of Results For Trimethylsilylation of Industrial Slags
For Present Work and Investigation Reported By Masson¹²³

Table 57a

Comparison of Iron Blast Furnace Slag Compositions

Slag	Slag composition (mole fraction)					
	SiO ₂	FeO	CaO	MgO	MnO	Al ₂ O ₃
Sydney Steel Corp'n(Masson ¹²³)	0.37	0.002	0.41	0.15	0.006	0.06
B.S.C. Scunthorpe	0.34	0.006	0.44	0.12	0.006	0.08
B.S.C. Scunthorpe Slag Converted to CaO-SiO ₂ Composition	0.39	-	0.61	-	-	-

Table 57b

Comparison of Silicate Anion Derivative Proportions For
Trimethylsilylated Iron Blast Furnace Slags

Slag	Prop'n. of Silicate Anion Deriv. (%)				
	SiO ₄ ⁴⁻	Si ₂ O ₇ ⁶⁻	Si ₃ O ₁₀ ⁸⁻	Si ₄ O ₁₂ ⁸⁻	Si ₃ O ₁₀ ⁸⁻
Sydney Steel Corp'n(Masson ¹²³)	34.20	37.20	0.24	11.20	17.10
B.S.C. Scunthorpe	29.40	41.20	5.90	5.90	17.65

Table 57c

Comparison of Open Hearth and LD Slag Compositions

Slag	Slag Composition (mole fraction)					
	SiO ₂	FeO	CaO	MgO	MnO	Al ₂ O ₃
OH Slag: Sydney Steel Corp'n(Masson ¹²³)	0.18	0.19	0.40	0.18	0.04	0.01
LD Slag: B.S.C. Scunthorpe	0.14	0.28	0.49	0.008	-	0.003

Table 57d

Comparison of Silicate Anion Derivative Proportions For
Trimethylsilylated Open Hearth and LD Slags

Slag	Proportion of Silicate Anion Deriv(%)				
	Si ₄ ⁴⁻	Si ₂₇ ⁶⁻	Si ₉ ⁶⁻	Si ₁₂ ⁸⁻	Si ₁₀ ⁸⁻
OH Slag: Sydney Steel Corp'n(Masson ¹²³)	65.3	22.3	1.0	3.6	7.74
LD Slag: B.S.C. Scunthorpe	61.5	23.1	-	7.7	7.7

Table 58

Slag Compositions For Droplet Experiments Assuming
Iron Oxide Present As FeO (cf Table 7a)

Slag	Composition							
	Mass %				Mole fraction			
	CaO	FeO	SiO ₂	S	CaO	FeO	SiO ₂	S
KC1	38.06	30.88	30.80	0.27	0.42	0.26	0.31	0.01
KC2	27.67	44.01	28.17	0.15	0.31	0.39	0.30	0.01
KC3	16.57	55.08	28.26	0.09	0.19	0.50	0.31	0.01
KC4	10.21	61.78	27.69	0.32	0.12	0.57	0.30	0.01
KC5	0.86	65.30	33.54	0.30	0.01	0.61	0.38	0.01
KC6	-	71.87	27.81	0.32	-	0.68	0.31	0.01

Table 59

Interfacial Slag Compositions During
Continuous Phase Controlled Decarburisation Assuming
Complete FeO Denudation of Bulk Slags in Table 58

Slag	Composition					
	Mass %			Mole fraction		
	CaO	SiO ₂	S	CaO	SiO ₂	S
KC1	55.06	44.55	0.39	0.57	0.43	0.01
KC2	49.42	50.31	0.27	0.51	0.49	0.01
KC3	36.89	62.91	0.20	0.38	0.61	0.01
KC4	26.71	72.45	0.84	0.32	0.67	0.02
KC5	2.49	96.66	0.86	0.02	0.96	0.02
KC6	-	98.86	1.14	-	0.98	0.02

Table 60

Interaction Parameters Used To Calculate
Activity Coefficients of Sulphur and Oxygen

e_0^O	e_0^S	e_S^S	e_S^O
-0.20	-0.091	-0.0282	-0.18
Ref 166	Ref 166	Ref 50	Ref 166

Table 61

Flood 'Electrically Equivalent' Fractions And Equilibrium
Quotients Based On Slag Compositions In Table 58

Slag	$N_{Ca^{2+}}'$	$N_{Fe^{2+}}'$	K'
KC1	0.613	0.387	0.025
KC2	0.445	0.554	0.021
KC3	0.273	0.726	0.017
KC4	0.173	0.827	0.015
KC5	Acid	-	-
KC6	-	1.000	0.012

Table 62

Temkin Ionic Fractions Based On Slag
Compositions in Table 58

Slag	$N_{O^{2-}}$	$N_{S^{2-}}$
KC1	0.150	0.016
KC2	0.253	0.007
KC3	0.204	0.005
KC4	0.200	0.018
KC5	Acid	-
KC6	0.144	0.019

Table 63

Anionic Parameters Determined From Silicate Slag Models

For Slag KC6 71.87 Mass % FeO-27.81 Mass % SiO₂-0.32 Mass % S

Toop and Samis : $N_{O^{2-}} = 0.747$, $N_{S^{2-}} = 0.016$

Masson Model : $a_{MO} = N_{O^{2-}} = 0.557$

Table 64

Predicted Equilibrium Sulphur Concentrations for

Metal Droplets Based On Temkin's Model

Slag	Predicted S Concentration mass %					Actual S Conc'n after 20 mins. reaction		
	Oxygen Concentration mass %					Initial S Conc'n mass %		
	0.005	0.01	0.02	0.04	0.06	0.512	0.440	0.302
KC1	0.031	0.061	0.121	0.243	0.364	0.065	0.020	0.048

Slag	Predicted S Conc'n. mass %					Actual S Conc'n after 20 mins. reaction			
	Oxygen Concentration mass %					Approx. Initial S Conc'n mass %			
	0.005	0.01	0.02	0.04	0.06	0.120	0.080	0.050	0.030
KC1	0.031	0.061	0.121	0.243	0.364	0.022	0.033	0.035	0.026
KC2	0.008	0.016	0.032	0.064	0.096	0.014	0.026	0.037	0.022
KC3	0.007	0.014	0.028	0.057	0.085	0.024	0.018	0.023	0.015
KC4	0.026	0.052	0.104	0.209	0.313	0.034	0.032	0.040	0.039
KC6	0.038	0.077	0.153	0.307	0.460	0.028	0.032	0.027	0.027

Table 65

Predicted Equilibrium Sulphur Concentrations For
Metal Droplets Based On The Flood Model

Slag	Predicted S Concentration mass %					Actual S Conc'n after 20 mins reaction		
	Oxygen Concentration mass %					Initial S Conc'n mass %		
	0.005	0.01	0.02	0.04	0.06	0.512	0.440	0.302
KC1	0.021	0.042	0.082	0.165	0.247	0.065	0.020	0.048

Slag	Predicted S Concentration mass %					Actual S Conc'n after 20 mins reaction			
	Oxygen Concentration mass %					Initial S Conc'n mass %			
	0.005	0.01	0.02	0.04	0.06	0.120	0.080	0.050	0.030
KC1	0.021	0.042	0.082	0.165	0.247	0.022	0.033	0.035	0.026
KC2	0.006	0.013	0.026	0.052	0.078	0.014	0.026	0.037	0.022
KC3	0.007	0.014	0.028	0.057	0.085	0.024	0.018	0.023	0.015
KC4	0.029	0.059	0.118	0.237	0.355	0.034	0.032	0.040	0.039
KC6	0.054	0.109	0.217	0.435	0.651	0.028	0.032	0.027	0.027

Table 66

Predicted Equilibrium Sulphur Concentrations For
Metal Droplets Based On Silicate Slag

Models Applied to Slag KC6 (71.87 Mass % FeO

-27.81 Mass % SiO₂ -0.32 Mass % S

Slag Model	Equil Quotient	Predicted S Conc'n mass %					Actual S Conc'n after 20 mins reaction			
		Oxygen Concentration mass %					Initial S Conc'n mass %			
		0.005	0.00	0.02	0.04	0.06	0.110	0.080	0.056	0.030
Masson	0.017	0.010	0.020	0.040	0.079	0.119	0.028	0.032	0.027	0.027
Masson	0.012	0.014	0.028	0.056	0.112	0.168	"	"	"	"
Toop and Samis	0.017	0.006	0.012	0.025	0.050	0.075	"	"	"	"
Toop and Samis	0.012	0.009	0.018	0.035	0.071	0.106	"	"	"	"

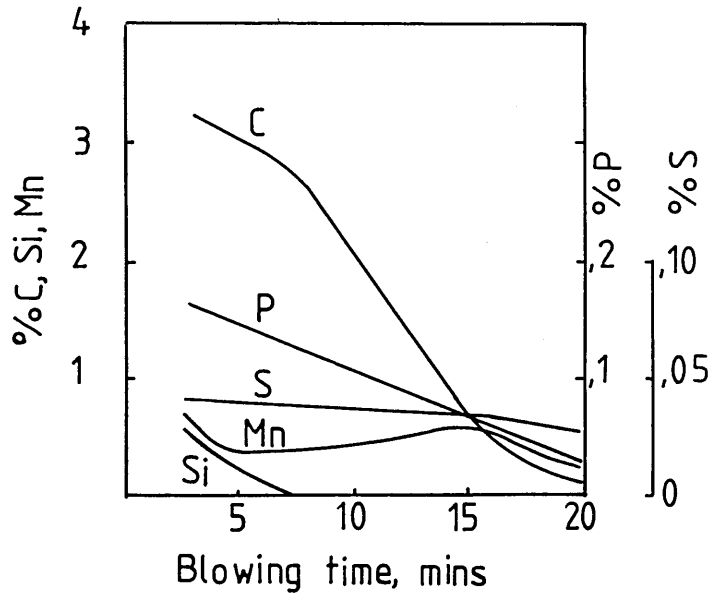


Fig. 1

LD Bath Composition During Blow

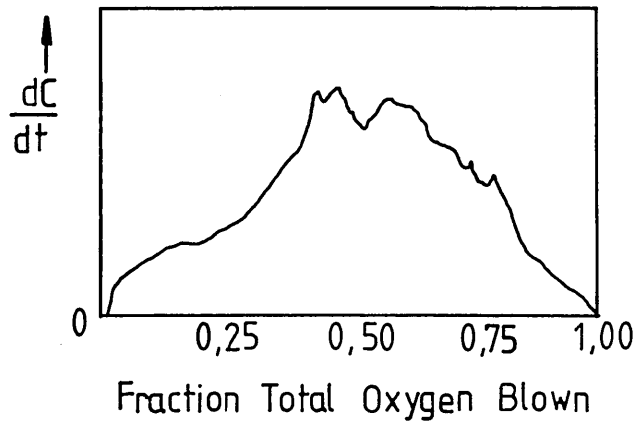


Fig. 2

Typical Decarburisation Rate Curve

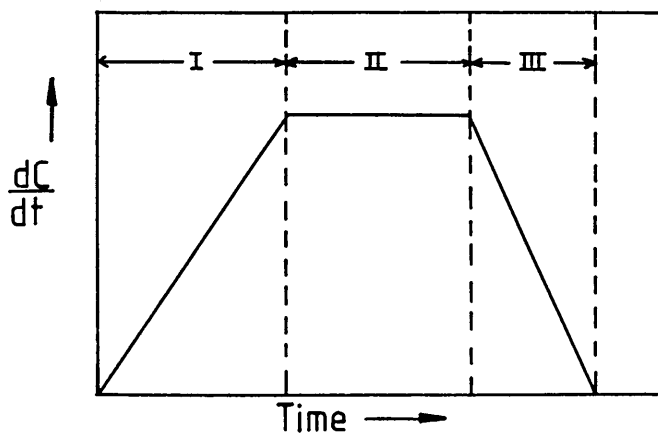
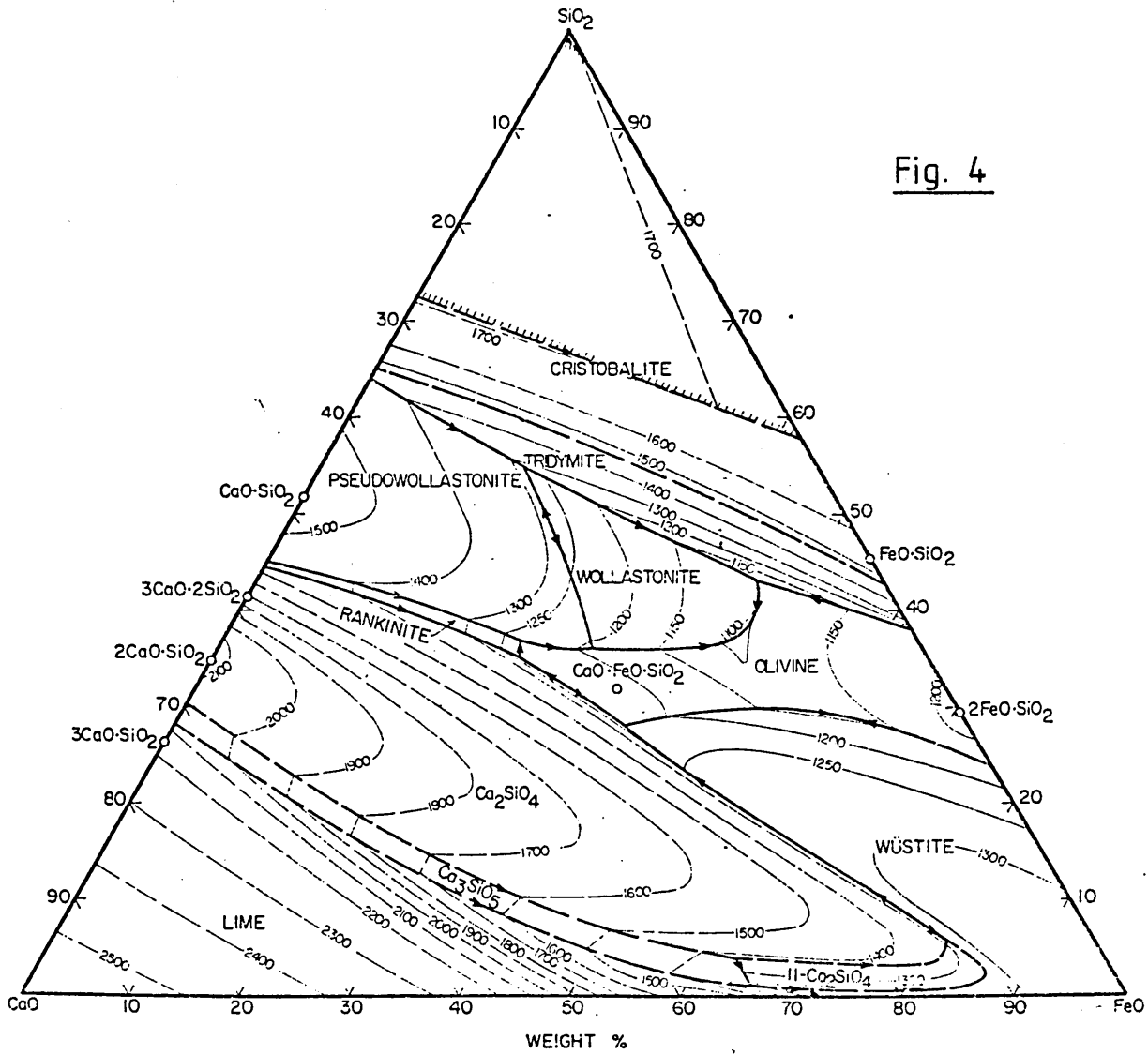


Fig. 3

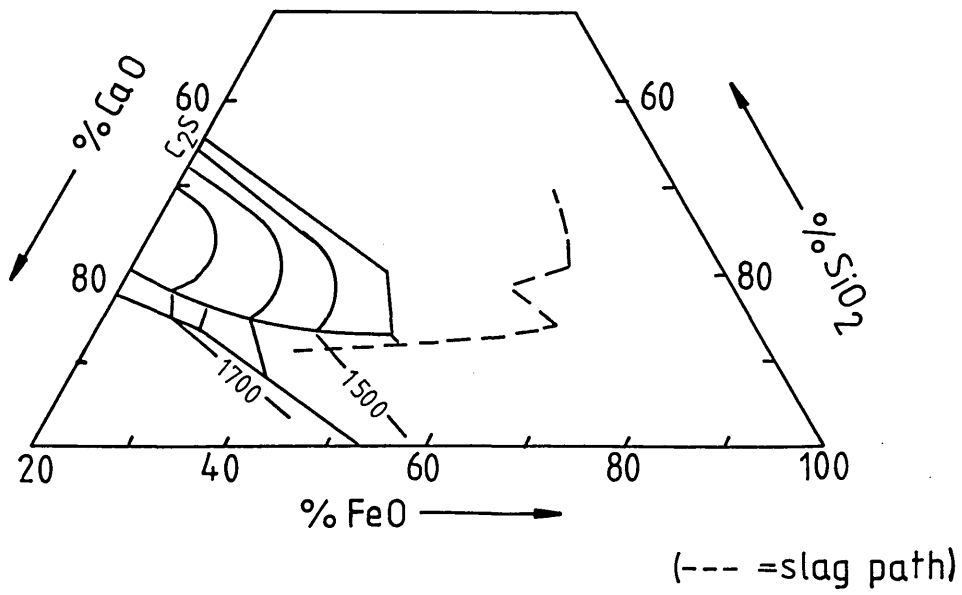
Idealised LD Decarburisation Rate Curve

Fig. 4



Phase Relations In CaO-FeO-SiO₂ System
In Contact With Metallic Iron (23)

Fig. 5



Typical Slag Formation Path (25)

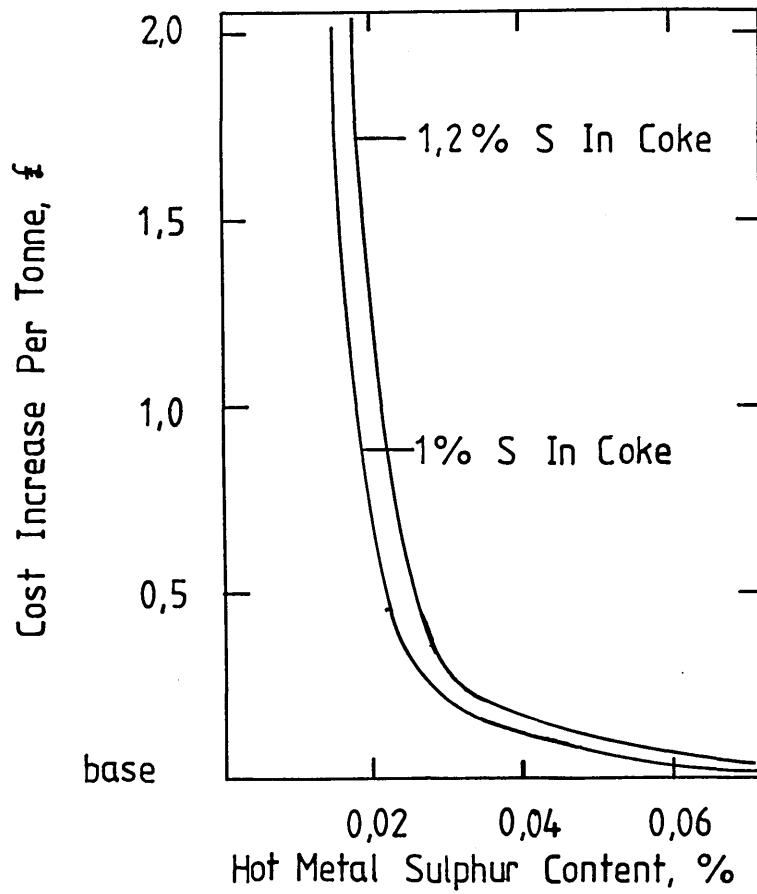
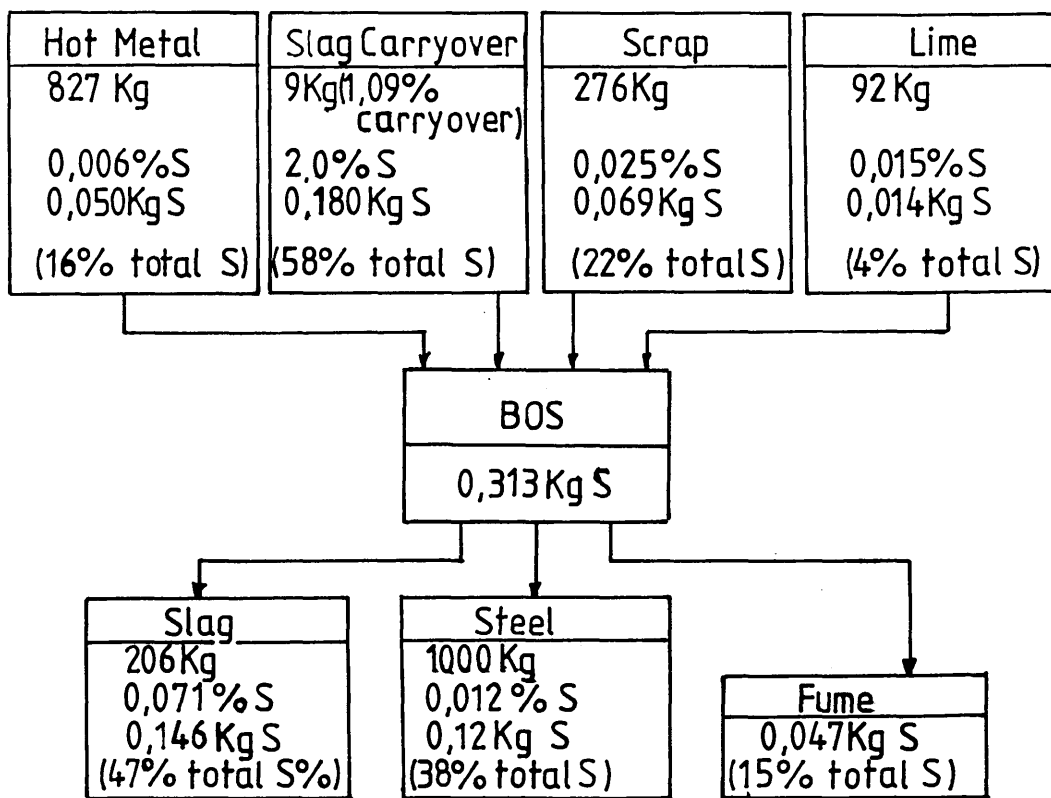
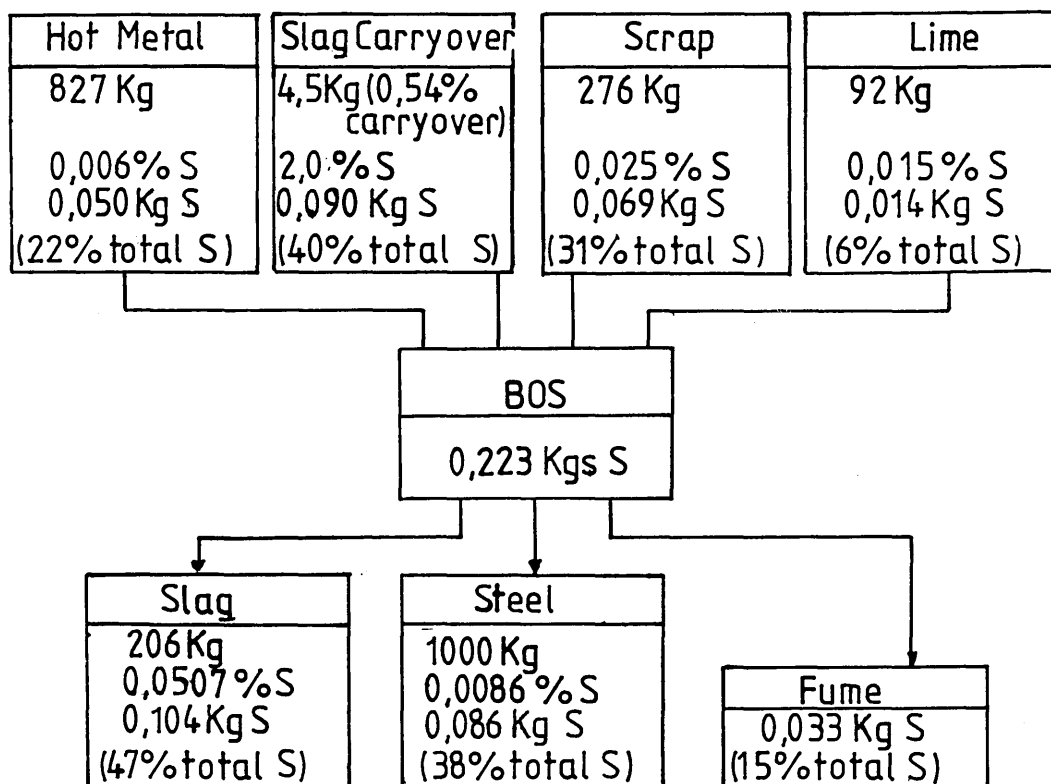


Fig. 6

Relationship Between Ironmaking Cost And
Sulphur In Iron(6)



(a) BOS Sulphur Balance: Effect Of Blast Furnace Slag Carryover On First Turndown Sulphur



(b) BOS Sulphur Balance As Above(a) Showing Effect Of 50% Reduction In B.F. Slag Carryover On 1st Turndown Sulphur (34)

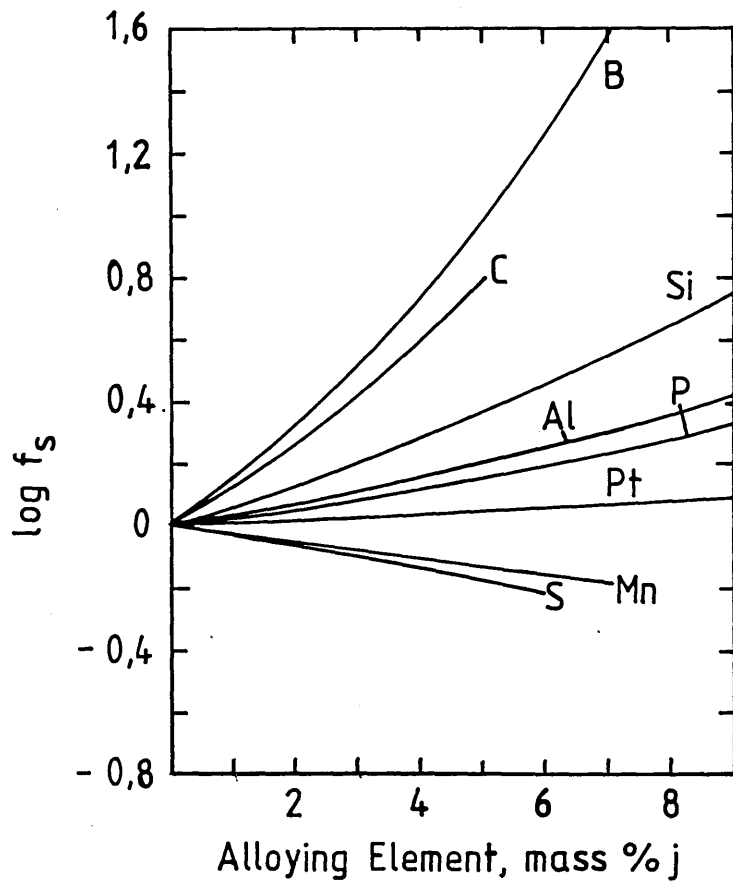


Fig. 8

Effect Of Alloying Element On Activity Coefficient Of Sulphur In Liquid Iron At 1550°C (50)

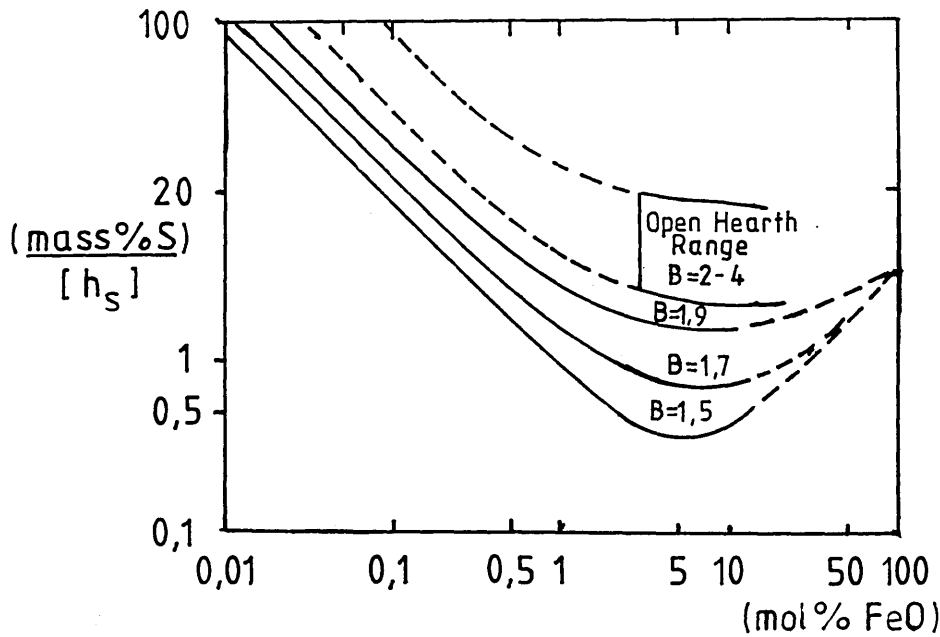
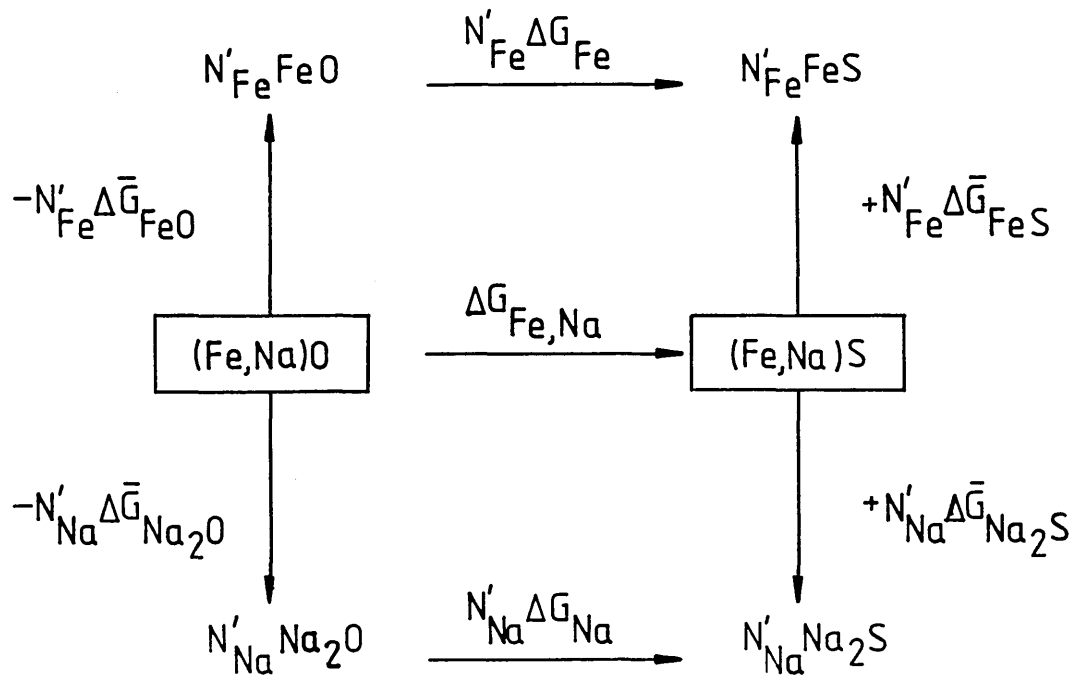


Fig. 9

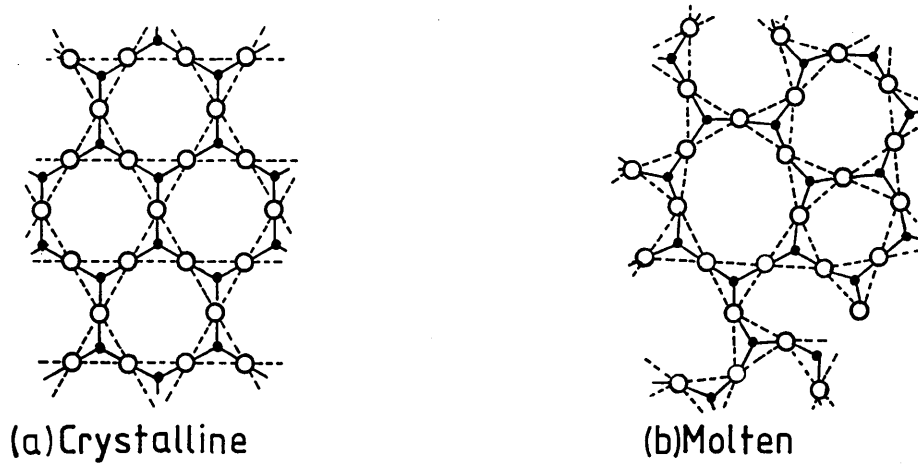
Effect Of Basicity And FeO Content Of Slag On Slag-Metal Sulphur Partition At 1600°C (66)

Fig. 10



Flood Model: Simplified Cyclic Argument(74)

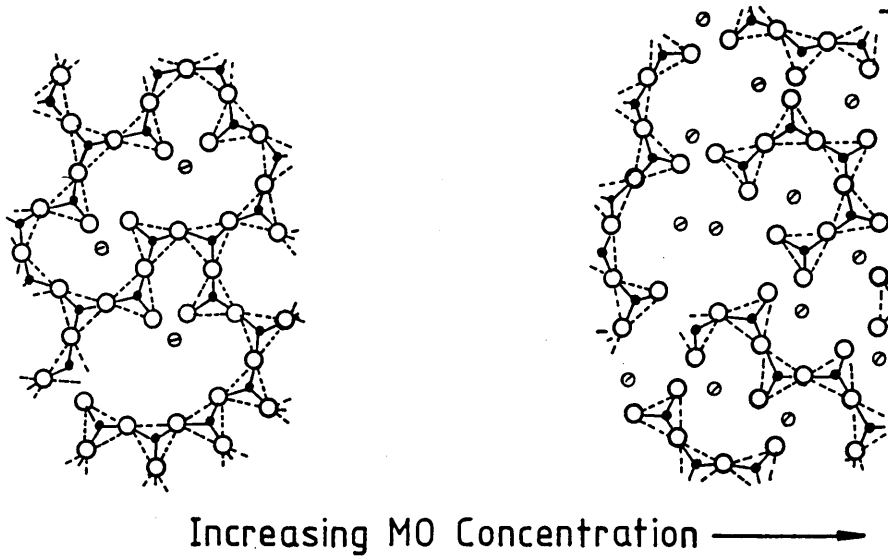
Fig. 11



Structural Representation Of Pure Silica

●=Silicon ○=Oxygen ◉=M²⁺ Cation

Fig. 12



Effect Of Basic Oxide Addition On Silica Structure

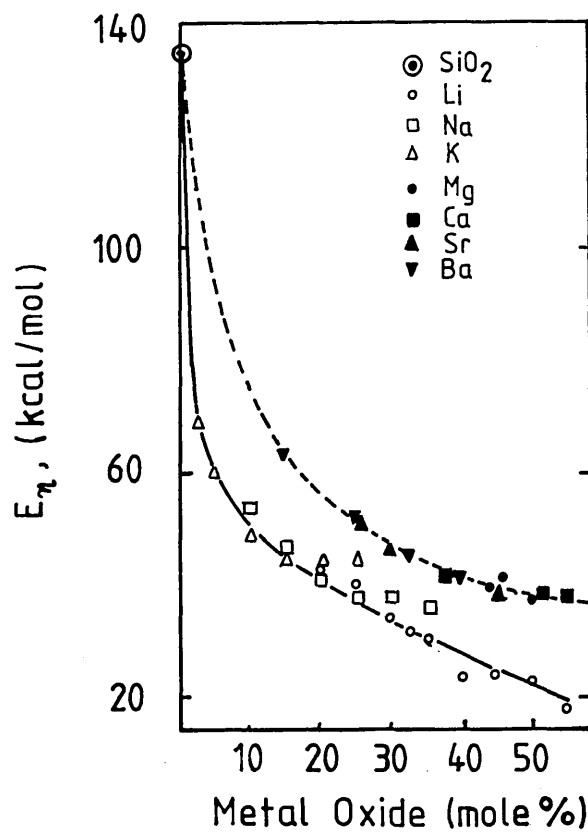


Fig. 13

Variation In Activation Energy For Viscous Flow In Binary Silicates With The Amount Of Metal Oxide Added.

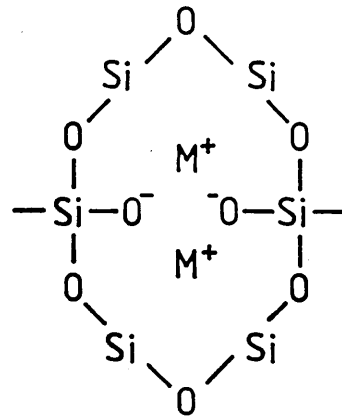
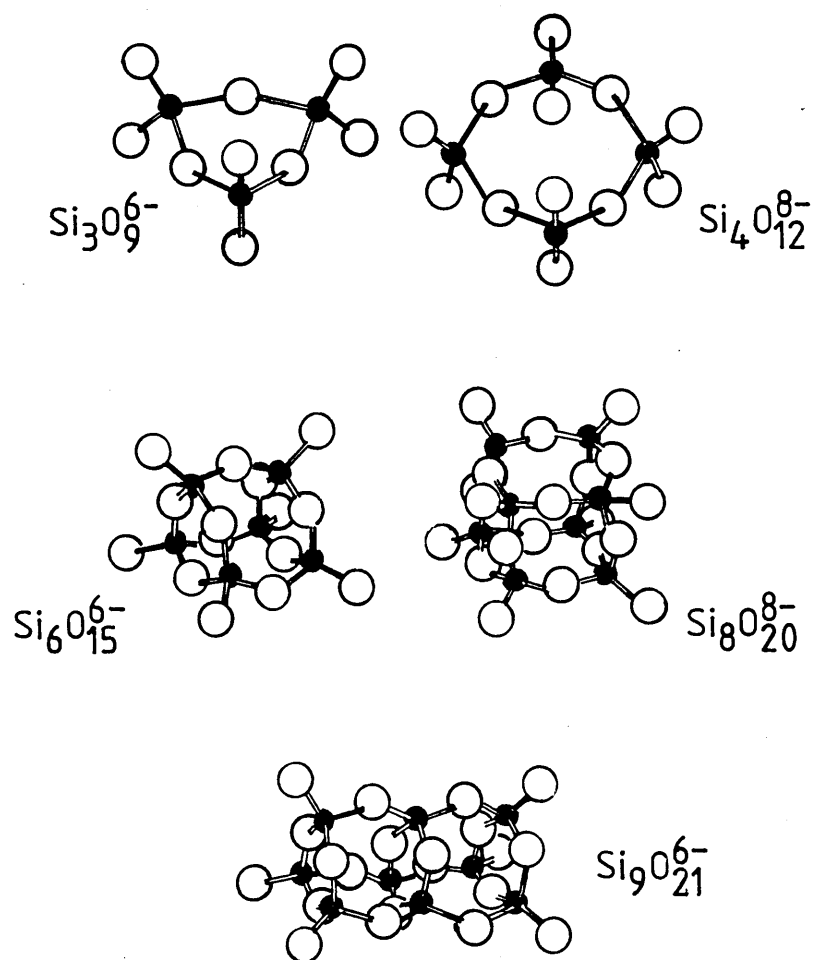


Fig. 14

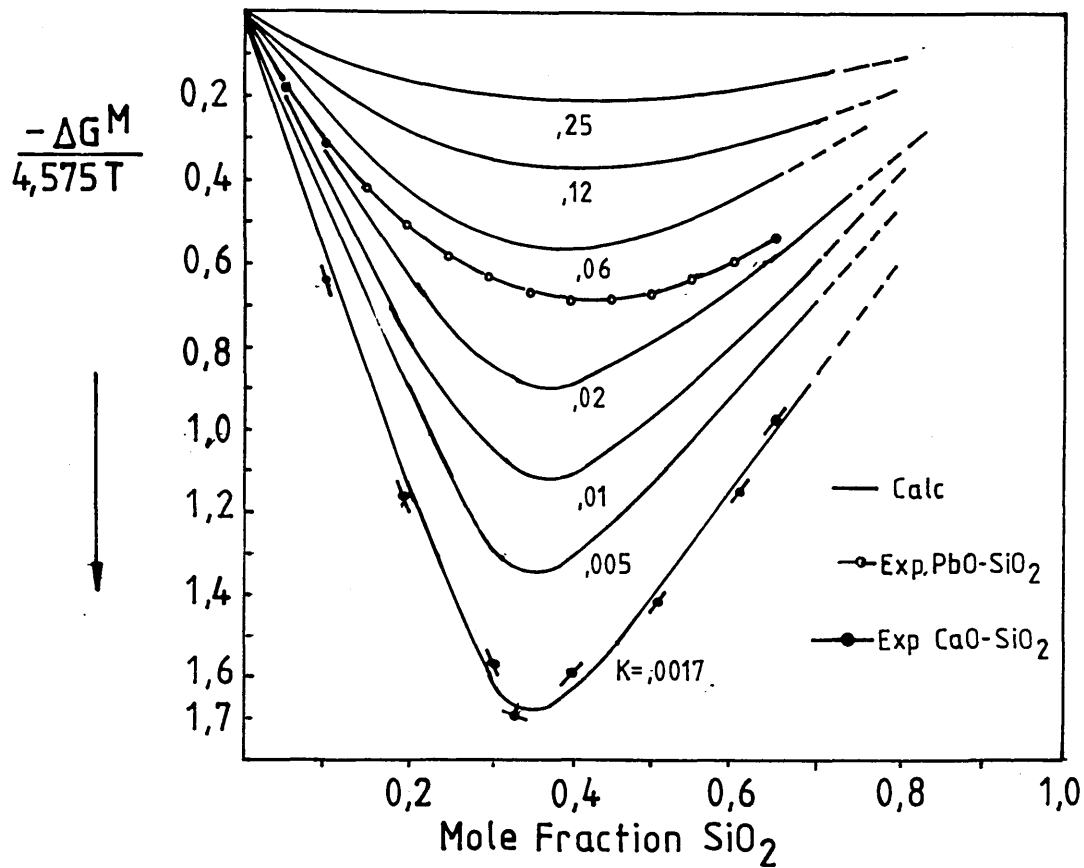
Cations Held In Silicate Cage

Fig. 15



Types Of Globular Anion Suggested By The
Discrete Anion Theory

Fig. 16



Calculated Binary Silicate Free Of Mixing Curves

For Various Values Of K : Toop And Samis Model (84)

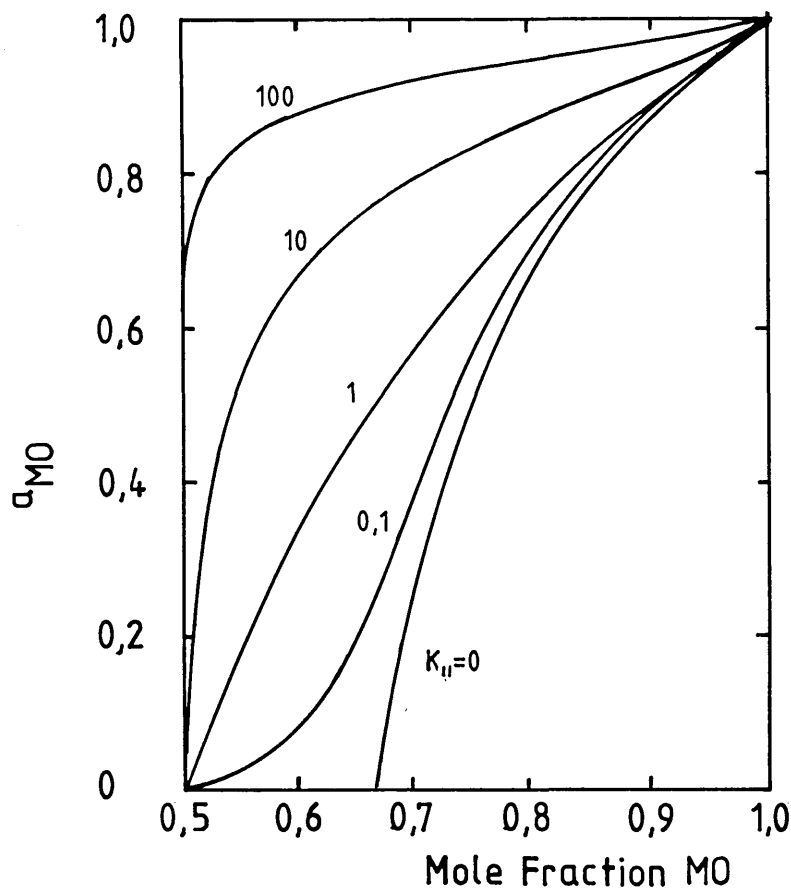


Fig. 17

Theoretical Curves Of Oxide Activity Versus Mole Fraction
MO : Masson Linear Chain Model (91)

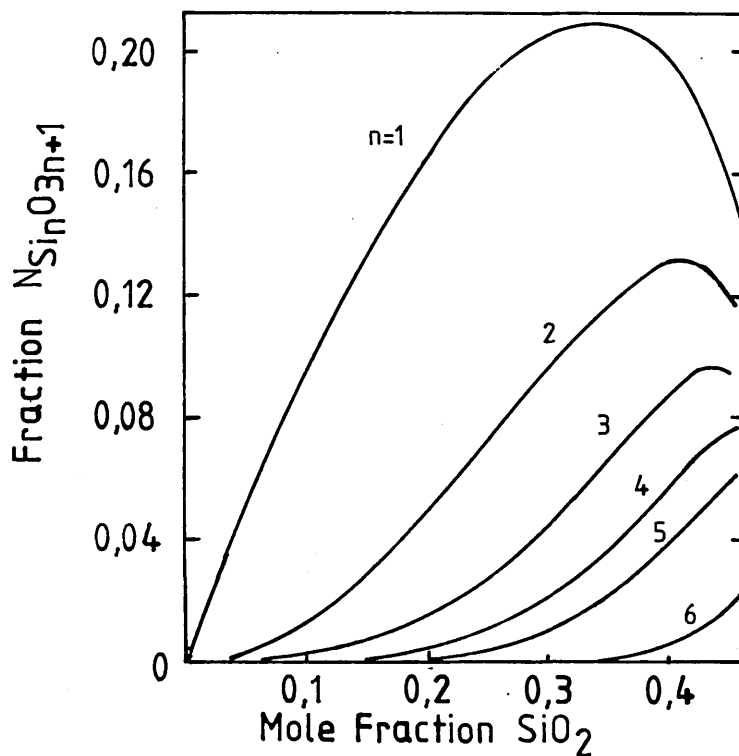


Fig. 18

Calculated Ionic Distributions For FeO-SiO₂ Melts At
1257-1307°C : Masson Linear Chain Model (91)

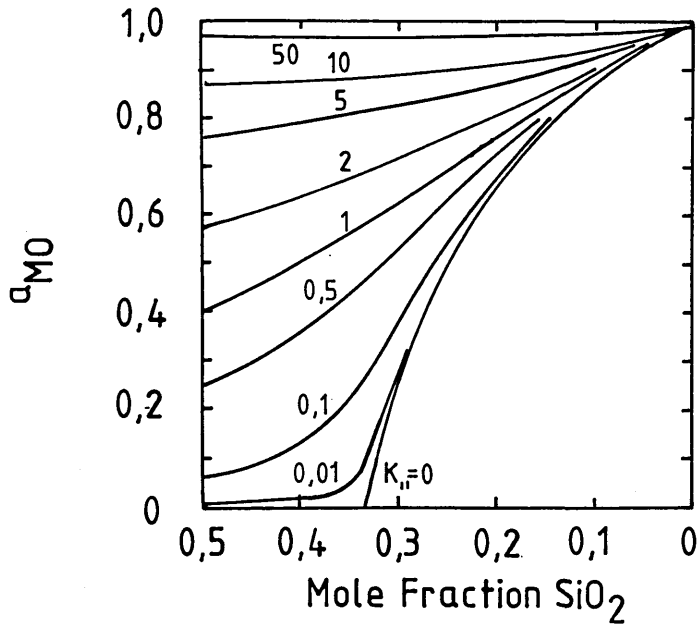


Fig. 19

Theoretical Curves Of Activity Of MO Versus Mole Fraction
 SiO_2 : Masson Branched Chain Model (92)

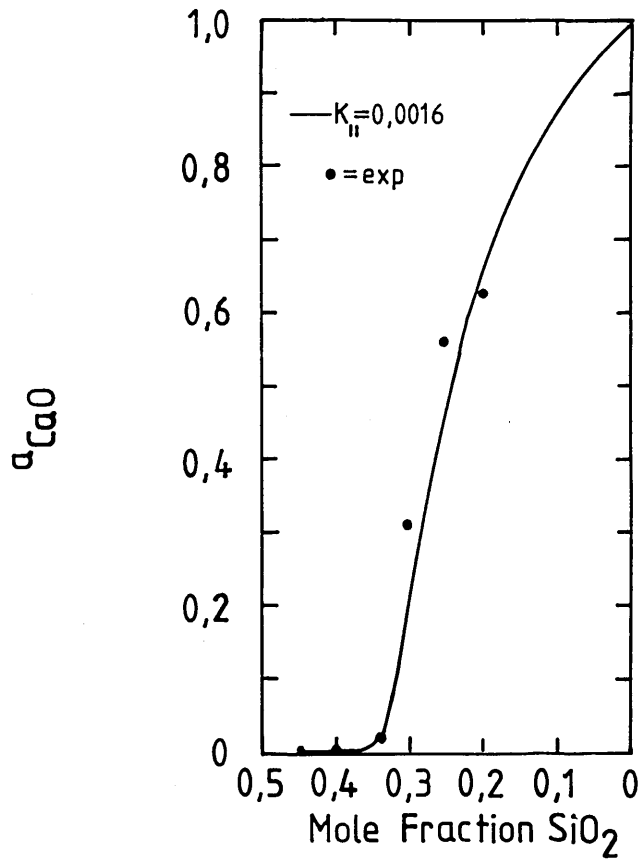


Fig. 20

Activity Of CaO Versus Mole Fraction SiO_2 For System
 $CaO-SiO_2$ At $1600^\circ C$: Masson Branched Chain Model (92)

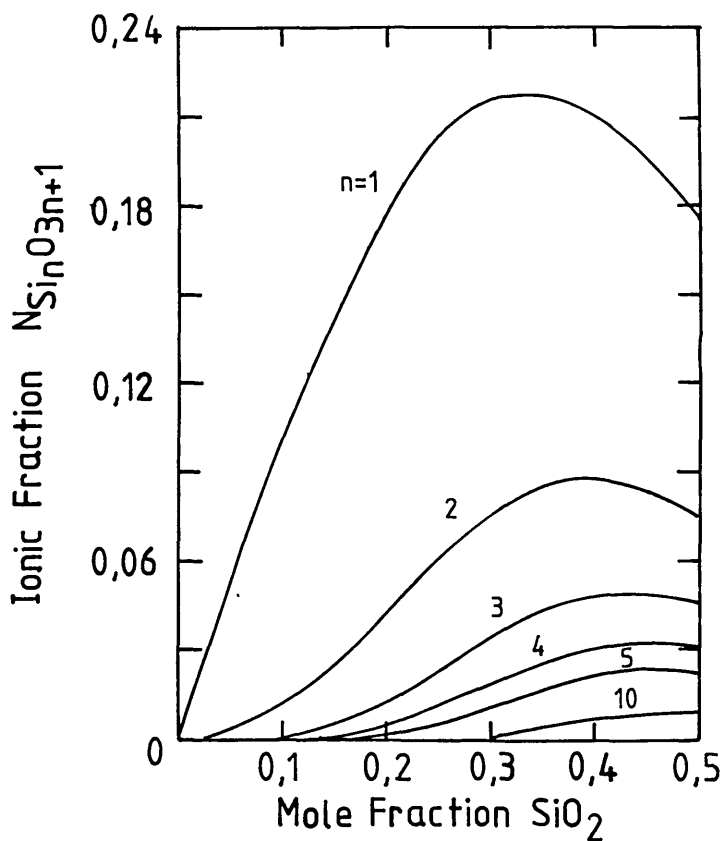


Fig. 21

Calculated Ionic Distributions For FeO-SiO₂ Melts At 1600°C

Masson Branched Chain Model (73)

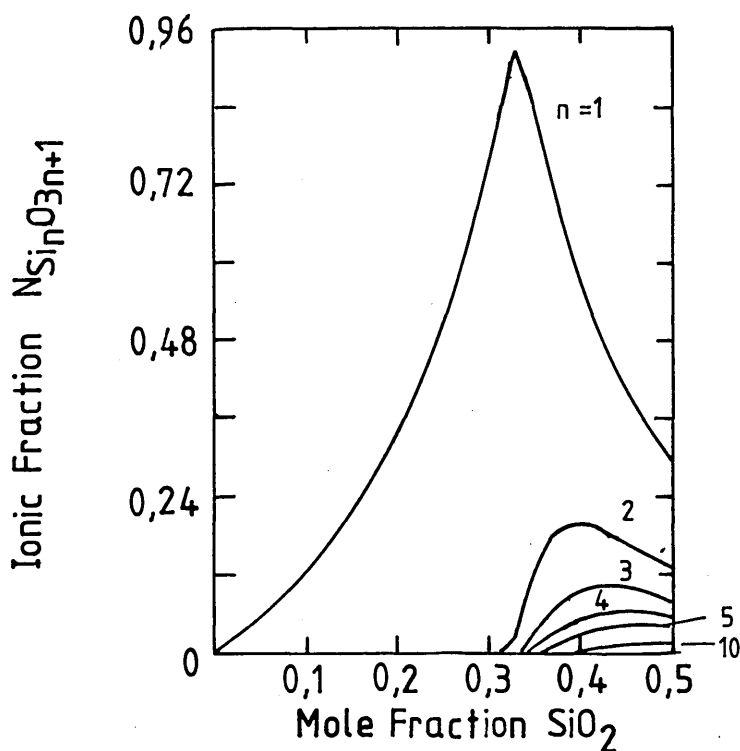
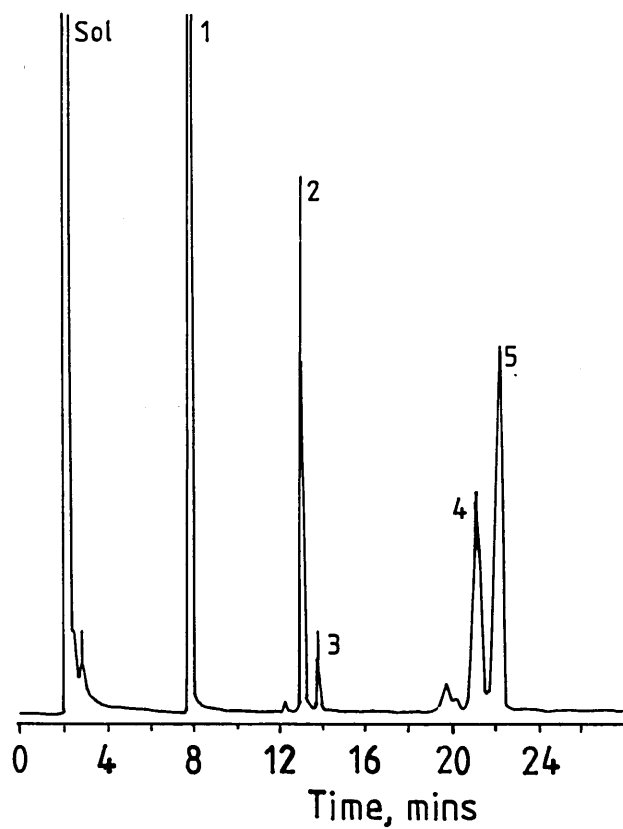


Fig. 22

Calculated Ionic Distributions For CaO-SiO₂ Melts At 1600°C

Masson Branched Chain Model (73)

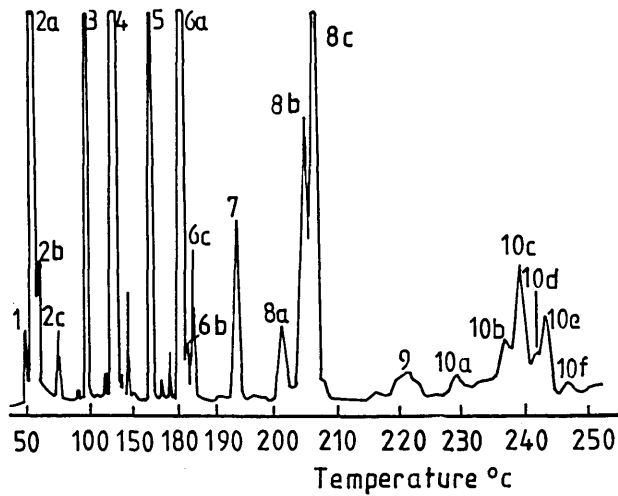
Fig. 23



Peak	Sol	1	2	3	4	5
Parent Ion	Solvent	SiO_4^{4-}	$\text{Si}_2\text{O}_7^{6-}$	$\text{Si}_3\text{O}_9^{6-}$	$\text{Si}_4\text{O}_{12}^{8-}$	$\text{Si}_3\text{O}_{10}^{8-}$

Chromatogram Of TMS Derivatives Of Silicate Anions
For Natrolite Mineral (113)

Fig. 24



Peak	1	2a	2b,2c,6b
Parent Ion	Cl ⁻	O ²⁻	Unknown

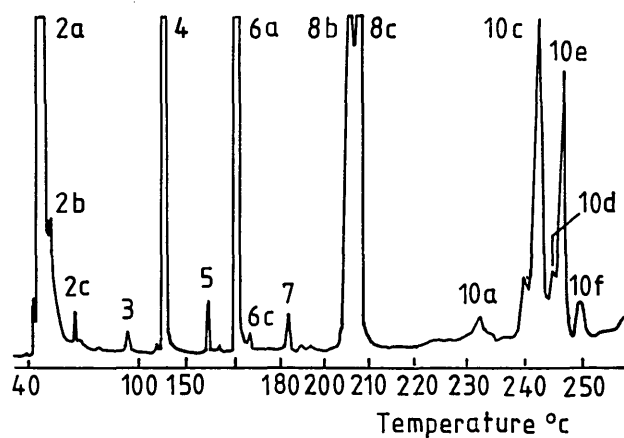
Peak	4	6a	6c	8a	8b	8c
Parent Ion	SiO ₄ ⁴⁻	Si ₂ O ₇ ⁶⁻	Si ₃ O ₉ ⁶⁻	Si ₃ O ₁₀ C ₃ H ₇ ⁷⁻ Si ₄ O ₁₂ C ₃ H ₇ ⁷⁻ Si ₆ O ₁₆ ⁸⁻	Si ₄ O ₁₂ ⁸⁻	Si ₃ O ₁₀ ⁸⁻

Peak	10a	10b	10c	10d	10e	10f
Parent Ion	mainly Si ₉ O ₂₃ ¹⁰⁻	mainly Si ₈ O ₂₁ ¹⁰⁻	mainly Si ₇ O ₁₉ ¹⁰⁻	mainly Si ₆ O ₁₇ ¹⁰⁻	mainly Si ₅ O ₁₅ ¹⁰⁻	mainly Si ₄ O ₁₃ ¹⁰⁻

Peak	3	5,7,9
Parent Ion	PO ₄ ³⁻	Silicophosphates

Chromatogram For Open-Hearth Slag (123)

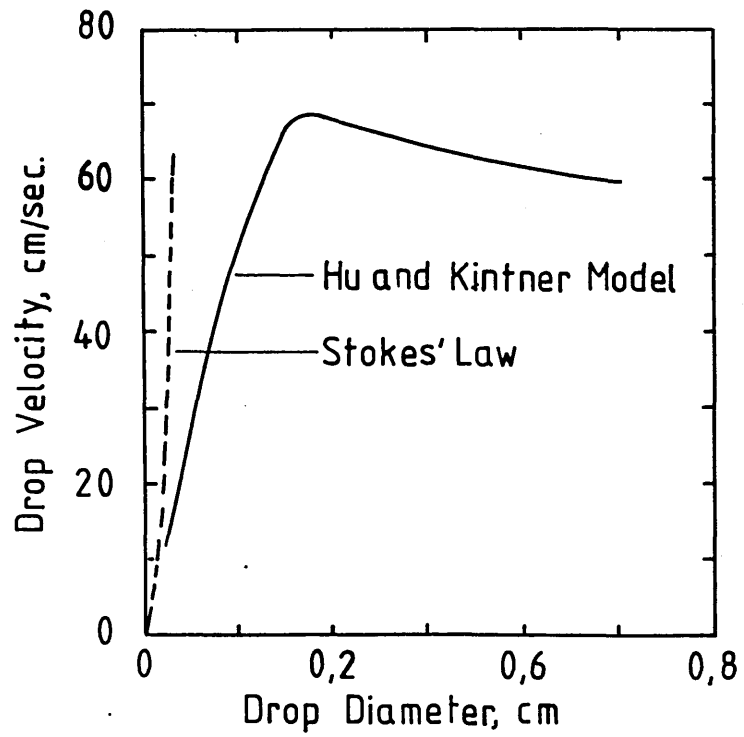
Fig. 25



Peak Identity As For Figure 24, Page 321

Chromatogram For Blast Furnace Slag (123)

Fig. 26



Velocity-Diameter Relationship: Mercury Drops In Water (125)

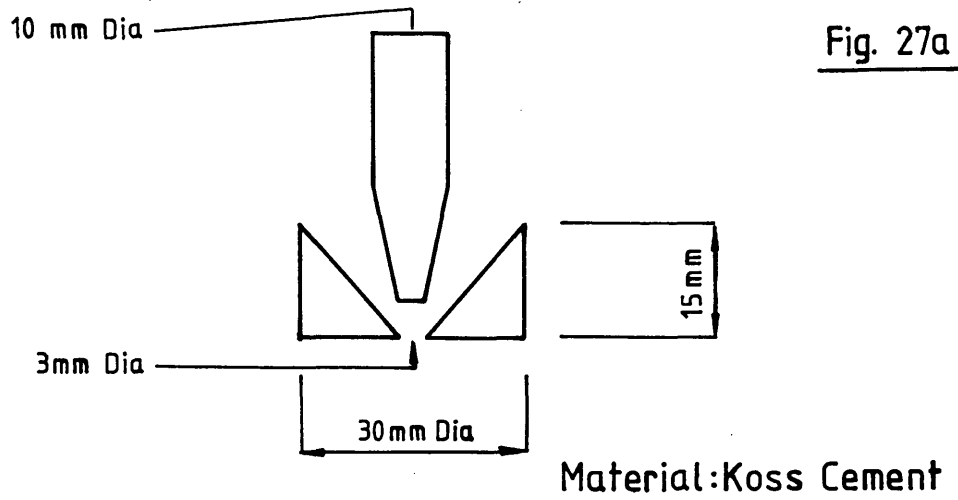


Fig. 27a

(a) Stopper And Seat Used For Wood's Metal Droplets

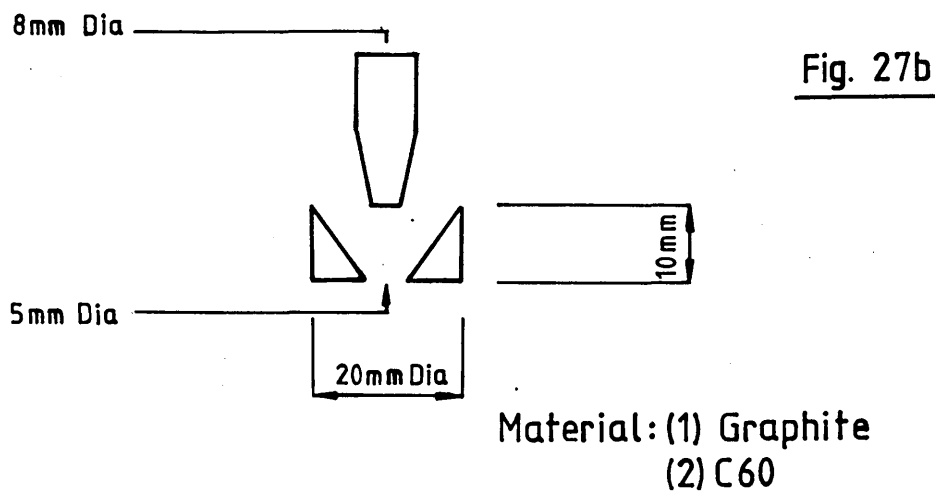


Fig. 27b

(b) Stopper And Seat For Fe-C-S Droplet Trials

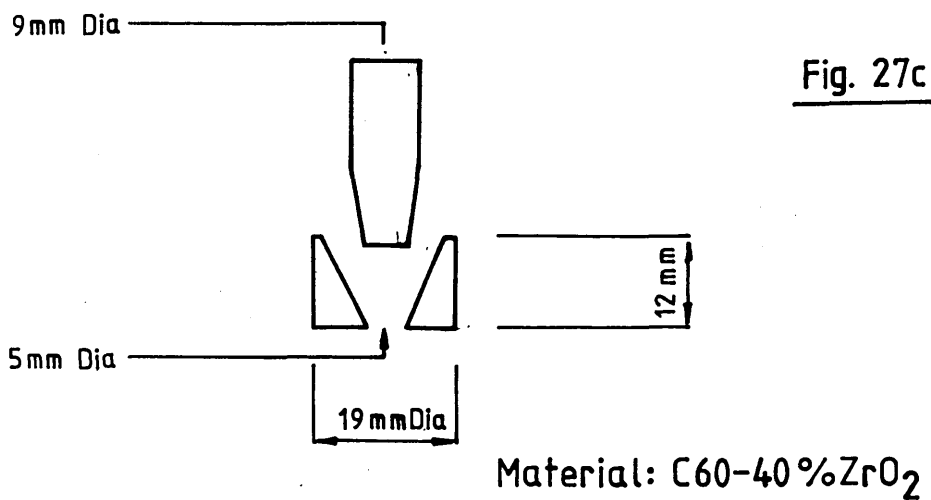
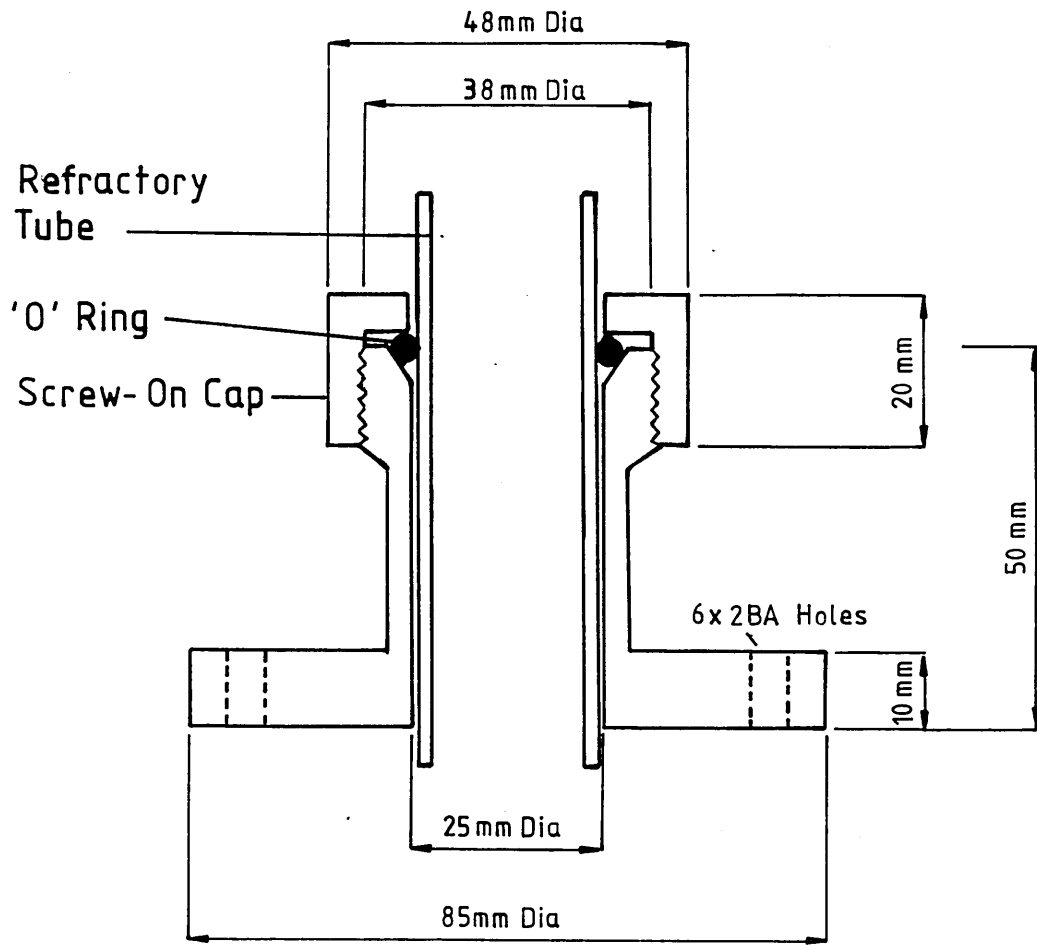


Fig. 27c

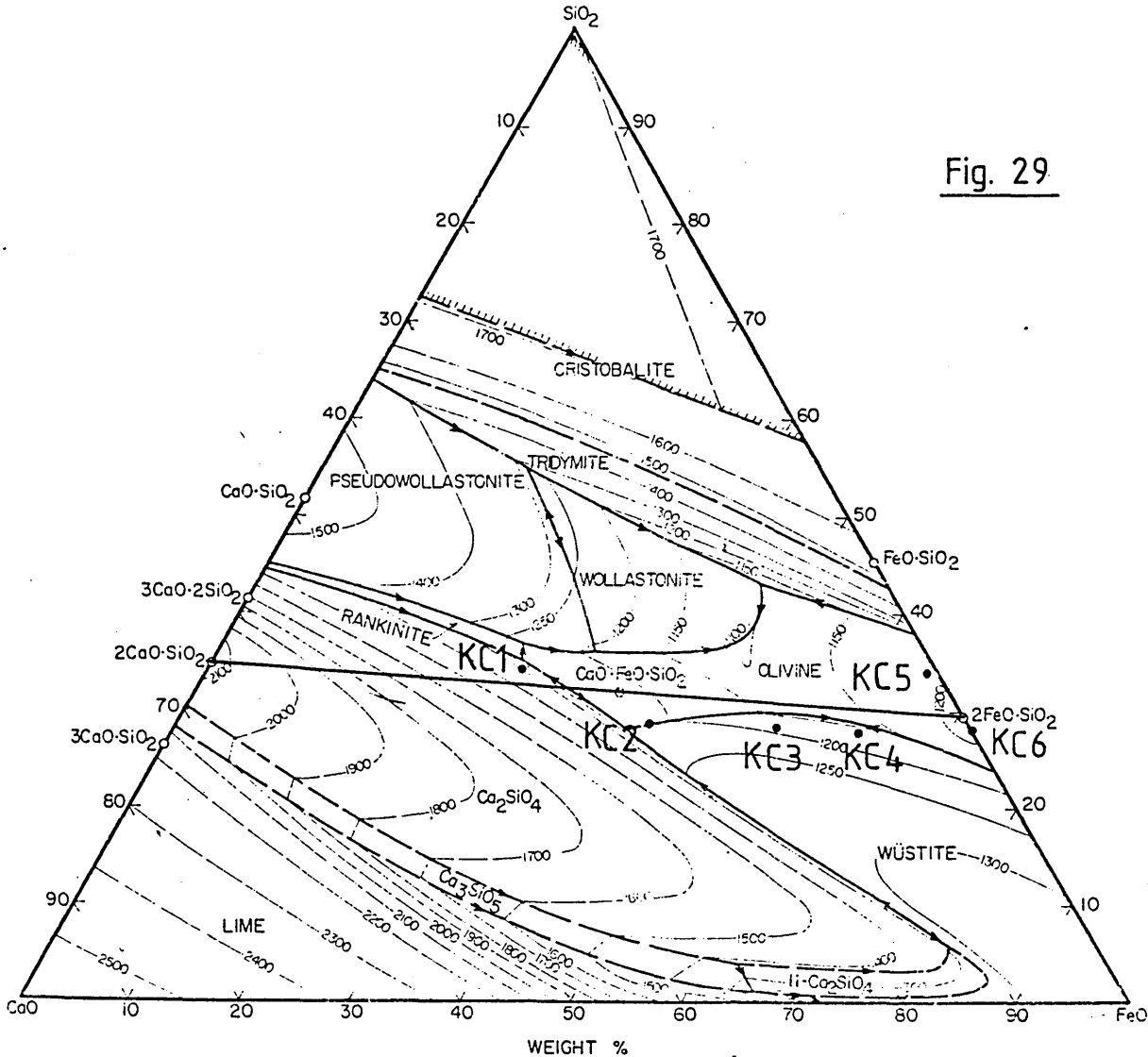
(c) Stopper And Seat For Droplet Experiments

Fig. 28



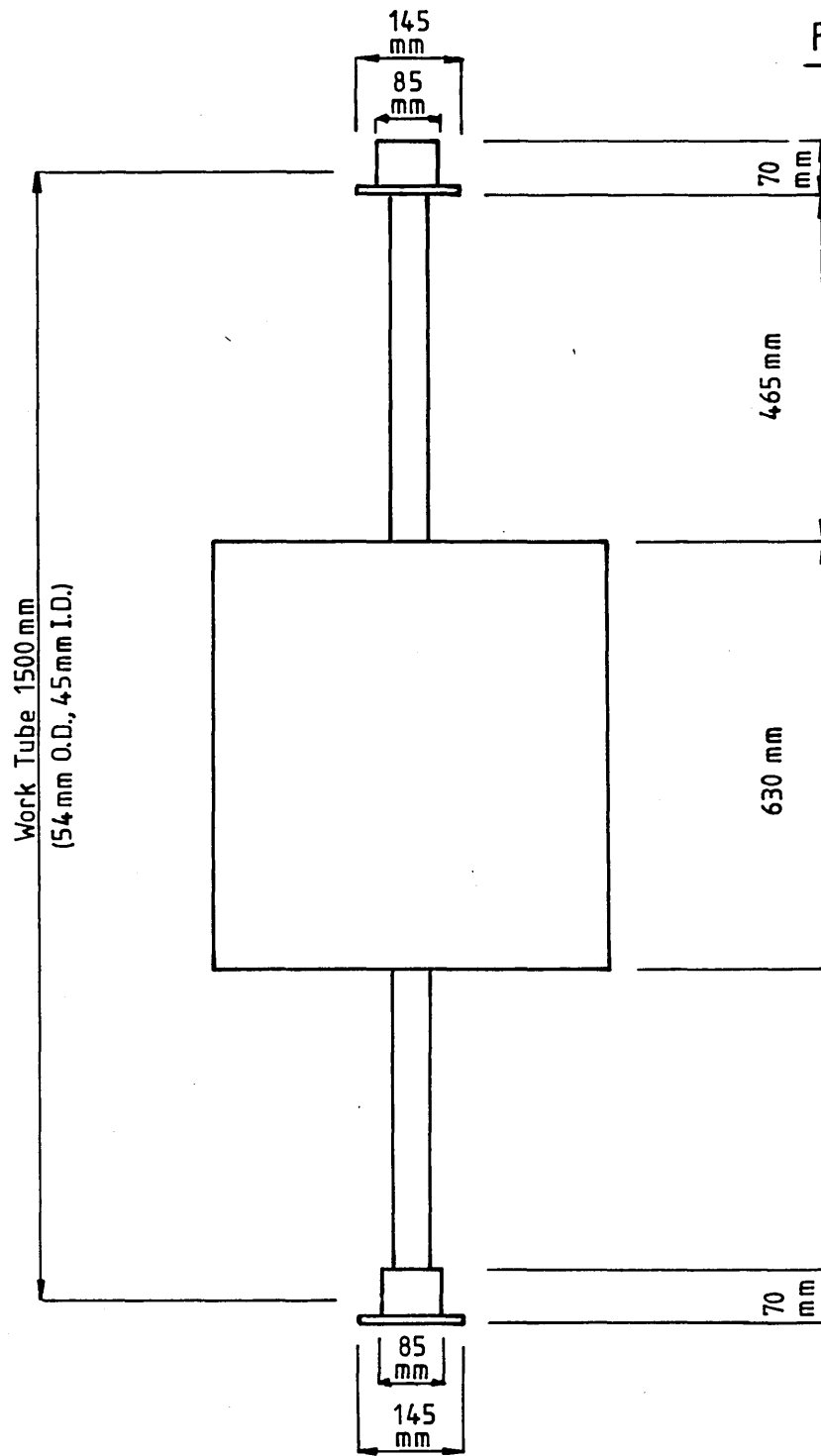
Wilson Seal For Suspending Stopper System

Fig. 29



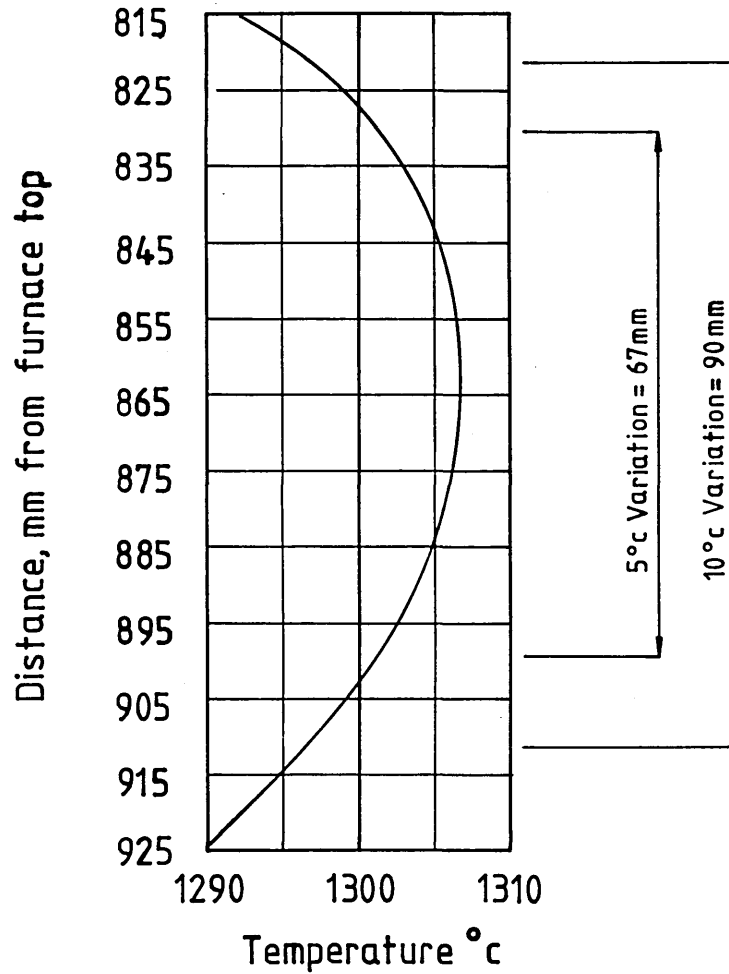
Slag Compositions Employed For Droplet Experiments

Fig. 30



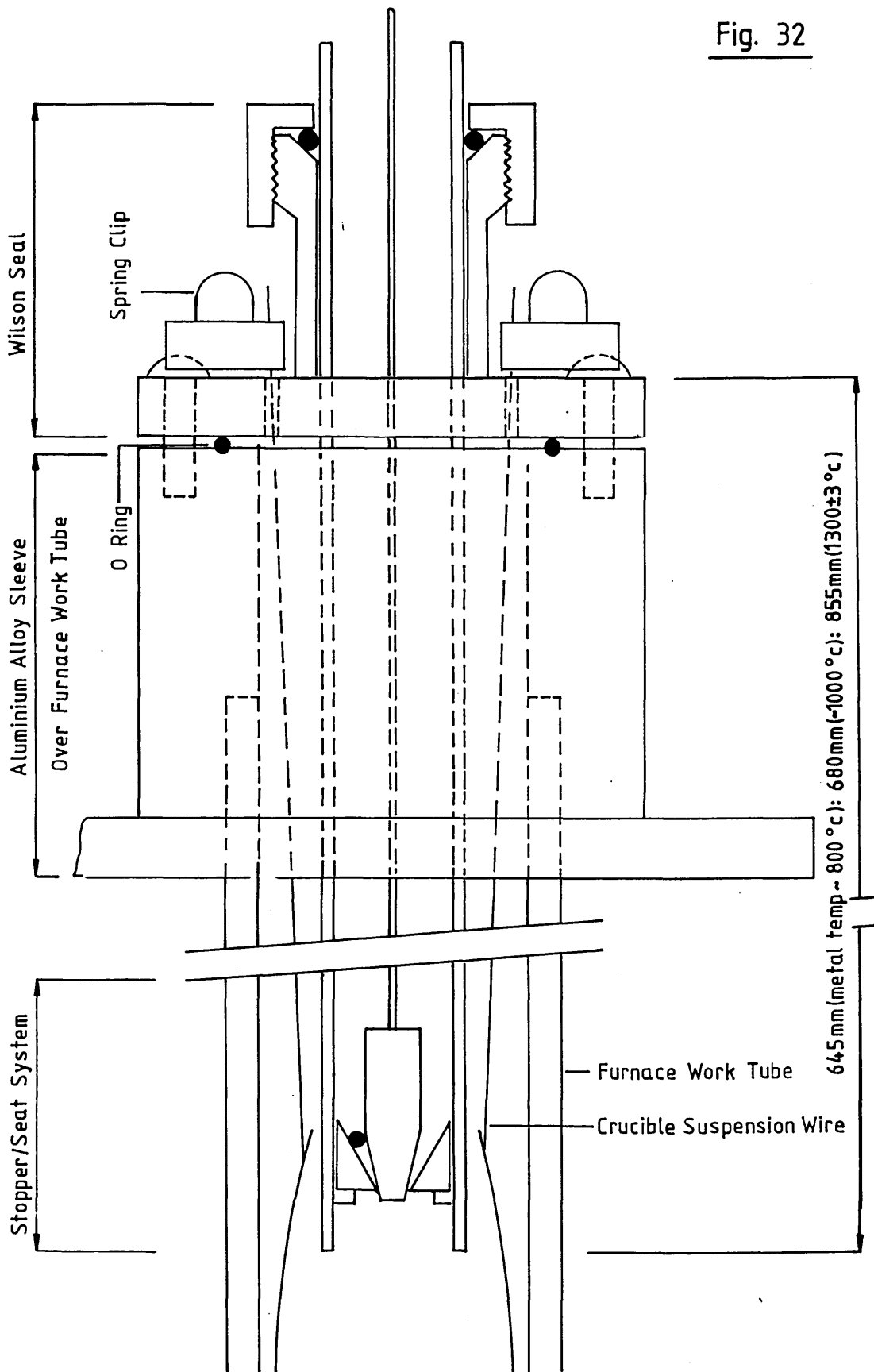
Schematic Diagram Of Furnace Employed For Droplet Experiments

Fig. 31



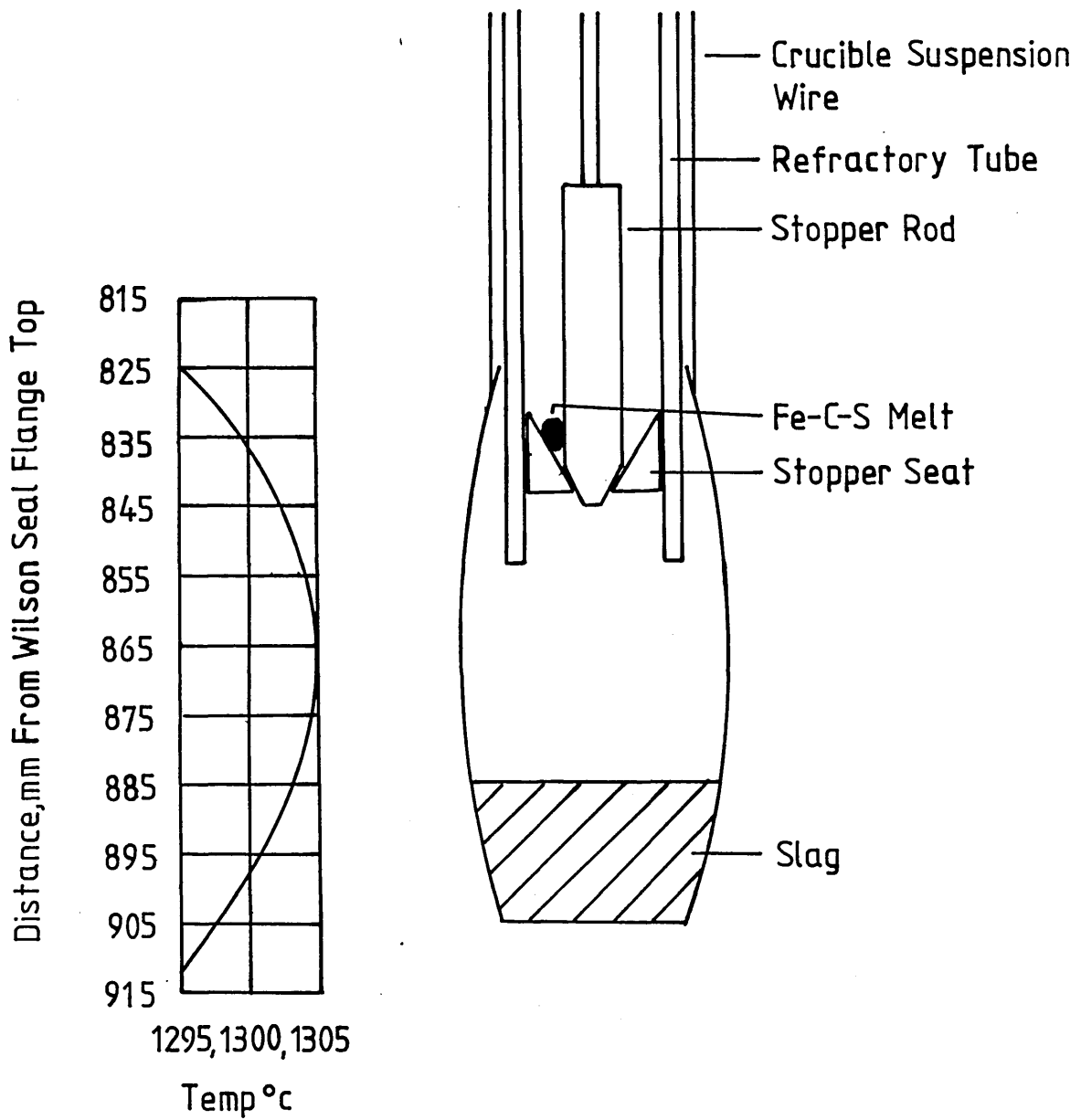
Typical Temperature Profile For The Furnace
Employed For Droplet Experiments

Fig. 32



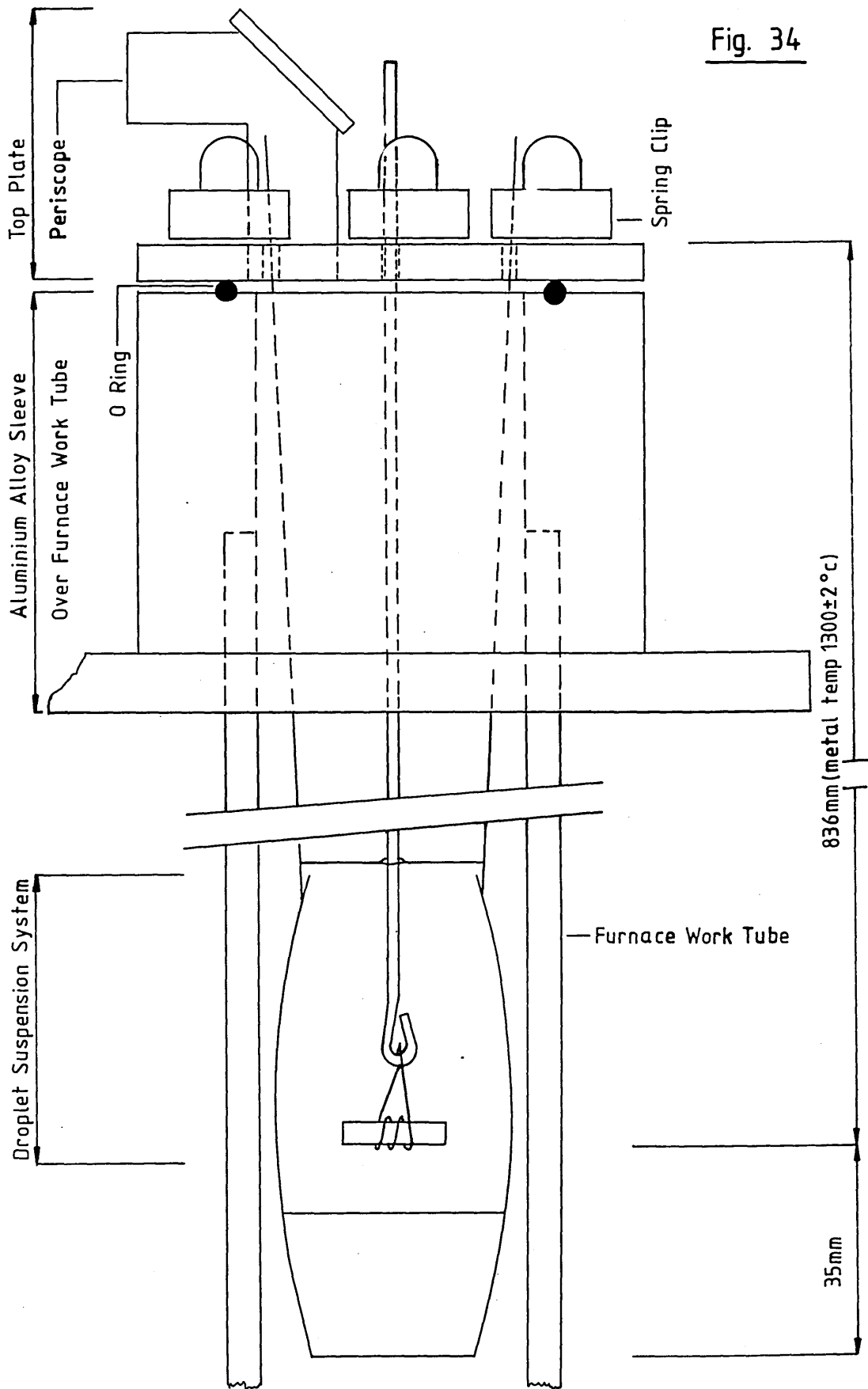
Arrangement Of Apparatus For Droplet Experiments
Using The Stopper And Seat Technique

Fig. 33



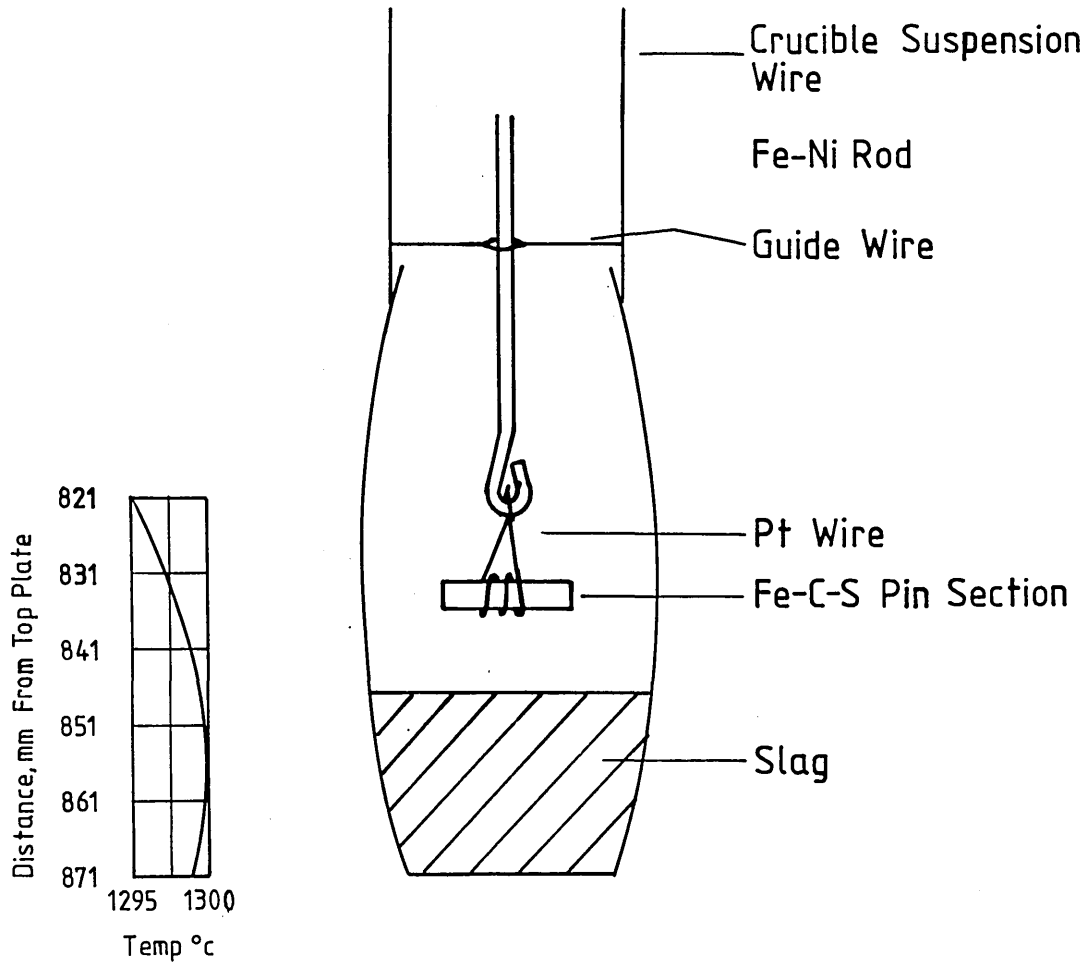
Relationship Between Temperature Profile Of Furnace
And Positioning Of Apparatus For Droplet Experiments
Using The Stopper And Seat Technique

Fig. 34



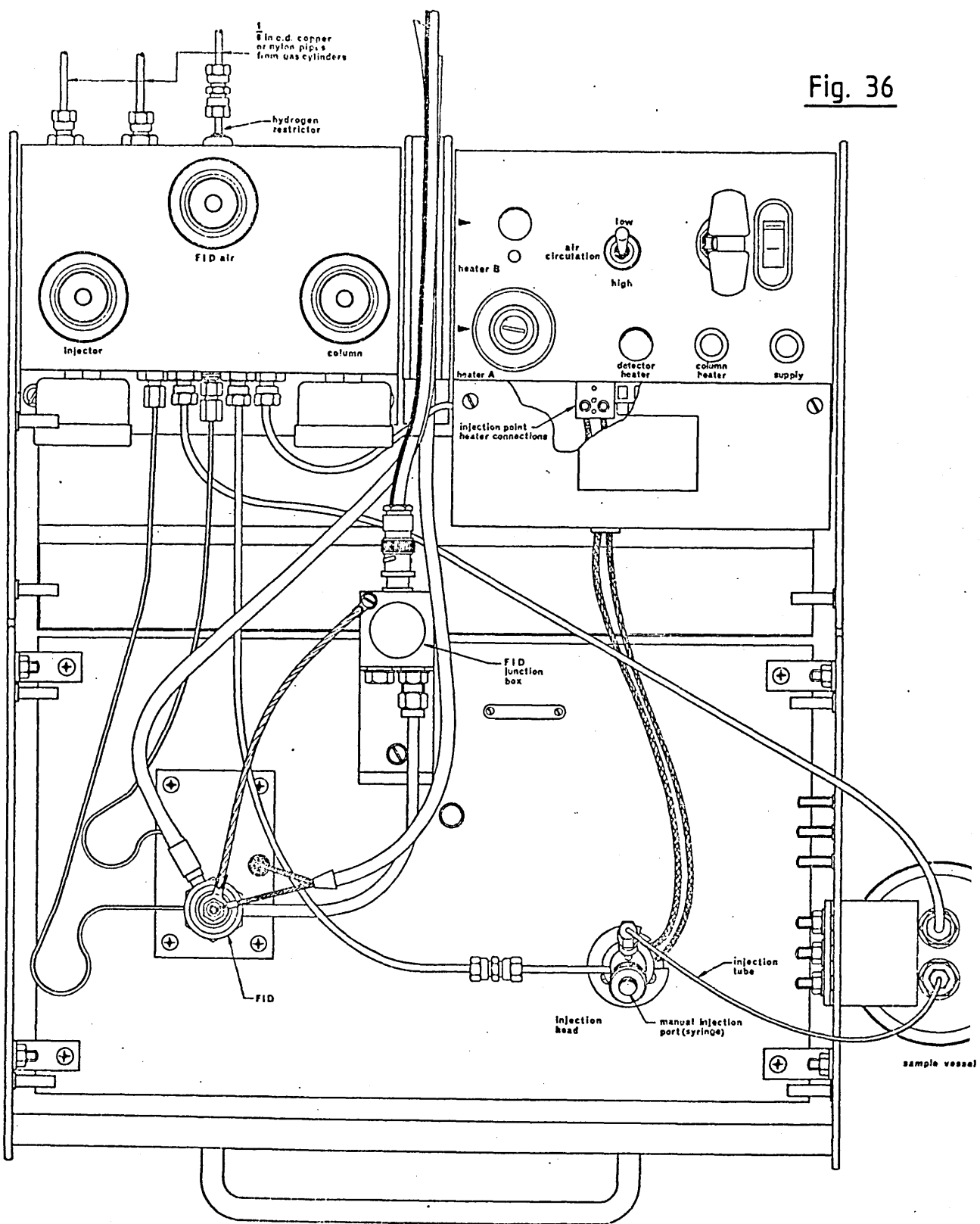
Arrangement Of Apparatus For Droplet Experiments
Using The Suspended Droplet Technique

Fig. 35



Relationship Between Temperature Profile Of Furnace
And Positioning Of Apparatus For Droplet Experiments
Using The Suspended Droplet Technique

Fig. 36



Plan View Of Analyser Unit – Pye Series 105
Gas Liquid Chromatograph

The Desulphurisation of Droplets Produced by the
Stopper and Seat Technique Using Slag KC1

Figure 37

The Desulphurisation of Droplets Containing 4.38 Mass % C and
0.512 Mass % S at Zero Reaction Time by Slag KC1 38.31 Mass % CaO
-28.52 Mass % FeO-1.90 Mass % Fe₂O₃-31.00 Mass % SiO₂-0.27 Mass % S

Figure 38

The Desulphurisation of Droplets Containing 4.71 Mass % C and 0.440
Mass % S at Zero Reaction Time by Slag KC1 38.31 Mass % CaO-28.52
Mass % FeO-1.90 Mass % Fe₂O₃-31.00 Mass % SiO₂-0.27 Mass % S

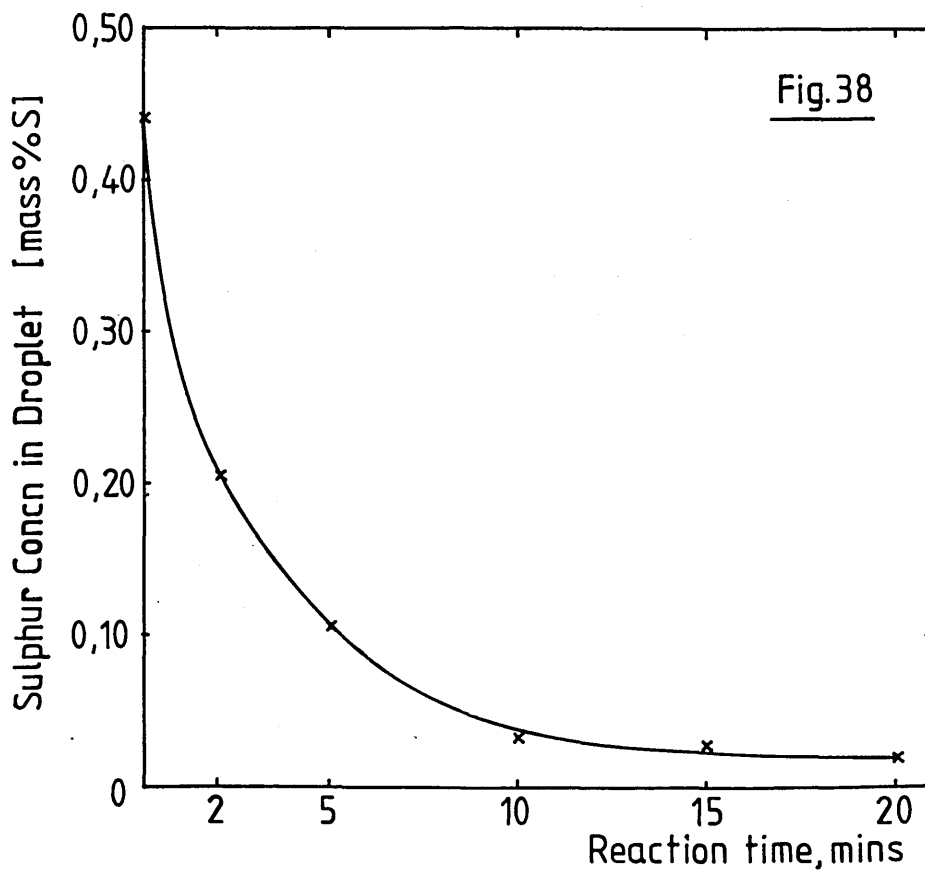
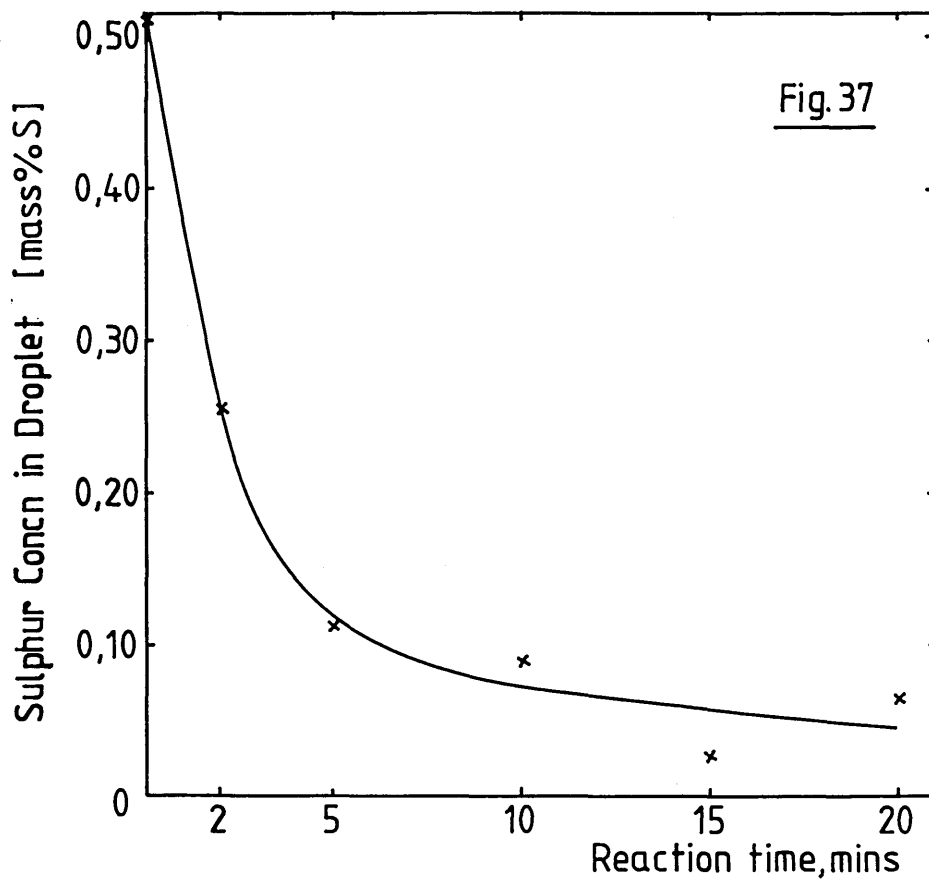


Figure 39

The Desulphurisation of Droplets Containing 4.60 Mass % C and
0.302 Mass % S at Zero Reaction Time by Slag KC1 38.31 Mass %
CaO-28.52 Mass % FeO-1.90 Mass % Fe₂O₃-31.00 Mass % SiO₂-0.27
Mass % S

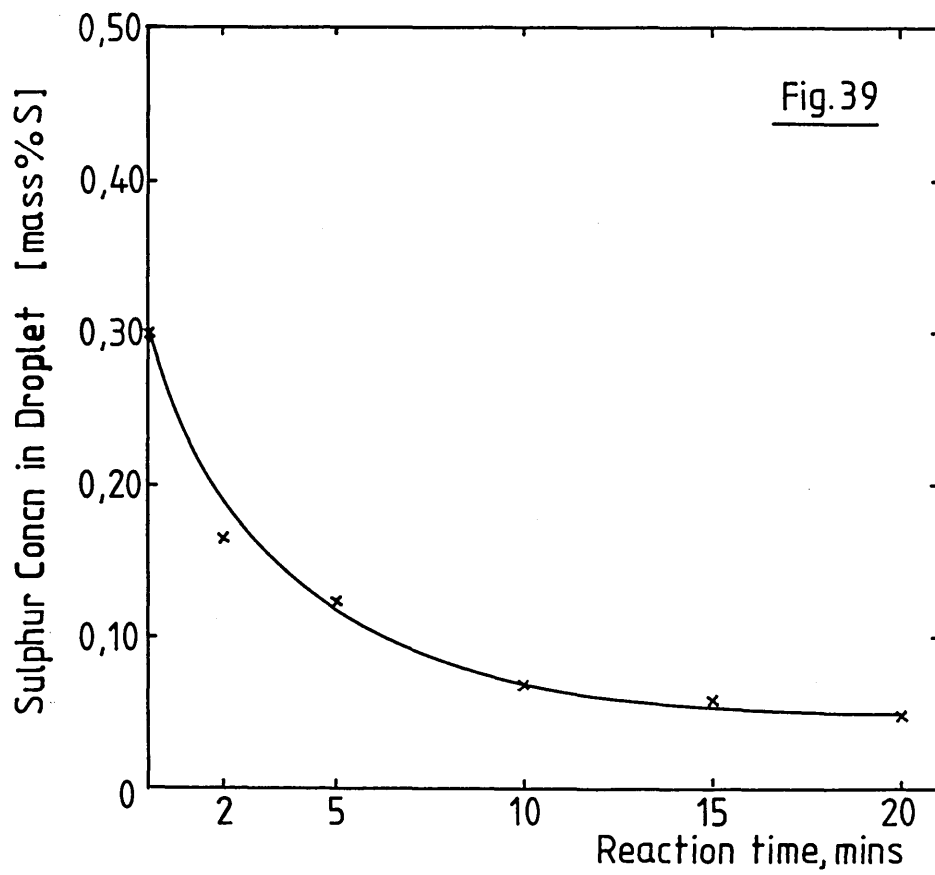


Figure 40

The Desulphurisation of Droplets Containing 4.20 Mass % C and 0.123 Mass % S (Run I) and 0.120 Mass % S (Run II) at Zero Reaction Time by Slag KC1, 38.31 Mass % CaO-28.52 Mass % FeO-1.90 Mass % Fe_2O_3 -31.00 Mass % SiO_2 -0.27 Mass % S

- NB: x denotes initial sulphur concentration of droplet
 equal to 0.123 mass %
- o denotes initial sulphur concentration of droplet
 equal to 0.120 mass %

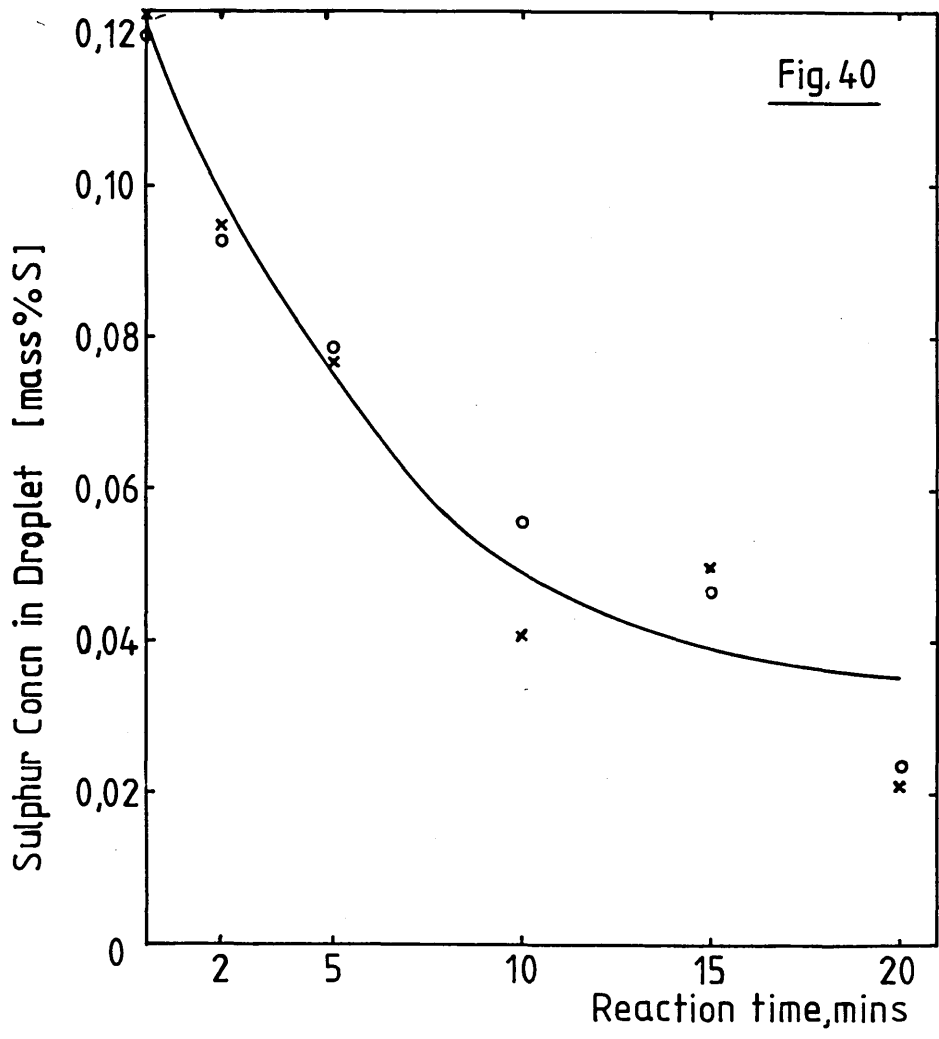


Figure 41

The Desulphurisation of Droplets Containing 4.55 Mass % C and 0.076
Mass % S at Zero Reaction Time by Slag KC1, 38.31 Mass % CaO-28.52
Mass % FeO-1.90 Mass % Fe₂O₃-31.00 Mass % SiO₂-0.27 Mass % S

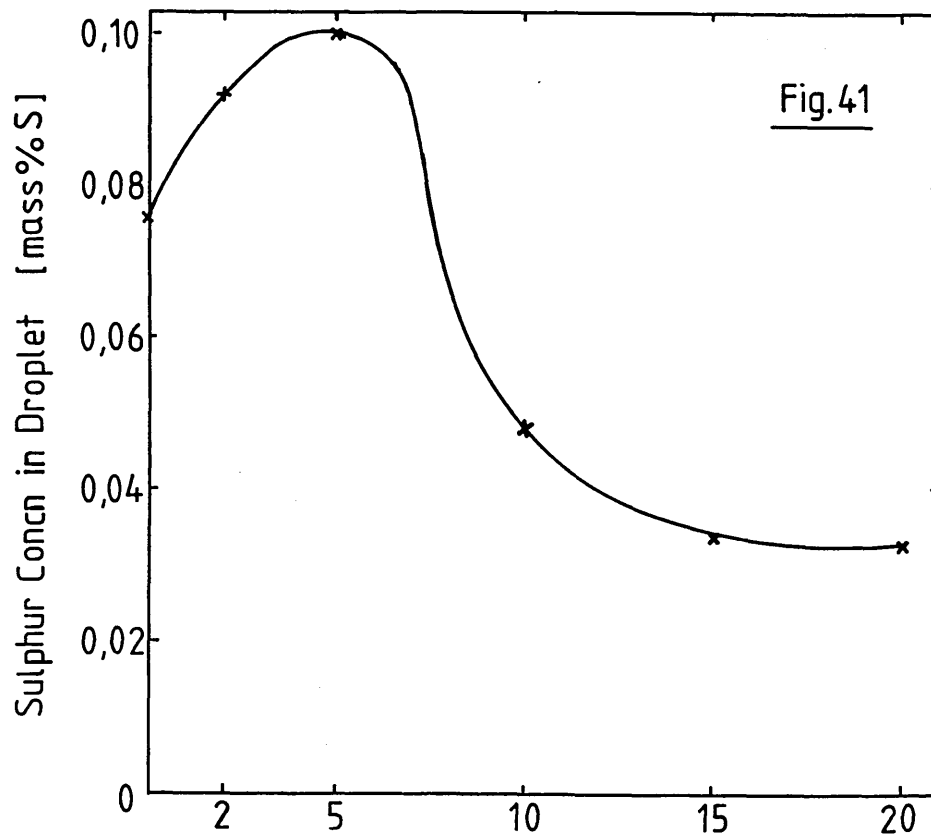


Fig.41

Figure 42a

The Desulphurisation of Droplets Containing 4.01 Mass % C and
0.057 Mass % S at Zero Reaction Time by Slag KC1, 38.31 Mass %
CaO-28.52 Mass % FeO-1.90 Mass % Fe₂O₃-31.00 Mass % SiO₂-0.27
Mass % S

Figure 42b

The Desulphurisation of Droplets Containing 4.01 Mass % C and
0.054 Mass % S at Zero Reaction Time by Slag KC1, 38.31 Mass % CaO
-28.52 Mass % FeO-1.90 Mass % Fe₂O₃-31.00 Mass % SiO₂-0.27 Mass % S

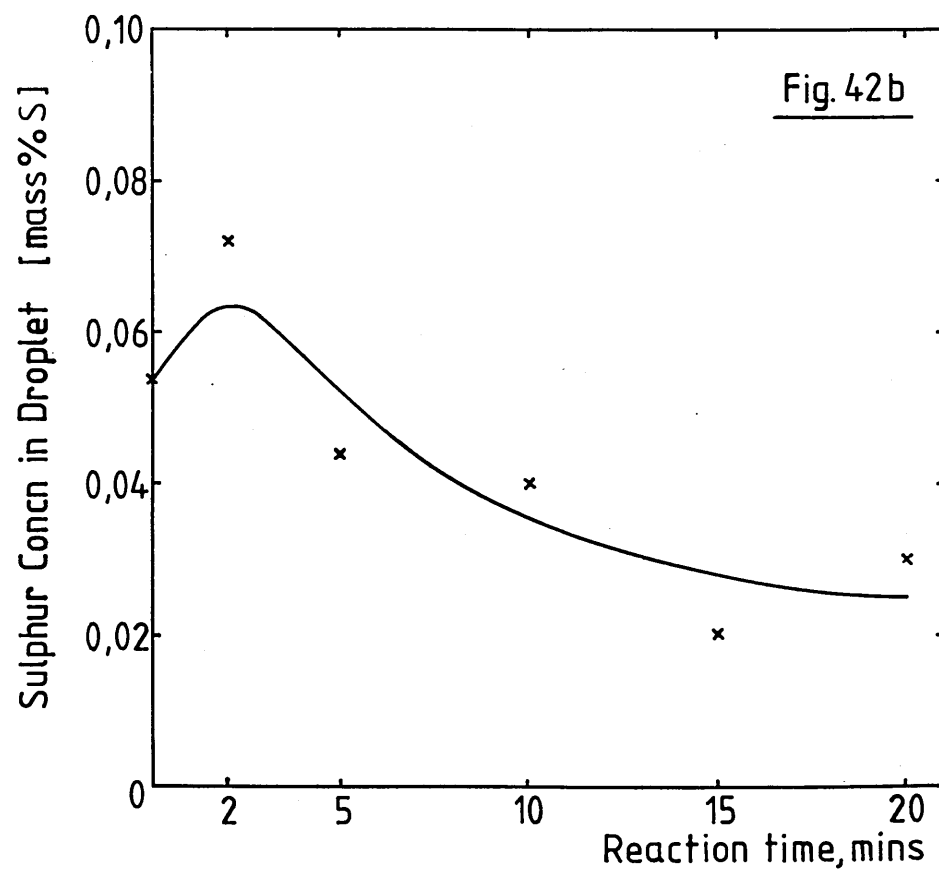
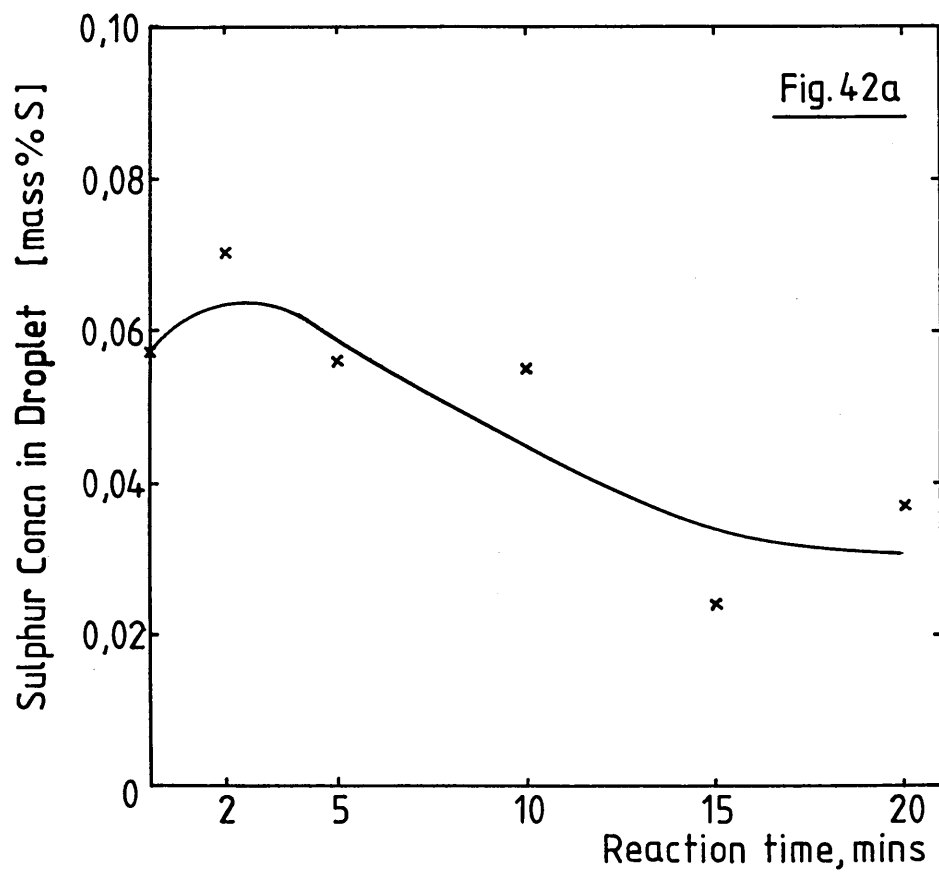
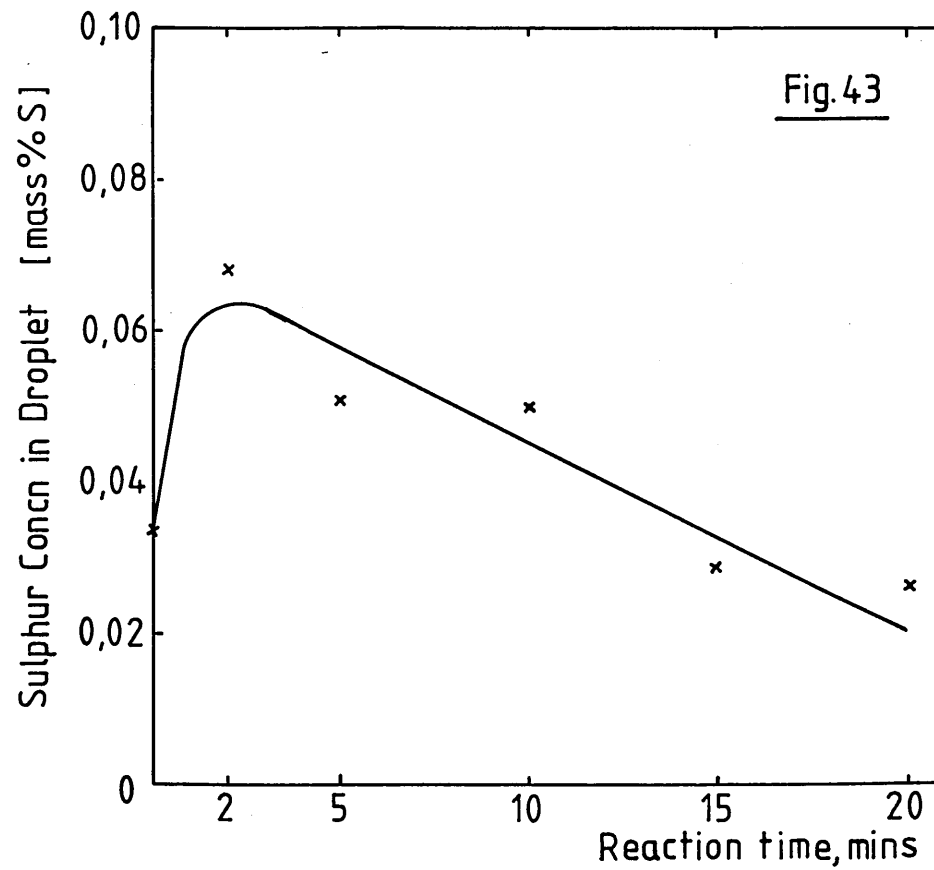
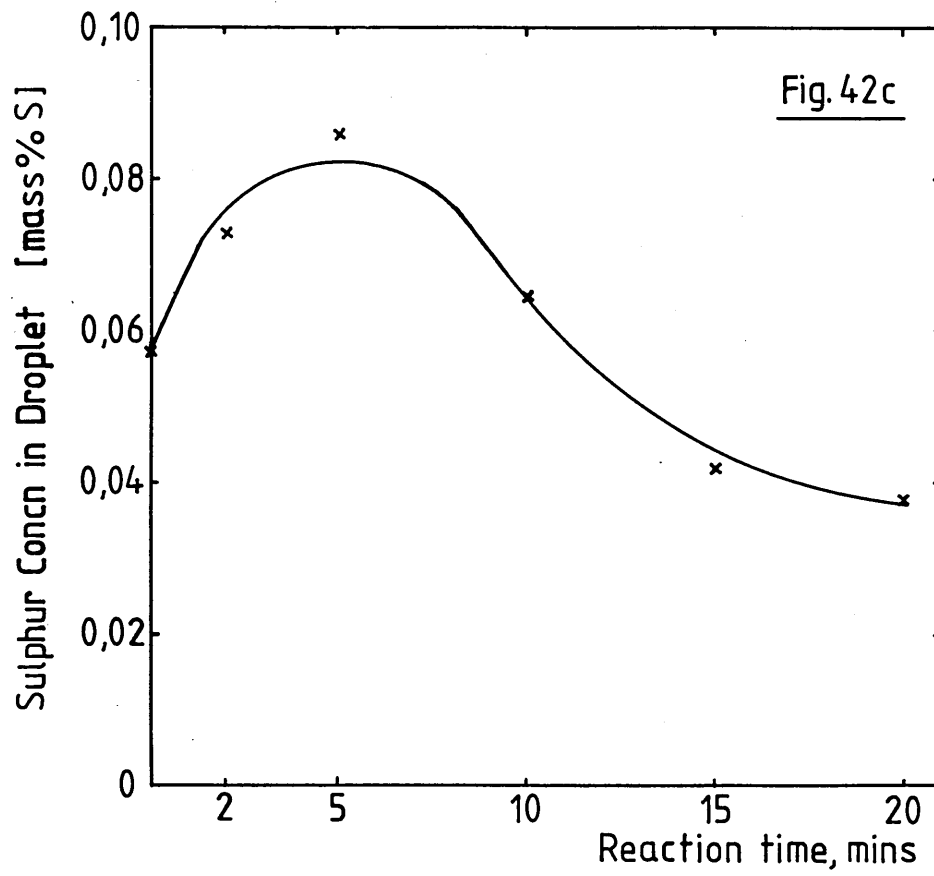


Figure 42c

The Desulphurisation of Droplets Containing 4.01 Mass % C and
0.057 Mass % S at Zero Reaction Time by Slag KC1, 38.31 Mass %
CaO-28.52 Mass % FeO-1.90 Mass % Fe₂O₃-31.00 Mass % SiO₂-0.27
Mass % S

Figure 43

The Desulphurisation of Droplets Containing 4.01 Mass % C and
0.034 Mass % S at Zero Reaction Time by Slag KC1, 38.31 Mass % CaO
-28.52 Mass % FeO-1.90 Mass % Fe₂O₃-31.00 Mass % SiO₂-0.27 Mass % S



Figures 44 and 45

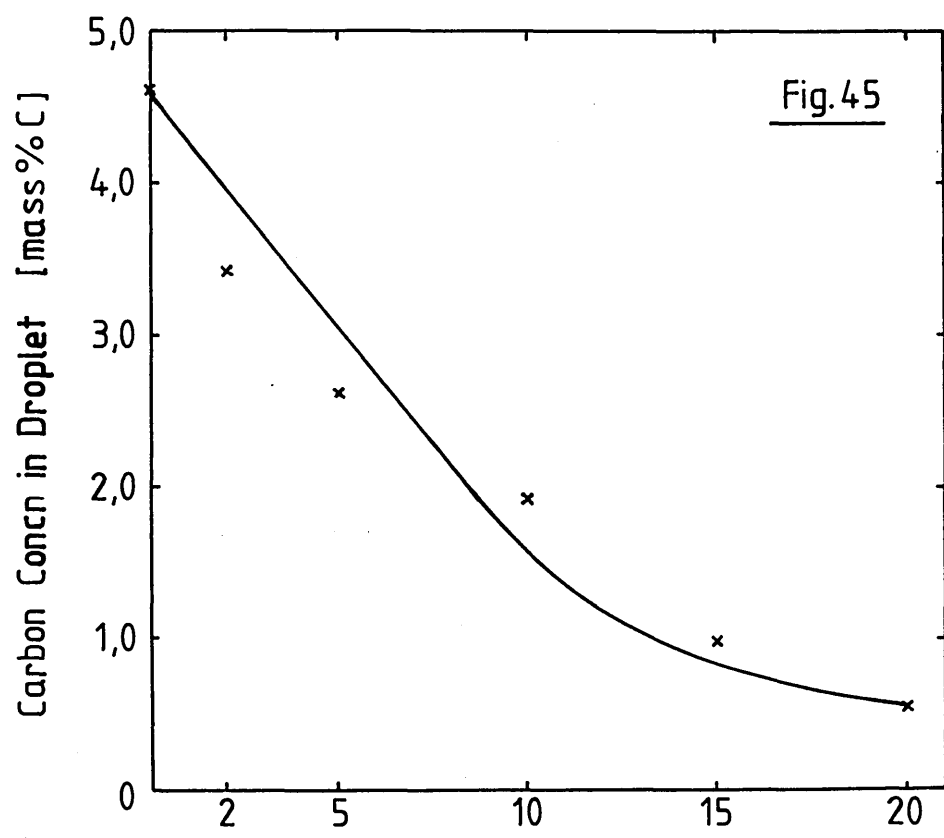
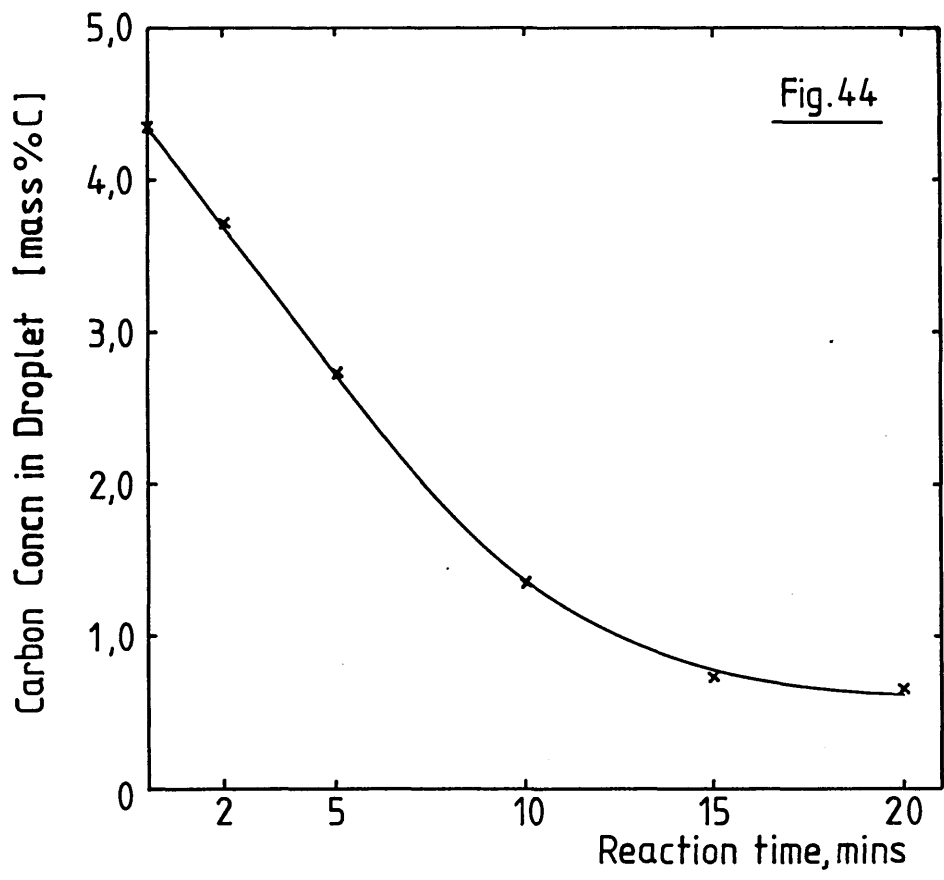
The Decarburisation of Droplets Produced by The Stopper
and Seat Technique Using Slag KC1

Figure 44

The Decarburisation of Droplets Containing 4.35 Mass % C and 0.111
Mass % S at Zero Reaction Time by Slag KC1, 38.31 Mass % CaO-28.52
Mass % FeO-1.90 Mass % Fe₂O₃-31.00 Mass % SiO₂-0.27 Mass % S

Figure 45

The Decarburisation of Droplets Containing 4.60 Mass % C and 0.050
Mass % S at Zero Reaction Time by Slag KC1, 38.31 Mass % CaO-28.52
Mass % FeO-1.90 Mass % Fe₂O₃-31.00 Mass % SiO₂-0.27 Mass % S



Figures 46a to 46d

The Desulphurisation of Droplets Produced by the Suspended Droplet Technique Using Slag KC2, 28.00 Mass % CaO-40.20 Mass % FeO-3.21 Mass % Fe₂O₃-28.50 Mass % SiO₂-0.15 Mass % S

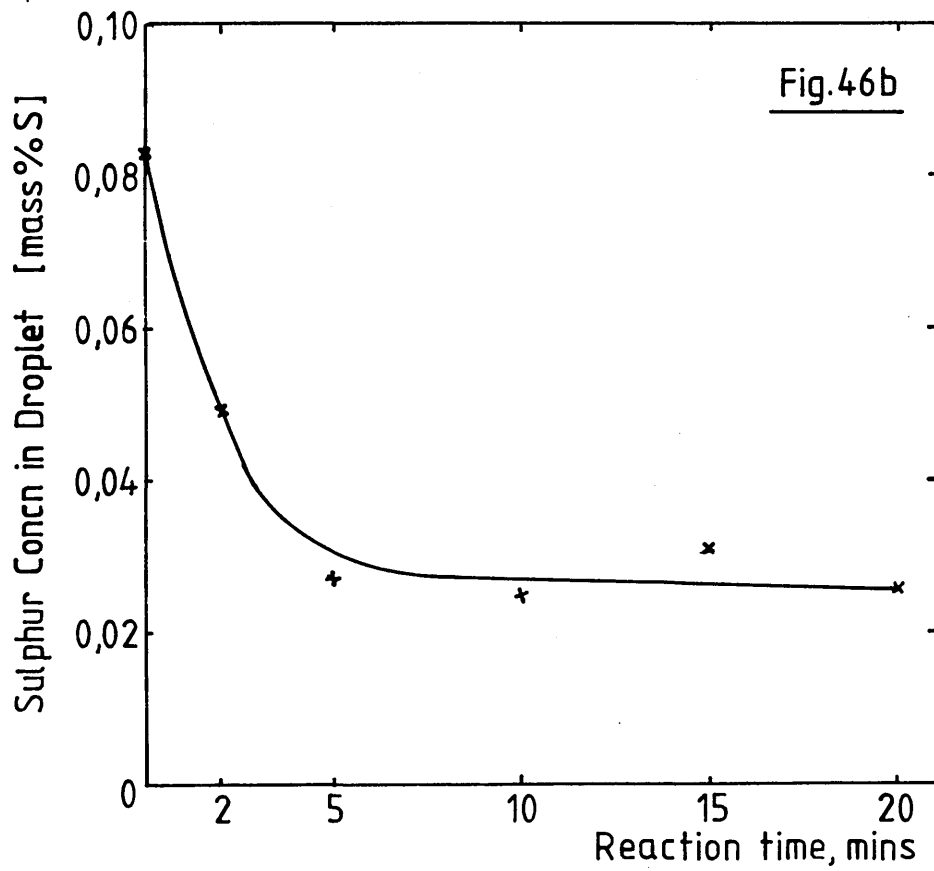
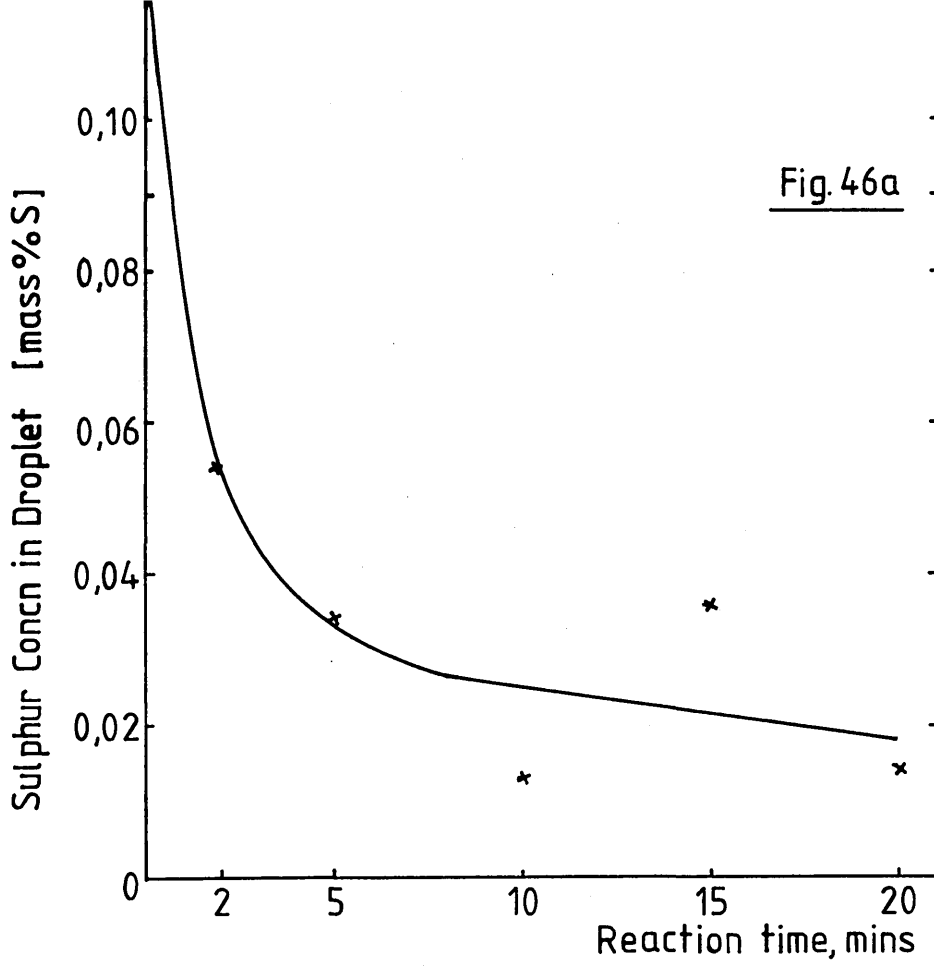
Initial Compositions of Metal Droplets:-

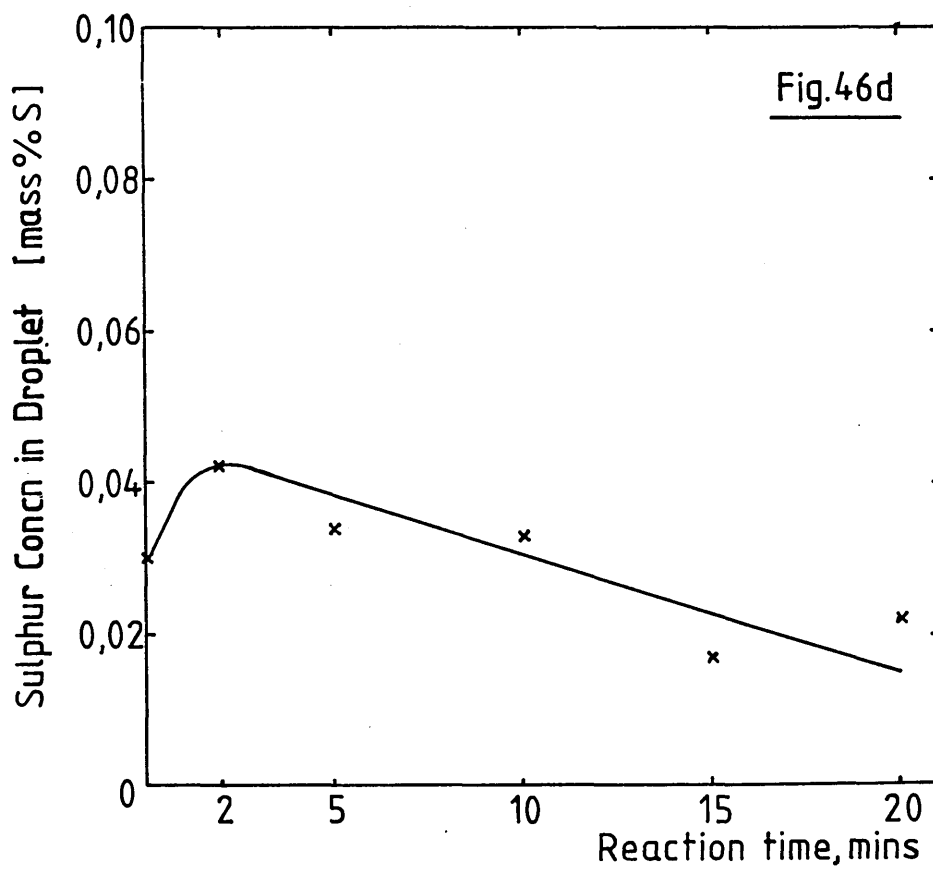
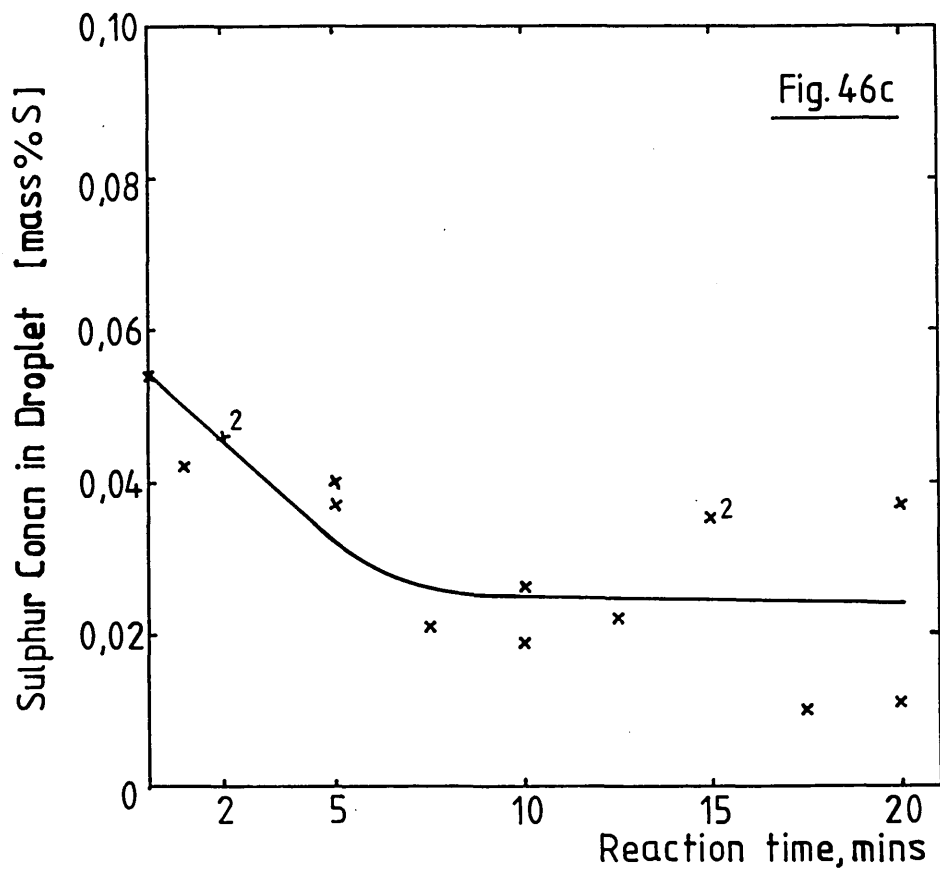
Figure 46a : Fe-4.20 Mass % C-0.120 Mass % S

Figure 46b : Fe-4.55 Mass % C-0.083 Mass % S

Figure 46c : Fe-4.01 Mass % C-0.054/0.055/0.054 Mass % S

Figure 46d : Fe-4.01 Mass % C-0.030 Mass % S





Figures 47a to 47d

The Desulphurisation of Droplets Produced by the Suspended Droplet
Technique Using Slag KC3, 17.01 Mass % CaO-46.10 Mass % FeO-7.72
Mass % Fe₂O₃-29.00 Mass % SiO₂-0.09 Mass % S

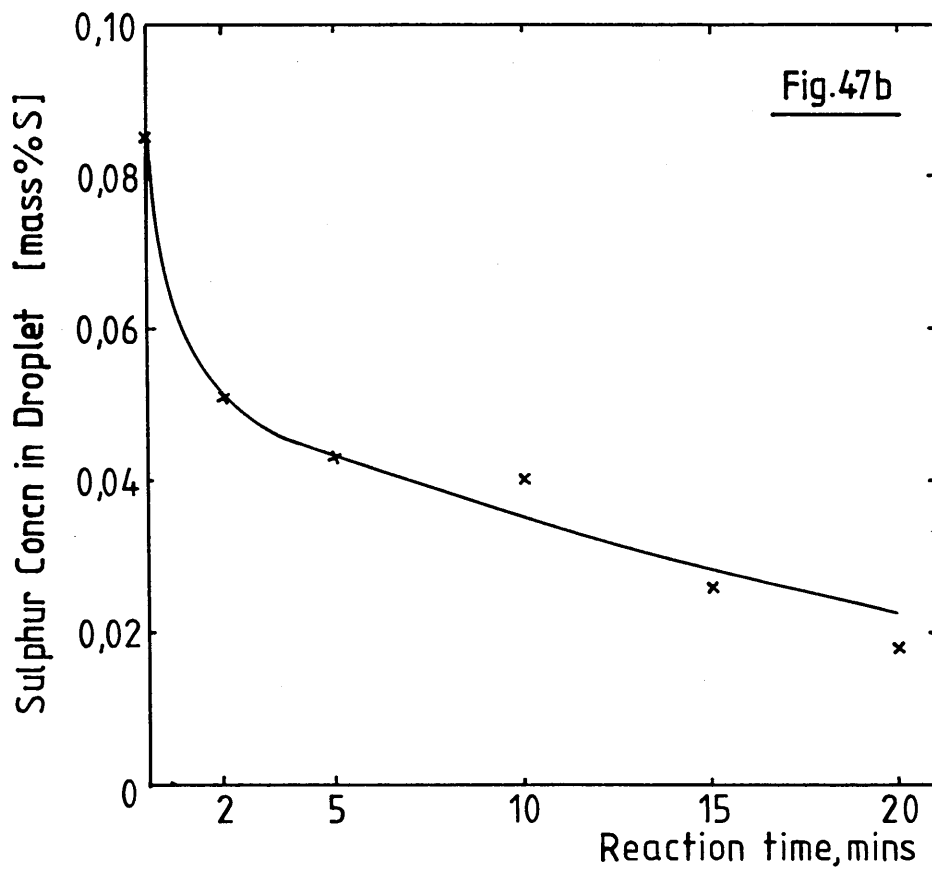
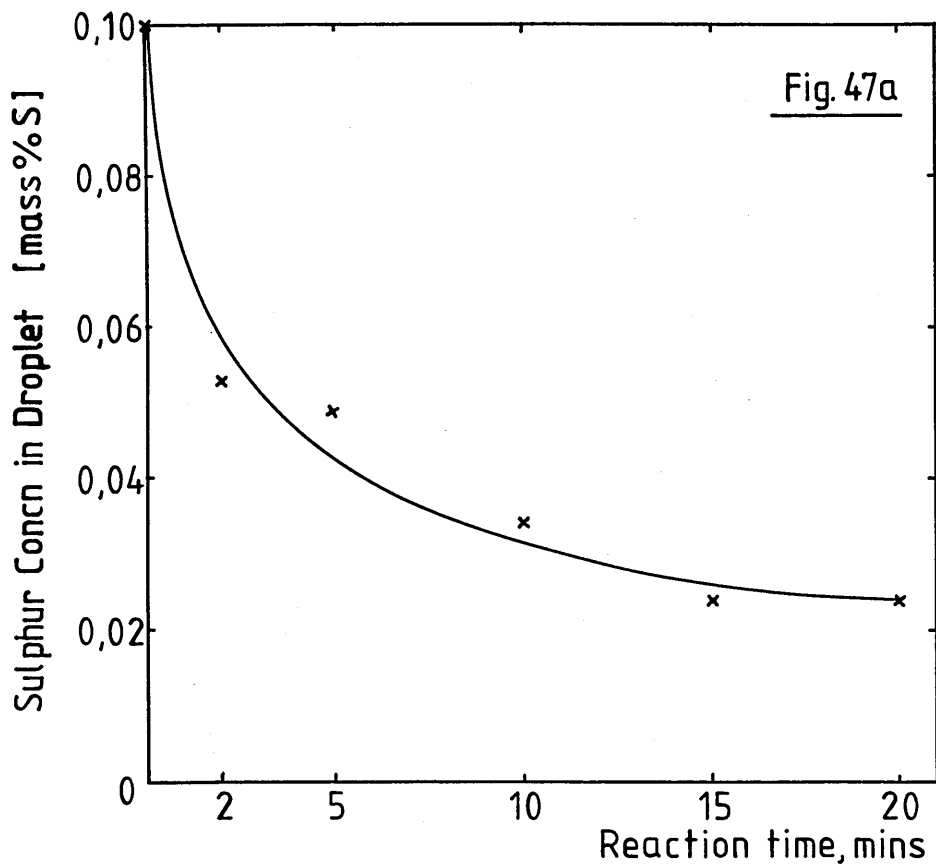
Initial Compositions of Metal Droplets:-

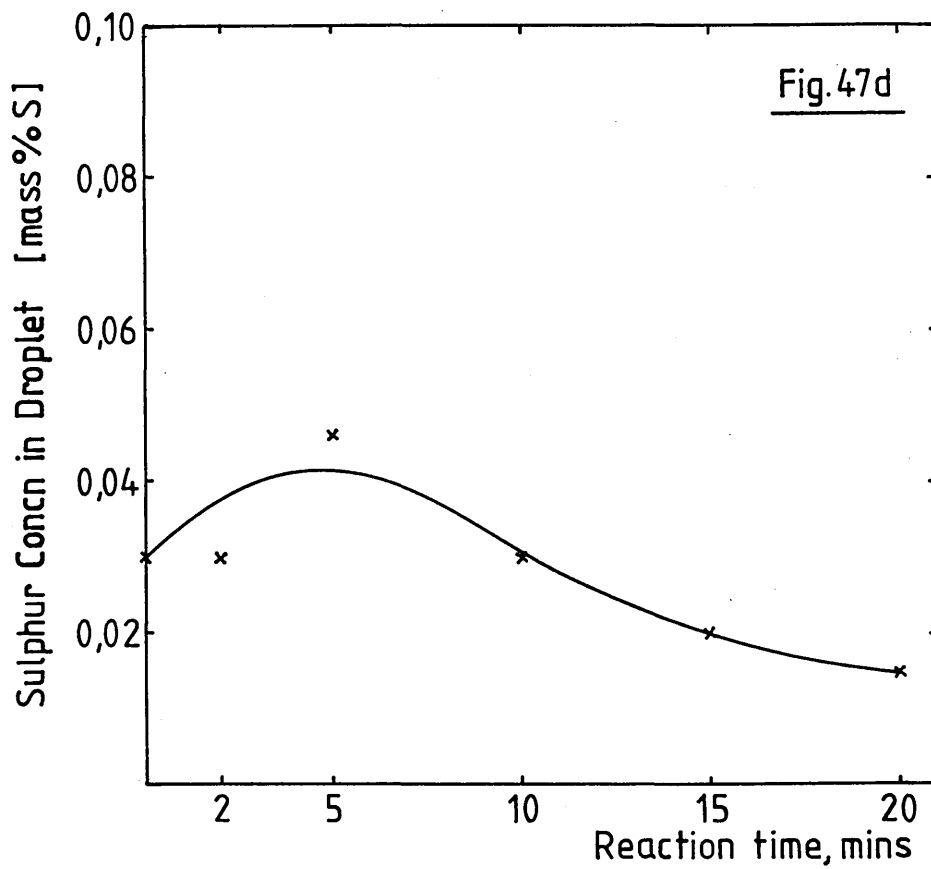
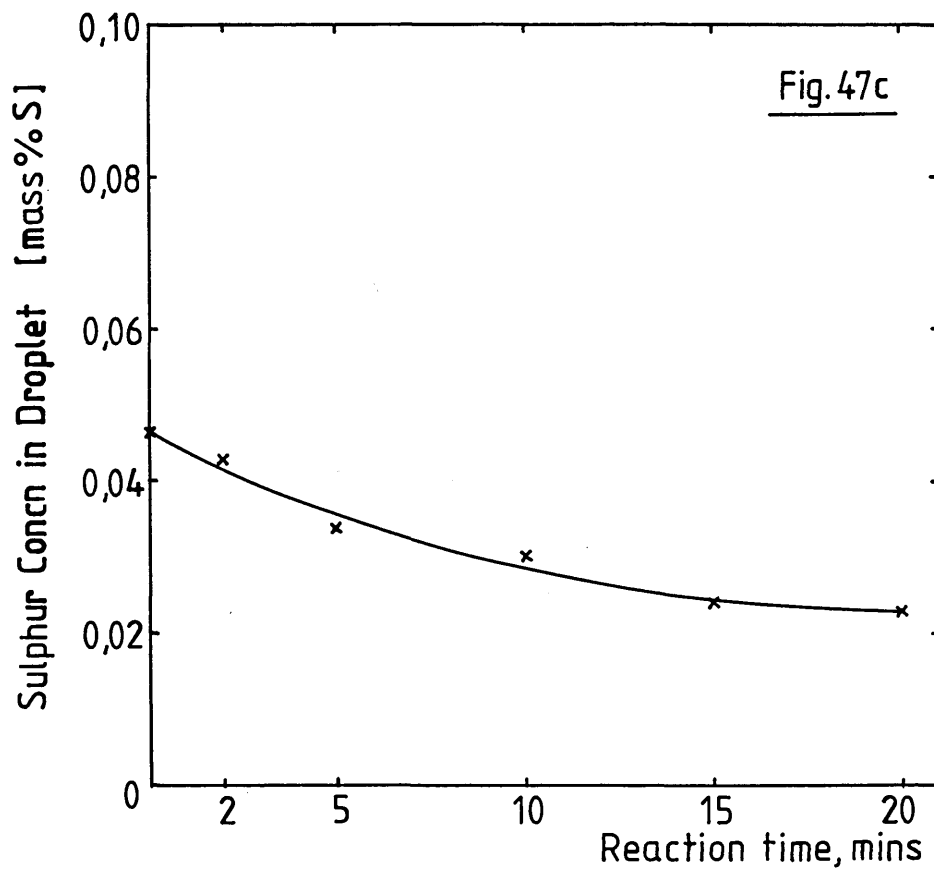
Figure 47a : Fe-4.20 Mass % C-0.100 Mass % S

Figure 47b : Fe-4.55 Mass % C-0.085 Mass % S

Figure 47c : Fe-4.01 Mass % C-0.046 Mass % S

Figure 47d : Fe-4.01 Mass % C-0.030 Mass % S





Figures 48a to 48d

The Desulphurisation of Droplets Produced by the Suspended Droplet
Technique Using Slag KCl₄, 10.04 Mass % CaO-55.20 Mass % FeO-5.72
Mass % Fe₂O₃-28.20 Mass % SiO₂-0.33 Mass % S

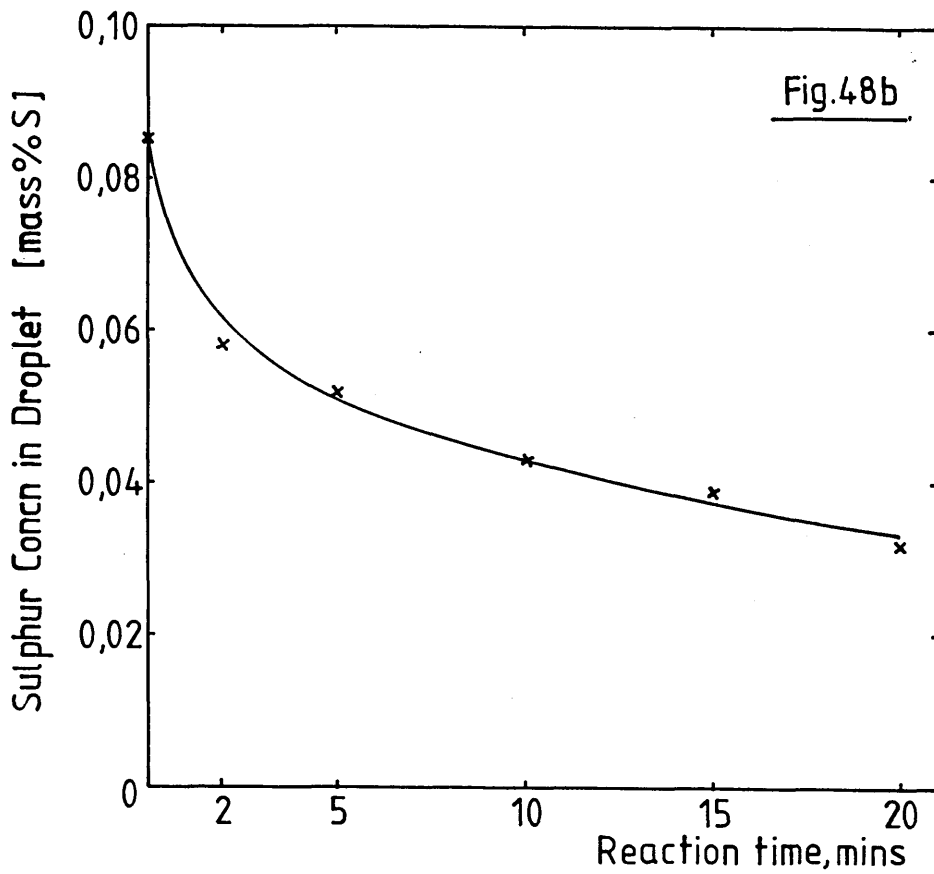
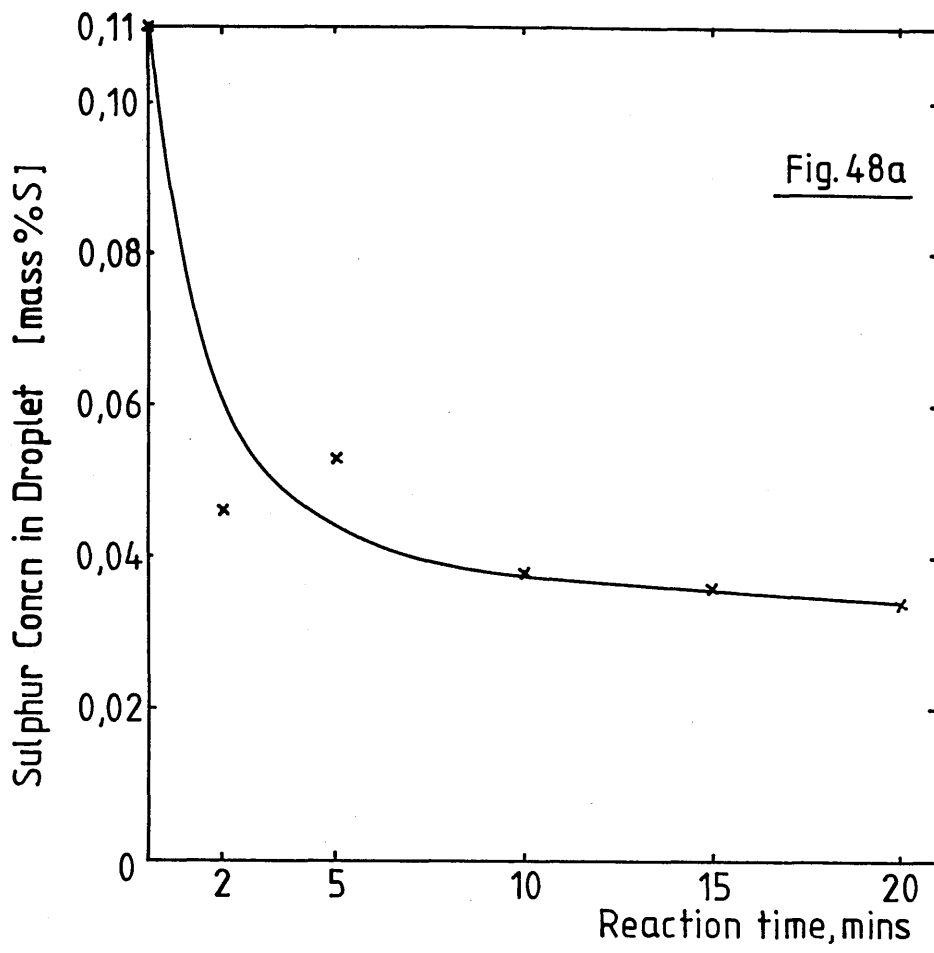
Initial Compositions of Metal Droplets:-

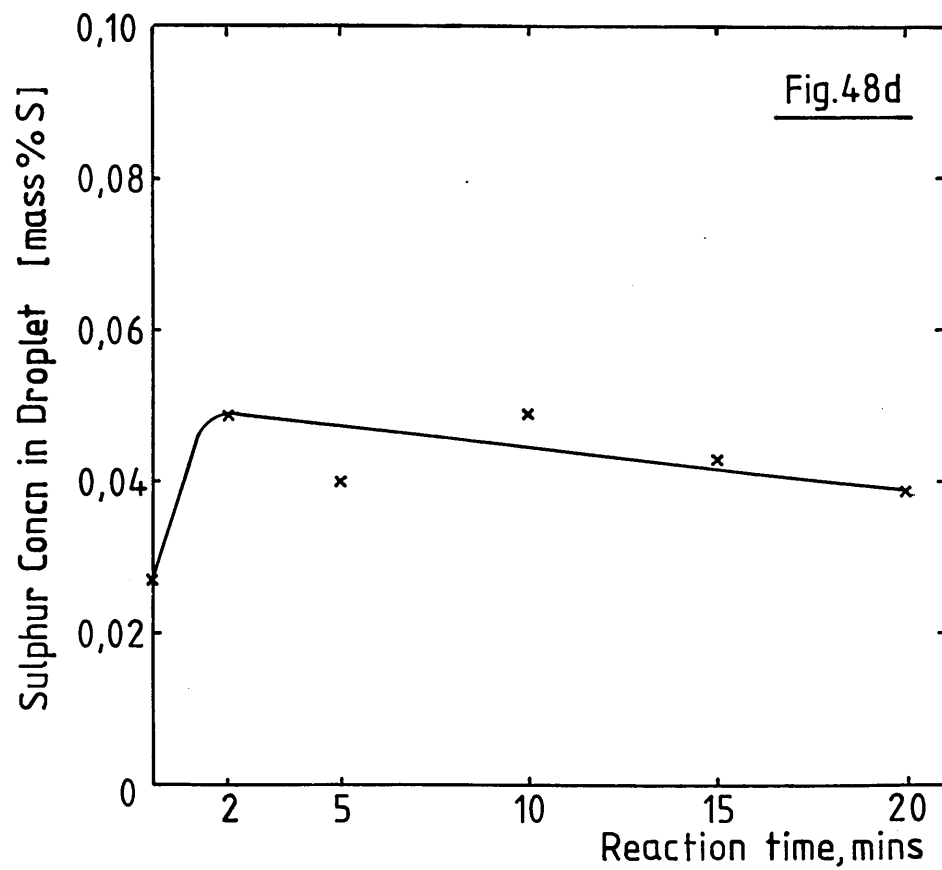
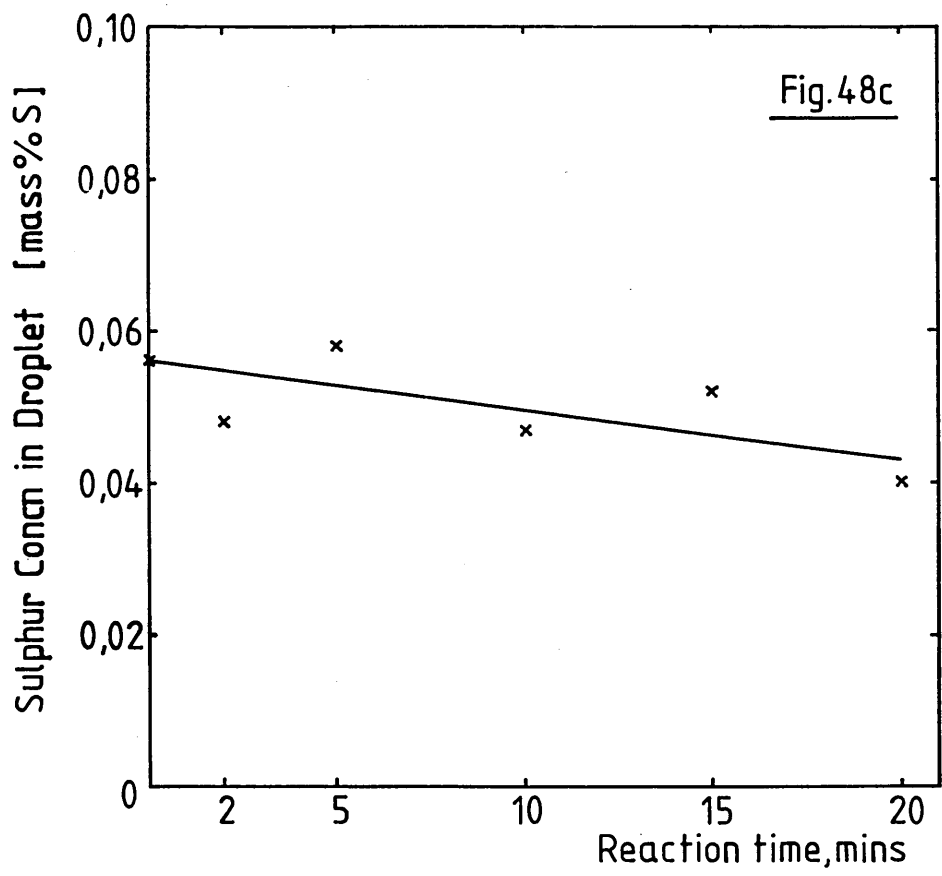
Figure 48a : Fe-4.20 Mass % C-0.110 Mass % S

Figure 48b : Fe-4.55 Mass % C-0.085 Mass % S

Figure 48c : Fe-4.01 Mass % C-0.056 Mass % S

Figure 48d : Fe-4.01 Mass % C-0.027 Mass % S





Figures 49a to 49d

The Desulphurisation of Droplets Produced by the Suspended Droplet
Technique Using Slag KC5, 0.87 Mass % CaO-62.80 Mass % FeO-2.23
Mass % Fe₂O₃-33.80 Mass % SiO₂-0.30 Mass % S

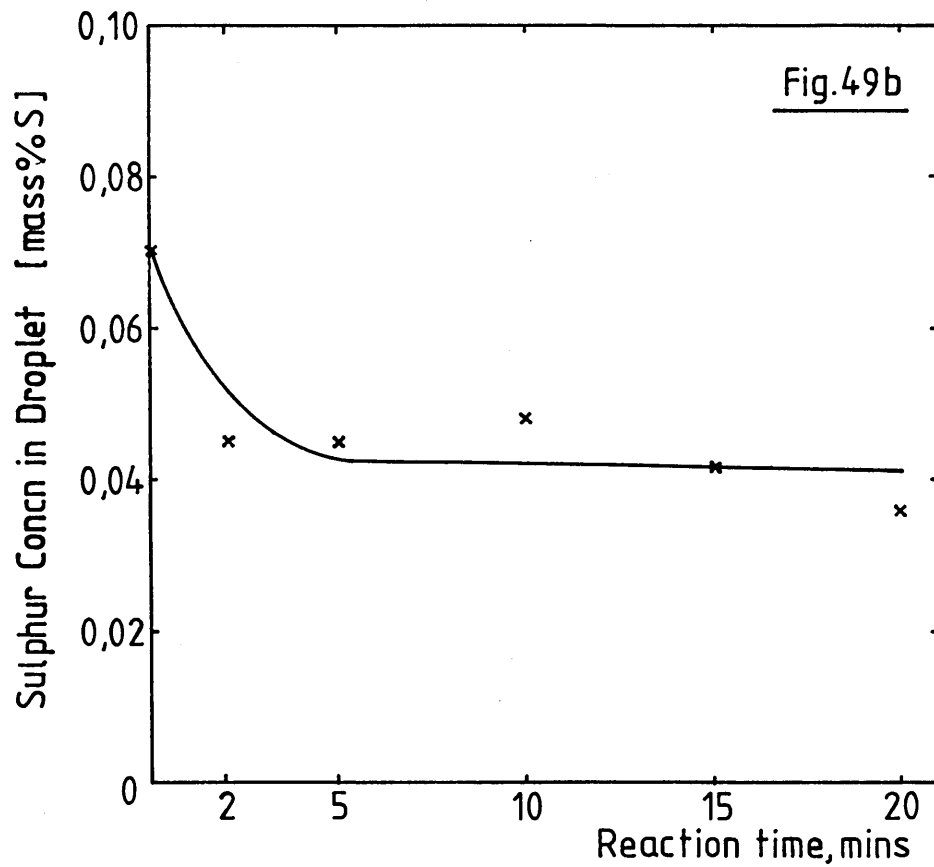
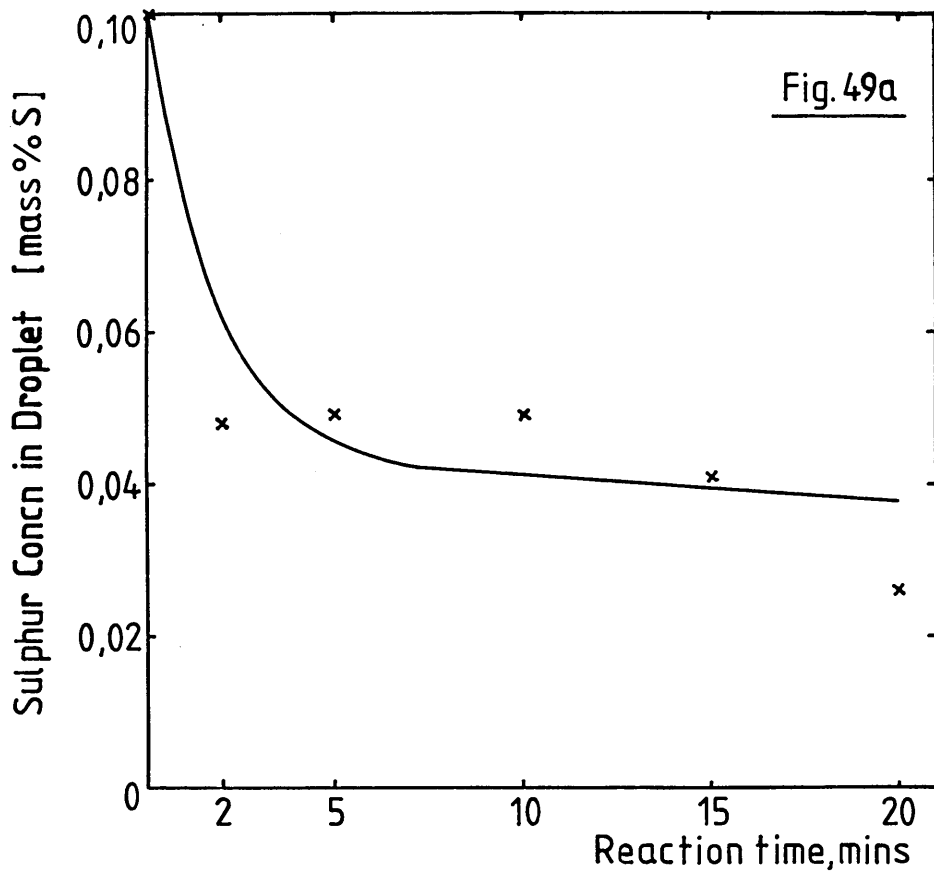
Initial Compositions of Metal Droplets:-

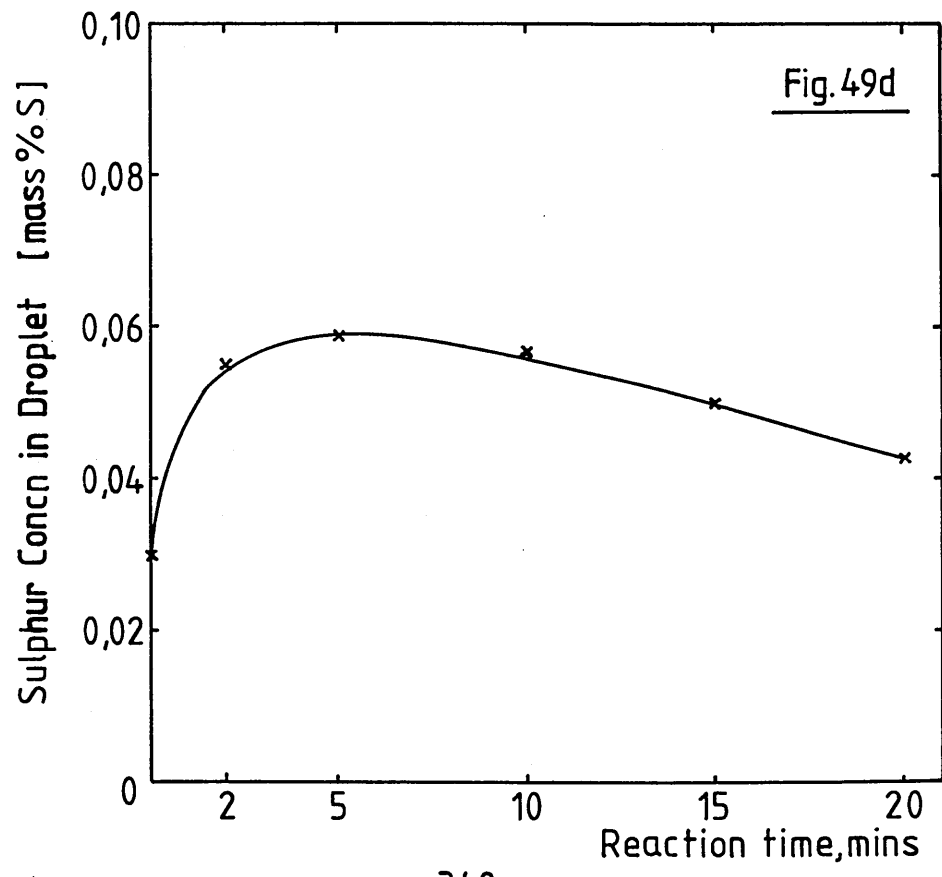
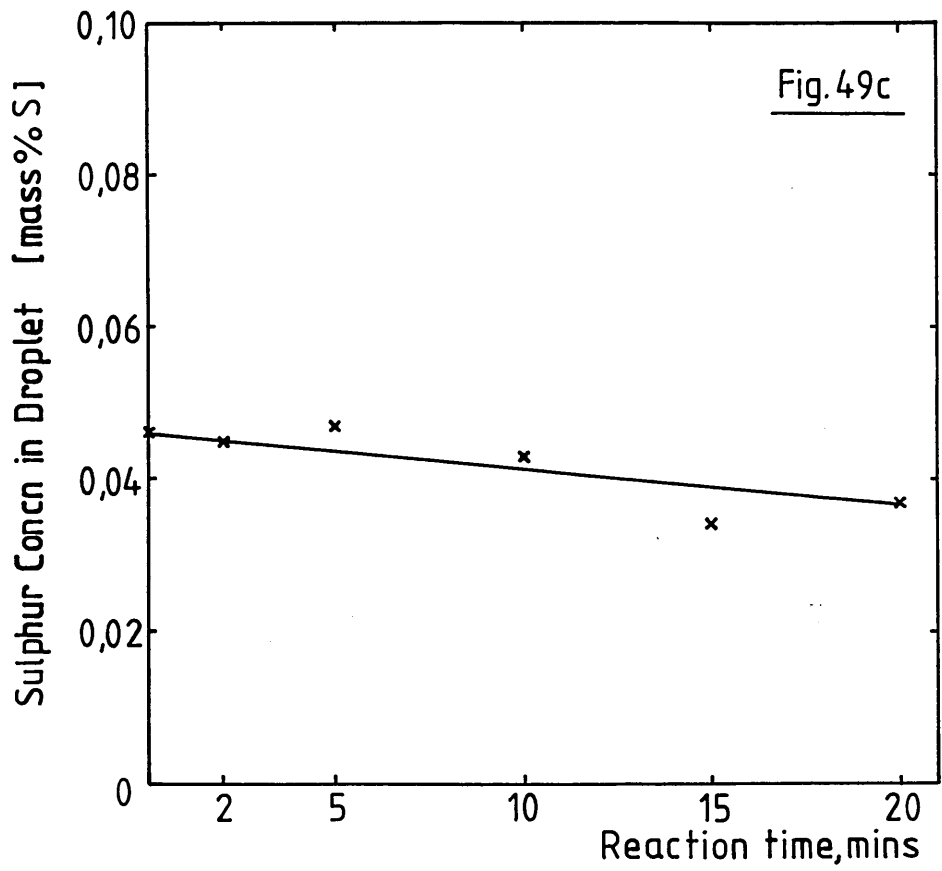
Figure 49a : Fe-4.20 Mass % C-0.102 Mass % S

Figure 49b : Fe-4.55 Mass % C-0.070 Mass % S

Figure 49c : Fe-4.01 Mass % C-0.046 Mass % S

Figure 49d : Fe-4.01 Mass % C-0.030 Mass % S





Figures 50a to 50d

The Desulphurisation of Droplets Produced by the Suspended Droplet
Technique Using Slag KC6, 67.63 Mass % FeO-3.50 Mass % Fe₂O₃-
28.00 Mass % SiO₂-0.32 Mass % S

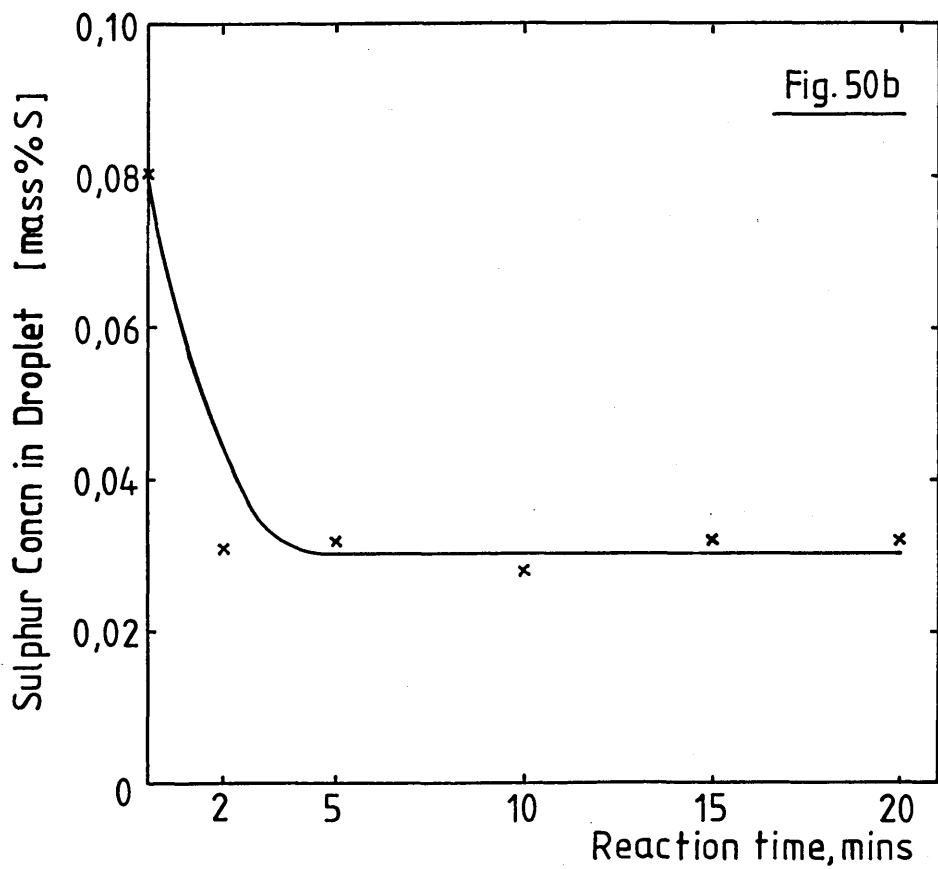
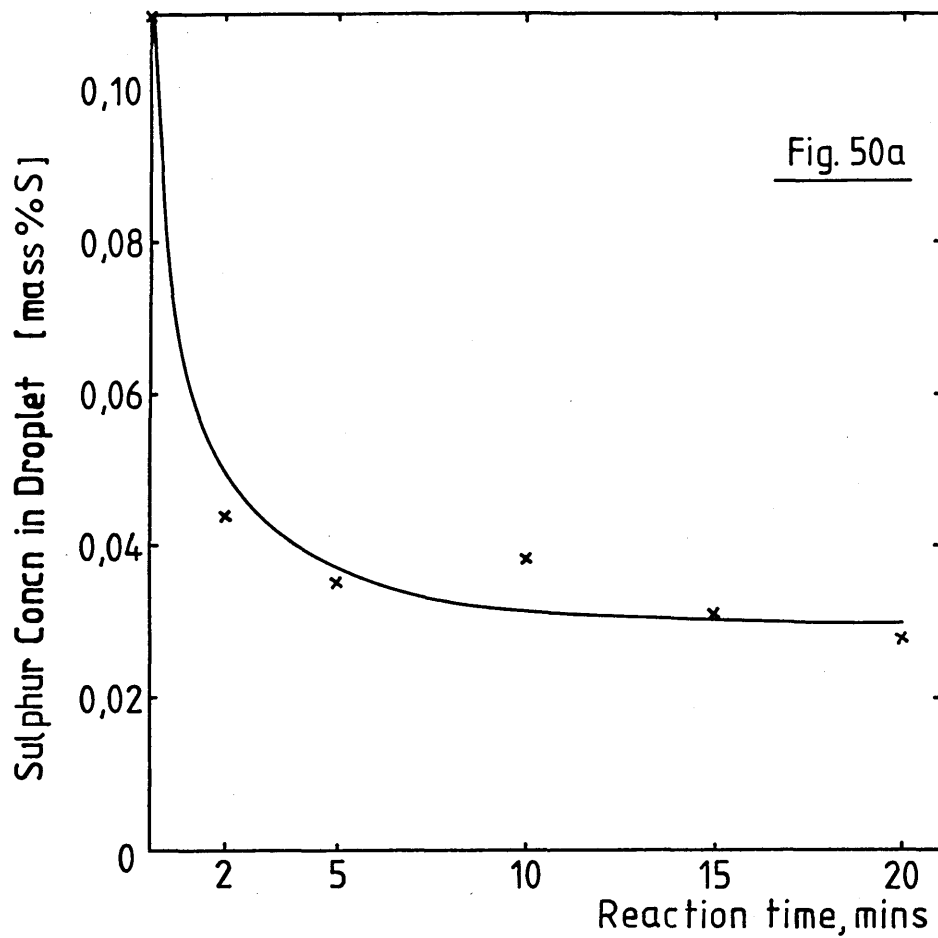
Initial Compositions of Metal Droplets:-

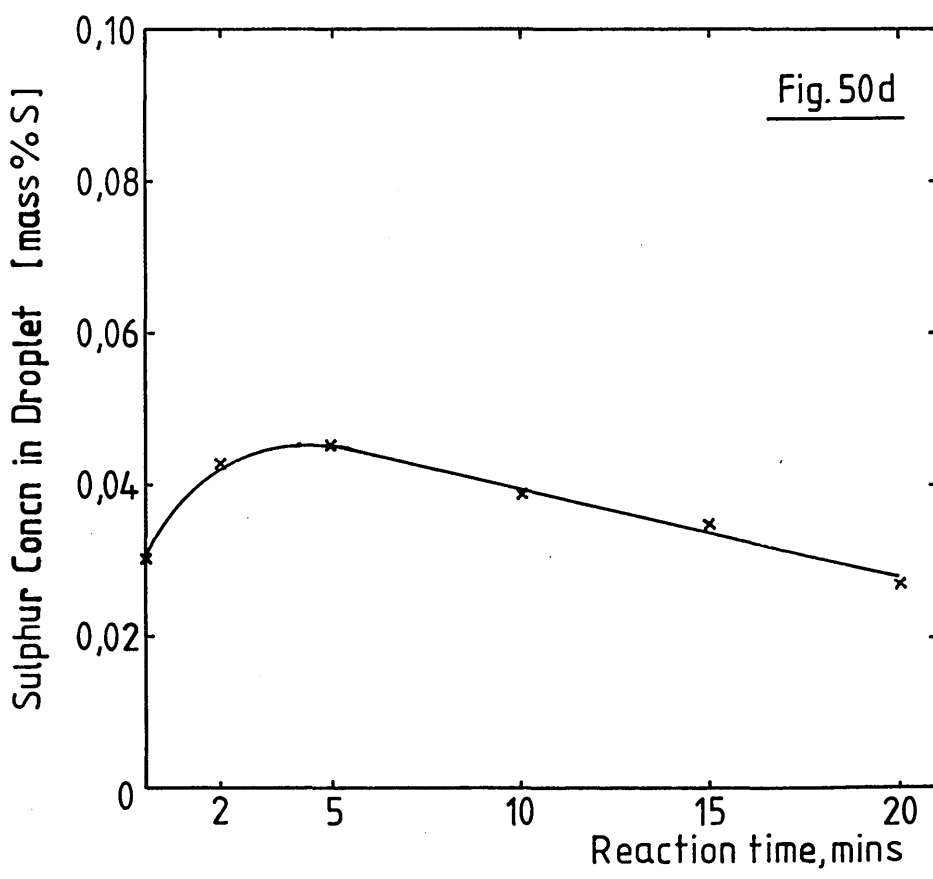
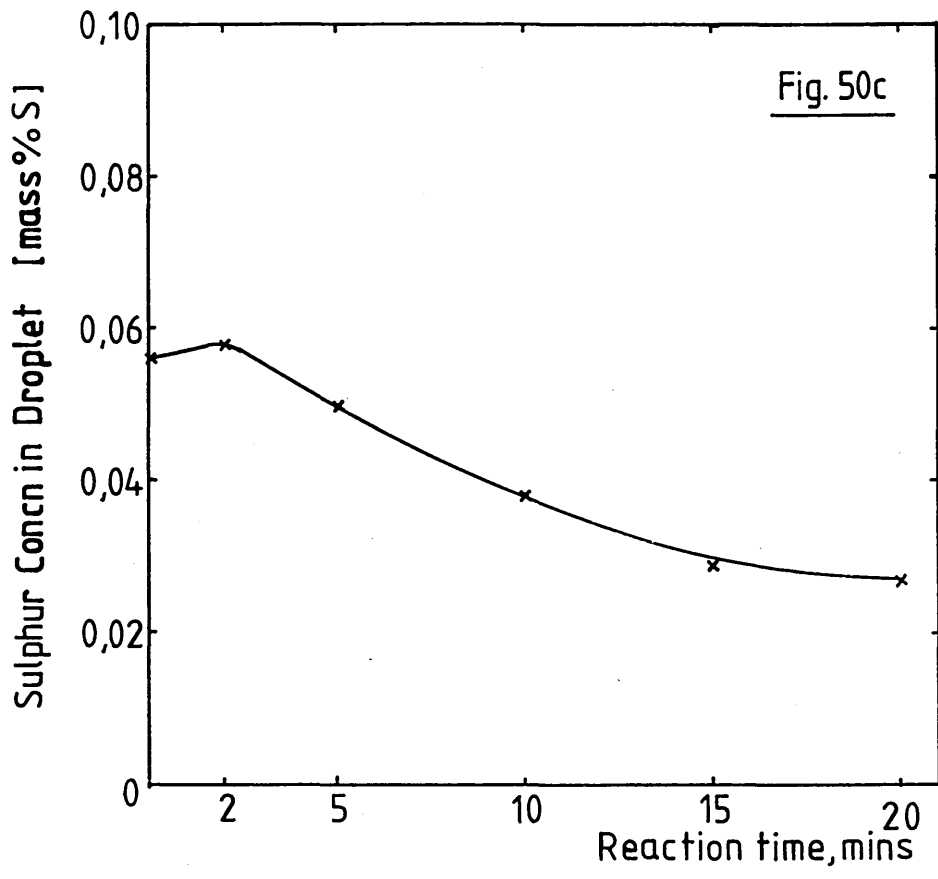
Figure 50a : Fe-4.20 Mass % C-0.110 Mass % S

Figure 50b : Fe-4.55 Mass % C-0.080 Mass % S

Figure 50c : Fe-4.01 Mass % C-0.056 Mass % S

Figure 50d : Fe-4.01 Mass % C-0.030 Mass % S





Figures 51 to 55

The Decarburisation of Droplets Produced by the Suspended
Droplet Technique Using Slags KC2 to KC6

Figure 51

The Decarburisation of Droplets Containing 4.00 Mass % C and 0.050
Mass % S at Zero Reaction Time by Slag KC2, 28.00 Mass % CaO-40.20
Mass % FeO-3.21 Mass % Fe₂O₃-28.50 Mass % SiO₂-0.15 Mass % S

Figure 52

The Decarburisation of Droplets Containing 4.23 Mass % C and 0.111
Mass % S at Zero Reaction Time by Slag KC3, 17.01 Mass % CaO-46.10
Mass % FeO-7.72 Mass % Fe₂O₃-29.00 Mass % SiO₂-0.09 Mass % S

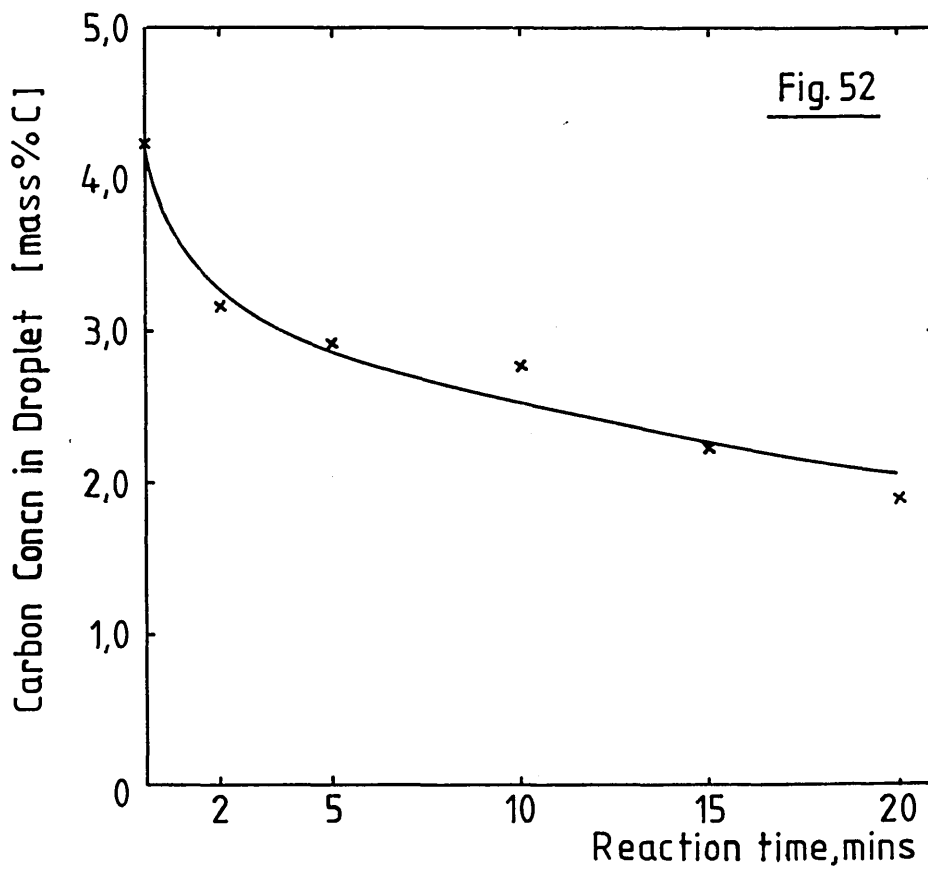
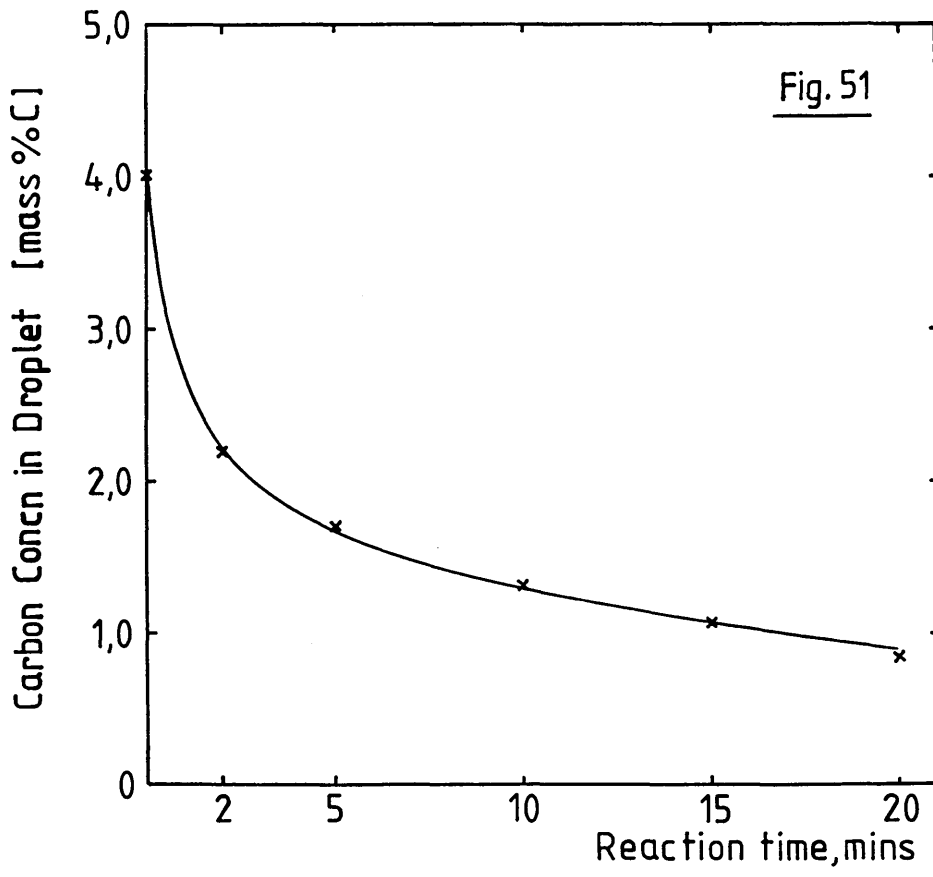


Figure 53a

The Decarburisation of Droplets Containing 4.41 Mass % C and 0.111 Mass % S at Zero Reaction Time by Slag KCl₄, 10.04 Mass % CaO-55.20 Mass % FeO-5.72 Mass % Fe₂O₃-28.20 Mass % SiO₂-0.33 Mass % S

Figure 53b

The Decarburisation of Droplets Containing 4.72 Mass % C and 0.083 Mass % S at Zero Reaction Time by Slag KCl₄, 10.04 Mass % CaO-55.20 Mass % FeO-5.72 Mass % Fe₂O₃-28.20 Mass % SiO₂-0.33 Mass % S

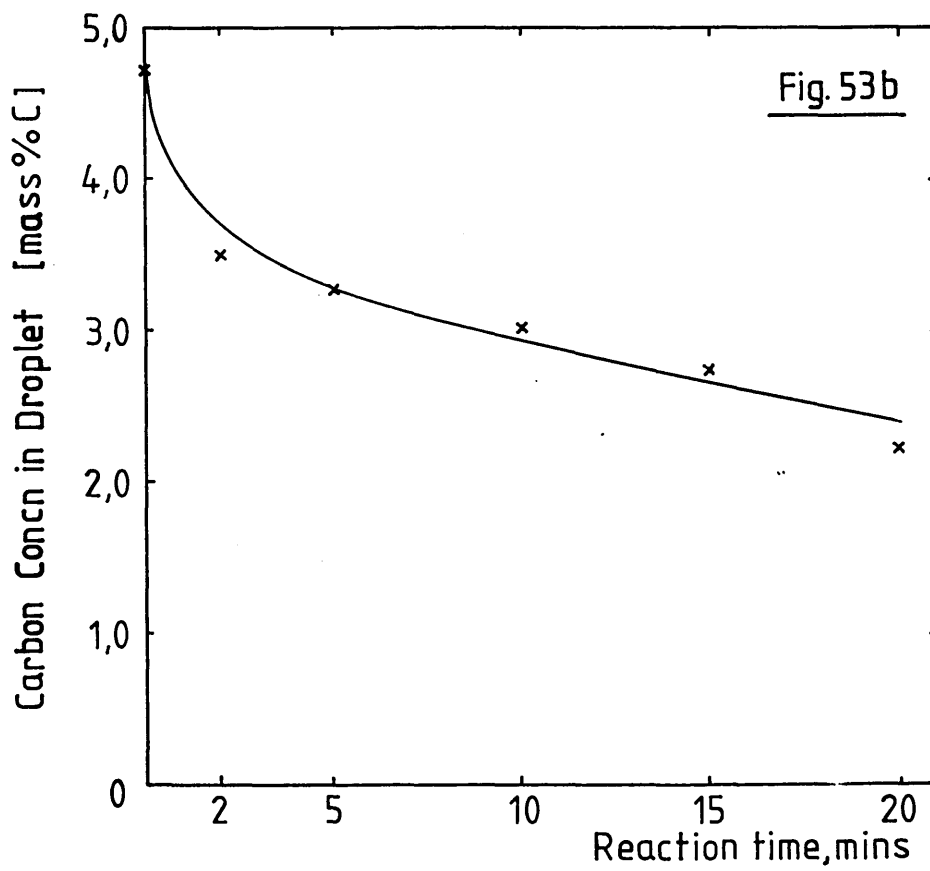
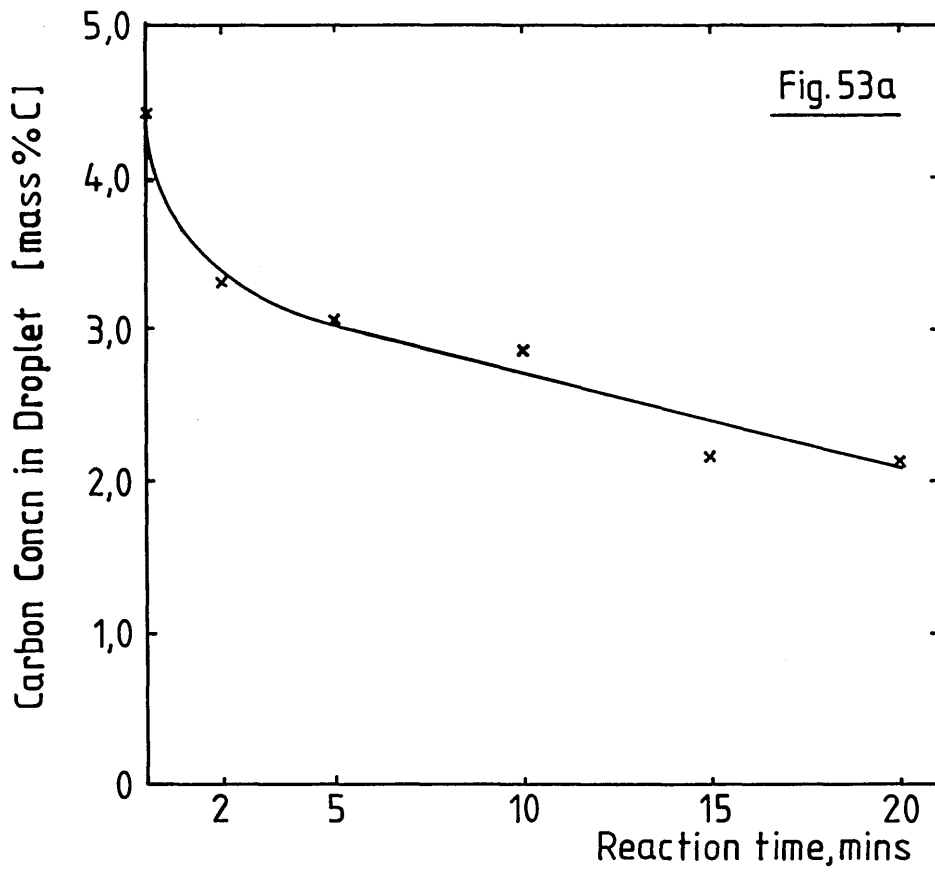


Figure 53c

The Decarburisation of Droplets Containing 4.10 Mass % C and 0.030
Mass % S at Zero Reaction Time by Slag KCl, 10.04 Mass % CaO-55.20
Mass % FeO-5.72 Mass % Fe₂O₃-28.20 Mass % SiO₂-0.33 Mass % S

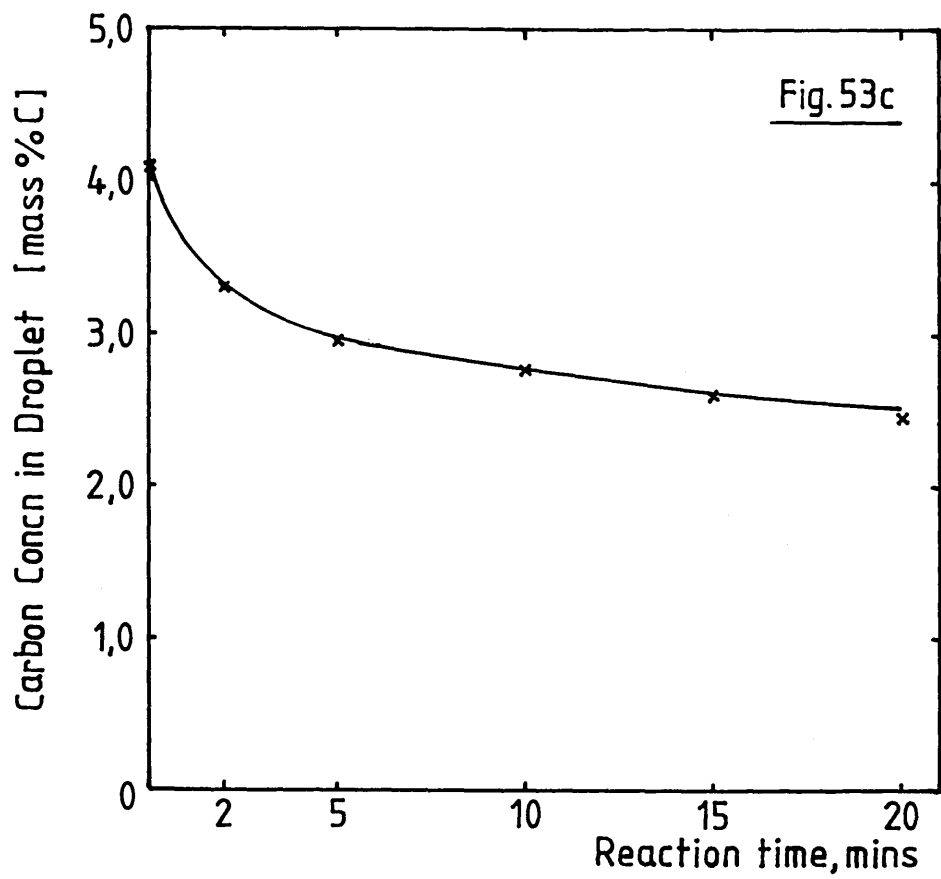
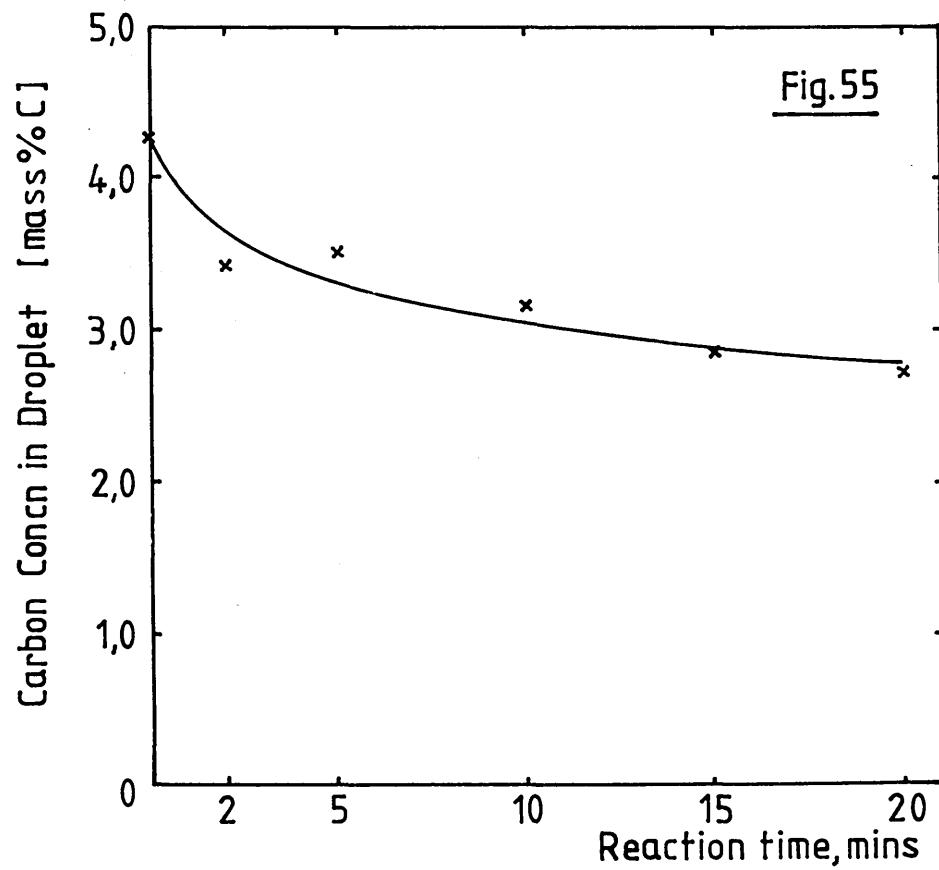
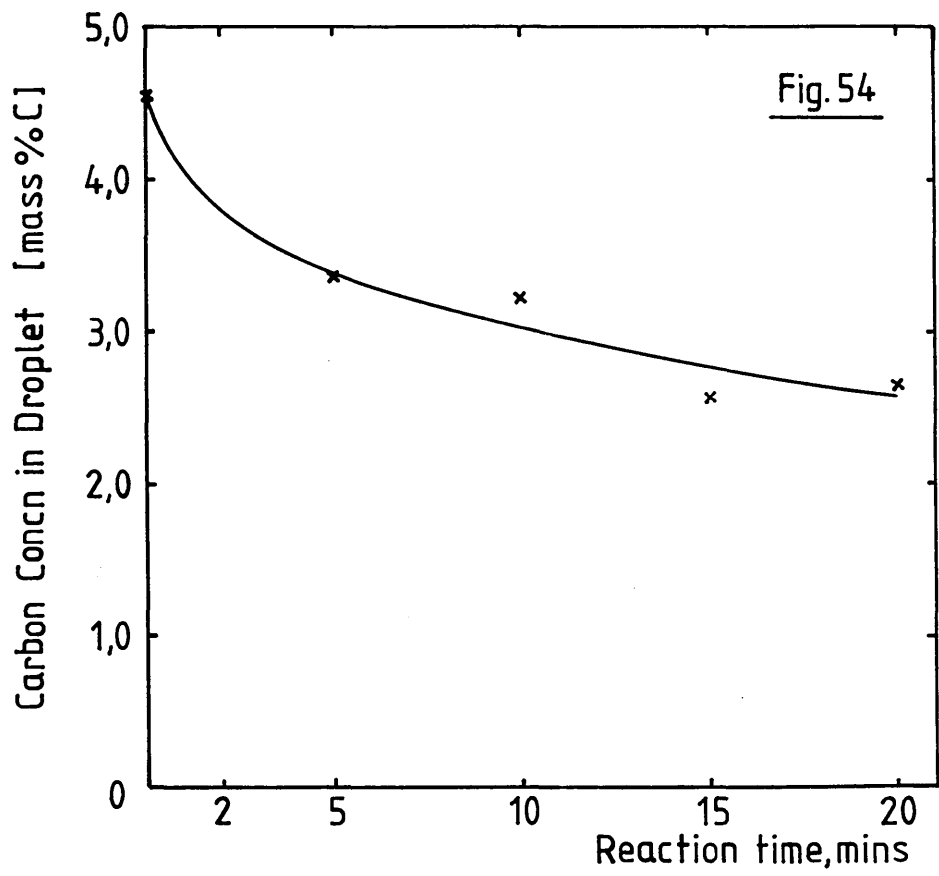


Figure 54

The Decarburisation of Droplets Containing 4.53 Mass % C and 0.083
Mass % S at Zero Reaction Time by Slag KC5, 0.87 Mass % CaO-62.80
Mass % FeO-2.23 Mass % Fe₂O₃-33.80 Mass % SiO₂-0.30 Mass % S

Figure 55

The Decarburisation of Droplets Containing 4.26 Mass % C and 0.111
Mass % S at Zero Reaction Time by Slag KC6, 67.63 Mass % FeO-3.50 Mass
% Fe₂O₃-28.00 Mass % SiO₂-0.32 Mass % S



Figures 56 and 57

Chromatograms Obtained by GLC From
Trimethylsilylation Experiments Using the Lentz Technique

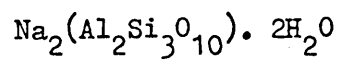
Figure 56

Blank Sample - Lentz Technique

Peak Label	1	IS
Parent Ion	SiO_4^{4-}	IS
Attenuation	20×10^2	10×10^4

Figure 57

Natrolite Mineral



All peaks : 5×10^4 Attenuation

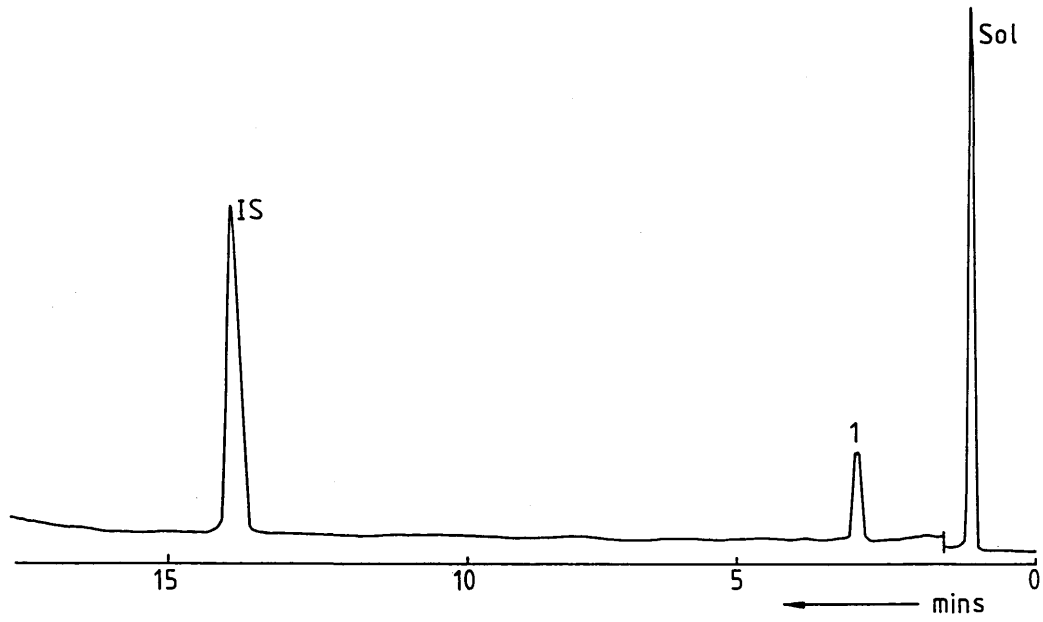


Fig. 56

Blank Sample - Lentz Technique

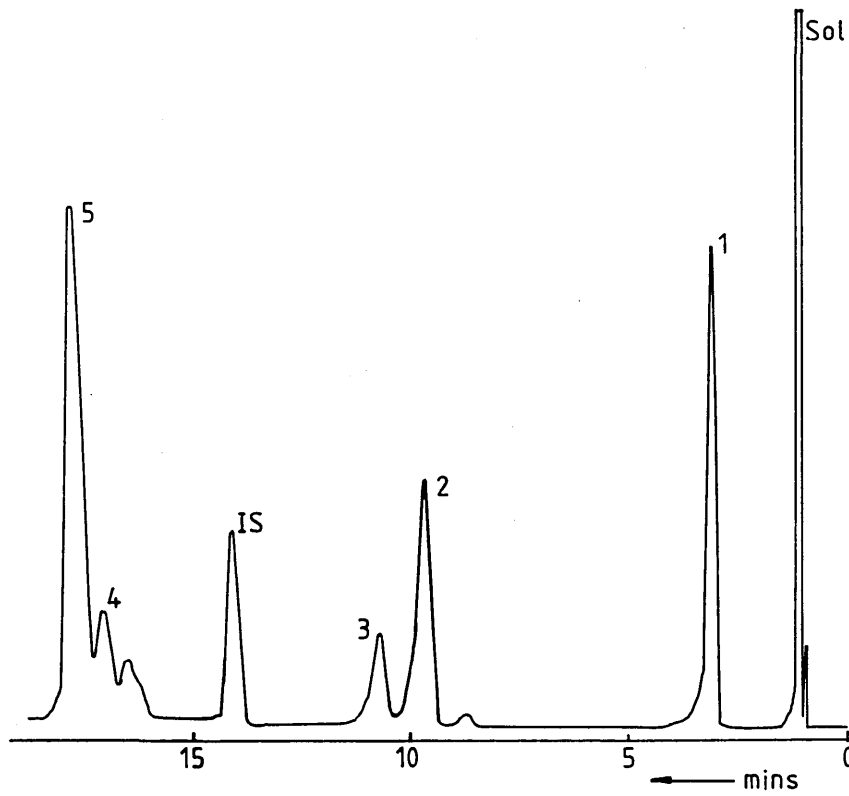


Fig. 57

Natrolite - Lentz Technique

Figures 58 to 86

Chromatograms Obtained by GLC From
Trimethylsilylation Experiments Using the Masson Technique

Figure 58

Blank Sample - Masson Technique - Untreated TMCS

Peak Label	1	IS
Parent Ion	SiO_4^-	IS
Attenuation	2×10^4	10×10^4

Figure 59

Blank Sample - Masson Technique - Pretreated TMCS

Peak Label	1	IS
Parent Ion	SiO_4^-	IS
Attenuation	20×10^2	10×10^4

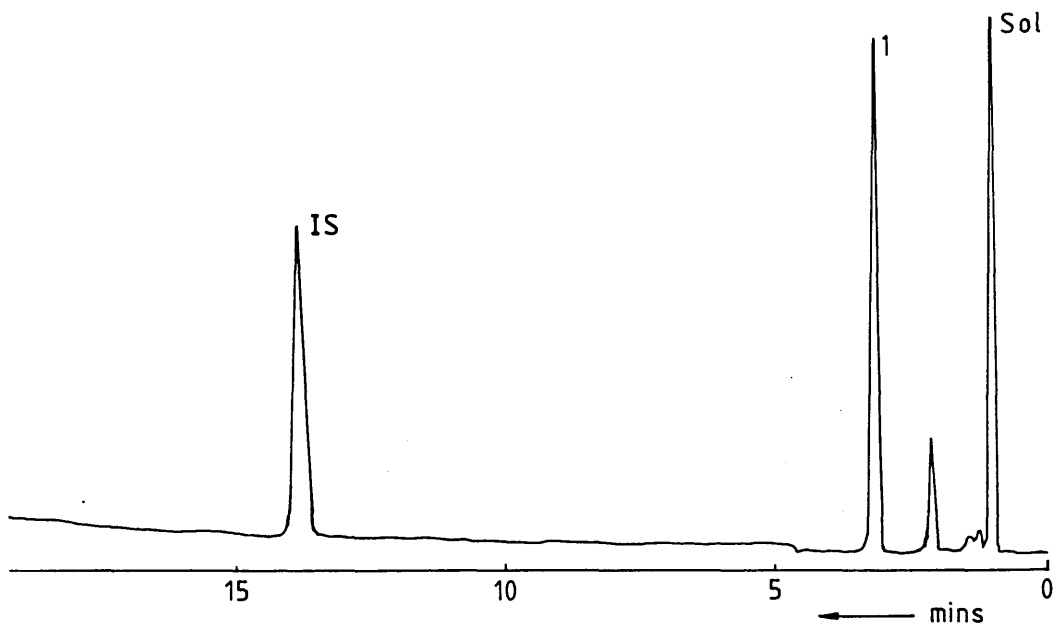


Fig. 58

Blank Sample-Masson Technique-Untreated TMCS

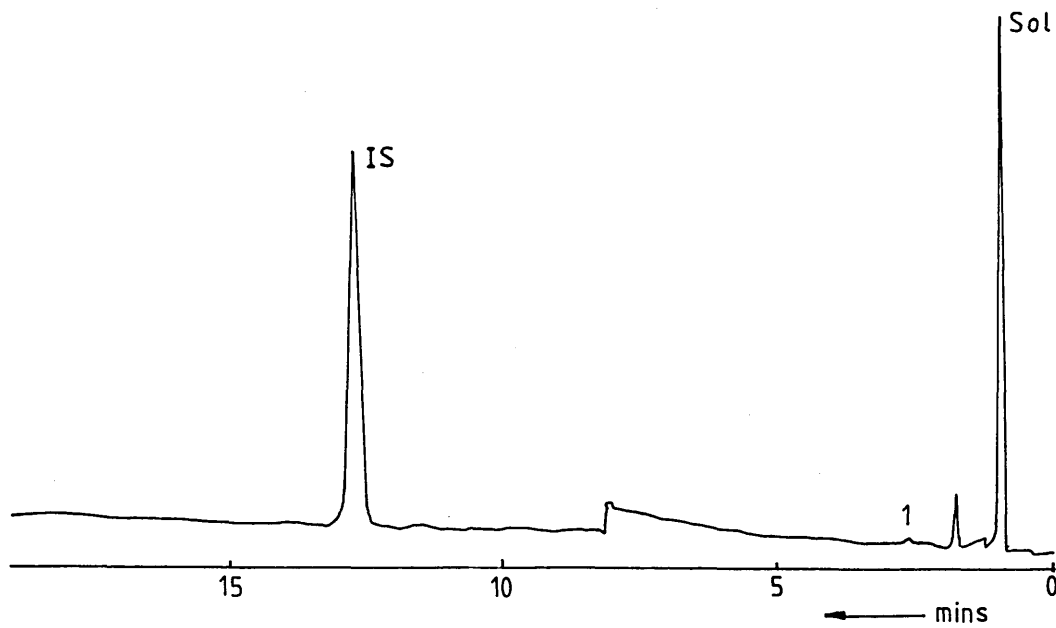
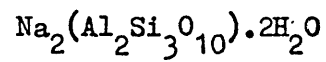


Fig. 59

Blank Sample - Masson Technique - Pretreated TMCS

Figure 60

Natrolite Mineral (Run I)



Peak Label	1	2	3	IS	4	5
Parent Ion	SiO_4^{4-}	$\text{Si}_2\text{O}_7^{6-}$	$\text{Si}_3\text{O}_9^{6-}$	IS	$\text{Si}_4\text{O}_{12}^{8-}$	$\text{Si}_3\text{O}_{10}^{8-}$
Attenuation	1×10^4	1×10^4	1×10^4	10×10^4	1×10^4	5×10^4

Figure 61

Natrolite Mineral (RunII)

Peak Label	1	2	3	IS	4	5
Parent Ion	SiO_4^{4-}	$\text{Si}_2\text{O}_7^{6-}$	$\text{Si}_3\text{O}_9^{6-}$	IS	$\text{Si}_4\text{O}_{12}^{8-}$	$\text{Si}_3\text{O}_{10}^{8-}$
Attenuation	1×10^4	1×10^4	1×10^4	10×10^4	1×10^4	5×10^4

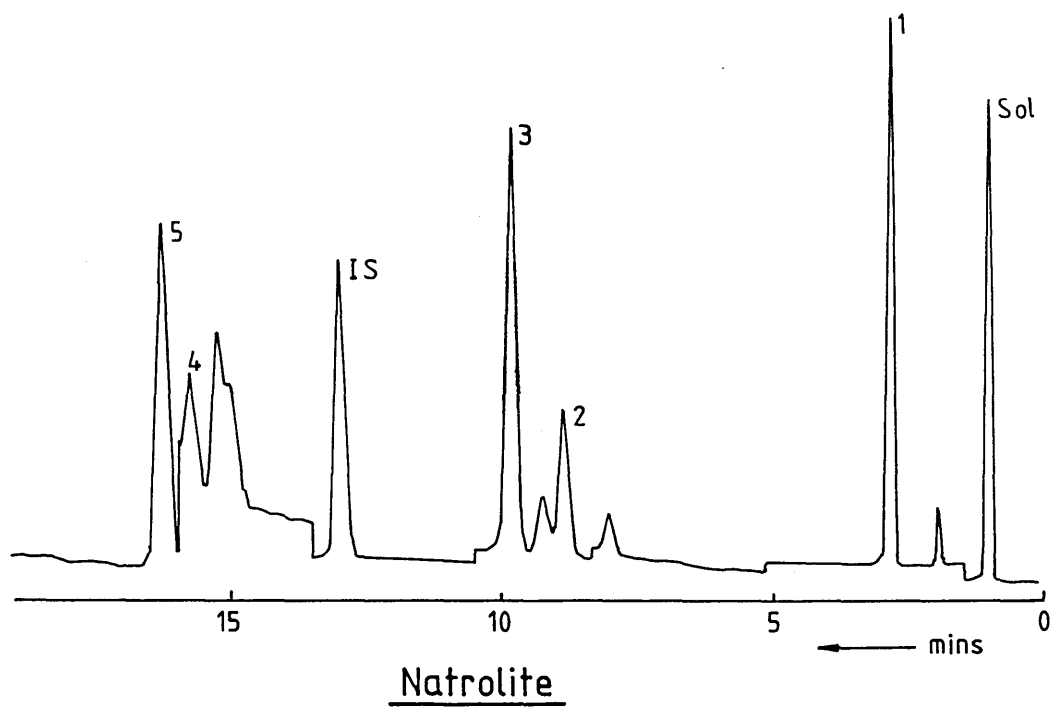


Fig.60

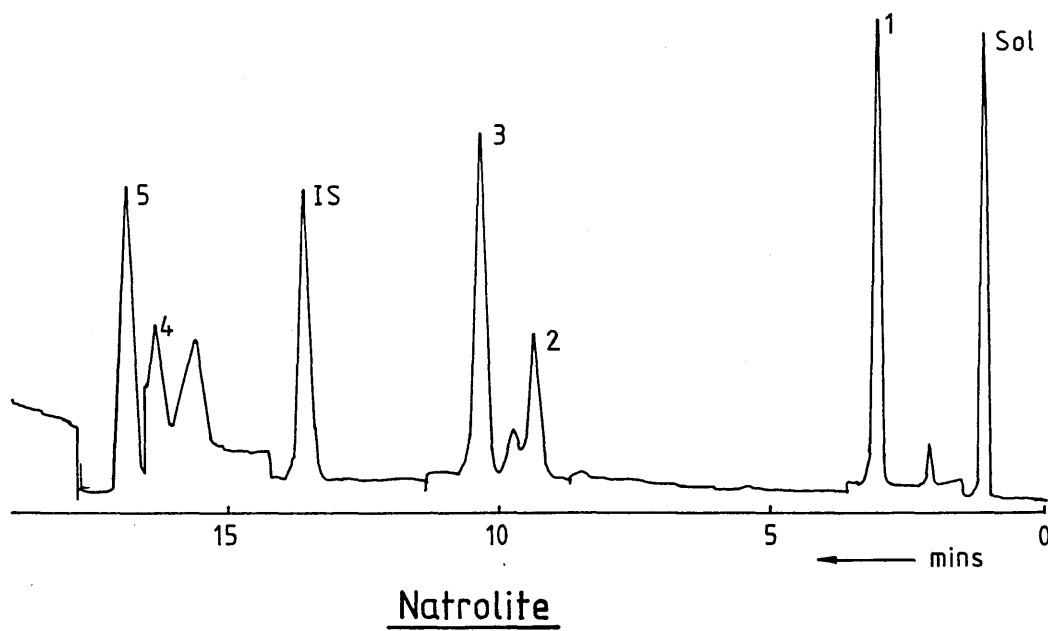
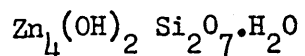


Fig.61

Figure 62

Hemimorphite Mineral (Run I)



Peak Label	1	2	3	IS	4	5
Parent Ion	SiO_4^{4-}	$\text{Si}_2\text{O}_7^{6-}$	$\text{Si}_3\text{O}_9^{6-}$	IS	$\text{Si}_4\text{O}_{12}^{8-}$	$\text{Si}_3\text{O}_{10}^{8-}$
Attenuation	1×10^4	5×10^4	50×10^2	10×10^4	1×10^4	1×10^4

Figure 63

Hemimorphite Mineral (Run II)

Peak Label	1	2	3	IS	4	5
Parent Ion	SiO_4^{4-}	$\text{Si}_2\text{O}_7^{6-}$	$\text{Si}_3\text{O}_9^{6-}$	IS	$\text{Si}_4\text{O}_{12}^{8-}$	$\text{Si}_3\text{O}_{10}^{8-}$
Attenuation	1×10^4	5×10^4	50×10^2	10×10^4	1×10^4	1×10^4

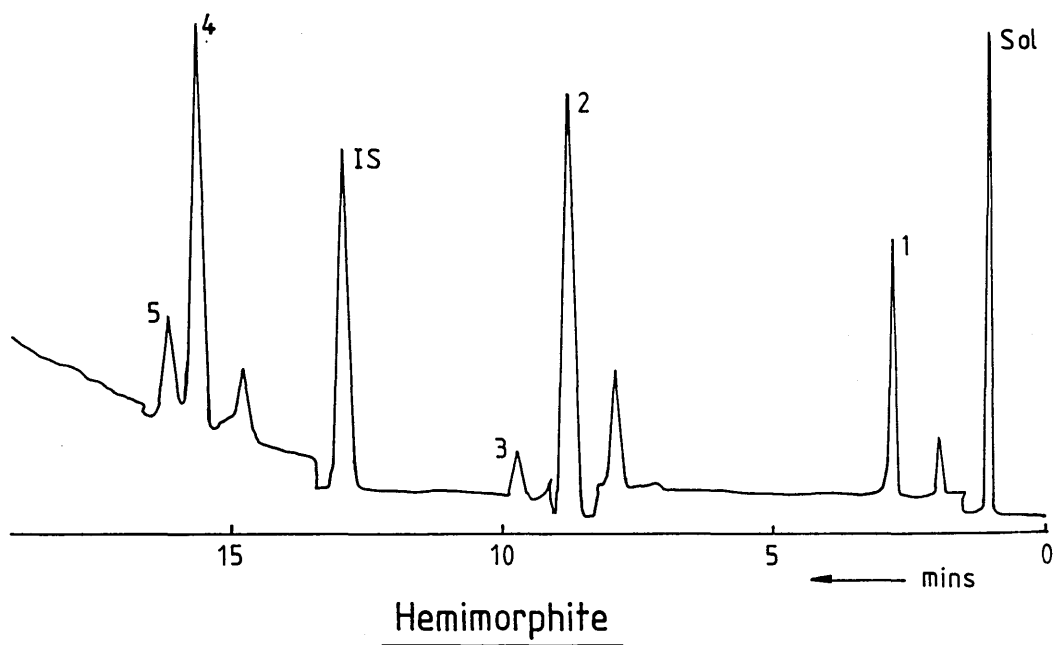


Fig.62

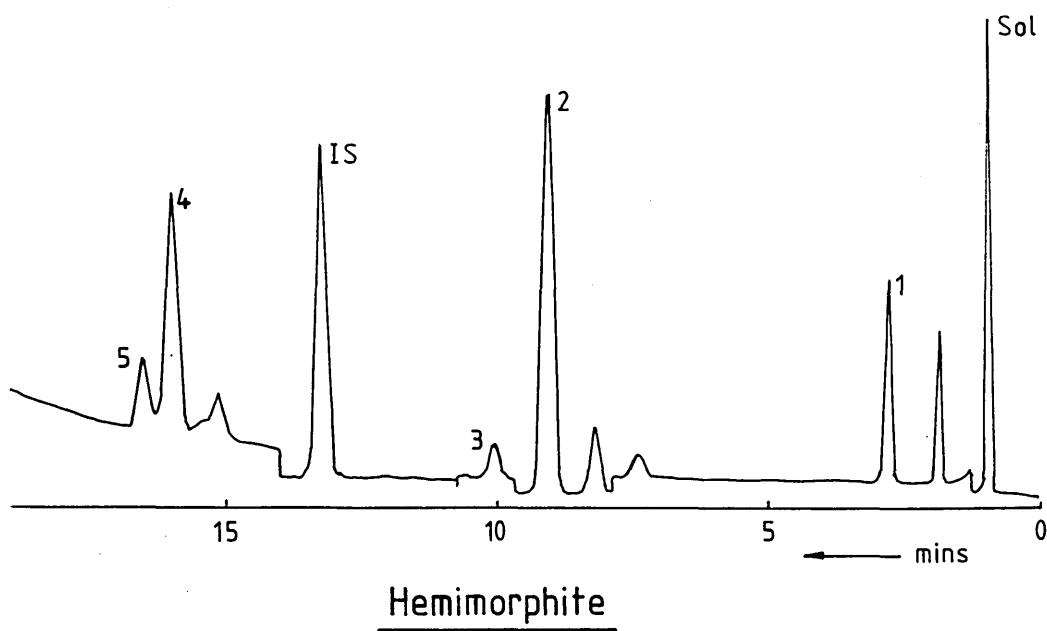
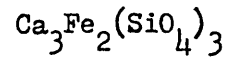


Fig.63

Figure 64

Andradite Mineral



Peak Label	1	2	3	IS	4	5
Parent Ion	SiO_4^{4-}	$\text{Si}_2\text{O}_7^{6-}$	$\text{Si}_3\text{O}_9^{6-}$	IS	$\text{Si}_4\text{O}_{12}^{8-}$	$\text{Si}_3\text{O}_{10}^{8-}$
Attenuation	50×10^2	20×10^2	20×10^2	10×10^4	20×10^2	20×10^2

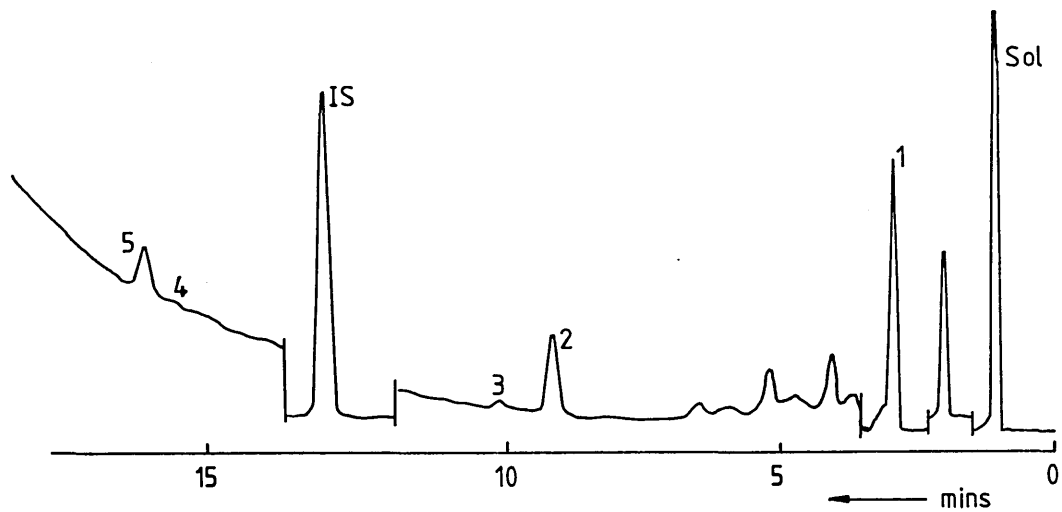


Fig. 64

Andradite

Figure 65

Hemimorphite (0.75g) + Natrolite (0.75g)

Peak Label	1	2	3	IS	4	5
Parent Ion	SiO_4^{4-}	$\text{Si}_2\text{O}_7^{6-}$	$\text{Si}_3\text{O}_9^{6-}$	IS	$\text{Si}_4\text{O}_{12}^{8-}$	$\text{Si}_3\text{O}_{10}^{8-}$
Attenuation	1×10^4	5×10^4	50×10^2	10×10^4	1×10^4	1×10^4

Figure 66

Hemimorphite (0.5g) + Natrolite (1.0g)

Peak Label	1	2	3	IS	4	5
Parent Ion	SiO_4^{4-}	$\text{Si}_2\text{O}_7^{6-}$	$\text{Si}_3\text{O}_9^{6-}$	IS	$\text{Si}_4\text{O}_{12}^{8-}$	$\text{Si}_3\text{O}_{10}^{8-}$
Attenuation	1×10^4	2×10^4	1×10^4	10×10^4	2×10^4	2×10^4

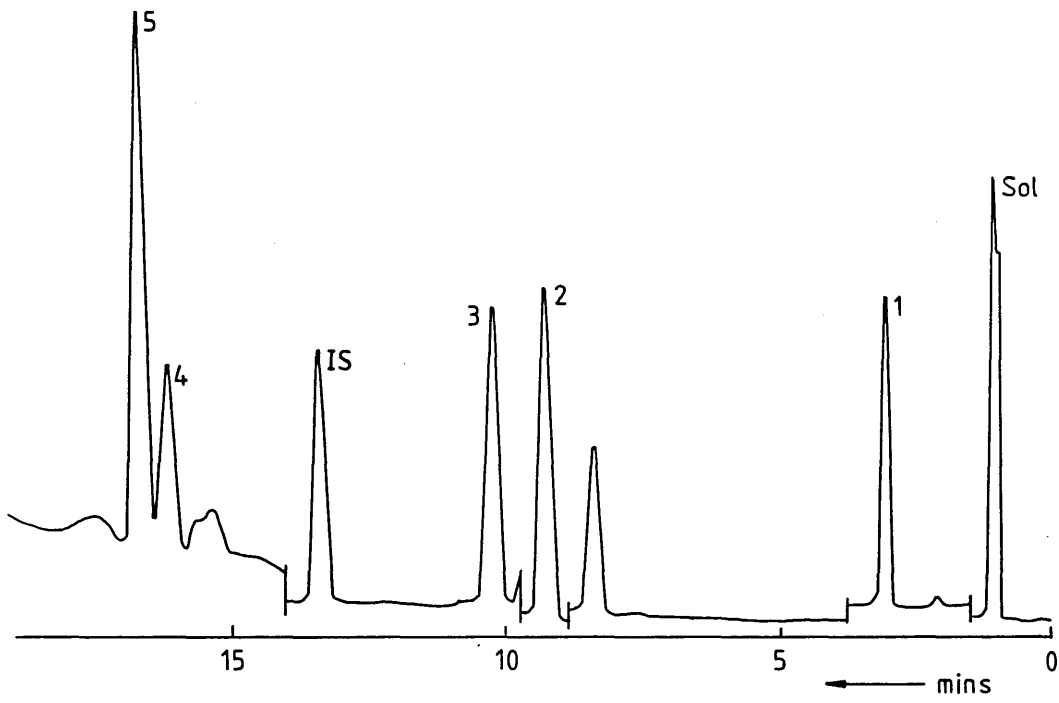


Fig.65

Hemimorphite (0,75g) + Natrolite (0,75g)

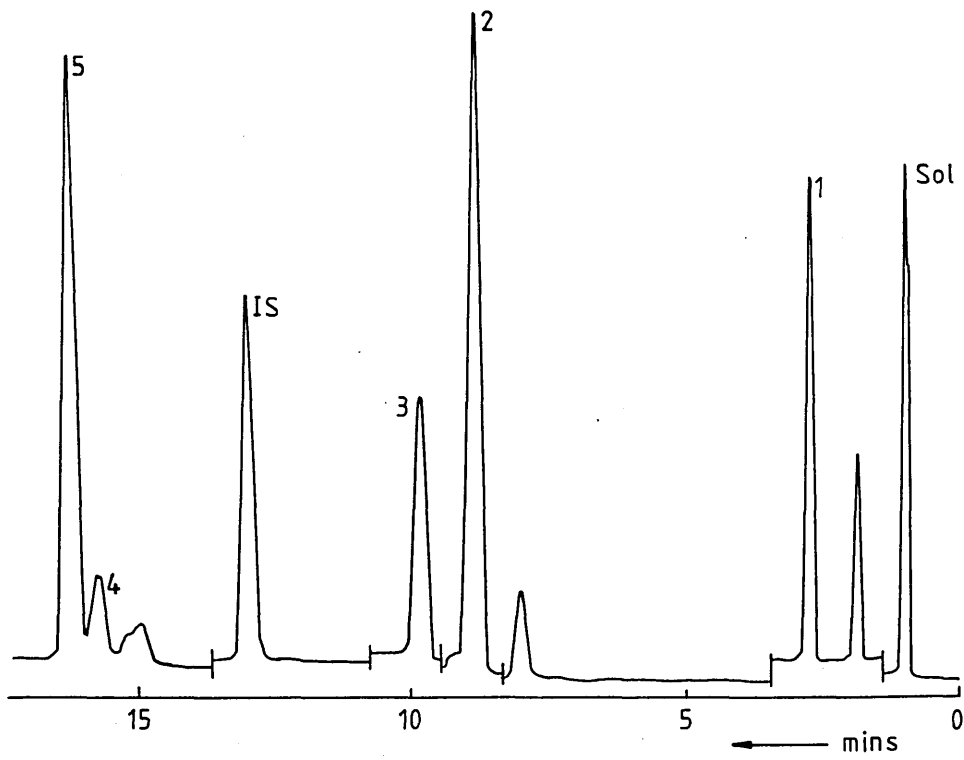


Fig.66

Hemimorphite (0,5g) + Natrolite (1,0g)

Figure 67

Iron Blast Furnace Slag

34.02 Mass % SiO₂-0.78 Mass % FeO-41.00 Mass % CaO-7.95 Mass % MgO-
0.95 Mass % MnO-13.90 Mass % Al₂O₃

Peak Label	1	2	3	IS	4	5
Parent Ion	SiO ₄ ⁴⁻	Si ₂ O ₇ ⁶⁻	Si ₃ O ₉ ⁶⁻	IS	Si ₄ O ₁₂ ⁸⁻	Si ₃ O ₁₀ ⁸⁻
Attenuation	1x10 ⁴	1x10 ⁴	50x10 ²	10x10 ⁴	50x10 ²	50x10 ²

Figure 68

LD Slag

13.00 Mass % SiO₂-30.90 Mass % FeO-42.70 Mass % CaO-4.70 Mass % MgO
-0.45 Mass % Al₂O₃-1.87 Mass % P₂O₅

Peak Label	1	2	3	IS	4	5
Parent Ion	SiO ₄ ⁴⁻	Si ₂ O ₇ ⁶⁻	Si ₃ O ₉ ⁶⁻	IS	Si ₄ O ₁₂ ⁸⁻	Si ₃ O ₁₀ ⁸⁻
Attenuation	2x10 ⁴	50x10 ²	50x10 ²	10x10 ⁴	50x10 ²	50x10 ²

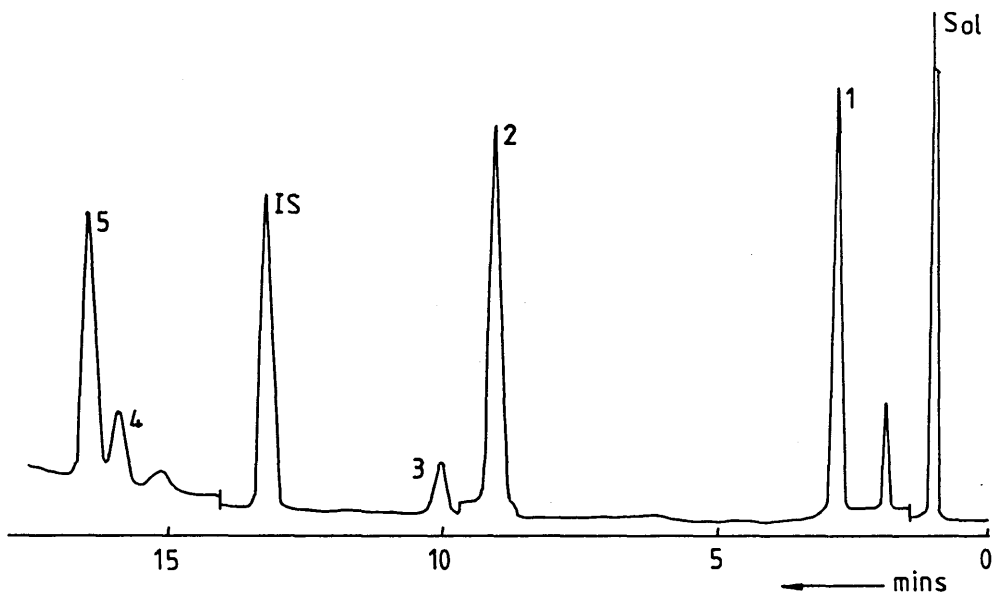


Fig. 67

B.S.C. Scunthorpe Blast Furnace Slag

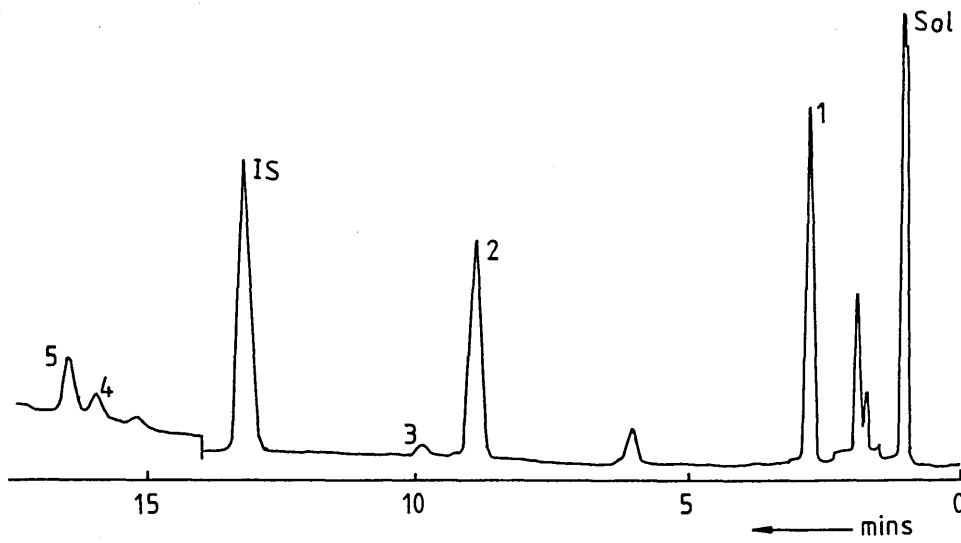


Fig. 68

B.S.C. Appleby-Frodingham LD Slag

Figure 69

Slag 1

82.61 Mass % FeO-9.27 Mass % Fe₂O₃-8.12 Mass % SiO₂.(0.10x SiO₂)

Peak Label	1	2	3	IS	4	5
Parent Ion	SiO ₄ ⁴⁻	Si ₂ O ₇ ⁶⁻	Si ₃ O ₉ ⁶⁻	IS	Si ₄ O ₁₂ ⁸⁻	Si ₃ O ₁₀ ⁸⁻
Attenuation	2x10 ⁴	50x10 ²	50x10 ²	10x10 ⁴	50x10 ²	50x10 ²

Figure 70

Slag 2

82.61 Mass % FeO-7.13 Mass % Fe₂O₃-15.84 Mass % SiO₂.(0.19x SiO₂)

Peak Label	1	2	3	IS	4	5
Parent Ion	SiO ₄ ⁴⁻	Si ₂ O ₇ ⁶⁻	Si ₃ O ₉ ⁶⁻	IS	Si ₄ O ₁₂ ⁸⁻	Si ₃ O ₁₀ ⁸⁻
Attenuation	10x10 ⁴	1x10 ⁴	1x10 ⁴	10x10 ⁴	50x10 ²	50x10 ²

Fig.69

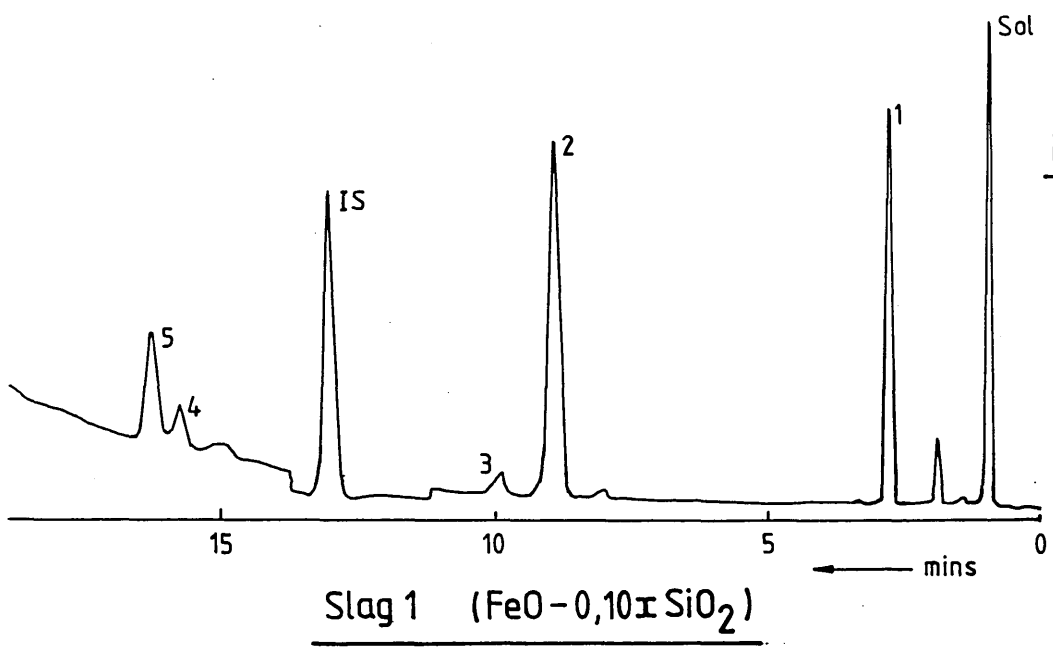


Fig.70

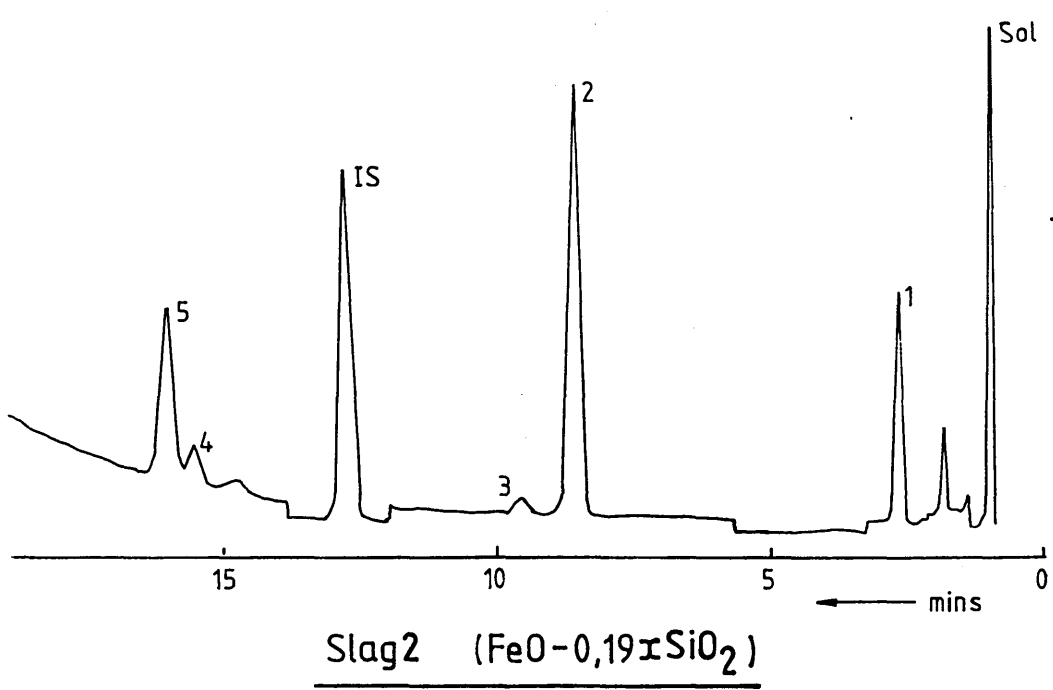


Figure 71

Slag 3

68.44 Mass % FeO-2.39 Mass % Fe₂O₃-29.10 Mass % SiO₂. (0.33x SiO₂)

Peak Label	1	2	3	IS	4	5
Parent Ion	SiO ₄ ⁴⁻	Si ₂ O ₇ ⁶⁻	Si ₃ O ₉ ⁶⁻	IS	Si ₄ O ₁₂ ⁸⁻	Si ₃ O ₁₀ ⁸⁻
Attenuation	10x10 ⁴	2x10 ⁴	1x10 ⁴	10x10 ⁴	50x10 ²	50x10 ²

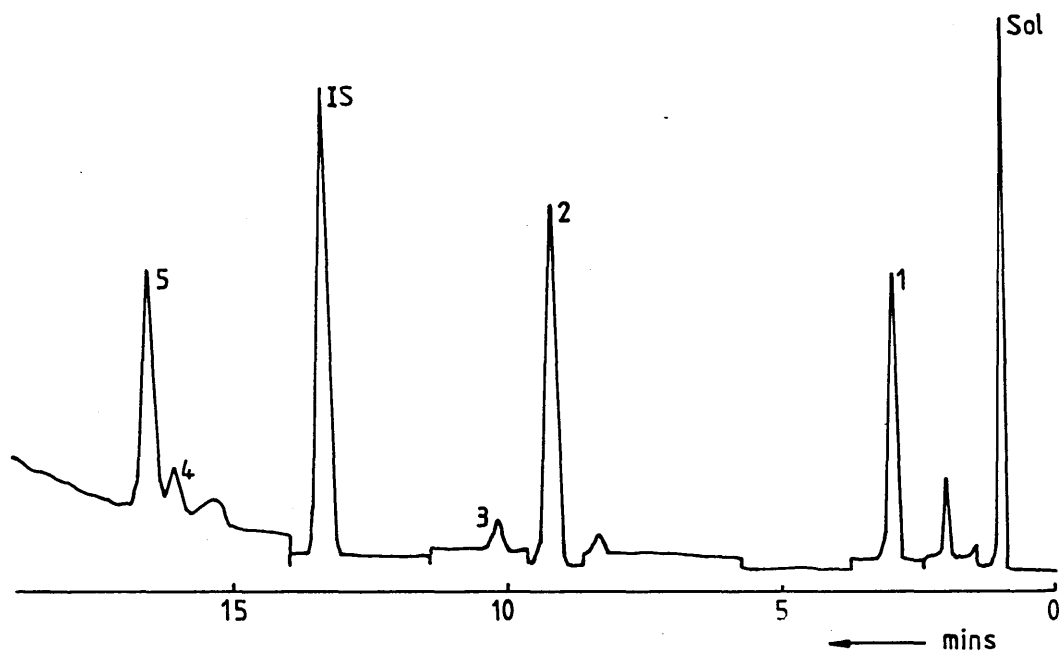


Fig.71

Slag 3 (FeO-0,33SiO₂)

Figure 72

Slag BF3 : Quenched

62.85 Mass % FeO-1.66 Mass % Fe₂O₃-34.80 Mass % SiO₂ (0.39x SiO₂)

Peak Label	1	2	3	IS	4	5
Parent Ion	SiO ₄ ⁴⁻	Si ₂ O ₇ ⁶⁻	Si ₃ O ₉ ⁶⁻	IS	Si ₄ O ₁₂ ⁸⁻	Si ₃ O ₁₀ ⁸⁻
Attenuation	5x10 ⁴	1x10 ⁴	50x10 ²	10x10 ⁴	50x10 ²	50x10 ²

Figure 73

Slag BF3 : Slow Cooled

Peak Label	1	2	3	IS	4	5
Parent Ion	SiO ₄ ⁴⁻	Si ₂ O ₇ ⁶⁻	Si ₃ O ₉ ⁶⁻	IS	Si ₄ O ₁₂ ⁸⁻	Si ₃ O ₁₀ ⁸⁻
Attenuation	5x10 ⁴	2x10 ⁴	50x10 ²	10x10 ⁴	50x10 ²	50x10 ²

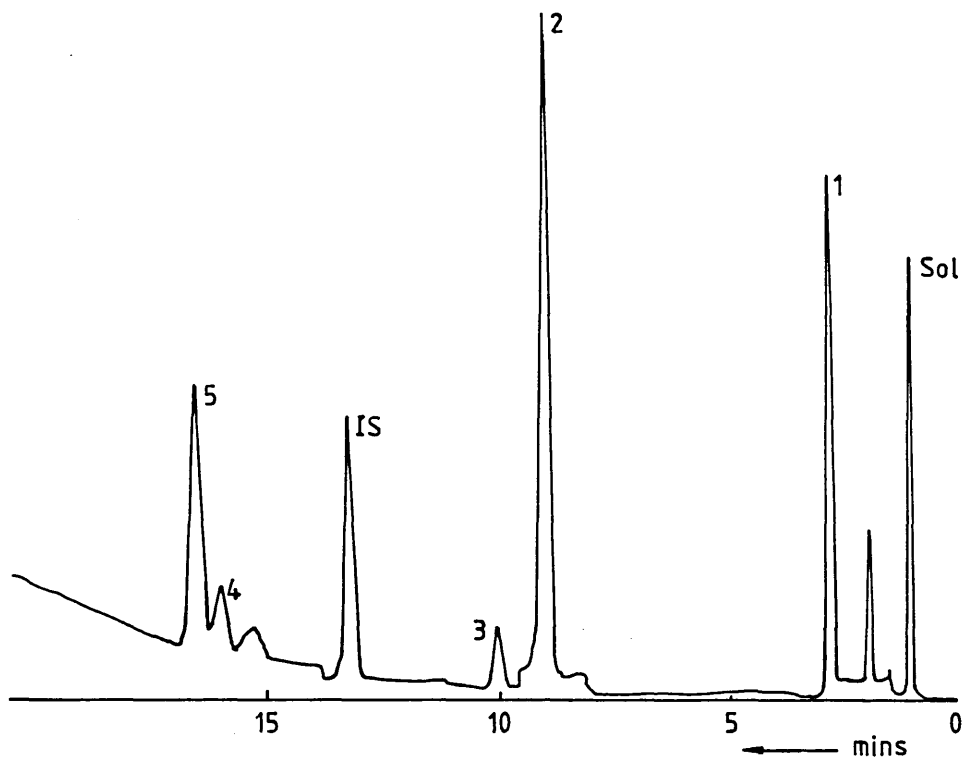


Fig.72

Slag BF3 Quenched (FeO-0,39SiO₂)

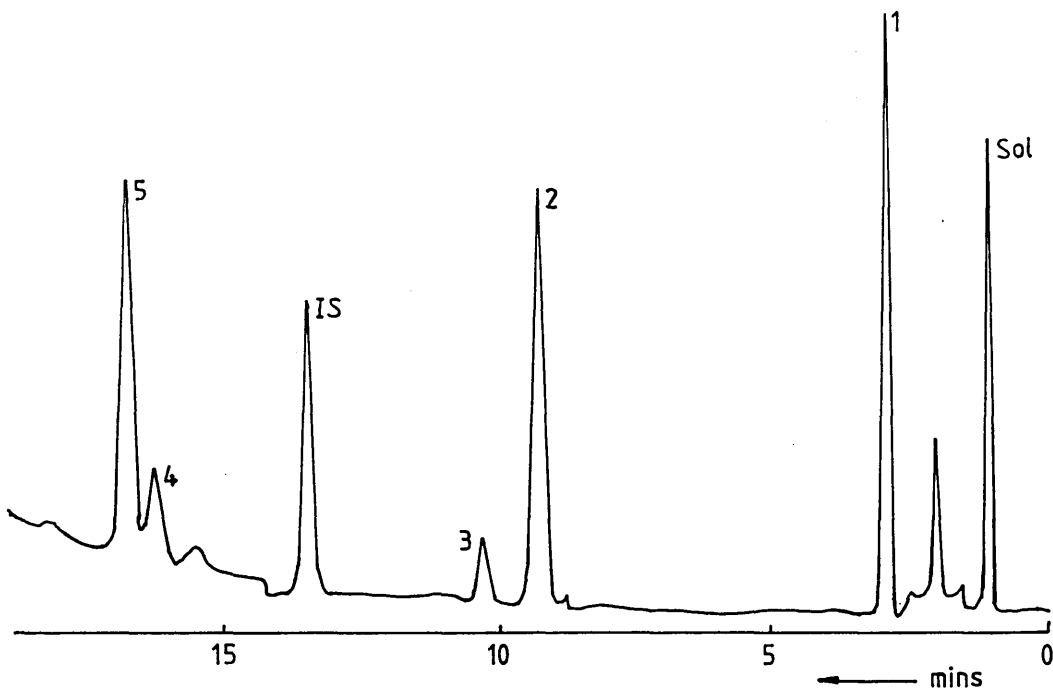


Fig.73

Slag BF3 Slow Cooled (FeO-0,39SiO₂)

Figure 74

Slag 4 : Quenched

57.00 Mass % FeO-2.13 Mass % Fe₂O₃-40.70 Mass % SiO₂ (0.46x SiO₂)

Peak Label	1	2	3	IS	4	5
Parent Ion	SiO ₄ ⁴⁻	Si ₂ O ₇ ⁶⁻	Si ₃ O ₉ ⁶⁻	IS	Si ₄ O ₁₂ ⁸⁻	Si ₃ O ₁₀ ⁸⁻
Attenuation	5x10 ⁴	2x10 ⁴	50x10 ²	10x10 ⁴	50x10 ²	50x10 ²

Figure 75

Slag 4 : Slow Cooled

FeO-0.46x SiO₂

Peak Label	1	2	3	IS	4	5
Parent Ion	SiO ₄ ⁴⁻	Si ₂ O ₇ ⁶⁻	Si ₃ O ₉ ⁶⁻	IS	Si ₄ O ₁₂ ⁸⁻	Si ₃ O ₁₀ ⁸⁻
Attenuation	5x10 ⁴	2x10 ⁴	50x10 ²	10x10 ⁴	50x10 ²	50x10 ²

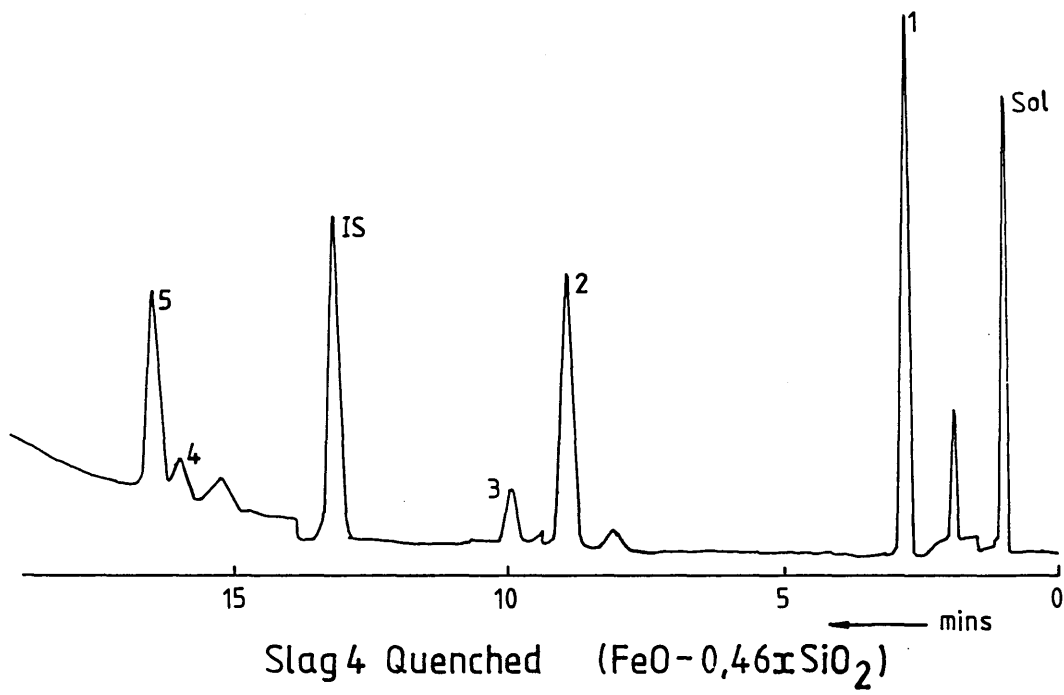


Fig.74

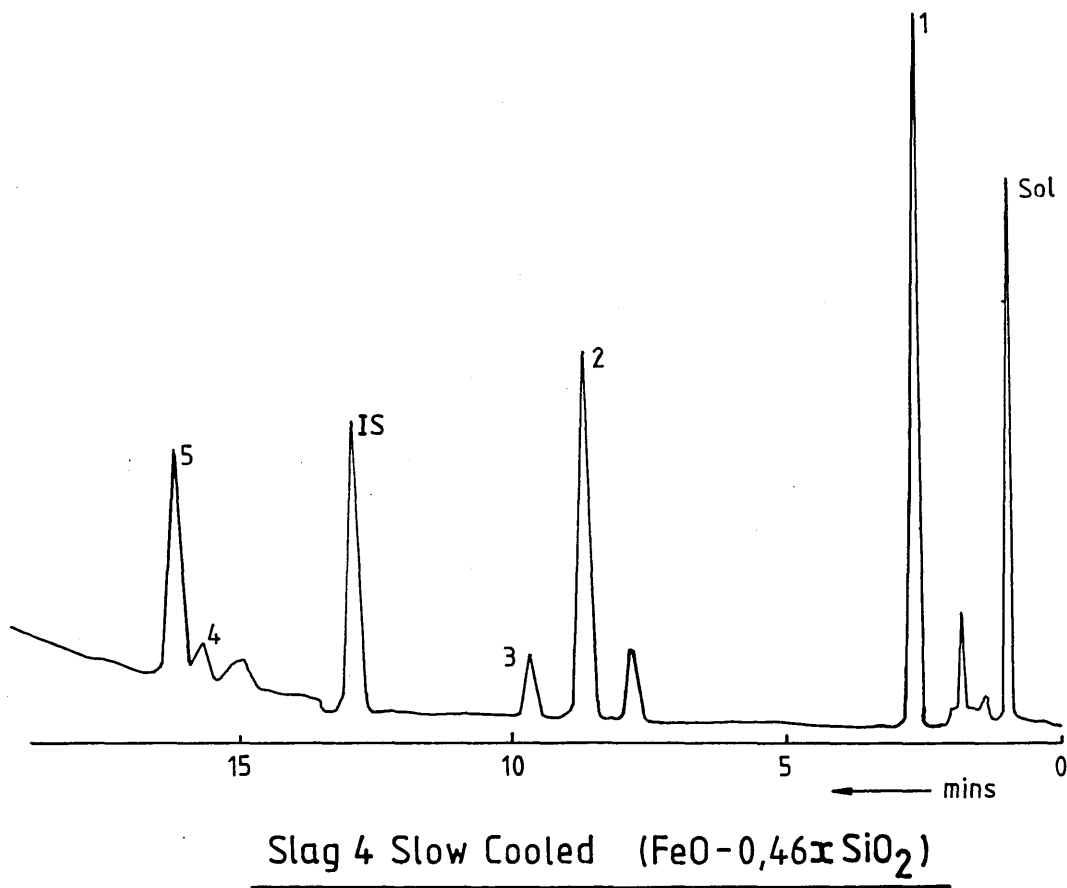


Fig.75

Figure 76

Slag 5

50.57 Mass % FeO-1.61 Mass % Fe₂O₃-47.82 Mass % SiO₂ (0.53x SiO₂)

Peak Label	1	2	3	IS	4	5
Parent Ion	SiO ₄ ⁴⁻	Si ₂ O ₇ ⁶⁻	Si ₃ O ₉ ⁶⁻	IS	Si ₄ O ₁₂ ⁸⁻	Si ₃ O ₁₀ ⁸⁻
Attenuation	5x10 ⁴	1x10 ⁴	50x10 ²	10x10 ⁴	50x10 ²	50x10 ²

Figure 77

Slag 6

(1.29 Mass % CaO-61.44 Mass % FeO-1.34 Mass % Fe₂O₃-35.93 Mass % SiO₂)

Peak Label	1	2	3	IS	4	5
Parent Ion	SiO ₄ ⁴⁻	Si ₂ O ₇ ⁶⁻	Si ₃ O ₉ ⁶⁻	IS	Si ₄ O ₁₂ ⁸⁻	Si ₃ O ₁₀ ⁸⁻
Attenuation	5x10 ⁴	2x10 ⁴	50x10 ²	10x10 ⁴	50x10 ²	50x10 ²

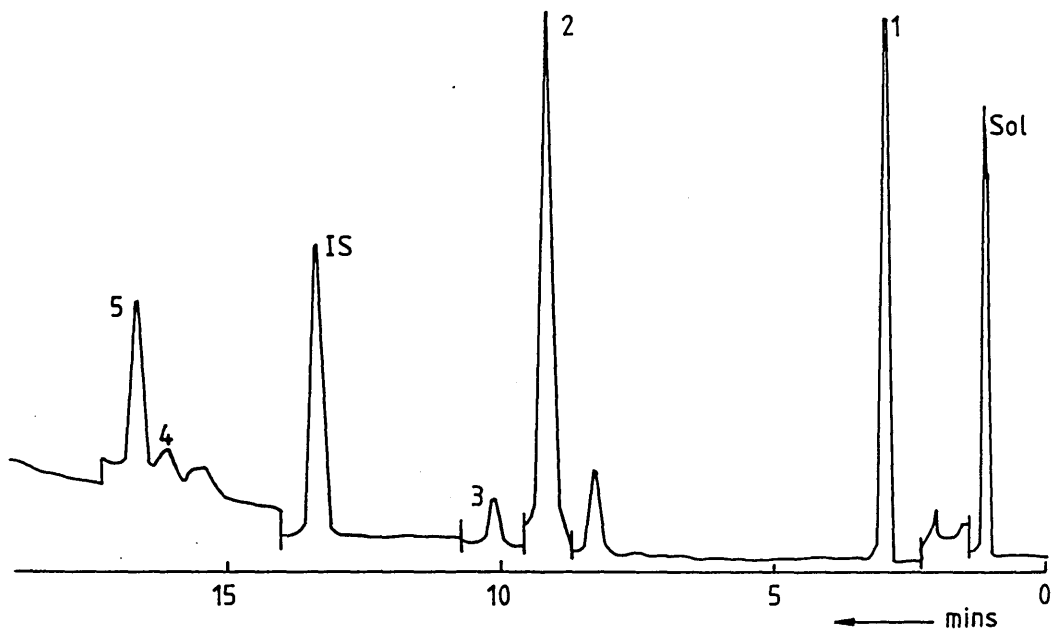


Fig.76

Slag 5 (FeO-0,53±SiO₂)

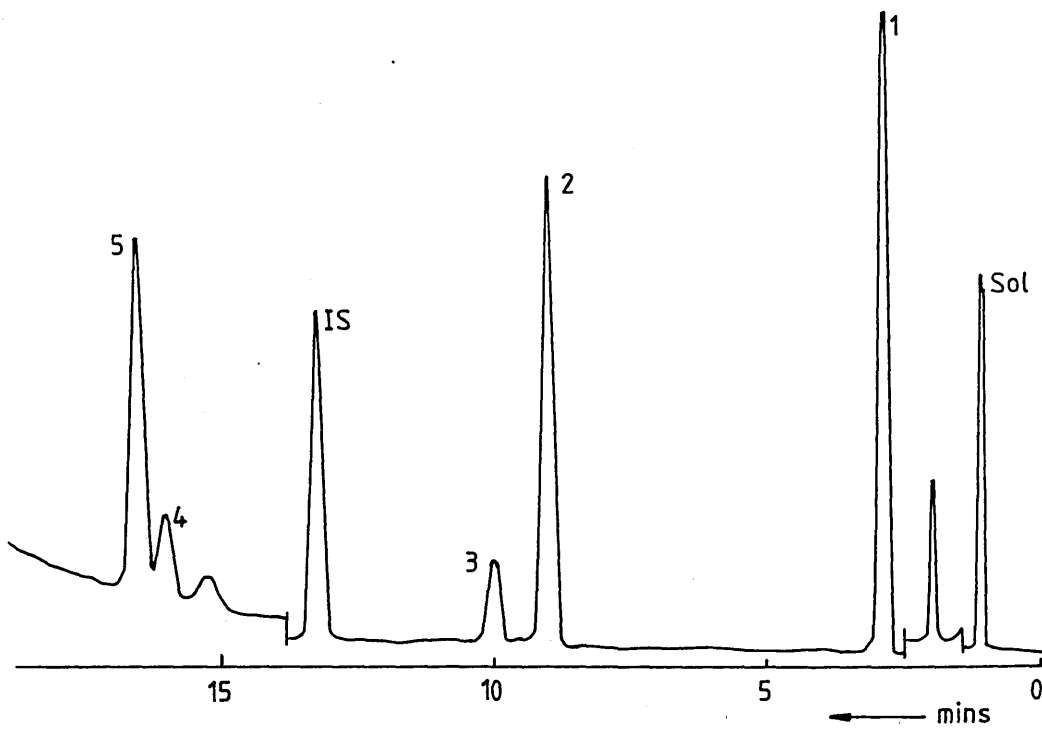


Fig.77

Slag 6

(1,29mass% CaO- 61,44mass% FeO- 35,93mass% SiO₂)

Figure 78

Slag KC1

(38.31 Mass % CaO-28.52 Mass % FeO-1.90 Mass % Fe₂O₃-31.00 Mass % SiO₂)

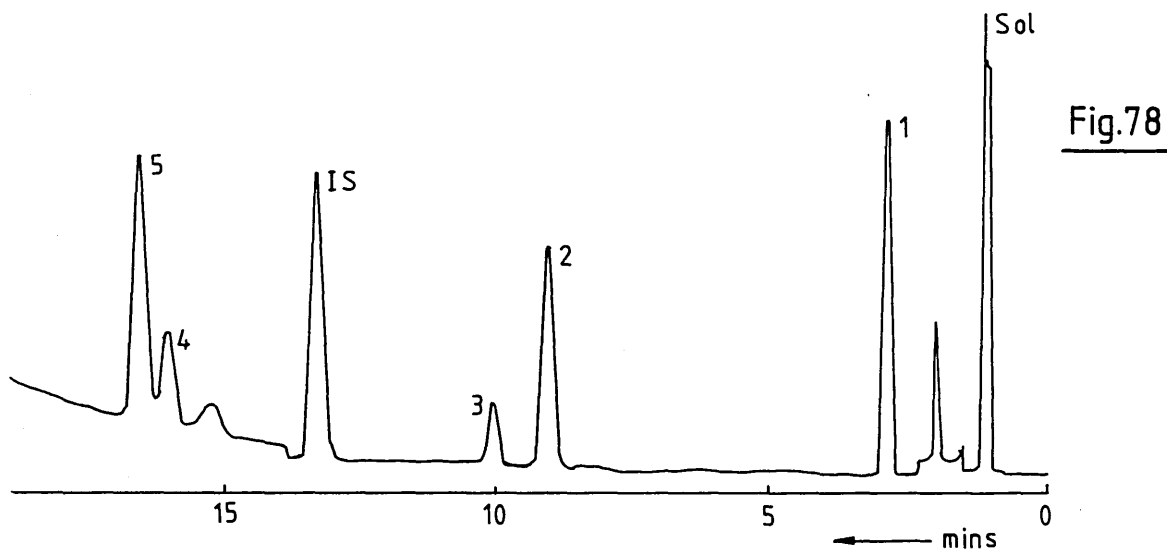
Peak Label	1	2	3	IS	4	5
Parent Ion	SiO ₄ ⁴⁻	Si ₂ O ₇ ⁶⁻	Si ₃ O ₉ ⁶⁻	IS	Si ₄ O ₁₂ ⁸⁻	Si ₃ O ₁₀ ⁸⁻
Attenuation	5x10 ⁴	2x10 ⁴	50x10 ²	10x10 ⁴	50x10 ²	50x10 ²

Figure 79

Slag KC2

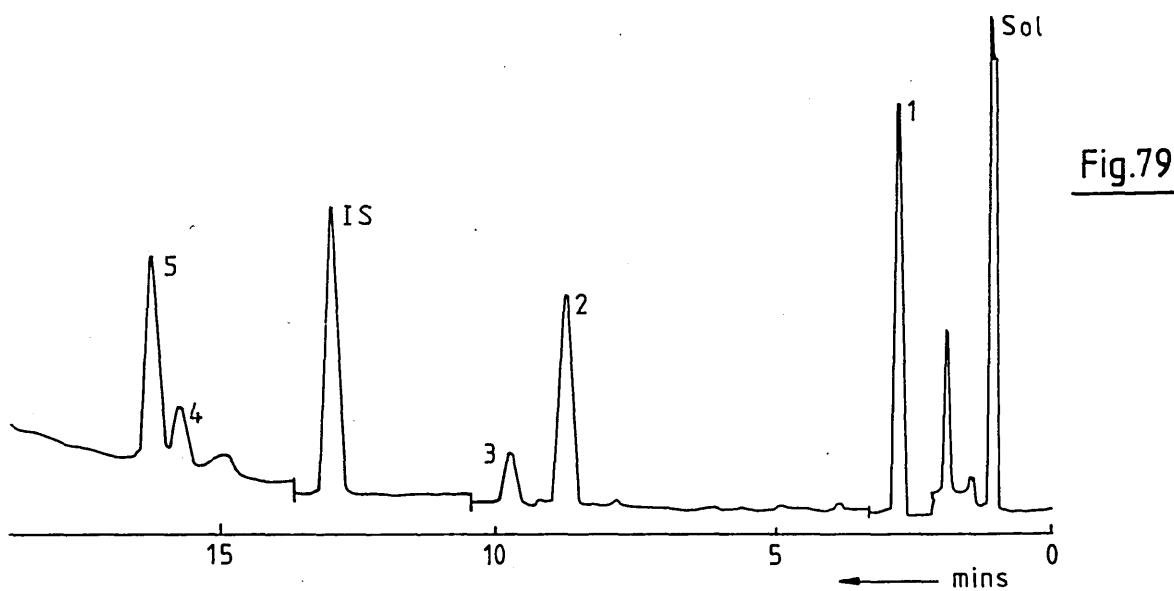
(28.00 Mass % CaO-40.20 Mass % FeO-3.21 Mass % Fe₂O₃-28.50 Mass % SiO₂)

Peak Label	1	2	3	IS	4	5
Parent Ion	SiO ₄ ⁴⁻	Si ₂ O ₇ ⁶⁻	Si ₃ O ₉ ⁶⁻	IS	Si ₄ O ₁₂ ⁸⁻	Si ₃ O ₁₀ ⁸⁻
Attenuation	5x10 ⁴	2x10 ⁴	50x10 ²	10x10 ⁴	50x10 ²	50x10 ²



Slag KC1

(38,31mass%CaO-28,52mass%FeO-31,00mass%SiO₂)



Slag KC2

(28,00mass%CaO-40,20mass%FeO-28,50mass%SiO₂)

Figure 80

Slag KC3

(17.01 Mass % CaO-46.10 Mass % FeO-7.72 Mass % Fe₂O₃-29.00 Mass % SiO₂)

Peak Label	1	2	3	IS	4	5
Parent Ion	SiO ₄ ⁴⁻	Si ₂ O ₇ ⁶⁻	Si ₃ O ₉ ⁶⁻	IS	Si ₄ O ₁₂ ⁸⁻	Si ₃ O ₁₀ ⁸⁻
Attenuation	5x10 ⁴	2x10 ⁴	50x10 ²	10x10 ⁴	50x10 ²	50x10 ²

Figure 81

Slag KCl₄

(10.04 Mass % CaO-55.20 Mass % FeO-5.72 Mass % Fe₂O₃-28.20 Mass % SiO₂)

Peak Label	1	2	3	IS	4	5
Parent Ion	SiO ₄ ⁴⁻	Si ₂ O ₇ ⁶⁻	Si ₃ O ₉ ⁶⁻	IS	Si ₄ O ₁₂ ⁸⁻	Si ₃ O ₁₀ ⁸⁻
Attenuation	5x10 ⁴	2x10 ⁴	50x10 ²	10x10 ⁴	50x10 ²	50x10 ²

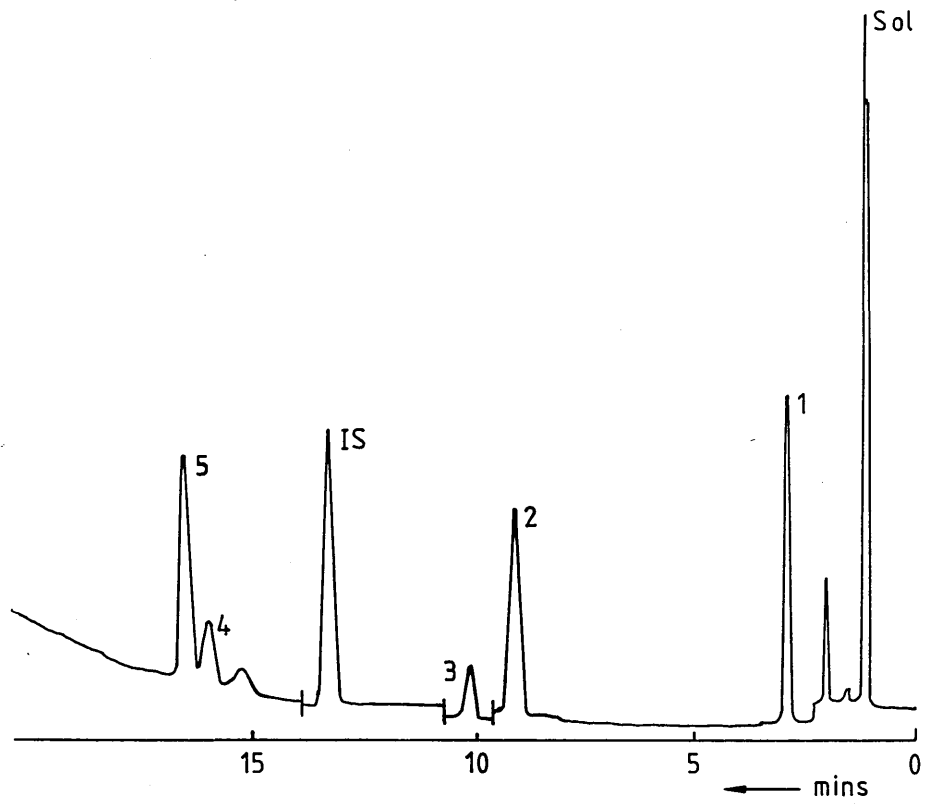


Fig. 80

Slag KC3

(17,01mass% CaO-46,10mass% FeO-29,00mass% SiO₂)

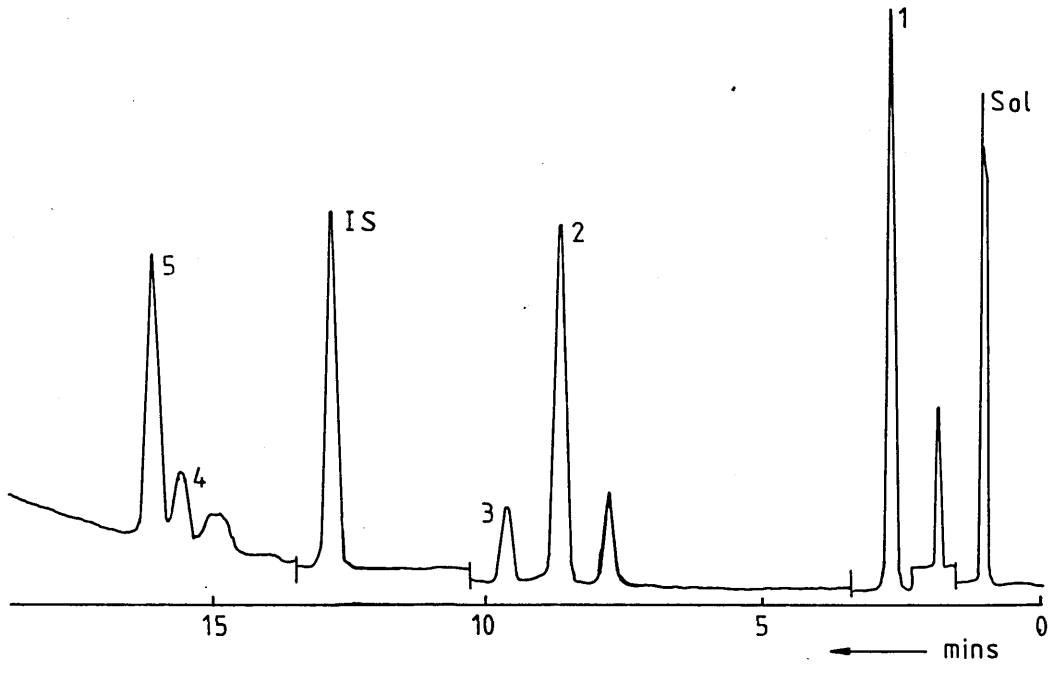
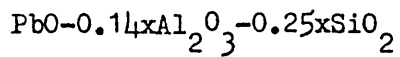


Fig. 81

Slag KC4

(10,04mass% CaO-55,20mass% FeO-28,20mass% SiO₂)

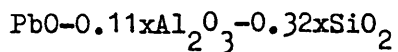
Figure 82



(84.00 Mass % PbO-8.31 Mass % Al_2O_3 -7.40 Mass % SiO_2)

Peak Label	1	2	3	IS	4	5
Parent Ion	SiO_4^{4-}	$\text{Si}_2\text{O}_7^{6-}$	$\text{Si}_3\text{O}_9^{6-}$	IS	$\text{Si}_4\text{O}_{12}^{8-}$	$\text{Si}_3\text{O}_{10}^{8-}$
Attenuation	$2x10^4$	$1x10^4$	$50x10^2$	$10x10^4$	$50x10^2$	$50x10^2$

Figure 83



(78.00 Mass % PbO-6.80 Mass % Al_2O_3 -9.70 Mass % SiO_2)

Peak Label	1	2	3	IS	4	5
Parent Ion	SiO_4^{4-}	$\text{Si}_2\text{O}_7^{6-}$	$\text{Si}_3\text{O}_9^{6-}$	IS	$\text{Si}_4\text{O}_{12}^{8-}$	$\text{Si}_3\text{O}_{10}^{8-}$
Attenuation	$2x10^4$	$1x10^4$	$50x10^2$	$10x10^4$	$50x10^2$	$50x10^2$

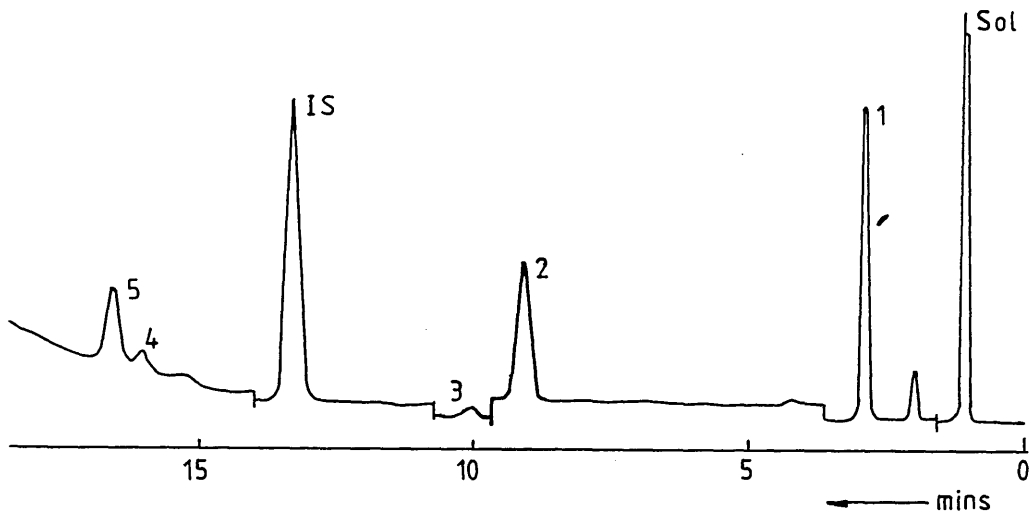


Fig. 82

PbO-0,25xSiO₂ Melt

(84,00mass%PbO- 8,31mass%Al₂O₃-7,40mass%SiO₂)

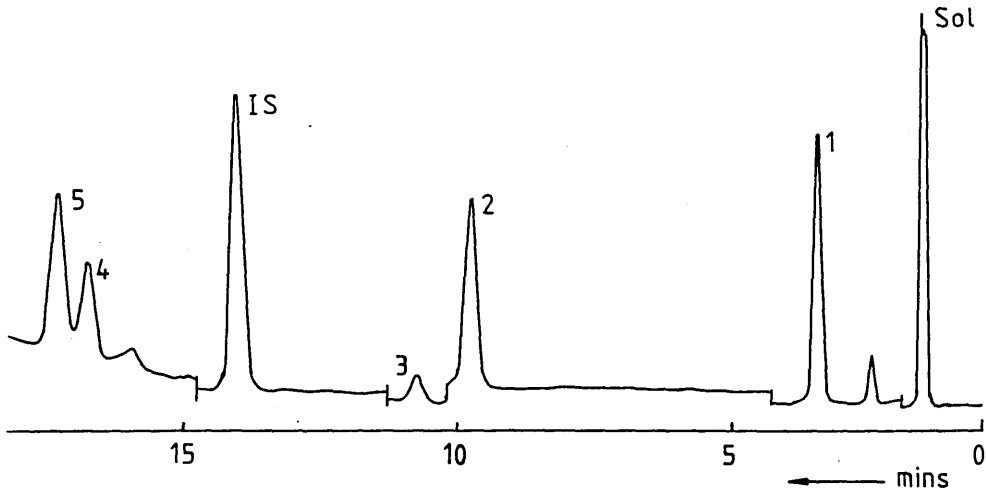
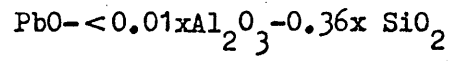


Fig. 83

PbO-0,32xSiO₂ Melt

(78,00mass%PbO-6,80mass%Al₂O₃-9,70mass%SiO₂)

Figure 84



(86.40 Mass % PbO - 0.20 Mass % Al_2O_3 - 13.20 Mass % SiO_2)

Peak Label	1	2	3	IS	4	5
Parent Ion	SiO_4^{4-}	$Si_2O_7^{6-}$	$Si_3O_9^{6-}$	IS	$Si_4O_{12}^{8-}$	$Si_3O_{10}^{8-}$
Attenuation	$2x10^4$	$1x10^4$	$50x10^2$	$10x10^4$	$50x10^2$	$50x10^2$

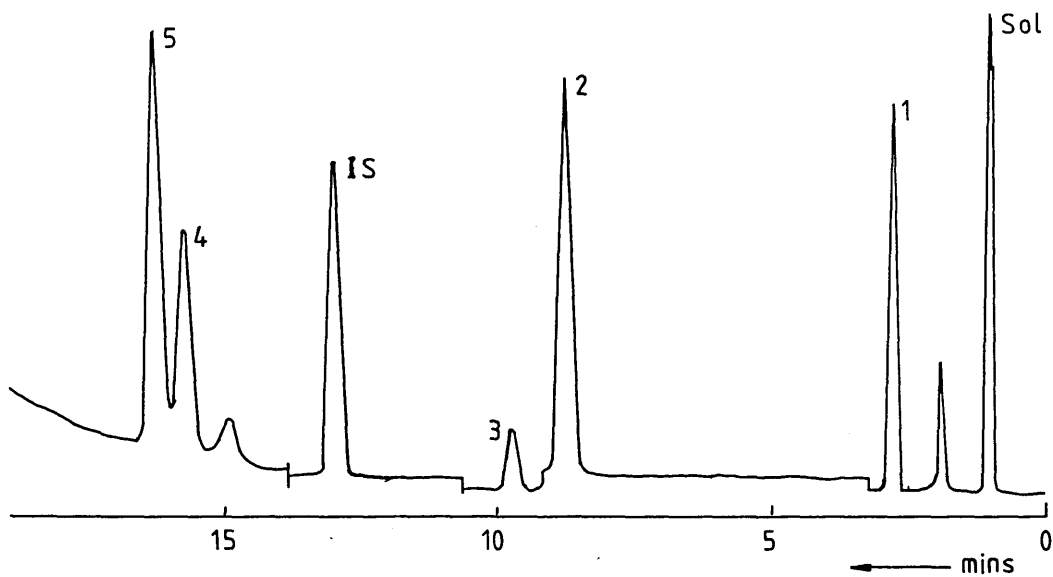


Fig. 84

PbO-0,36 x SiO₂ Melt

(86,40 mass% PbO- 0,20 mass% Al₂O₃-13,20 mass% SiO₂)

Figure 85

Precipitated Silica (BDH Reagent)

Peak Label	1	IS
Parent Ion	SiO_4^{4-}	IS
Attenuation	50×10^2	10×10^4

Figure 86

Fused SiO_2 Rod Sample

Peak Label	1	IS
Parent Ion	SiO_4^{4-}	IS
Attenuation	20×10^2	10×10^4

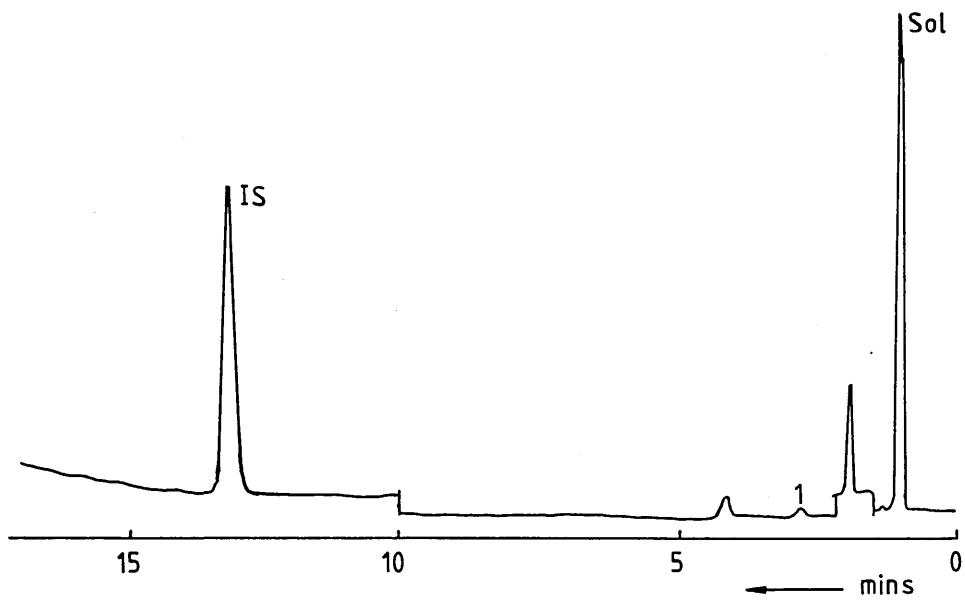


Fig. 85

Precipitated Silica

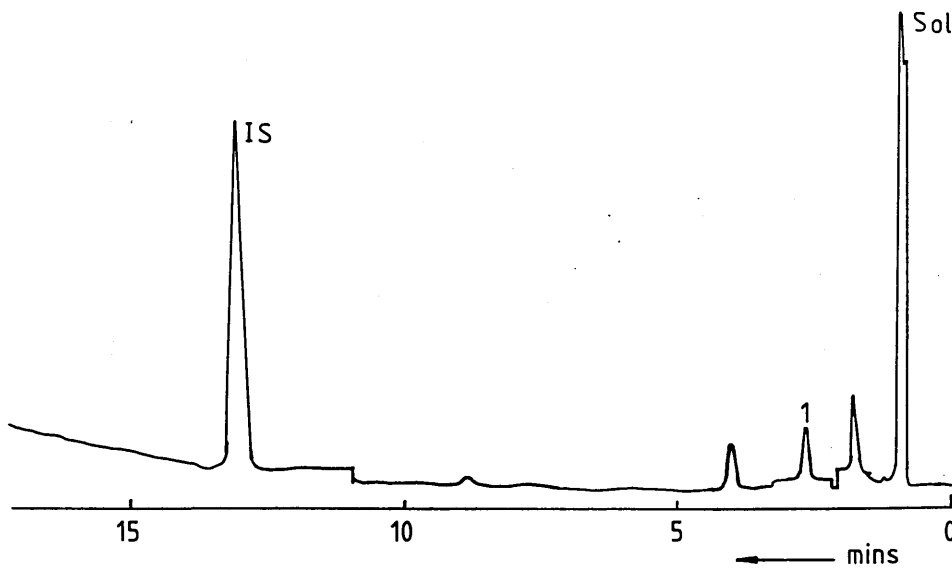
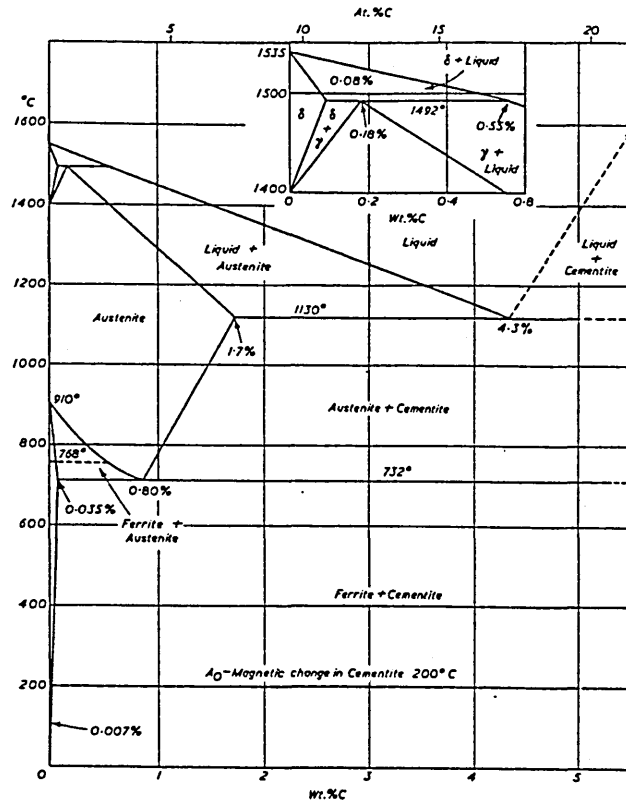


Fig. 86

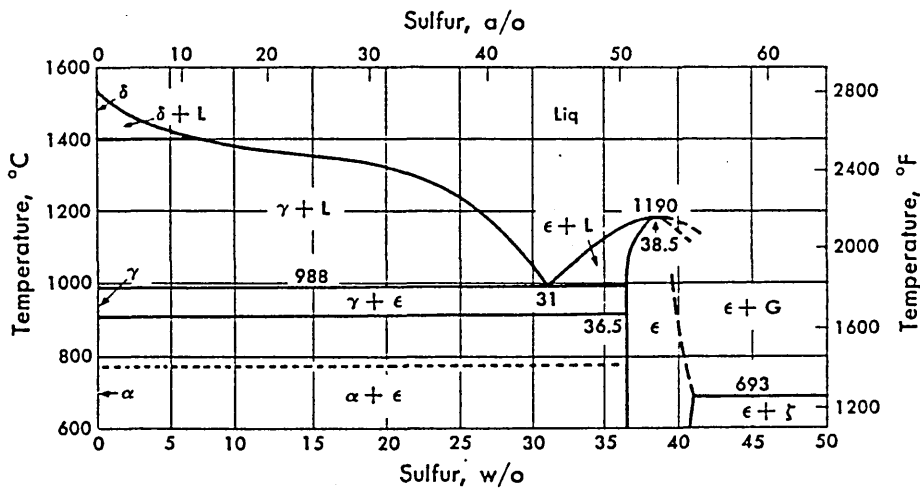
Fused Silica

Fig. 87a



Fe-C Equilibrium Diagram ¹⁶⁵

Fig. 87b



Fe-S Equilibrium Diagram ¹⁶⁶

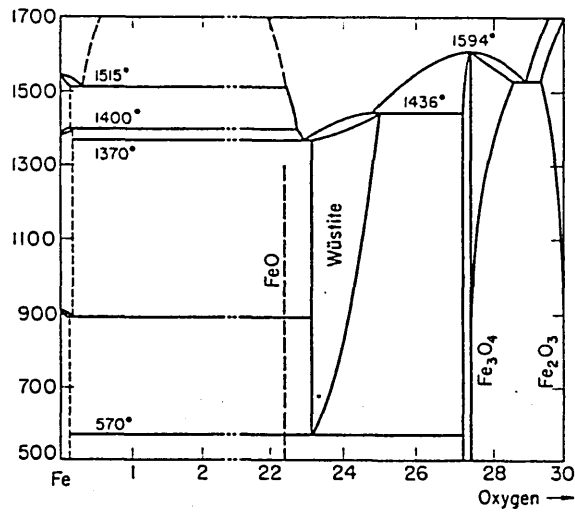


Fig. 87c

Fe-O₂ Equilibrium Diagram¹⁶⁷

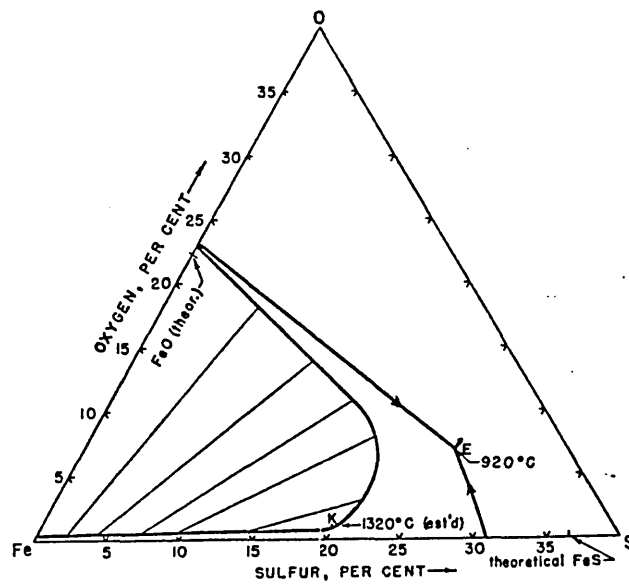


Fig. 87d

Fe-O-S Equilibrium Diagram¹⁶⁸

Fig.88a

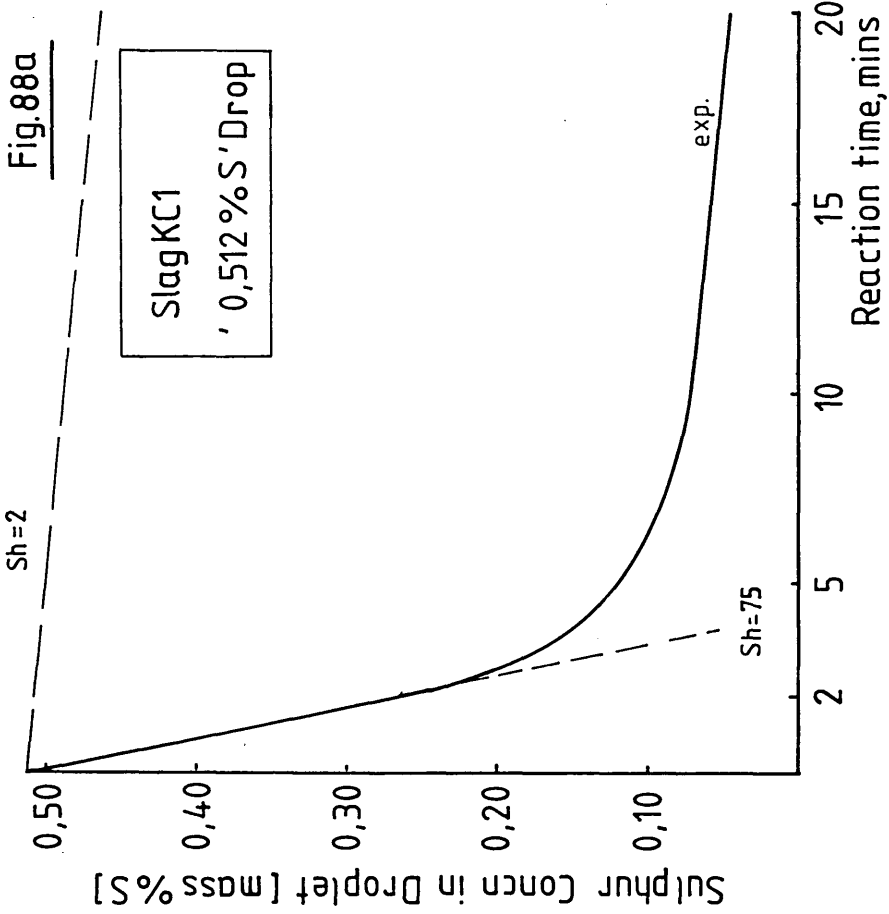
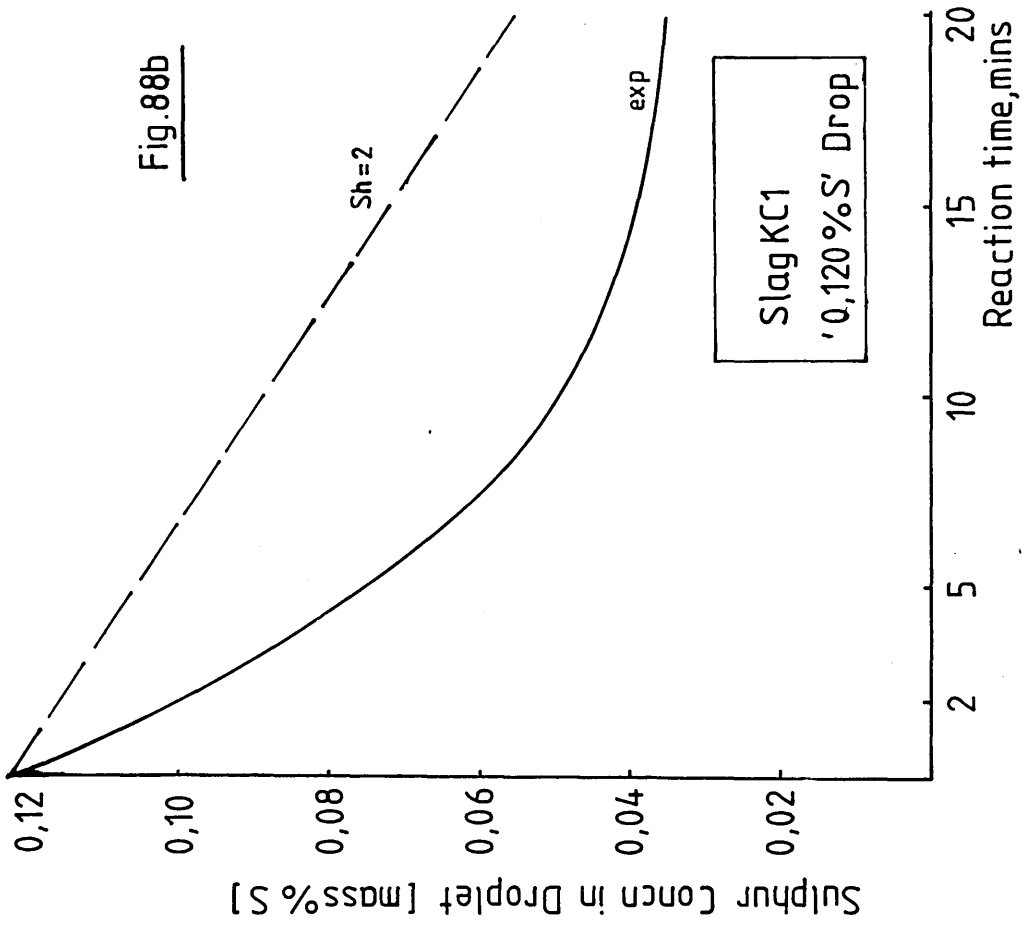
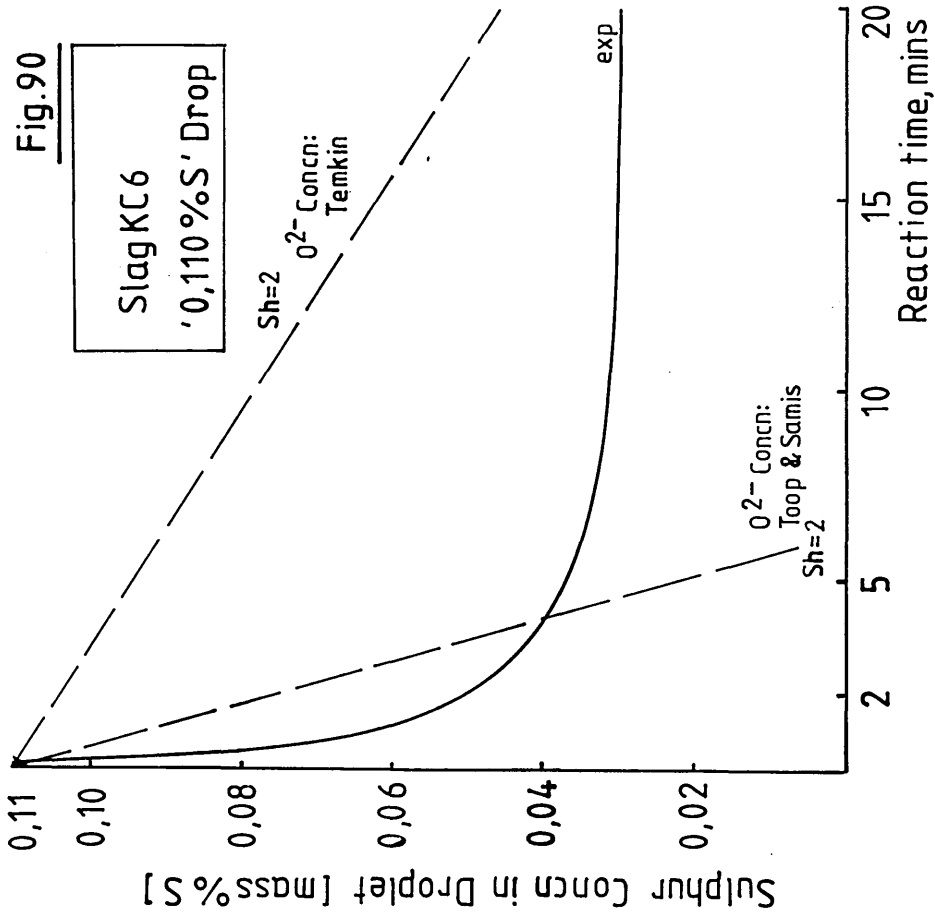
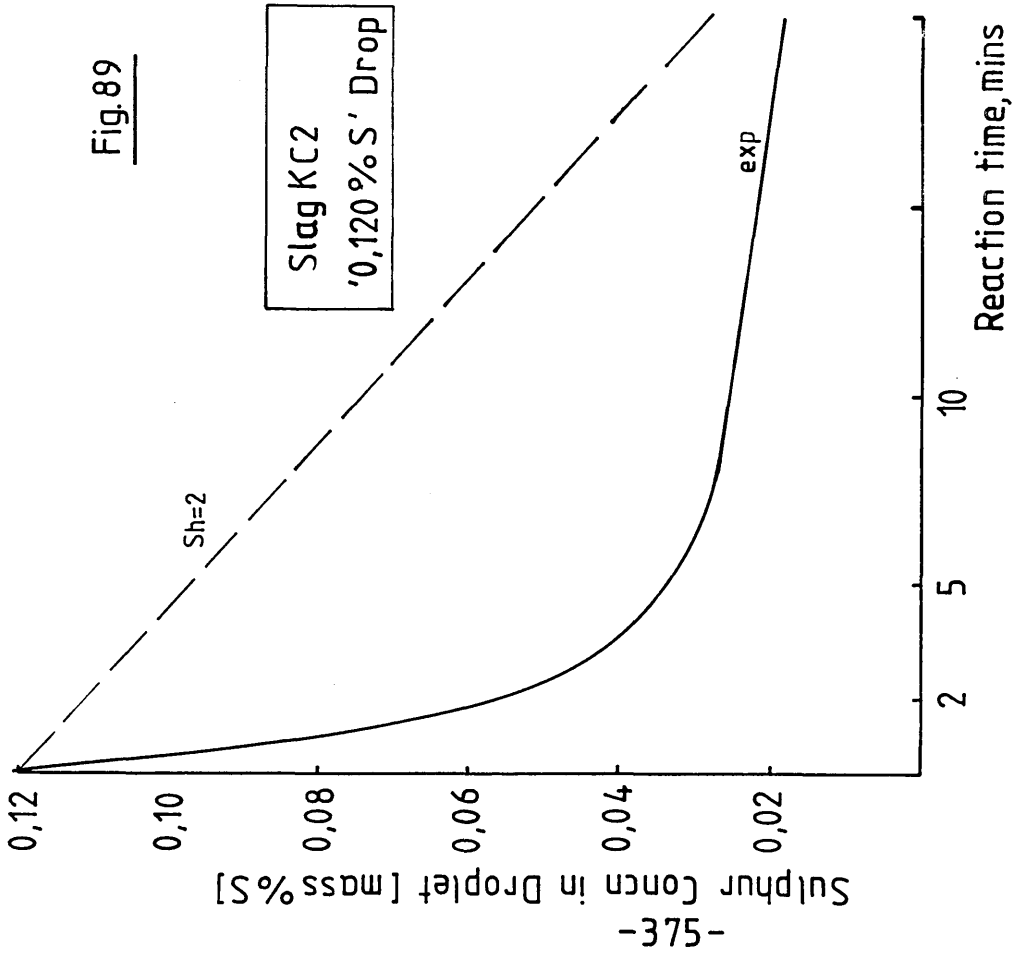


Fig.88b



Sulphur Concentrations in Droplets ; Comparison Between Experimental Results And Predictions Based On Mass Transfer Model Assuming Continuous Phase Control



Sulphur Concentrations in Droplets ; Comparison Between Experimental Results And Predictions Based On Mass Transfer Model Assuming Continuous Phase Control

Fig.91a

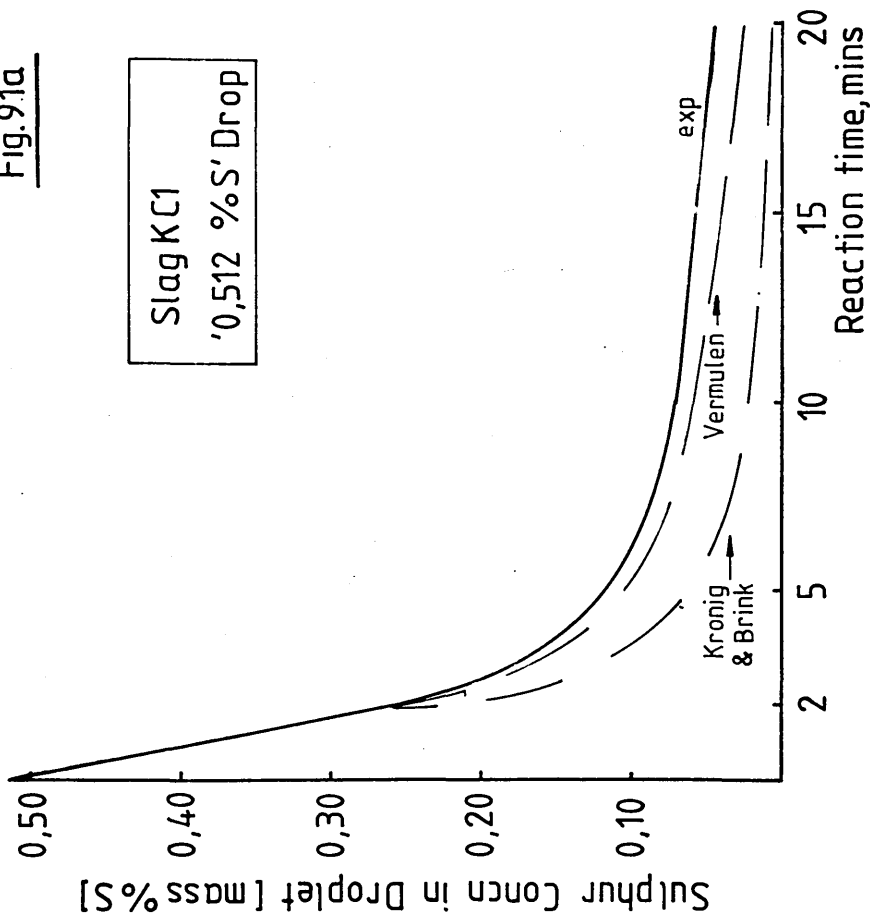
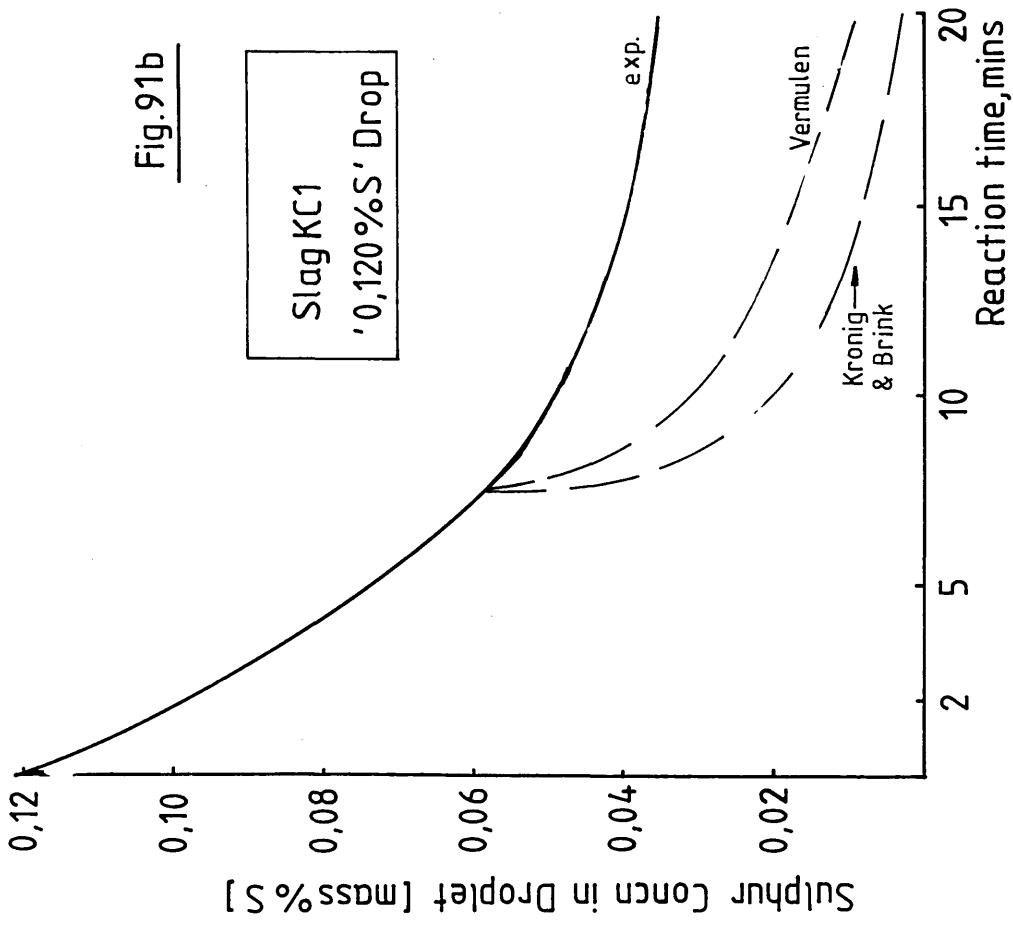
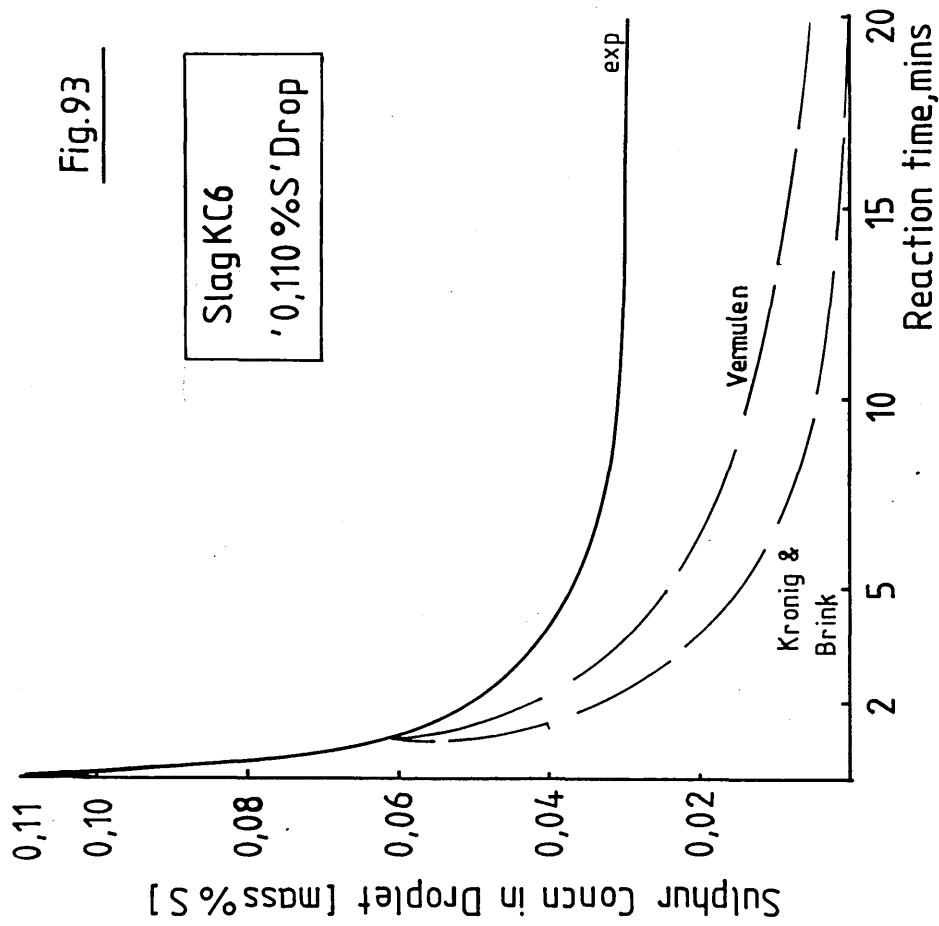
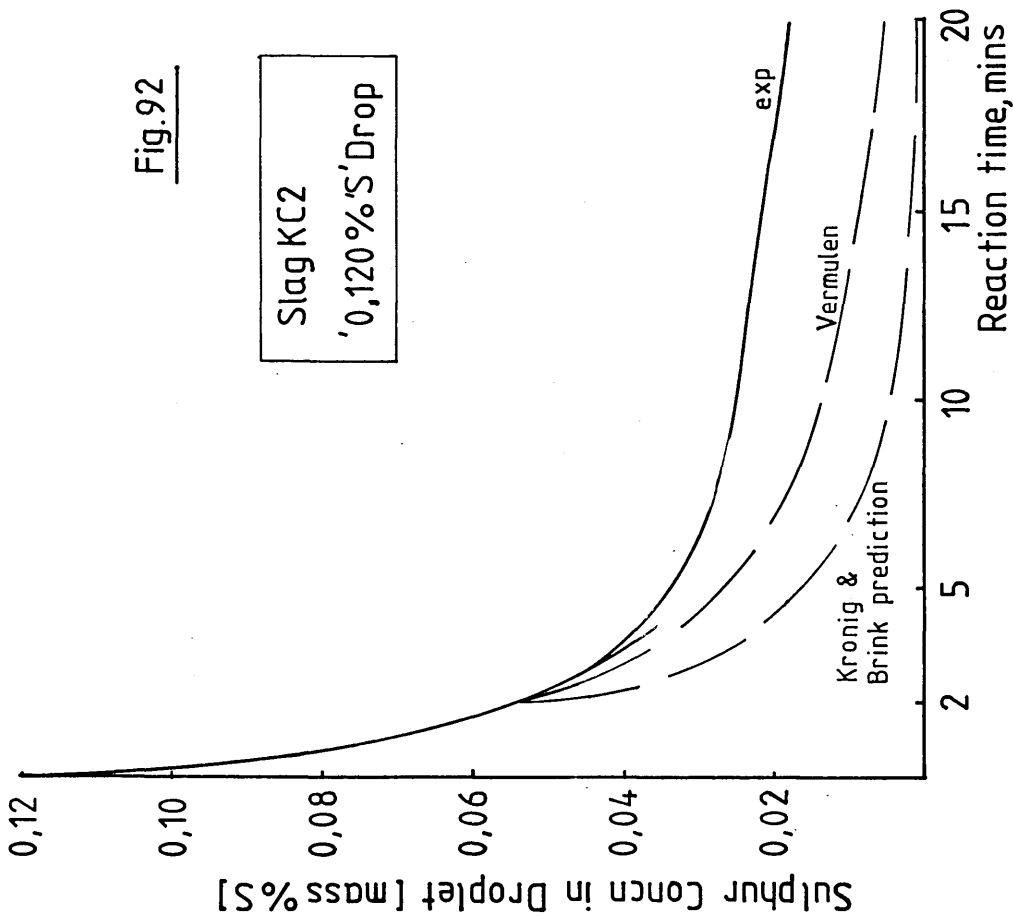


Fig.91b



Sulphur Concentrations in Droplets ; Comparison Between Experimental Results And Predictions Based On Diffusion Control Of Sulphur In The Dispersed Phase



Sulphur Concentrations in Droplets ; Comparison Between Experimental Results And Predictions Based On Diffusion Control Of Sulphur In The Dispersed Phase

Plates 1a to 1g

Profiles of Seven Woods Metal Droplets At
Different Stages of Free Fall

Free Fall Distances:-

Plate 1a = 58 mm

Plate 1b = 67 mm

Plate 1c = 70 mm

Plate 1d = 78 mm

Plate 1e = 82 mm

Plate 1f = 97 mm

Plate 1g = 104 mm

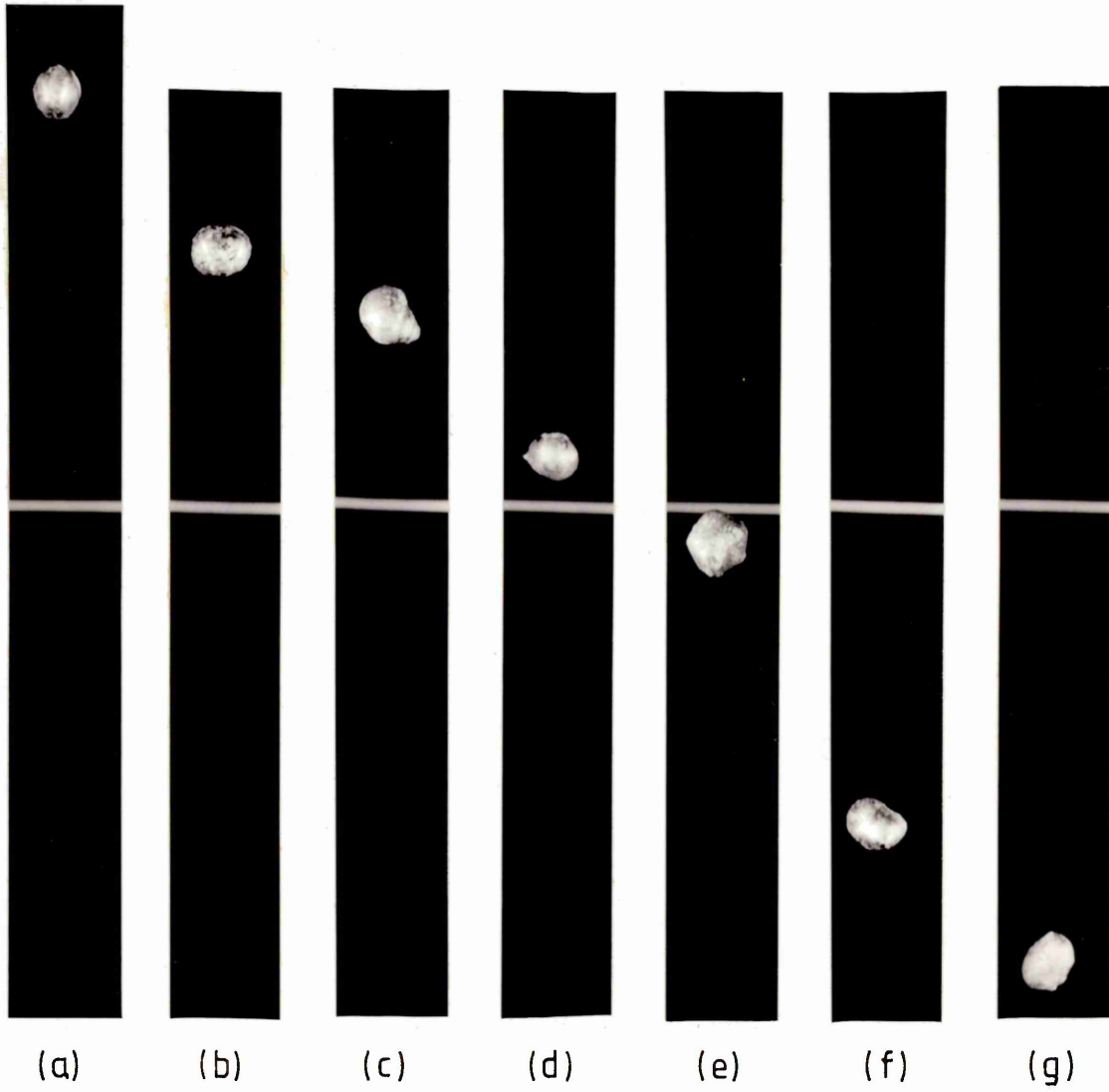
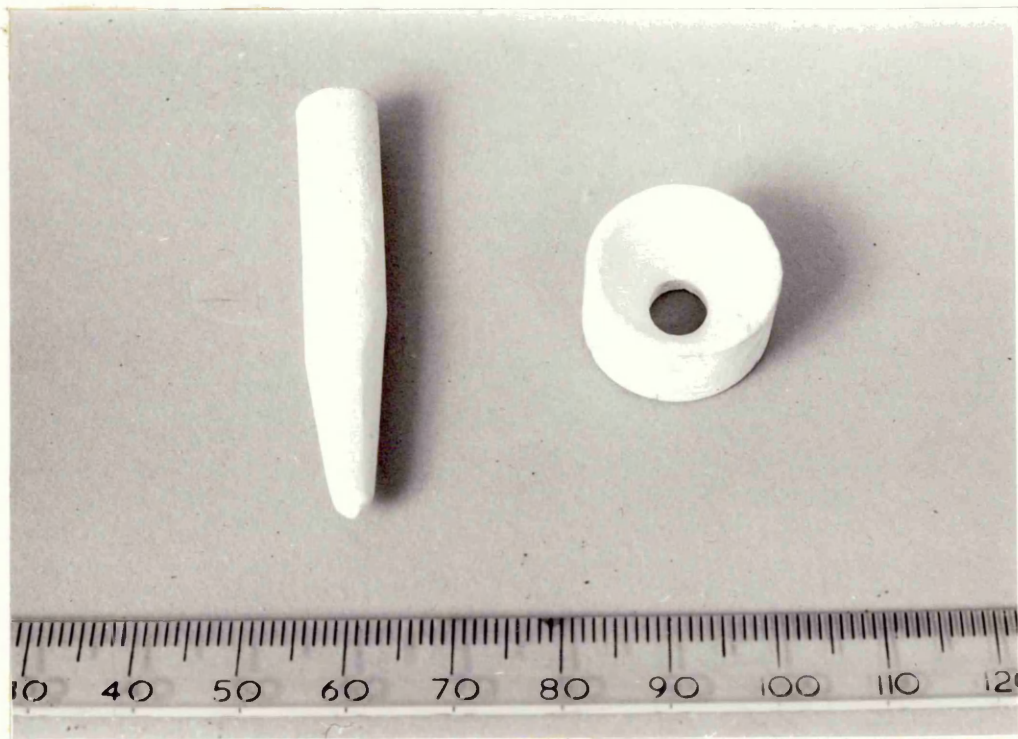
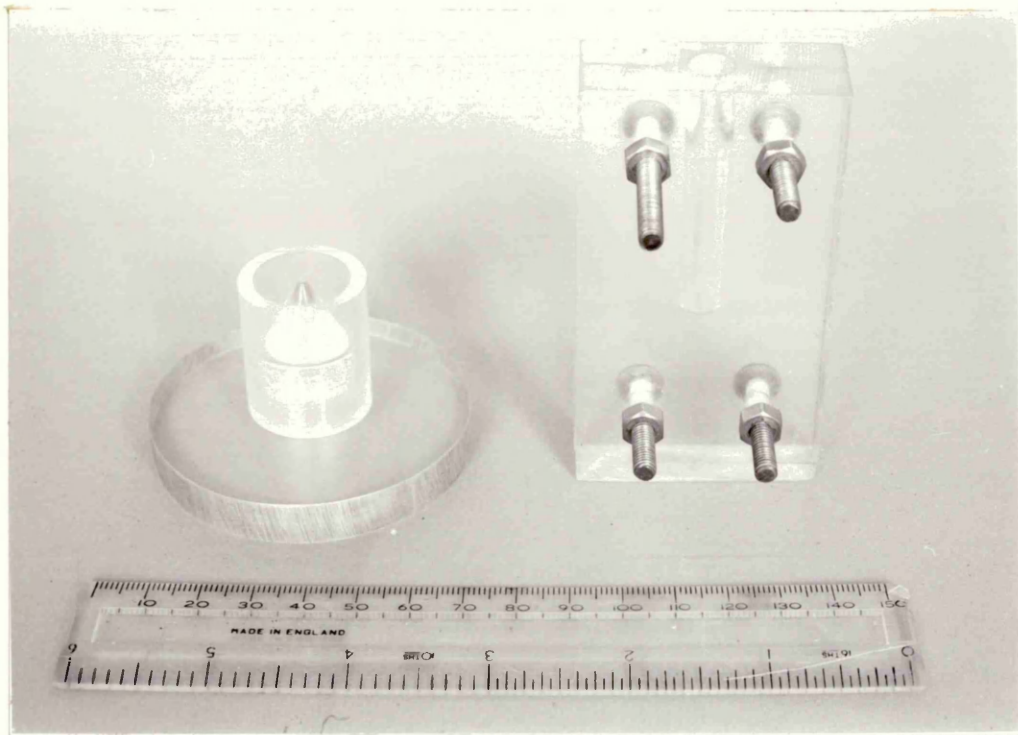


Plate 2a

Perspex Moulds Used In The Manufacture
of Stopper and Seat Components

Plate 2b

Stopper and Seat Components Made From
 Al_2O_3 -40 mass % ZrO_2

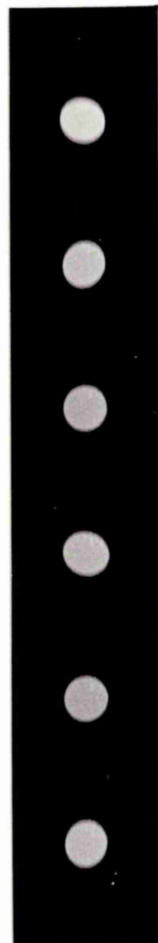


Plates 3a and 3b

Examples of Fe-C-S Droplet Profiles During
Different Stages of Free Fall



(a)



(b)

Plate 4

Carbolite Vertical Tube Furnace Employed For
Droplet Experiments

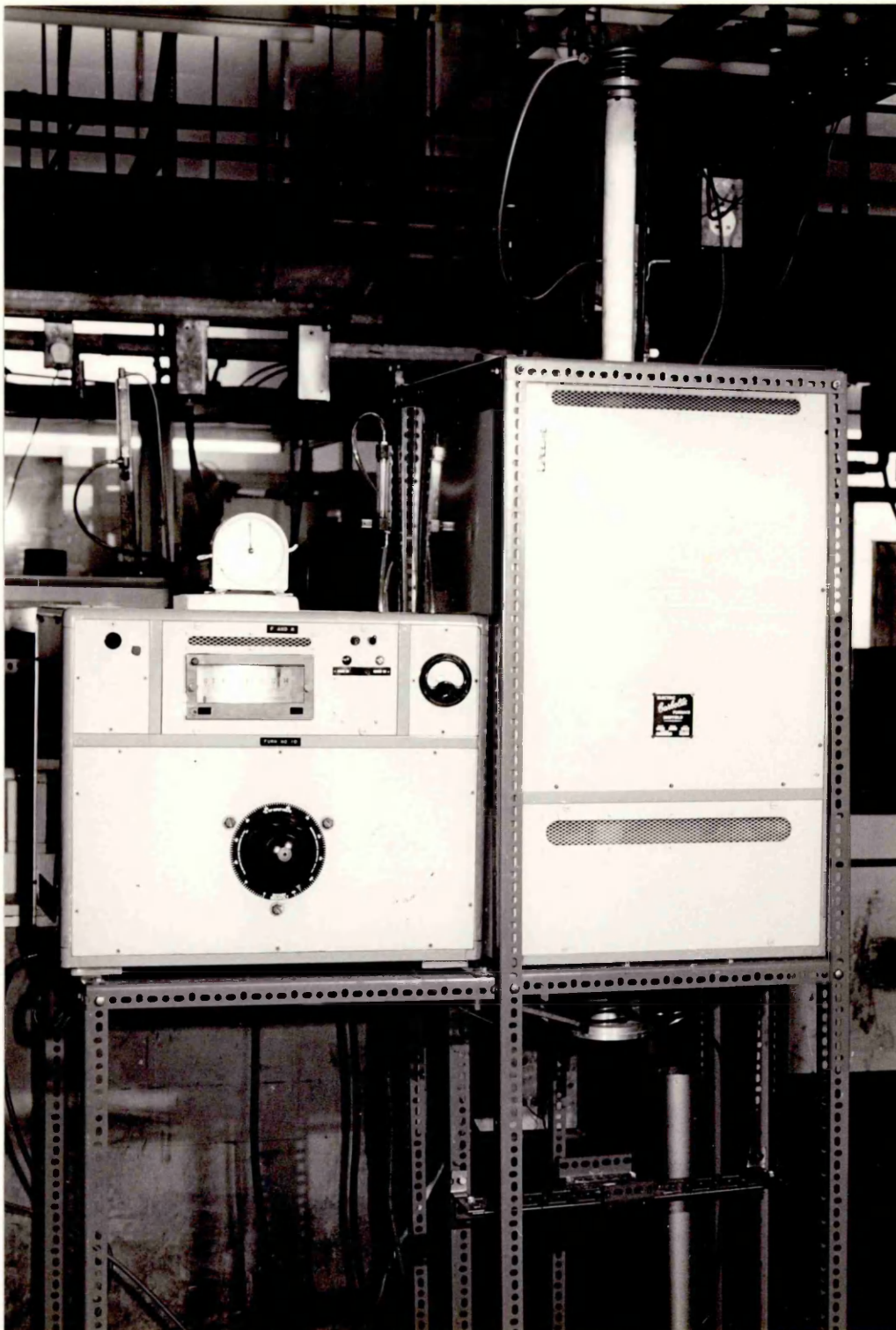


Plate 5

Distillation Unit Used For the Purification of
Trimethylchlorosilane

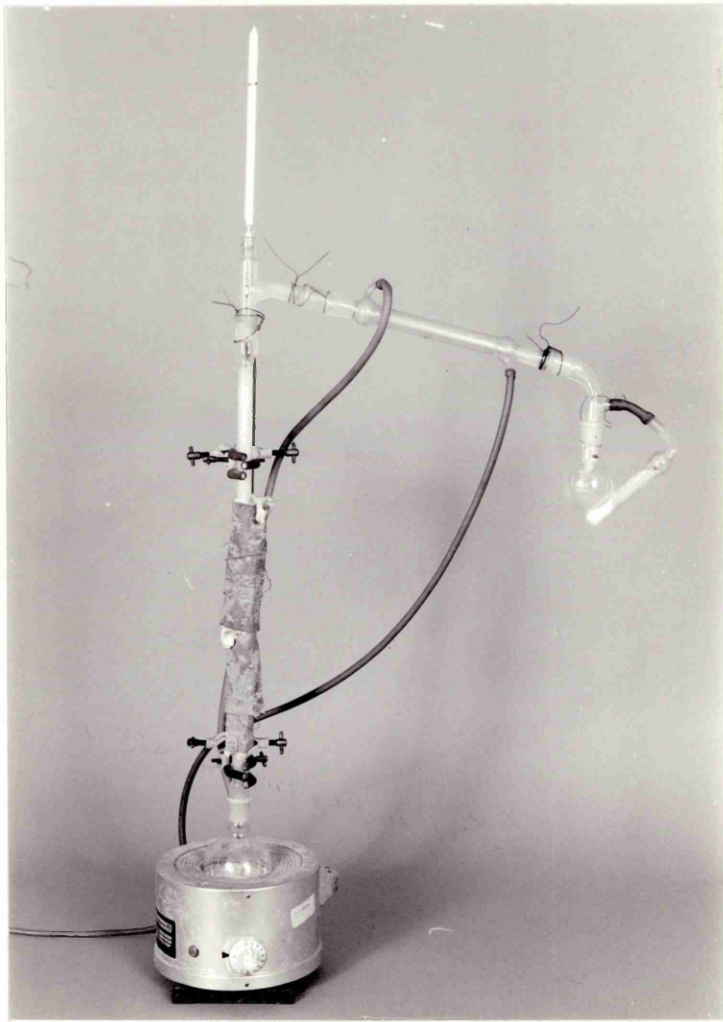
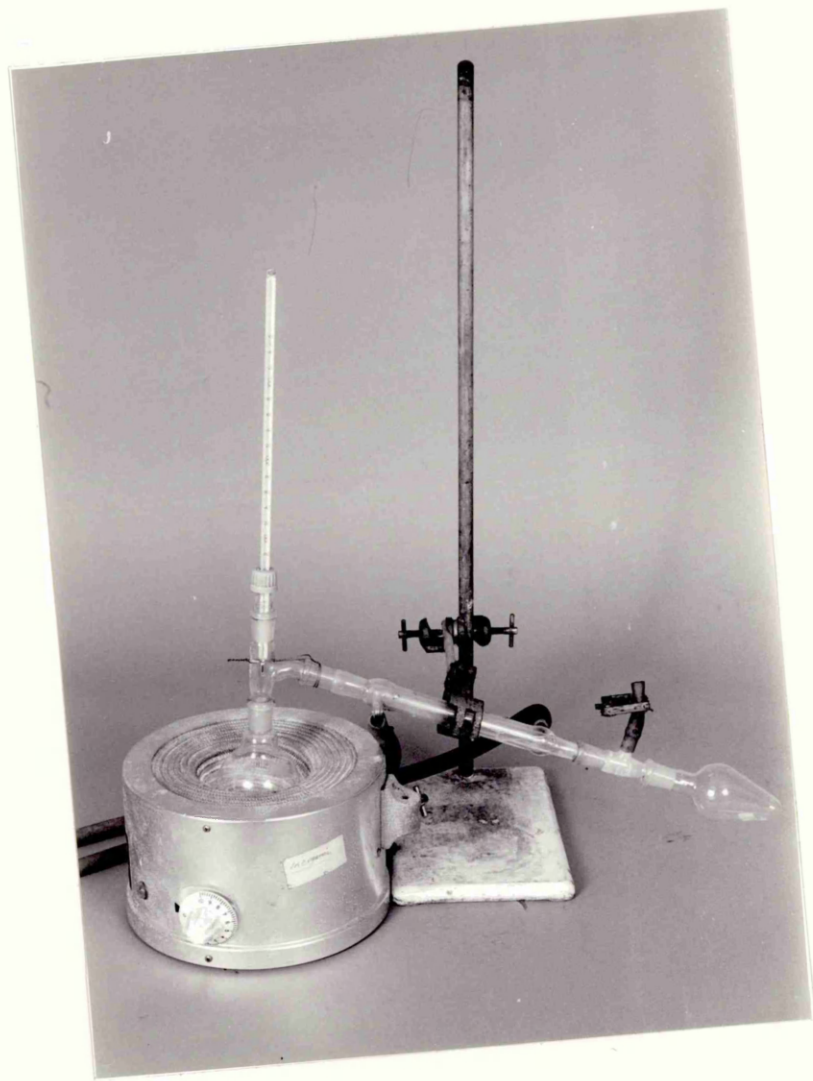
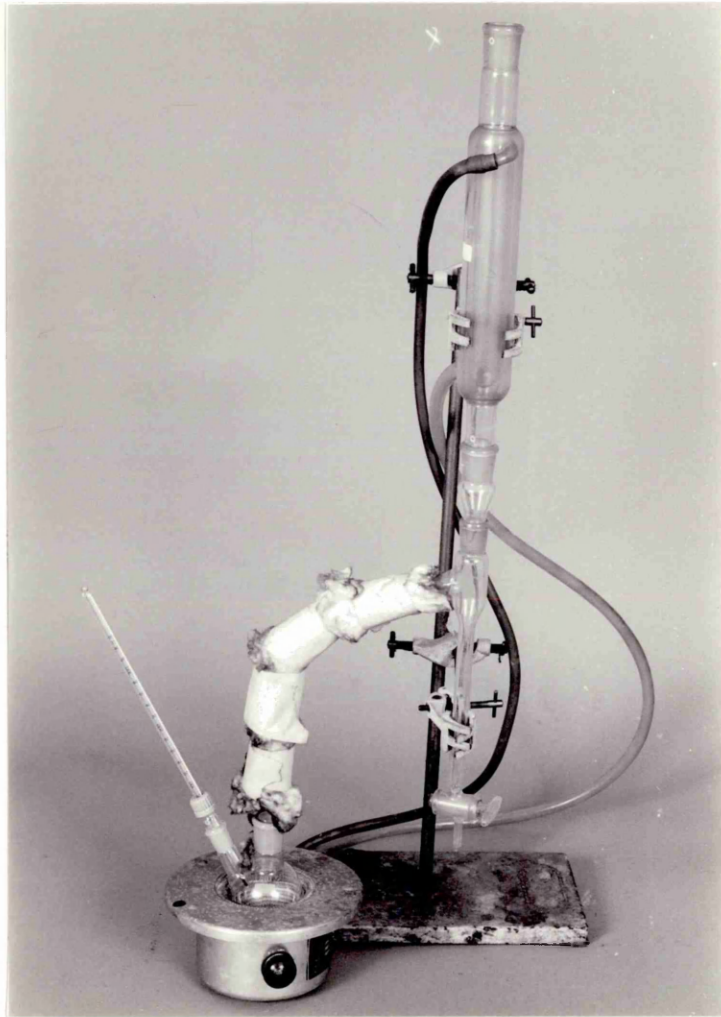
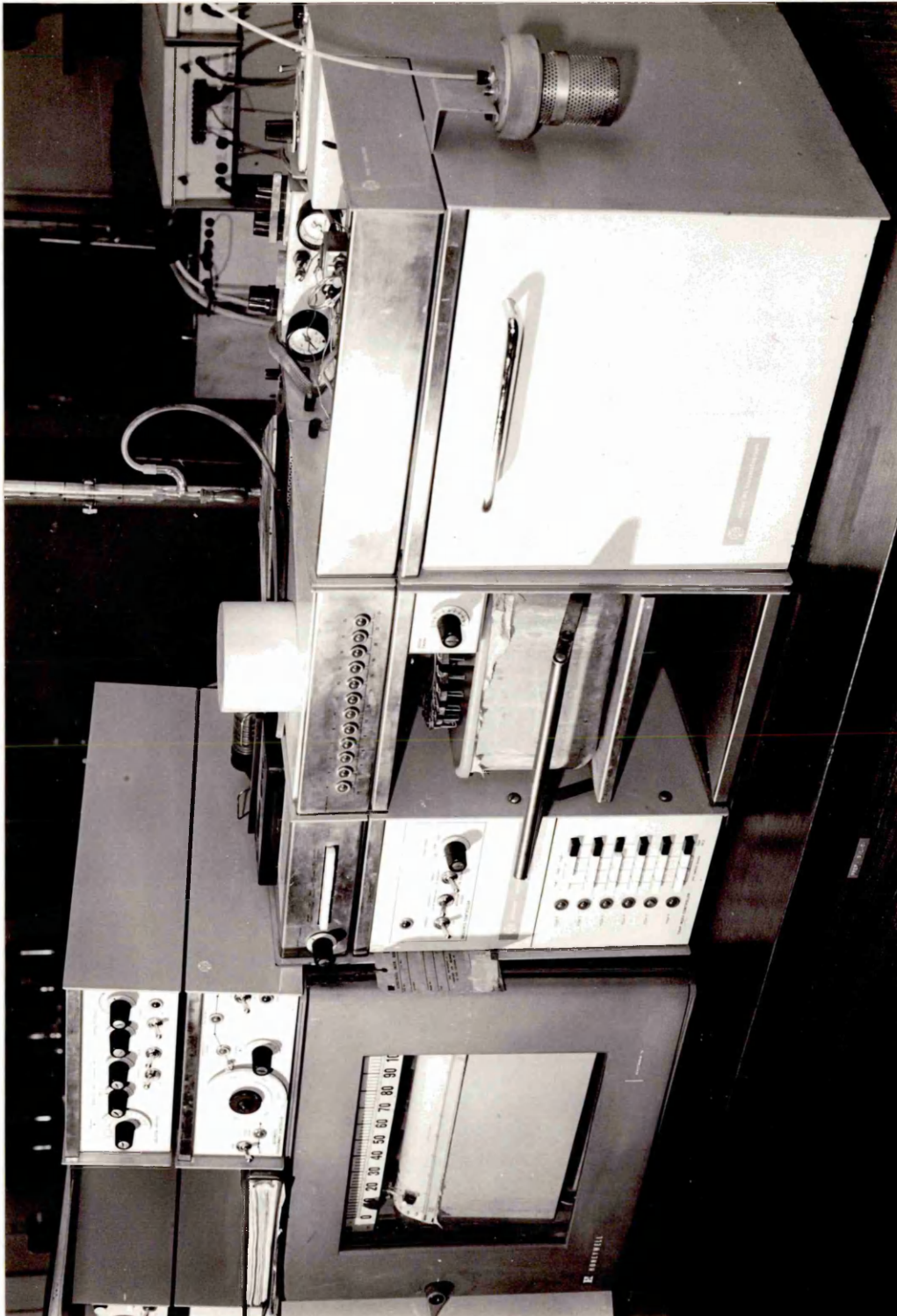


Plate 6

Distillation Unit Used For The Removal of Unreacted
Trimethylchlorosilane During The Masson
Trimethylsilylation Technique







Plates 9a to 9e

Typical Appearances of Reacted Droplets From The
Stopper and Seat Droplet Experiments

Initial Droplet Composition: Fe-4.20 mass % C-0.123 mass % S
Slag KC1: 38.31 mass % CaO-28.52 mass % FeO-1.90 mass % Fe₂O₃
-31.00 mass % SiO₂-0.27 mass % S

Plate 9a

Droplet Reaction Time = 2 mins.

Final Sulphur Content = 0.095 mass % S

Plate 9b

Droplet Reaction Time = 5 mins.

Final Sulphur Content = 0.077 mass % S



Plate 9c

Droplet Reaction Time = 10 mins.

Final Sulphur Content = 0.041 mass % S

Plate 9d

Droplet Reaction Time = 15 mins.

Final Sulphur Content = 0.050 mass % S

Plate 9e

Droplet Reaction Time = 20 mins.

Final Sulphur Content = 0.021 mass % S

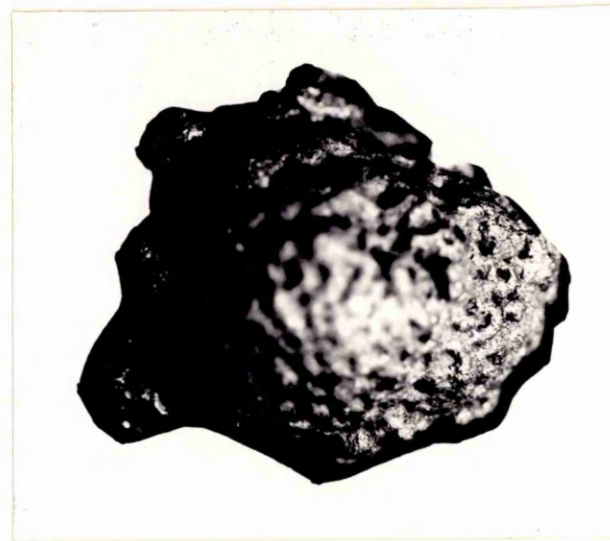
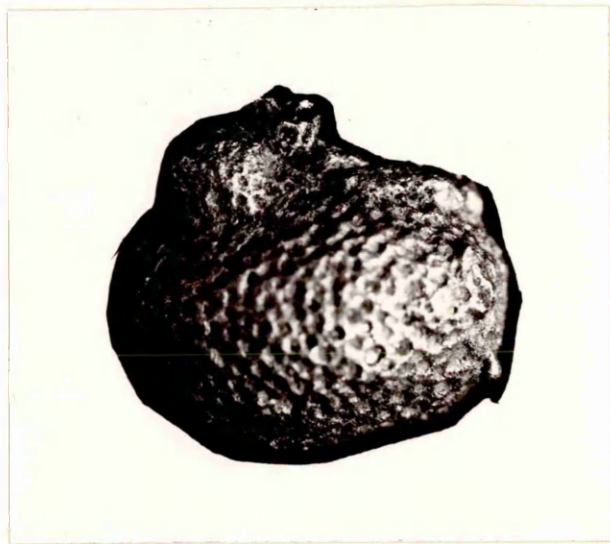
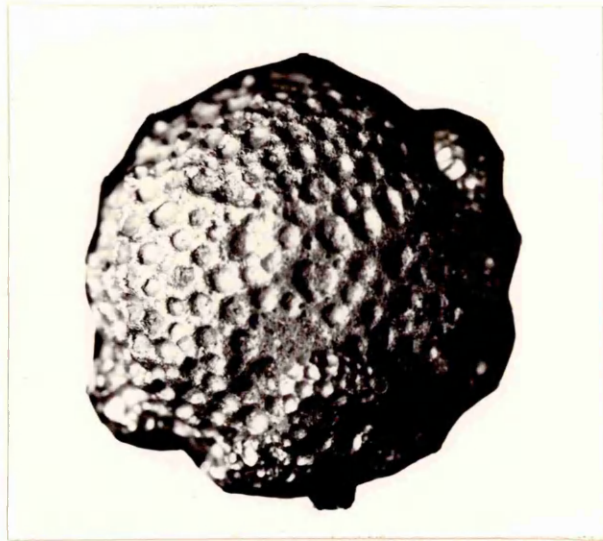
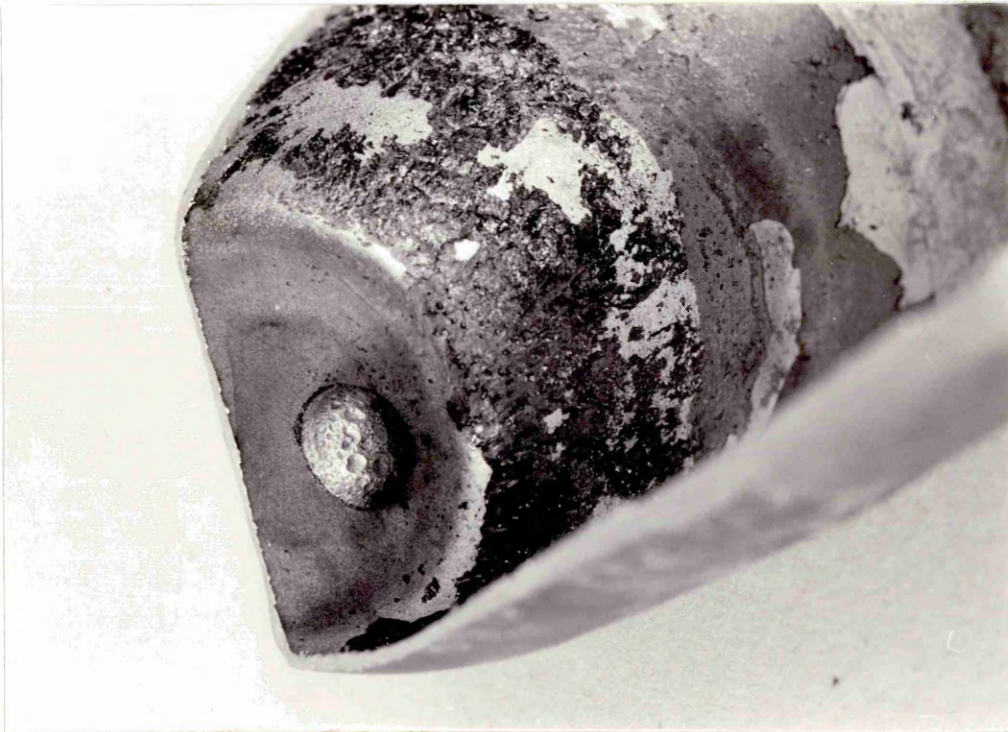


Plate 10

Example of Welding Between Metal Droplet
And Iron Crucible



Plates 11a to 11d

SEM-EDAX Data From a Qualitative Study of
The Interaction Between The ZrO_2 Coating
of a Crucible And Slag KCl , 38.31 % CaO -
28.52% FeO -1.90 % Fe_2O_3 -31.00 % SiO_2 -0.27 % S

Plate 11a

Slag-Crucible Image

Plate 11b

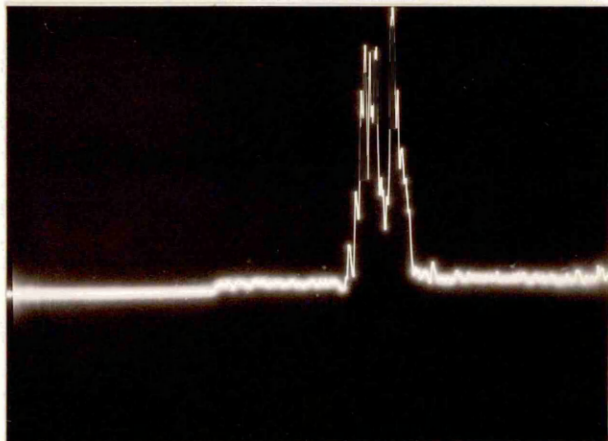
Zirconium Distribution For Field Of
View Shown in 11a

Plate 11c

Zirconium Concentration Profile For
A Line Scan Taken Perpendicular To
Crucible Wall

Plate 11d

Scanning Map For All Detectable
Elements



Plates 12a to 12d

SEM-EDAX Data From a Qualitative Study of
The Interaction Between The ZrO_2 Coating
of a Crucible and Slag K_2CO_3 , 28.60 % CaO -
40.20 % FeO -3.21 % Fe_2O_3 -28.50 % SiO_2 -0.15 % S

Plate 12a

Slag-Crucible Image

Plate 12b

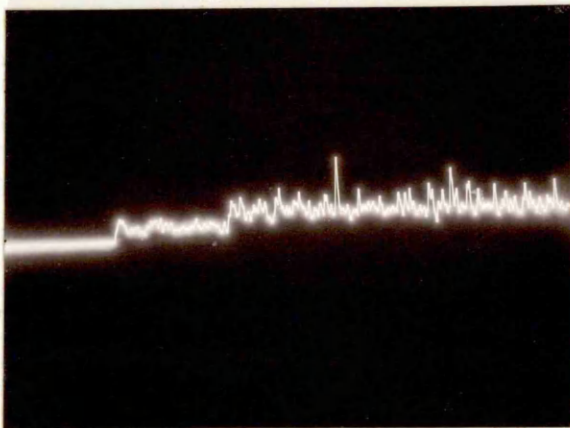
Zirconium Distribution For Field Of
View Shown in 12a

Plate 12c

Zirconium Concentration Profile For
A Line Scan Taken Perpendicular To
Crucible Wall

Plate 12d

Scanning Map For All Detectable
elements



Plates 13a to 13e

Typical Appearances Of Reacted Droplets
From Suspended Droplet Experiments.
Initial Droplet Composition: Fe-4.01 %
C-0.027 % S. Slag KCl₄, 10.40 % CaO-
55.20 % FeO-5.72 % Fe₂O₃-28.20 % SiO₂-
0.33% S

Plate 13a

Droplet Reaction Time = 2 mins

Final Sulphur Content = 0.049 mass % S

Plate .13b

Droplet Reaction Time = 5 mins

Final Sulphur Content = 0.040 mass % S

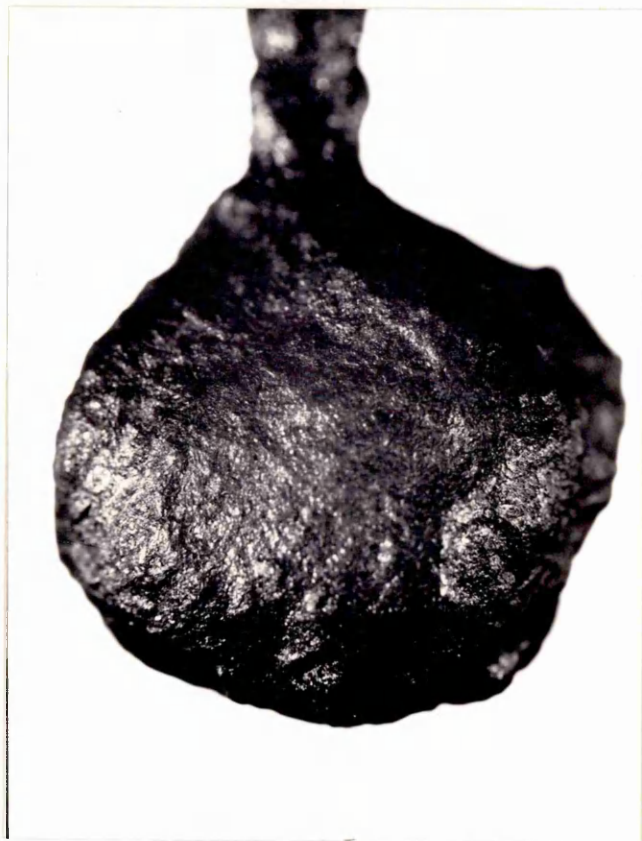
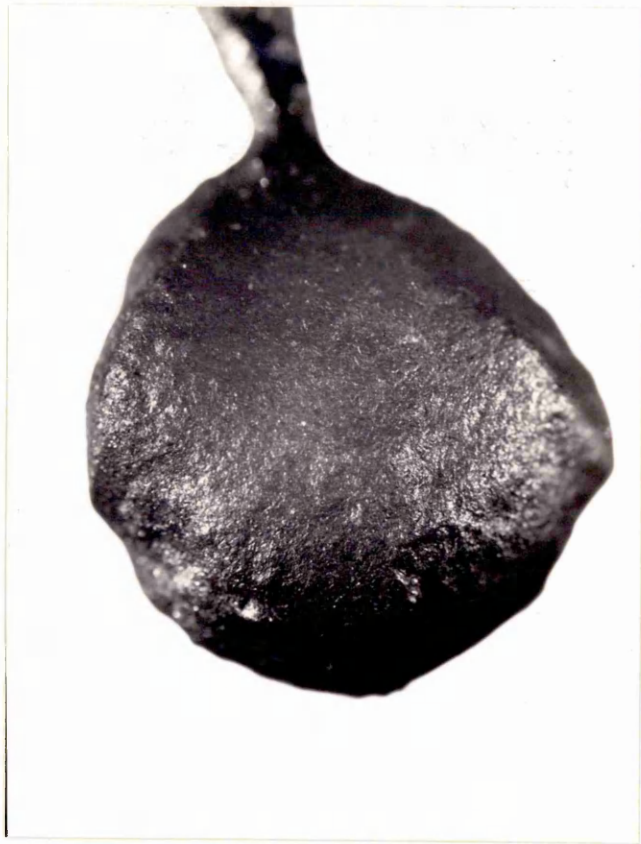


Plate 13c

Droplet Reaction Time = 10 mins.
Final Sulphur Content = 0.049 mass % S

Plate 13d

Droplet Reaction Time = 15 mins.
Final Sulphur Content = 0.043 mass % S

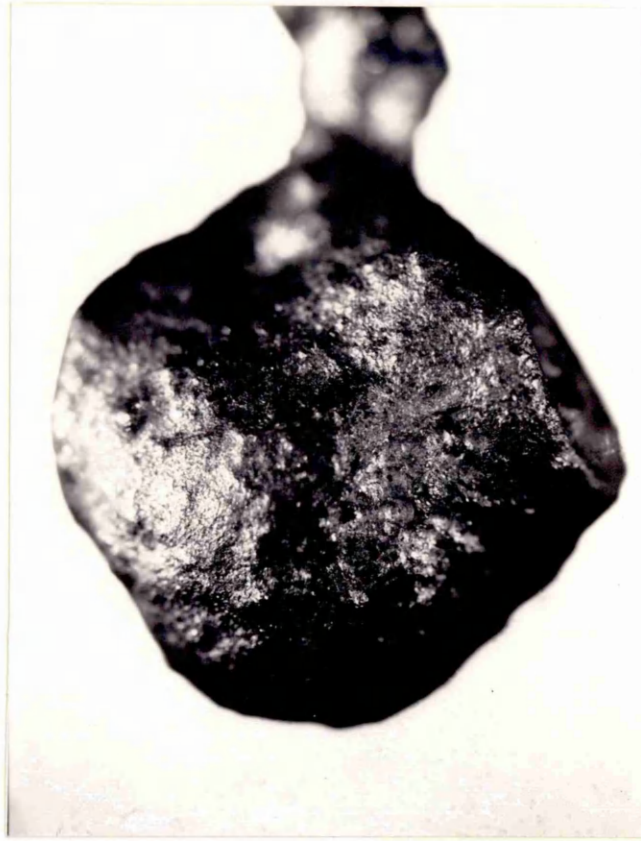


Plate 13e

Droplet Reaction Time = 20 mins.

Final Sulphur Content = 0.039 mass % S

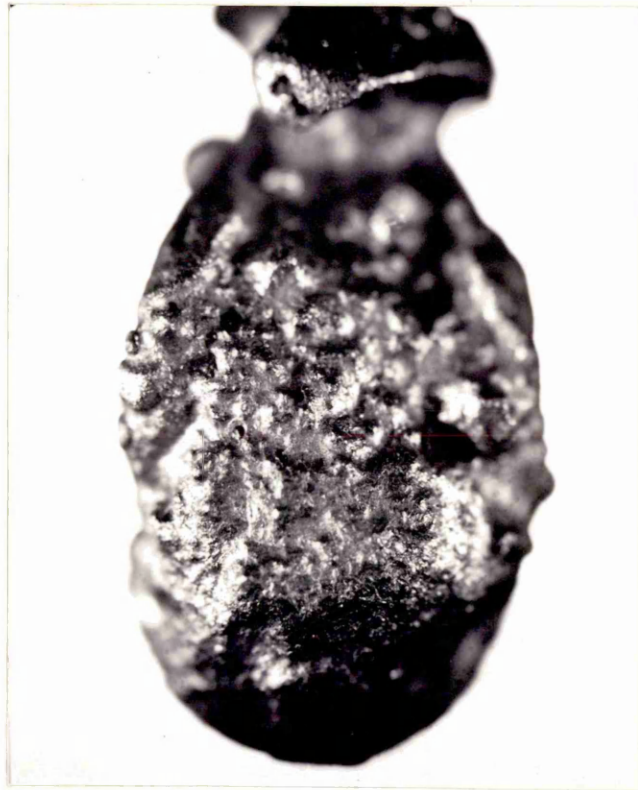


Plate 14a

General View Of A Pin Section And Subsequent
Reacted Droplet.

Plate 14b

General View Of Reacted Droplets From Suspended
Droplet Experiments.

Reaction Times From Left To Right:-

2, 5, 10, 15 and 20 mins. respectively.

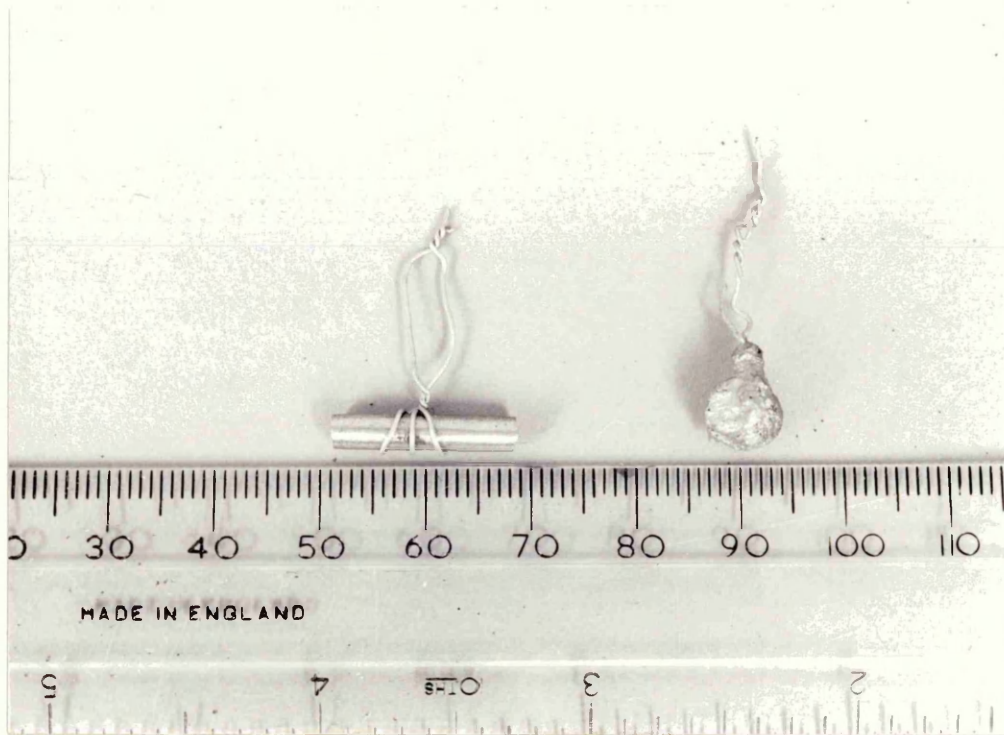


Plate 15

View of Fe-Pt Interface From A Sectioned Droplet.

Droplet Reaction Time = 35 mins.

Slag: KC₂, 28.00 % CaO-40.20 % FeO-3.21 % Fe₂O₃-
28.50 % SiO₂-0.15 % S

Magnification: X63

Appendix 1a

Calculation Of Silicate Anionic Fractions Of An

Iron Blast Furnace Slag Based On GLC Data

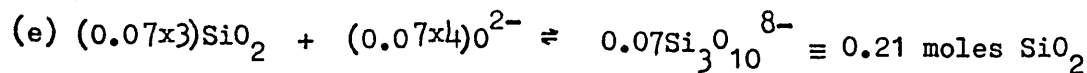
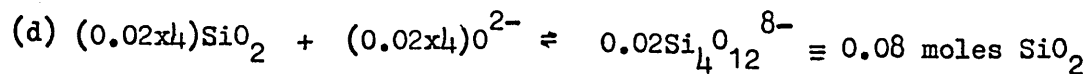
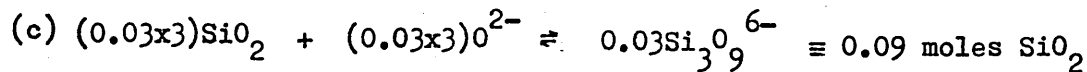
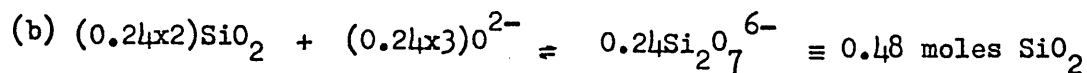
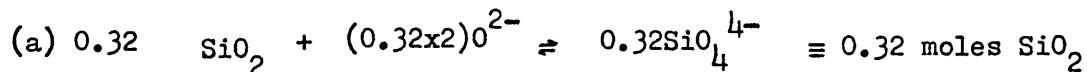
The percentage proportions of silicate anion derivatives detected were (Table 50a):-

	$\frac{\text{SiO}_4^{4-}}{4}$	$\frac{\text{Si}_2\text{O}_7^{6-}}{7}$	$\frac{\text{Si}_3\text{O}_9^{6-}}{9}$	$\frac{\text{Si}_4\text{O}_{12}^{8-}}{12}$	$\frac{\text{Si}_3\text{O}_{10}^{8-}}{10}$
%	29.4	41.2	5.9	5.9	17.6

Assuming that the detector response factors are identical for all the above species and disregarding the mass due to TMS groups, the percentages can be considered to represent mass percentages of silicate groups. The number of moles/100g slag for each species becomes:-

	$\frac{\text{SiO}_4^{4-}}{4}$	$\frac{\text{Si}_2\text{O}_7^{6-}}{7}$	$\frac{\text{Si}_3\text{O}_9^{6-}}{9}$	$\frac{\text{Si}_4\text{O}_{12}^{8-}}{12}$	$\frac{\text{Si}_3\text{O}_{10}^{8-}}{10}$
moles/ 100g slag	0.32	0.24	0.03	0.02	0.07

The total parts of SiO_2 used to produce the above amounts of silicate becomes:-



Total parts SiO_2 used = 1.18 moles SiO_2

The fractional parts of SiO_2 used for conversion to respective anions are:-

$$\text{SiO}_2 \longrightarrow \text{SiO}_4^{4-} = \frac{0.32}{1.18} = 0.27$$

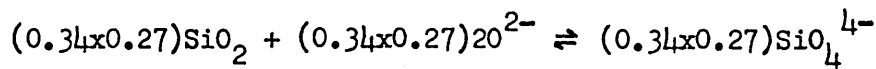
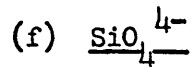
$$\text{SiO}_2 \longrightarrow \text{Si}_2\text{O}_7^{6-} = \frac{0.48}{1.18} = 0.41$$

$$\text{SiO}_2 \longrightarrow \text{Si}_3\text{O}_9^{6-} = \frac{0.09}{1.18} = 0.08$$

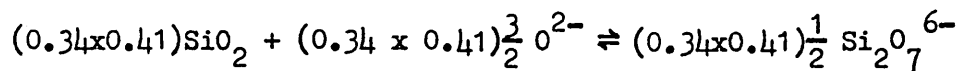
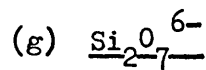
$$\text{SiO}_2 \longrightarrow \text{Si}_4\text{O}_{12}^{8-} = \frac{0.08}{1.18} = 0.07$$

$$\text{SiO}_2 \longrightarrow \text{Si}_3\text{O}_{10}^{8-} = \frac{0.21}{1.18} = 0.18$$

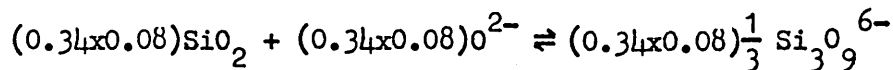
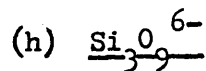
The mole fraction of SiO_2 in the blast furnace slag is 0.34 and, therefore, the oxygen consumed to produce the 5 silicate anions is calculated as follows:-



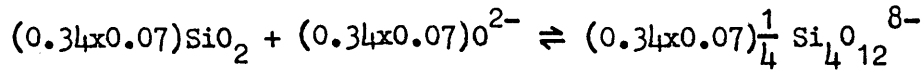
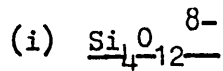
$$\therefore \text{Oxygen consumed} = 0.34 \times 0.27 \times 2 = 0.18 \text{ moles } \text{O}^{2-} / \text{mole slag}$$



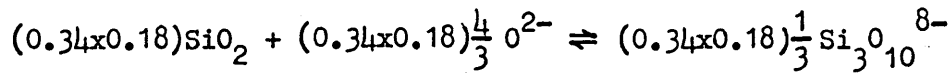
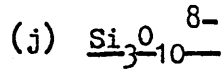
$$\therefore \text{Oxygen consumed} = 0.34 \times 0.41 \times \frac{3}{2} = 0.21 \text{ moles } \text{O}^{2-} / \text{mole slag}$$



$$\therefore \text{Oxygen consumed} = 0.34 \times 0.08 = 0.03 \text{ moles } \text{O}^{2-} / \text{mole slag}$$



$$\therefore \text{Oxygen consumed} = 0.34 \times 0.07 = 0.02 \text{ moles } \text{O}^{2-} / \text{mole slag}$$



$$\therefore \text{Oxygen consumed} = 0.34 \times 0.18 \times \frac{4}{3} = 0.08 \text{ moles } \text{O}^{2-} / \text{mole slag}$$

$$\therefore \text{Total Oxygen consumed to produce silicate anions} = \underline{0.52 \text{ moles } \text{O}^{2-} / \text{mole slag}}$$

If the small concentration of Al_2O_3 in the slag is ignored then the above amount of oxygen will be accommodated by the contribution of oxygen anions in the slag by the oxides CaO, FeO, MgO and MnO thus allowing an oxygen balance to be evaluated:-

	CaO	FeO	MgO	MnO
mole fraction:	0.44	0.006	0.12	0.006

$$\begin{aligned} \text{O}^{2-} \text{ on dissociation} &= (0.44 + 0.006 + 0.12 + 0.006) \\ &= 0.57 \text{ moles/mole slag} \end{aligned}$$

$$\therefore \text{Free } \text{O}^{2-} = 0.57 - 0.52 = \underline{0.05 \text{ moles } \text{O}^{2-} / \text{mole slag}}$$

To Determine Anionic Fractions:-

For anionic species O^{2-} , SiO_4^{4-} , $\text{Si}_2\text{O}_7^{6-}$, $\text{Si}_3\text{O}_9^{6-}$, $\text{Si}_4\text{O}_{12}^{8-}$ and $\text{Si}_3\text{O}_{10}^{8-}$, the anionic fraction of a species is defined as:-

$$N_{\text{silicate anion}} =$$

$$n_{\text{silicate anion}}$$

$$\frac{n_{\text{O}^{2-}} + n_{\text{SiO}_4^{4-}} + n_{\text{Si}_2\text{O}_7^{6-}} + n_{\text{Si}_3\text{O}_9^{6-}} + n_{\text{Si}_4\text{O}_{12}^{8-}} + n_{\text{Si}_3\text{O}_{10}^{8-}}}{},$$

and so on, where $n_{\text{SiO}_4^{4-}}$ etc. is obtained from the equation (f) to (j) and $n_{\text{O}^{2-}} = 0.05 n_{\text{SiO}_4^{4-}}$

Thus:-

$$N_{\text{SiO}_4^{4-}} = 0.36$$

$$N_{\text{Si}_2\text{O}_7^{6-}} = 0.28$$

$$N_{\text{Si}_3\text{O}_9^{6-}} = 0.04$$

$$N_{\text{Si}_4\text{O}_{12}^{8-}} = 0.02$$

$$N_{\text{Si}_3\text{O}_{10}^{8-}} = 0.08$$

Appendix 1b

Determination of the Probable Anionic Constitution of a
PbO-0.36xSiO₂ Slag Based On The Toop and Samis Slag Model ⁸⁴

The calculation involves the determination of (O^-) , (O^{2-}) and (O^0) :-

(i) Calculation of (O^-)

(O^-) , the number of moles of singly bonded oxygen atoms per mole of slag, can be determined from the following equation (Section 2.3.2(a), equation 2.5):-

$$4K = \frac{[4x_{SiO_2} - (O^-)][2 - 2x_{SiO_2} - (O^-)]}{(O^-)^2}$$

where K is the Toop and Samis equilibrium constant with a value of 0.04 for the PbO-SiO₂ system. Thus, for a PbO-SiO₂ slag with a mole fraction of SiO₂ equal to 0.36:-

$$4 \times 0.04 = \frac{[4 \times 0.36 - (O^-)][2 - 2 \times 0.36 - (O^-)]}{(O^-)^2}$$

$$0.16(O^-)^2 = [1.44 - (O^-)][1.28 - (O^-)]$$

which reduces to a quadratic equation:-

$$0.84(O^-)^2 - 2.72(O^-) + 1.8432 = 0$$

where $(O^-) = 0.902$

(ii) Calculation of (O^{2-})

(O^{2-}) , the number of moles of free oxygen anions per mole of slag, is determined from the following equation (Section 2.3.2(a), equation 2.4):-

$$(O^{2-}) = (1-x_{SiO_2}) - \frac{(O^-)}{2}$$

$$\underline{(O^{2-}) = 0.189}$$

(iii) Calculation of (O^0)

(O^0) , the number of moles of doubly bonded oxygen atoms per mole of slag, is determined from the equation (Section 2.3.2(a), equation 2.3):-

$$(O^0) = \frac{4x_{SiO_2} - (O^-)}{2}$$

$$\underline{(O^0) = 0.269}$$

(iv) Determination of the Number of Silicon Atoms per Silicate Anion

The number of silicon atoms per ion can be determined by use of the graph in Figure A1.

To use the graph a value of the following term is required:-

$$\frac{O^-}{O^- + O^0 + Si^{(iv)}}$$

For the slag composition $\text{PbO}-0.36\text{xSiO}_2$, the ionic fraction $\text{Si}^{(\text{iv})}$, equals 0.36. Therefore,

$$\frac{\text{O}^-}{\text{O}^- + \text{O}^0 + \text{Si}^{\text{iv}}} = \frac{0.902}{0.902 + 0.269 + 0.360} = 0.589$$

From Figure A1, the number of silicon atoms per ion corresponding to the above proportion of singly bonded oxygen atoms, 0.589, can be read off as 2.85, i.e. 3.

Thus, the most likely silicate anion is $\text{Si}_3\text{O}_{10}^{8-}$

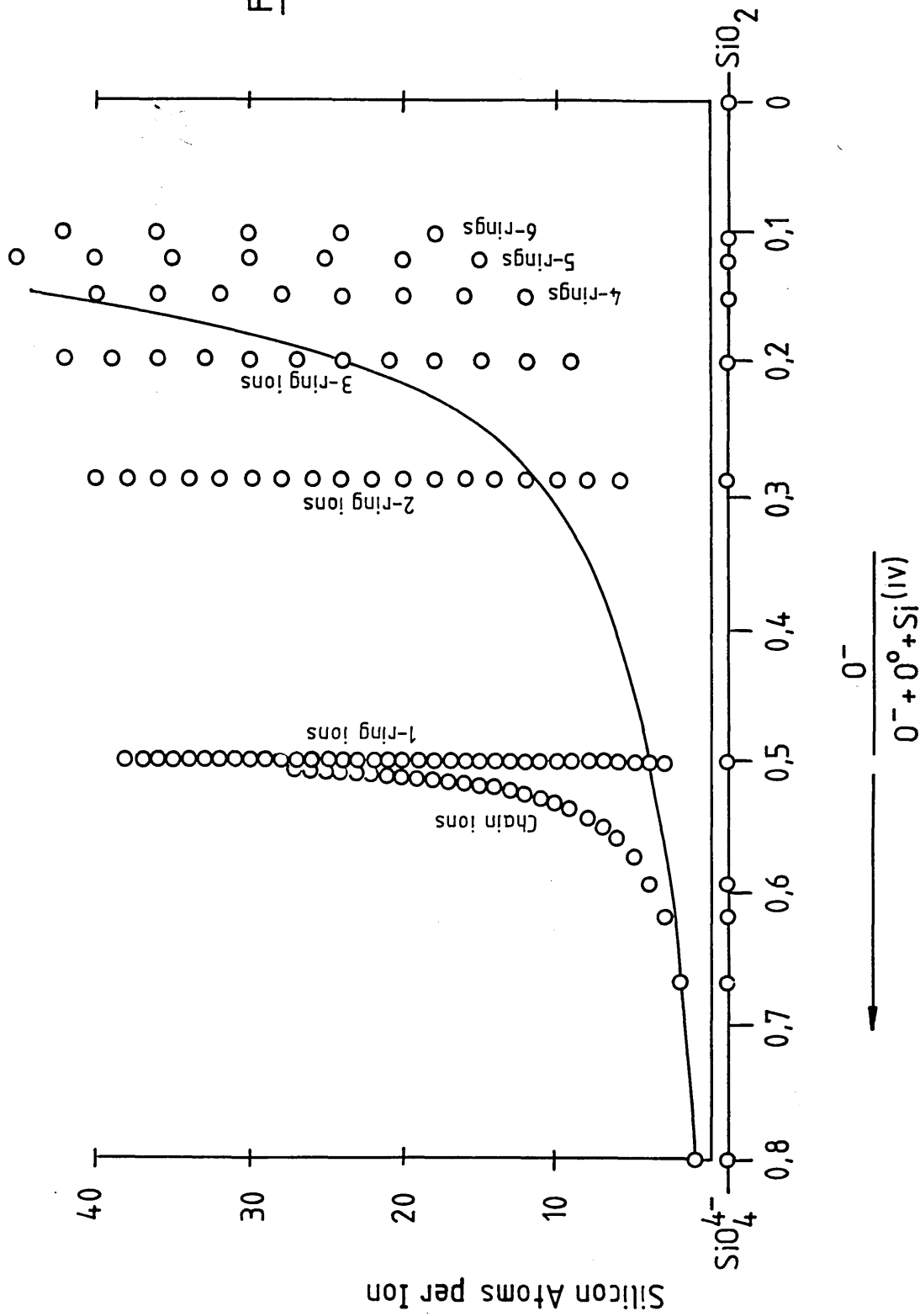


Fig. A1

Plot of the Proportion of Singly Bonded Oxygen Atoms Versus the Number of Silicon Atoms per Ion for a Simple Basic Oxide-Silica Melt - Toop and Samis